**Institute of Production Engineering and Building Research**

Abdelaziz Ibrahim Omara

# Further development of a mobile wind energy plant for a low-pressure irrigation system

Published as: Landbauforschung Völkenrode Sonderheft 275

Braunschweig
**Federal Agricultural Research Centre (FAL)**
2004

Sonderheft 275
*Special Issue*

FAL
Bundesforschungsanstalt für Landwirtschaft

*Landbauforschung*
*Völkenrode*
*FAL Agricultural Research*

# Further development of a mobile wind energy plant for a low-pressure irrigation system

**Abdelaziz Ibrahim Abdelaziz Aly Omara**

# TABLE OF CONTENT / *INHALTSVERZEICHNIS*

# LIST OF TABLES / *TABELLENVERZEICHNIS*

# LIST OF FIGURES / *ABBILDUNGSVERZEICHNIS*

# LIST OF SYMBOLS / *ABKÜRZUNGSVERZEICHNIS*

| Symbol<br>*Zeichen* | Meaning<br>*Bedeutung* | Unit<br>*Einheit* |
|---|---|---|
| **A** | Ampere | **----** |
| **AAMEP** | MoWEC average actual mean monthly energy production on N.W. coast of Egypt | **kWh/ month** |
| **AC** | Alternating-current | **----** |
| **$A_{ef}$** | Effective area MoWEC-rotors | **m²** |
| **AHE** | Required hydraulic energy | **kWh/ year** |
| **AMAEP** | MoWEC actual mean annual energy production | **kWh/ year** |
| **AMEP** | MoWEC actual mean monthly energy production | **kWh/ month** |
| **AOM** | Annual operation and maintenance | **€/year** |
| **$A_r$** | Area swept by rotor blades | **m²** |
| **b** | Rotor wing element width | **m** |
| **°C** | Degree of temperatures (Celsius) | **----** |
| **Ca** | Annual fuel or maintenance costs | **€ /year** |
| **$C_d$** | Drag-coefficient | **----** |
| **CFK** | Carbon fiber reinforced plastic | **----** |
| **$C_{Hwh}$** | Hazen-William's coefficient of the distributor hose | **----** |
| **$C_{HwL}$** | Hazen-William's coefficient of the lateral | **----** |
| **$C_{Hwm}$** | Hazen-William's coefficient of the Mainline | **----** |
| **$C_{Hwmf}$** | Hazen-William's coefficient of the Manifold | **----** |
| **cm** | Centimeter | **----** |
| **CIS** | Commonwealth of Independent States | **----** |
| **COE** | Cost of energy | **€ cent/ kWh** |
| **$C_p$** | Power coefficient | **----** |
| **$C_{p, max, d}$** | Optimal power-coefficient | **----** |
| **$C_{pm}$** | Lee-wind wheel power coefficient | **----** |
| **$C_{Pt}$** | MoWEC total power coefficient | **----** |
| **$C_r$** | Total aerodynamic coefficient | **----** |
| **$C_T$** | Torque coefficient | **----** |
| **dE** | Kinetic energy | **J** |
| **DH** | Distributor hoses | **----** |
| **Dh1** | Pressure head at hose inlet | **m** |
| **Dh2** | Pressure head at hose outlet | **m** |
| **DHE** | Distributor hose elevation | **---** |
| **$D_L$** | Lateral diameter | **mm** |

| Symbol<br>*Zeichen* | Meaning<br>*Bedeutung* | Unit<br>*Einheit* |
|---|---|---|
| **dm** | Air of mass element | **kg** |
| **$D_m$** | Mainline diameter | **mm** |
| **$D_{mf}$** | Manifold diameter | **mm** |
| **$d_{oh}$** | Hose diameter | **mm** |
| **dV** | Volume element | **m³** |
| **$D_{wi}$** | Lee-wind wheel inner ring diameter | **m** |
| **$D_{wo}$** | Lee-wind wheel outer diameter | **m** |
| **dx** | Distance element | **m** |
| **$d_e$** | Rotor wing element depth | **m** |
| **D** | Inside diameter of pipes | **m** |
| **$D_b$** | MoWEC ball race middle diameter | **m** |
| **DC** | Direct-current | **----** |
| **DDC** | Desert development center | **----** |
| **DDHE** | Different distributor hose elevation | **----** |
| **DDHL** | Different distributor hose length | **----** |
| **$E_{fh}$** | Hose outlet elevation | **m** |
| **EJ** | Exa Joule | **$10^{18}$ J** |
| **Emax** | Maximum simulated distributor hose outlet elevation | **cm** |
| **$ET_c$** | Crop evapotranspiration rate | **mm/day** |
| **$Et_o$** | Reference evapotranspiration | **mm/ day** |
| **EU** | Emission uniformity of distributor hoses | **%** |
| **f** | Friction factor | **----** |
| **F** | Christensens friction factor | **----** |
| **FAL** | Federal Agricultural Research Center | **----** |
| **FCR** | Fixed charge rate | **% year** |
| **$F_d$** | Drag force | **N** |
| **FDHW** | Theoretical friction loss of the hoses | **m/m** |
| **FLHW** | Lateral theoretical friction loss | **m/m** |
| **$F_T$** | Tangential force | **N** |
| **$F_{Tr}$** | Minimum tangential force | **N** |
| **g** | Gravitational constant | **m/s²** |
| **GFK** | Glass fiber reinforced plastic | **----** |
| **h2** | Pressure head at lateral outlet | **m** |

| Symbol<br>*Zeichen* | Meaning<br>*Bedeutung* | Unit<br>*Einheit* | Symbol<br>*Zeichen* | Meaning<br>*Bedeutung* | Unit<br>*Einheit* |
|---|---|---|---|---|---|
| **ha** | Hectare | **$10^4$ m²** | **MEP** | MoWEC mean monthly energy production | **kWh/ month** |
| **$h_{ac}$** | Actual head loss in the pipeline | **m** | **MIR** | Monthly irrigation requirement | **m³/10ha * month** |
| **HE** | Daily required hydraulic energy | **kWh/ day** | **MLF** | Lateral measured friction loss | **m/m** |
| **$h_f$** | Friction head loss in pipes | **m** | **mm** | Millimeter | **----** |
| **$h_{mc}$** | Minor losses at pipe fittings | **m** | **MoWEC** | Mobile Wind Energy Converter | **----** |
| **HSS** | Static suction head | **m** | **MTOE** | Million Ton Oil Equivalent | **----** |
| **h** | Hour | **----** | **MWD** | Mean monthly wind speed duration | **h/ month** |
| **H** | Vertical distance | **cm** | **MWS** | Mean monthly wind speed | **m/s** |
| **h1** | Pressure head at lateral inlet | **m** | **N** | Newton | **----** |
| **I** | Current | **A** | **$N_o$** | Number of outlets along the pipeline | **----** |
| **IC** | Initial installed cost | **€** | **$N_1$, $N_2$** | Rotational speed | **rpm** |
| **$I_g$** | Generator output current | **A** | **$n_1$** | Lee-wind wheel rotational speed | **rpm** |
| **IR** | Irrigation requirement | **l/tree * day** | **N.W.** | North West | **----** |
| **J** | Joule | **Nm** | **$n_g$** | Generator rotational speed | **rpm** |
| **K** | Kelvin degree | **----** | **$N_L$** | Lateral number | **----** |
| **$K_c$** | Crop coefficient | **----** | **$n_{oh}$** | Hose number per lateral side | **----** |
| **$K_{cover}$** | Cover crop coefficient | **----** | **P** | Water pressure within the pipe | **N/m²** |
| **$K_{canopy}$** | Canopy crop coefficient | **----** | **$P_{air}$** | Air pressure | **N/m²** |
| **kg** | Kilogram | **----** | **PE** | Polyethylene | **----** |
| **km** | Kilometer | **----** | **$P_g$** | Generator output power | **kW** |
| **kW** | Kilowatt | **$10^3$ W** | **PH** | Pressure head | **cm** |
| **kWh** | Kilowatt hour | **----** | **$P_N$** | Rotor actual mechanical power | **W** |
| **l** | Litre | **----** | **$P_{v1}$** | Wind power | **W** |
| **$L_o$** | Length of pipeline | **m** | **PTO** | Power take off | **----** |
| **$L_d$** | Delivery pipe length | **m** | **$q_{ohL}$** | average hose discharge in lowest 25% of discharge range | **l/h** |
| **LHBIS** | Low-head bubbler irrigation system | **----** | **$q_{ohA}$** | average discharge of all distributor hoses | **l/h** |
| **$L_L$** | Lateral length | **m** | **$q_{oh\ var}$** | Distributor hose flow variation | **%** |
| **$L_m$** | Mainline length | **m** | **$q_{oh\ max}$** | Maximum distributor hose discharge | **l/h** |
| **$L_{mf}$** | Manifold length | **m** | **$q_{oh\ min}$** | Minimum distributor hose discharge | **l/h** |
| **$L_{oh}$** | Hose length | **m** | **$q_{oh}$** | Distributor hose discharge | **l/h** |
| **$L_S$** | Suction pipe length | **m** | **Q** | Discharge in the pipe upstream of the distributor hose | **l/s** |
| **m** | Meter | **----** | **$Q_M$** | MoWEC water pumped | **m³/ month** |
| **$m_d$** | Exponent in Darcy-Weisbach equation | **----** | **$Q_c$** | Downstream Discharge | **l/s** |
| **MDF** | Measured friction loss in the hose | **m/m** | **R** | Electrical resistance of the heating elements | **Ω** |
| **MDN** | Number of days in each | **day/** | **RD** | Required discharge for 10 ha | **m³/h** |

| | | |
|---|---|---|
| | month | **month** |

| **Symbol** *Zeichen* | **Meaning** *Bedeutung* | **Unit** *Einheit* |
|---|---|---|
| **RHL** | Required pressure head at each lateral inlet | **m** |
| **$R_e$** | Reynolds number | **----** |
| **RHM** | Required pressure head at mainline inlet | **m** |
| **RHMF** | Required pressure head at the inlet of the manifold | **m** |
| **$r_p$** | Pulley radius | **cm** |
| **rpm** | Revolution per minute | **----** |
| **$R_T$** | Total speed reduction ratio of the Lee-wind wheel system | **----** |
| **rw** | Speed reduction ratio in lee-wind wheel system | **----** |
| **$R_{wo}$** | Lee-wind wheel outer ring radius | **m** |
| **R** | Rotor radius | **m** |
| **r** | Radius of the roll wheel in lee-wind wheel system | **m** |
| **$R_{air}$** | Gas constant of the air | **Ws/kg$_*$ K** |
| **s** | Second | **----** |
| **S = 1** | Hose position on one lateral side | **----** |
| **S = 2** | Hose position on two lateral sides | **----** |
| **$S_L$** | Distributor hose spacing along the lateral (Tree spacing) | **m** |
| **$S_m$** | Lateral spacing along the manifold (Row spacing) | **m** |
| **$So_L$** | Longitudinal slope of the laterals | **%** |
| **SRH** | Simulated required pressure head at each manifold inlet | **cm** |
| **SS = 1** | Laterals position on one manifold side | **----** |
| **SS = 2** | Laterals position on two manifold sides | **----** |
| **t** | Time | **min** |
| **$T_{air}$** | Absolute air temperature | **K** |
| **TDH** | Total dynamic head | **m** |
| **$T_g$** | Generator torque | **Nm** |
| **TH** | Storage tank height | **m** |
| **TL** | Total loss | **m** |
| **$T_r$** | Torque required by MoWEC | **Nm** |
| **$T_w$** | Lee-wind wheel torque | **Nm** |
| **TSH** | Total static head | **m** |

| **Symbol** *Zeichen* | **Meaning** *Bedeutung* | **Unit** *Einheit* |
|---|---|---|
| **TWh** | Terra watt hour | **$10^{12}$ Wh** |
| **u** | Circumferential speed | **m/s** |
| **$U_g$** | Generator output voltage | **V** |
| **U** | Voltage between two conductors | **V** |
| **$U_{str}$** | Voltage between one conductor and the neutral point | **V** |
| **V** | Water velocity in pipes | **m/s** |
| **$v_1$** | Wind speed | **m/s** |
| **W** | Watt | **J/s** |
| **WEC** | Wind energy converter | **----** |
| **WU** | Water use rate | **l/tree$_*$ day** |
| **Z** | Elevation of pipe centerline | **m** |
| **€** | Euro | **----** |
| **$\rho_{air}$** | Air density | **kg/m³** |
| **$\omega$** | Angular velocity of rotor | **rad/s** |
| **$\lambda$** | Tip-speed-ratio | **----** |
| **$\alpha_c$** | Kinetic energy correction factor | **----** |
| **$\Delta h_p$** | Pressure head recovery across outlet | **m** |
| **$\alpha$** | Angle of attack | **degree** |
| **$\gamma$** | Specific weight of water | **N/m³** |
| **$\gamma_w$** | Specific gravity of water | **kN/m³** |
| **$\eta_g$** | Transmission efficiency | **%** |
| **$\eta_p$** | Pump efficiency | **%** |
| **$\theta$** | Lee-wind wheel horizontal axis-wind direction angle or angle between MoWEC-rotor axle and the wind direction | **degree** |
| **$\rho$** | Water density | **kg/m³** |
| **$\varphi$** | Lee-wind wheel blade angle | **degree** |
| **$\varphi_c$** | Current phase angle | **degree** |
| **$\Omega$** | Ohm | **----** |

# 1 INTRODUCTION

Worldwide energy demand is continually increasing due to the increase in the world's population, economic growth, and energy consumption [HEINLOTH (1997)]. At today's rate of increase the sources of fossil energy, which meet the majority of the current world energy demand, will not be sufficient in the centuries to come. Moreover, $CO_2$ emissions, which are the main causes of the greenhouse effect, and other atmospheric pollutants from energy generation based on fossil fuels cause environmental pollution [HASSAN (2003)].

Humans have found ways to secure their food from the Earth's land, beginning more than a million years ago with the hunter-gatherers. Much of the world's agriculture was - and still is- carried out by hand. Once fossil energy supplies became available about 200 years ago, intensive agricultural production developed. Although contemporary, energy - intensive agricultural systems are highly productive [PIMENTEL (1999)].

Now, at the turn of the century, we are faced with meeting the food needs of a rapidly expanding human population. Currently, more than 3 milliard people in the world are malnourished due to food shortages and poor distribution of some foods [WHO (1996)]. In addition, shortages of crop land, fresh water, fossil energy, and biological resources now plague agricultural production in many parts of the world. Stores of fossil energy also have begun to decline. This trend will intensify after the year 2000 [PIMENTEL (1998a)].

## 1.1 Agricultural and irrigation systems in Egypt

The agricultural land base of Egypt totals about 3.25 million hectares covering three different production zones. The first is the old irrigated land with an area of 2.25 million hectares lying within the Nile Valley and Delta. It represents the most fertile soils in Egypt, which are alluvial, level, deep, dark brown and heavy to medium in texture. The second production zone is the "newly" reclaimed land, which is viewed as an opportunity for increasing the cultivated area by about 0.798 million hectares. This includes the newly reclaimed land of sandy, calcareous, and saline origin. The third zone is the rainfed area (about 0.21 million hectares) located along the Northwest Coast and in North Sinai [ABDEL-MONEM (1998)].

Egypt's agricultural land is, on average, highly productive and ideally suited to intensive agriculture. With good climatic conditions and a perennial source of irrigation water, agriculture is provided with excellent growing conditions, resulting in high crop yields. Crop productivity levels in Egypt are relatively high when compared to world standards. Due to intensive cropping, the total cropped area was estimated at about 5.082 million hectares, giving a cropping intensity of around 180% for the country as a whole [GOMAA (1996)]. The total

orchard area in Egypt is 13.1% of the agricultural land [PETER (2000)]. In Egypt, different irrigation systems are used to irrigate both the old lands and newly reclaimed areas. These systems are surface, sprinkler and localized irrigation. The area irrigated with the aid of these systems is illustrated in Table 1.1 [ICID (2002)].

Table 1.1: Irrigated area by different irrigation systems in Egypt. [ICID (2002)]

*Bewässerungsflächen und Bewässerungssysteme in Ägypten.*

| Irrigated area | **Surface** | **Sprinkler** | **Localised** | Total |
|---|---|---|---|---|
| ha | 2,746,000 | 450,000 | 104,000 | 3,300,000 |
| % | 83.21 | 13.64 | 3.15 | 100 |

The irrigation system in the old lands (S) of the Nile Valley and delta is a combined gravity and water lifting system. But the irrigation system in the newly reclaimed areas (M) is based on a succession of pumping stations from the main canal or well to the fields with a total lift of 20 to 30 m. For this purpose, new irrigation systems such as micro-irrigation and sprinklers are used. The places of surface and modern irrigation systems are shown in Figure 1.1 [DERBALA (2003)].


Figure 1.1: The places of surface irrigation (S) and modern irrigation (M) systems in Egypt.

*Die Orte mit Oberflächenbewässerung (S) und mit modernen (M) Bewässerungssystemen in Ägypten.*

The present water supply barely sustains the current demand in Egypt, and the demand for water is increasing since currently the population is growing by about one million a year. Egypt is expected to face a population of about 86 million by the year 2025 [ABU-ZEID (1992)]. The present share of land is 0.05 ha per capita. This is an exceedingly small share compared to 0.22 ha per capita in most countries of the Near East Region and the world average of 0.28 ha per capita [GADDAS (2000)]. Egypt's real current challenge is the management and development of the limited natural resources such as water, land, and energy in order to meet the increasing requirements of a steadily growing population. Extensive research and numerous studies have been carried out in different fields with regard to the saving and use of renewable energy, the development of water resources and the improvement of irrigation and drainage methods well as the means of protecting the environment from pollution.

Egypt is located in the north-eastern corner of the African continent with a total area of about 1,002,000 km². Total population is about 74.719 million on 1st July 2003. The majority of Egypt's population lives in the Nile Valley and its Delta in an area that amounts to less than 4% of the country's land area. Thus, 96% of the area is primarily desert [CIA (2003)]. There is great pressure to reclaim the desert to meet the needs of a population which is increasing at a rate close one million a year [ABU-ZEID (1992)]. Egypt lies in the Saharan hyper arid climatic zone where the evapotranspiration exceeds rainfall and water resources are very limited. Water sufficiency represents the main future problem expected for Egypt as well as the other countries in the region. The river Nile represents the main source of water in Egypt where the population is concentrated in its valley. The Egyptian annual share from the Nile water reaches 55.5 billion cubic meters according to the 1959 agreement between Egypt and Sudan. Agriculture in Egypt is almost entirely dependent on irrigation; the country has no effective rain except in a narrow band along the northern coastal areas. Most of Egypt's water is used within the agricultural sector (84% for agriculture, 8% for industry, 5% for municipalities, and 3% for navigation) [ABU-ZEID (1994)]. Table 1.2 shows the current and expected water requirement by the year 2025, as compared with the actual requirement in the year 1997. It is clear that the water requirements will reach 81 billion cubic meters by the year 2025 with a deficiency of 14.9 billion cubic meters. A volume of 9.5 billion cubic meters can be replaced by upper Nile projects. It is possible to replenish the water deficit through improved usage efficiency provided by recent irrigation techniques and other methods [EL-KADY (1999), GAD (2003) and YEHIA (2003)].

Table 1.2: Water requirements in Egypt by the year 2025 as compared with the year 1997.
*Wasserverbrauch in Ägypten bis zum Jahr 2025, im Vergleich zu 1997.*

| **Usage sector** | **Year 1997** $[10^9\ m^3]$ | **Year 2025** $[10^9\ m^3]$ |
|---|---|---|
| Agriculture | 50.1 | 64.0 |
| House use | 4.5 | 7.3 |
| Industry | 7.5 | 7.3 |
| Others* | 3.0 | 2.4 |
| Total requirements | 65.1 | 81.0 |
| Available | 66.1 | 66.1 |
| Difference | +1.0 | -14.9 |

*Winter closure and evaporation from irrigation networks

## 1.2 Energy situation in the World

Energy resources can be divided into renewable and non-renewable resources. Non-renewable resources can be divided into a) fossil fuels which are divided into coal, crude oil and natural gas and b) uranium ores – nuclear power. Renewable resources can be divided into geothermal, hydro-electric, solar, wave, tidal, wind, biomass, etc. Fossil fuels are the most widely used energy resources. Renewable energy resources can be defined as energy resources that are replaced rapidly by natural processes. Renewable energy is beginning to grow out of its fledgling status and has experienced exponential growth in usage over recent years. There can be no doubt that it will play a major role in the global, regional and local energy supply systems of the 21st century and beyond. Non-renewable energy resources are energy resources that are not replaced or are replaced only very slowly by natural processes; i.e., they are being used up at rates much greater than the rates of formation of new resources. The problem with non-renewable energies, in addition to limited resources, is that they cause environmental pollution. Burning fossil fuel produces $CO_2$ and other atmospheric pollutants [HASSAN (2003)].

The WEC/FAO (1999) wrote in a recent publication: “Three milliard people live in rural areas around the world, nearly 90 percent of them in developing countries. The vast majorities are overwhelmingly dependent on burning wood, dung and crop residues to provide energy for cooking, heating and light, often using inefficient technologies. In the poorest rural households, the amount of energy consumed is less than what is needed for a minimum standard of living”.

A breakdown of world primary energy consumption in 1995 illustrates that oil is the dominant fuel, contributing some 40%, followed by coal at 29.5%. Coal was once the dominant world fuel, but is now losing ground rapidly to oil and natural gas, which has a 25.5% share. Hydroelectricity and nuclear energy are used far less, accounting for around 2.5% each. In

1995, worldwide annual primary energy consumption reached 338.4 EJ [ENQUETE-KOMMISSION (1995), QUASCHNING (1999), GODFREY (1996), ROGER (2000)]. In 2002, worldwide annual total energy consumption including non conventional energies reached 421.95 EJ. The distribution of utilization is shown in Figure 1.2 [ENERDATA (2003)].

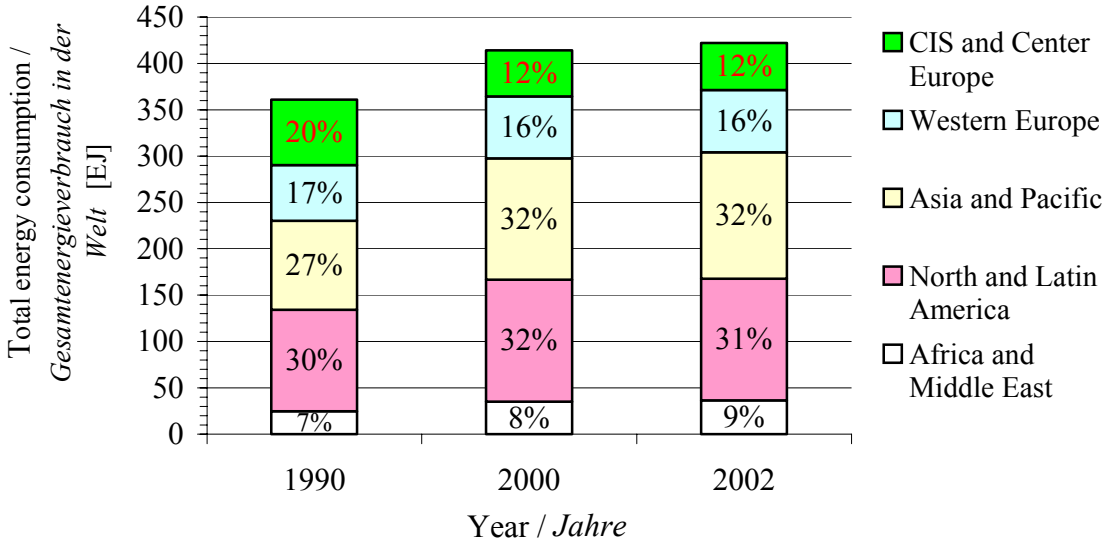


Figure 1.2: Worldwide total energy consumption. [after ENERDATA (2003)]
*Gesamtenergieverbrauch in der Welt.*

Current energy use expenditure is directly related to many factors, e.g. rapid population growth, urbanization and higher consumption rates. Indeed, energy use has been growing even faster than world population. From 1970 to 1995, energy use was increasing at a rate of 2.5% per year (doubling every 30 years) whereas the world population only grew by 1.7% (doubling approximately every 40 years) [DOE (1995), PRB (1996) and IEA (1995)]. From 1995 to 2015, energy use is projected to increase at a rate of 2.2% (doubling every 32 years) compared with a population growth rate of 1.5% (doubling every 47 years) [DOE (1995), PRB (1996) and IEA (1995)].

The world supply of oil is projected to last approximately 50 years at current production rates [BP (1994), IVANHOE (1995), CAMPBELL (1997), DUNCAN (1997), YOUNGQUIST (1997) and DUNCAN (1998)]. Worldwide, the natural gas supply is adequate for about 50 years and coal for about 100 years [BP (1994), BARTLETT (1995) and YOUNGQUIST (1997)]. These projections, however, are based on current consumption rates and current population numbers. If world population continued to grow at a rate of 1.5% and if all people in the world were to enjoy a standard of living and energy consumption rate similar to that of the average American, then the world's fossil fuel reserves would last only about 15 years [CAMPBELL (1997) and YOUNGQUIST (1997)].

A hopeful sign is that major oil companies are beginning to take renewable energy seriously and to factor renewable energies into the energy mix required to meet future demand. For example, SHELL (1996) speculates that perhaps ten different sources will each have a market share between 5 and 15 percent by the year 2060, see Figure 1.3. The scenario shows that the use of fossil energies is going to increase over the next 30 years. By 2020/2030, however, they will reach their maximum amount and their use will begin to decrease. The growing world energy demand will then be satisfied by a substantial increase in renewable forms of energy, i.e. wind, biomass, solar, geothermal and yet undefined forms labelled "surprise".

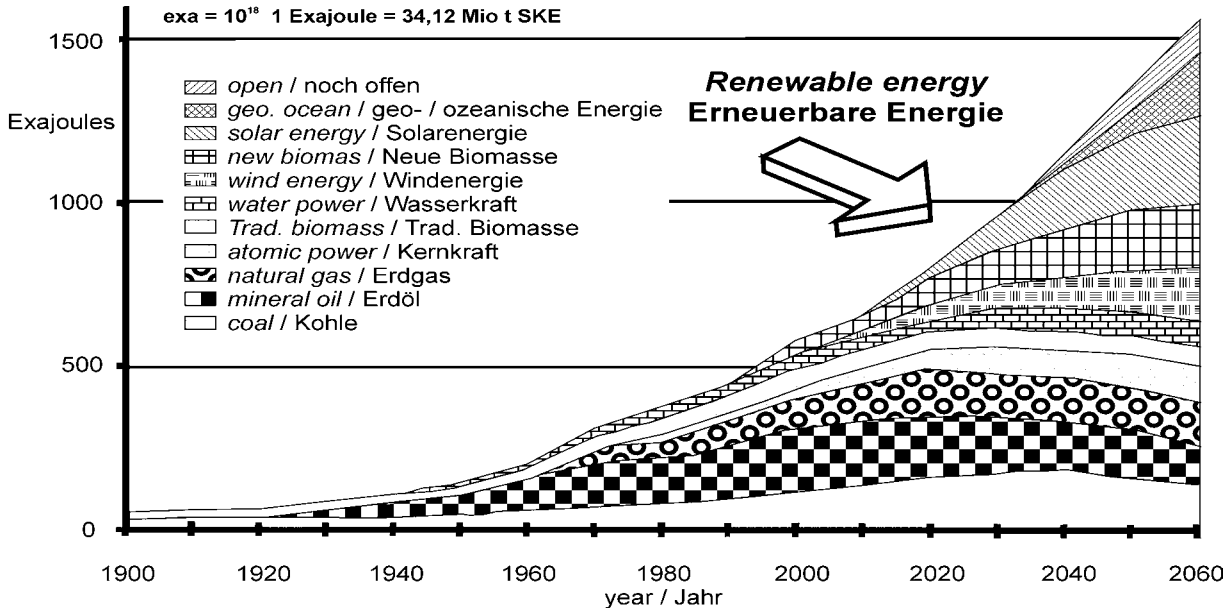


Figure 1.3: The scenario of ten different energy sources until the year 2060. [SHELL (1996)]
*Ein Energieszenario für zehn unterschiedliche Energiequellen bis zum Jahr 2060.*

## 1.3 Energy situation in Germany

Germany is one of the world's largest energy consumers. Germany imports most of the energy required to meet its energy needs because it has limited local energy resources (except for coal and natural gas). Total primary energy consumption in Germany for the year 2001 was 14.501 EJ [AGEB (2002)]. Current energy consumption is primarily based on petroleum (39.5 %), natural gas (21.5 %), as well as hard coal and lignite (13.1 and 11.2 % respectively) – the main causes of the greenhouse effect and climatic changes. They are followed by nuclear power (12.9 %) as well as hydro and wind power (together just under 0.8 %). Slightly less than 2 % was provided by the other renewable energies such as solar energy and biomass [AGEB (2002)]. In the case of final energy used by the consumer, transportation is the dominant sector (30 %). Households account for 29 % of overall final energy consumption, followed by industry (26 %), and crafts, trade, and services at 16 % [BMWi (2002)].

Germany's main renewable resources are hydro and wind power. The opening of Europe's largest wind farm in Paderborn, Germany, in 2001 has increased Germany's total wind power electricity capacity to 700 MW. The use of renewable energy sources for electricity production would increase by 6 % in 2000 to 21 % in 2020 [HASSAN (2003)].

## 1.4 Energy situation in Egypt

In Egypt, fossil fuels in addition to hydropower and non-commercial fuels, such as firewood, agricultural wastes and dried dung, are considered as the main energy resources. Petroleum fuels (e.g. oil and natural gas) are the most important energy sources for Egypt at present and will be for many years to come. The total production of oil and natural gas has been increased by about 60% over the last 18 years while, total production was 33 MTOE (Million Ton Oil Equivalent) in 1980/81, it has meanwhile grown to 55.482 MTOE in 1998/99. Hydropower resources are applied to supply a considerable amount of current electric energy consumption in Egypt. The energy generated from the Highdam, Aswandams, Esna and Naga Hammady barrage power stations in 1998/99 was 15.3 TWh (Terra Watt Hour) representing 22.5% of the total electricity generated. This hydropower is not counted within the term of renewable energy share. The total commercial energy demand of Egypt has increased from about 3 MTOE in 1959 to 30 MTOE in 1998/99 with an average annual growth rate of 4.57% [NREA (2001)].

Due to the socio-economic development, the electricity demand is growing rapidly in Egypt. Since 1980, the Ministry of Electricity and Energy has formulated a national strategy for the development of renewable energy applications and energy conservation measures. The strategy targets a 10% saving of the projected 2005 primary energy consumption through energy conservation measures and the supply of 3% of electricity production from renewable resources such as solar, wind and biomass technologies by the year 2010 [DANISH (1999) and UNEP (2001)].

In 1985, the American University in Cairo established the Desert Development Center (DDC), which undertakes research and development programs to investigate how desert reclamation can best be achieved. Because of the importance of adequate energy sources as part of the integrated development necessary to support new communities in the desert and in view of the ever-diminishing conventional (fossil/hydro) energy sources, the DDC has concentrated on investigating renewable energy sources. The harnessing of both solar and wind energy, is being investigated [MOBARAK (1991)].

In Egypt, like in most other developing countries, there is an increasing demand for energy. Wind energy can be very useful for lifting water or generating electricity in Egypt. BAZ (1981) indicated that the Ministry of energy and electricity in Egypt has carried out several studies to measure the wind speed and its duration at various favorable locations in Egypt. These studies determined the feasibility of using wind energy conversion systems especially along the coasts of the Red and Mediterranean seas. Annual available energy in Egypt in particular along the coasts of the Red and Mediterranean seas is 2250-3750 kWh/year per rated kilowatt output for wind machines designed for a rated wind speed of 11 m/s. GASCH (1996) reported that according to MOLLY (1990) the annual average wind speed along the coasts of the Red and Mediterranean seas of Egypt is 4.6 -5.6 m/s.

Wind energy is one of the most flexible of all renewable energy sources. It can be used for different purposes, such as irrigation, electricity generation, crop drying, grain grinding and many others after converting wind power to mechanical power in windmills. Current wind-powered pumping systems generally utilize bulky, slow-moving rotors and reciprocating pumps. These systems operate well in low-speed winds but reach peak water production in moderate winds around 7 to 8 m/s. Systems using a high-speed rotor coupled to a centrifugal pump could provide increased water production over a wide range of wind speeds and at a reduced cost [BRUSH (1987)].

The North West Coast of Egypt extends about 550 km from Alexandria to Al-Salloum and about 10-20 km south of the Mediterranean Sea shore, as indicated by EID (1995). Ground water is adequate and accessible along most parts of the N.W. Coast at a depth ranging from 5 to 50 m [BALBA (1981) and EL-MALLAH (1991)]. A report by the UNDP/FAO (1970) indicated that an area of 148,766 ha in this region is suitable for almost all crops and an area of 110,000 ha is suitable for fruit trees. The main problem encountered by the farmers who use traditional wind pumps on their farms on the North West Coast of Egypt is low capacity, which is attributed to short daily operating hours and a low discharge rate of the wind pump. The main type of wind pump that has been used is the so-called American farm wind pump. About 1000 wind pumps were manufactured by Military Factories at Helwan and were distributed on Bedouins in this region in the 1960’s. Several hundreds of these units are still in use today. They are preferred over diesel engine driven pumps which have very high water discharge rates, exhaust the well quickly and cause higher operating costs [FARAHAT (1999)].

# 2 OBJECTIVES AND TASKS

Traditional wind power (wind pump) has been used to power mechanical pumps; however, wind turbines that produce electricity and operate independently of the electric utility have numerous pumping applications. These independent systems allow the load to be located where power distribution from the utility may not be practical or economical. The wind energy systems which use a high-speed rotor coupled to a centrifugal pump could also provide increased water production over a wide range of wind speeds and at a reduced cost.

IRPS (2002a) has reported a new design of a wind energy plant for agricultural use according the following topics: the use of wind power at different locations shall be possible, which means mobile construction also suitable for road transport. Limited height of the wing tip through optimal rotor swept area; the wing tip of a prototype was 10 m. Simple design of yaw drive and safety technology. Use of different energy facilities like permanent-magnet synchronous generators, water pumps, and air compressors. Combination with other energy sources should be possible.

**MoWEC** is the prototype of a **mobile wind energy converter** with two rotors, which can be used to capture wind energy at different locations. The rotational energy, which is produced by the two three bladed rotors, leads on to two positions to a shaft for power take off (PTO) use. A three point fastening, similar to the three point hydraulic hitch on modern tractors, is used to connect the desired energy transformer to the PTO, like e.g. a mechanical water pump, a permanent magnet generator for stand alone use or with grid connection, an air-compressor for energy storage or other suitable equipment. There are lots of different designs in terms of heights, width and rated power possibilities. The wing heights in the present MoWEC prototype amount to 10 meters. The total rotor swept area is 80 m² because each of the two rotors has a diameter of 7.10 meters. The theoretical rated power is 20 kW at a wind speed of 11 m/s [IRPS (2002b)]. This first MoWEC-prototype has been used for test and advancement in the German Federal Agricultural Research Center (FAL) in Braunschweig since the beginning of the year 2002.

Up to now, the unsolved problem of this prototype in stand alone use is the lack of a simple automatic drive control system to winding the main rotors at low wind speeds and for automatic protection from damage caused by strong gusts of wind. Therefore, one of the aims of this study is to solve this problem with the aid of a specialized lee- wind wheel, which shall be used for yaw control at low and high wind velocities.

The power curve for a wind energy converter system (WECS) indicates the power output from WECS as a function of wind velocity at hub height. The power curve of a WECS is an

important parameter in wind plant energy yield prediction. More often the power curve measurements are included in the proposed warranty assessment procedures as part of wind plant commissioning. The power characteristics therefore need to be determined in a proper way. For this reason, the MoWEC-prototype will be operating to test the MoWEC elements and to measure the power curve in the field in order to define MoWEC performance, in particular the power coefficient value.

Combining a wind-electric system with an irrigation system for fruit and nut tree watering may open up vast regions of land heretofore untapped due to no utility supplied electricity. In general micro-irrigation is the broad classification of frequent, low volume, low-pressure application of water on or beneath the soil surface by drippers, drip emitters, spaghetti tubes, subsurface or surface drip tubes, low-head bubblers, and spray or mini-sprinkler systems. It is also referred to as drip or trickle irrigation. Existing closed-conduit irrigation systems are capable of saving water by increasing application uniformity. Therefore, one of the objectives of the present work is also the development of a water and energy saving irrigation system by selecting and studying one of the irrigation techniques for small orchard farms and studying the possibilities of the application of a MoWEC water pumping system based on this irrigation technique on the N.W. coast of Egypt.

## Tasks :

1. **Further development of the mobile wind energy converter (MoWEC) with the goal of allowing a yaw drive control system to be realized without external energy storage in particular for stand-alone use.**
2. **Measurement of the MoWEC power curve in stand alone use (prototype).**
3. **Selection, simulation and laboratory test of a water- and energy saving irrigation technique for small orchard farms which are suitable for wind energy use.**
4. **Layout of an orchard farm in Egypt with this irrigation system and water provision by MoWEC.**

## *Aufgaben:*

1. ***Weiterentwicklung der mobilen Windkraftanlage (MoWEC) mit dem Ziel, für den Inselbetrieb eine Windnachführung ohne externen Energiespeicher zu ermöglichen.***
2. ***Messung der MoWEC-Leistungskurve im Inselbetrieb (Prototyp).***
3. ***Auswahl, Simulation und Labortest einer für die Windenergie geeigneten wasser- und energiesparenden Bewässerungstechnik für kleine Obstbaumplantagen.***
4. ***Layout dieses Bewässerungssystems für eine Obstbaumplantage in Ägypten mit der Wasserversorgung durch MoWEC.***

# 3 LEVEL OF KNOWLEDGE

Wind energy is one of the most important sources of renewable energy. In areas with adequate mid-level wind speeds, the use of environmentally neutral wind power can reduce the use of fossil energy fuels. Wind energy can and will constitute a significant energy resource. However, it must be converted into a usable form. Wind power is used throughout the world to pump water for domestic, irrigation and livestock use. The intermittent nature of the wind is not as big a problem for pumping water as in the case of electric power generation since water can be stored on windy days and used later on days when the wind is calm. When one generates electrical power from the wind for applications other than pumping water, significant power can be lost storing it in batteries for later use. Combining a wind-electric system with an irrigation system for watering fruit trees may open up vast regions of land heretofore untapped due to no utility supplied electricity. In general micro-irrigation is the broad classification of frequent, low volume irrigation, and its low operating pressure makes it particularly well suited for combination with alternative energy such as wind energy water pumping systems.

## 3.1 Wind Energy

### 3.1.1 Causes of the wind

The sun's energy falling on the earth produces the large-scale motion of the earth atmosphere. Due to the heating of the air at the equatorial regions, the air becomes lighter and starts to rise. The rising air at the equator moves northward and southward. This movement ceases at about 30° N and 30° S, where the air begins to sink and a return flow of colder air takes place in the lowest layers of the atmosphere. The Coriolis acceleration due to the rotation of the earth causes the flow from the equator to the poles to be deflected towards the east, and the return flow towards the equator will be deflected towards the west producing the so-called trade winds. North of 30° and south of 30° south the atmospheric motion is characterized by westerly winds. The general large-scale motion of the atmosphere is illustrated in Figure 3.1 [JOHANSSON (1993), WMO (1981), MORTENSEN (1993) and DOBESCH (1999)].

In addition to the main global wind systems there are also local wind patterns, like sea breezes and mountain-valley winds. **Sea breezes** according Figure 3.2 a and b are generated in coastal areas as a result of the different heat capacities of sea and land, which give rise to different rates of heating and cooling. The land has a lower heat capacity than the sea and heats up quickly during the day, but at night it cools more quickly than the sea. During the day, the sea is therefore cooler than the land and this causes the cooler air to flow shoreward to replace the rising warm air on the land. During the night the direction of airflow is reversed.

**Mountain-valley winds** are created when cool mountain air warms up in the morning and, as it becomes lighter, begins to rise cool air from the valley below then moves up the slope to replace it. During the night the flow reverses, with cool mountain air sinking into the valley according Figure 3.2 c and d.

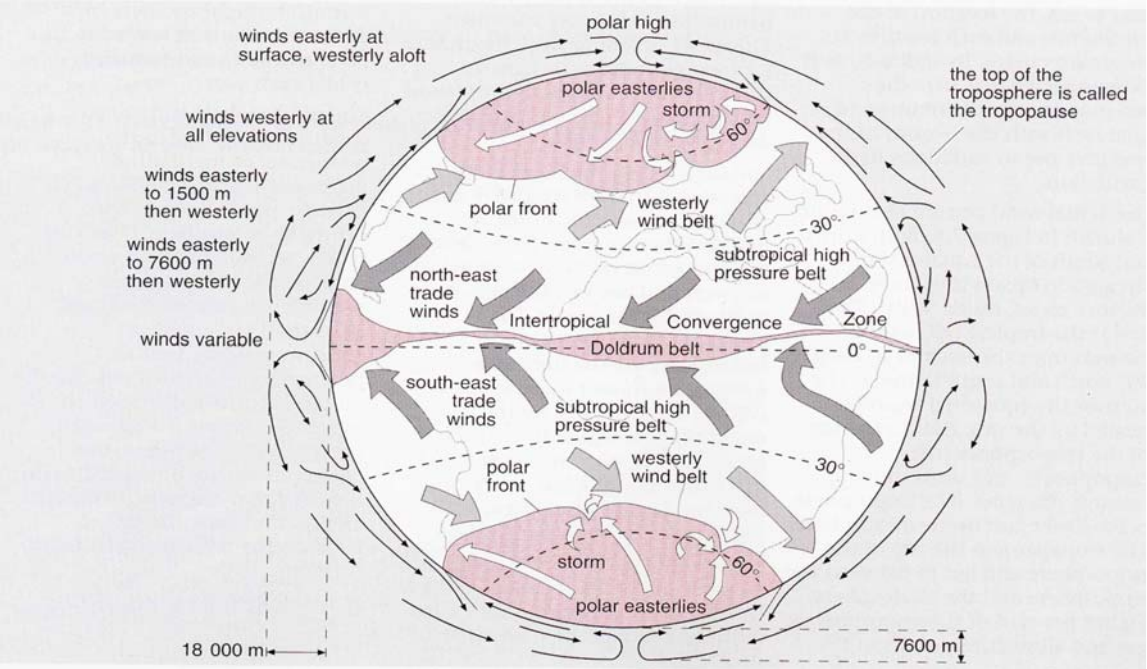


Figure 3.1: General circulation of winds over the surface of the earth. [GODFREY (1996)]
*Allgemeine Zirkulation der Winde über der Oberfläche der Erde.*

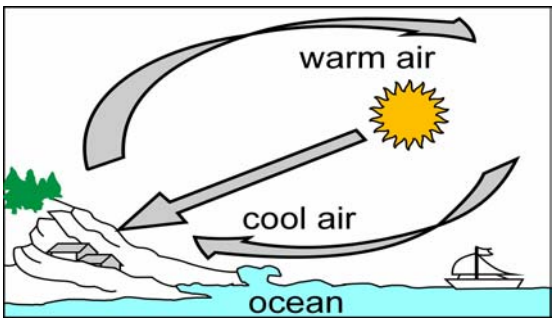


a) Sea breezes, during the day.

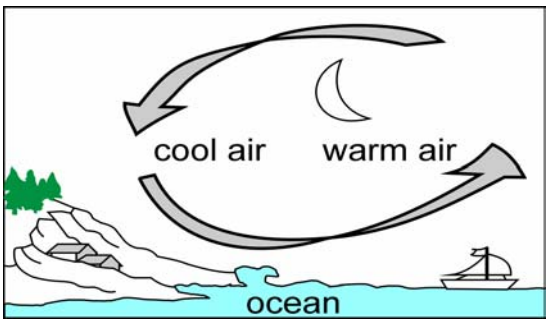


b) Sea breezes, during the night.

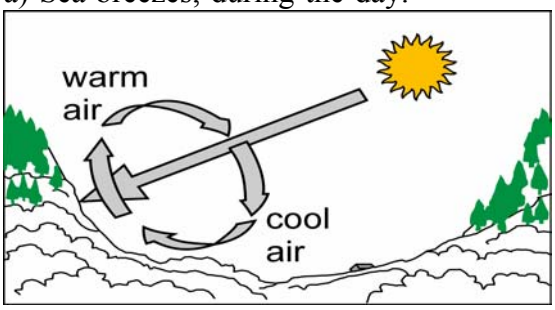


c) Mountain-valley winds, during the day.

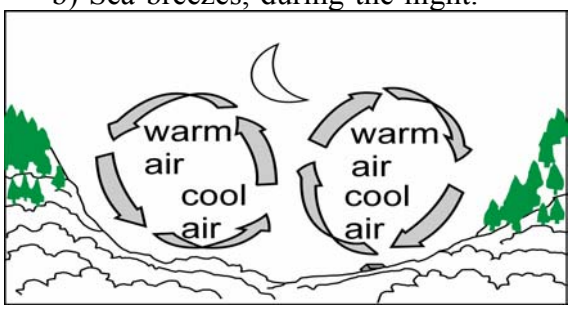


d) Mountain-valley winds, during the night.

Figure 3.2: How winds are created. [after GODFREY (1996)]
*Wie Winde entstehen.*

Figure 3.3 shows the annual available wind energy in different parts of the world in kWh/year per rated kilowatt output for wind machines designed for a rated wind speed of 11 m/s.

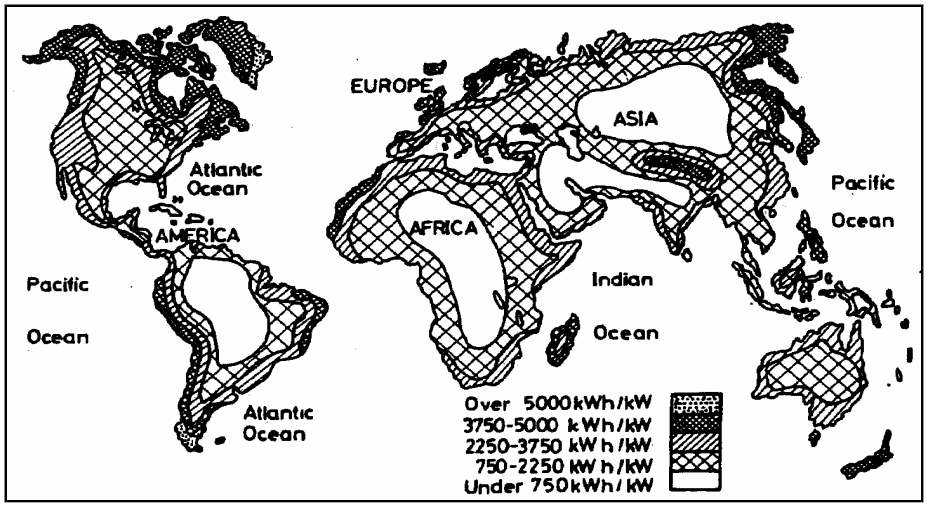


Figure 3.3: Annual availability of wind energy in the world in kWh/year. [JENS (1978)]
*Jährliche zu nutzende Windenergie in der Welt in kWh/ Jahr.*

### 3.1.2 Technical aspects of wind energy utilization

Utilizing wind energy entails installing a device that converts part of the kinetic energy in the atmosphere to, say, mechanically useful energy. This kind of conversion of wind energy into the motion of a body has been in use for a long time. Almost any physical construction that produces an asymmetric force in a wind flow can be made to rotate, translate or oscillate there by generating power. How this works is shown in the next sections.

#### 3.1.2.1 The power of a moving air mass

By referring to the power density of the airflow and a surface, which stands perpendicularly to the direction of flow, one can compute the kinetic energy dE given a mass element dm of the air and the speed v:

$$dE = \frac{1}{2} \cdot dm \cdot v^2 \qquad [J] \qquad (3.1.1)$$

It is: $dm = \rho_{air} \cdot dV$ [kg] (3.1.2)

Where: $\rho_{air}$ = air density in kg/m³, dV = volume element in m³ and v = speed in m/s.

With $dV = A_r \cdot dx$ [m³] and $dx = v \cdot dt$ [m]

$A_r$ is the rotor circle area in m², and dx is the distance element in m, see Figure 3.4.
One can write Equation (3.1.2) as follows:

$$dm = \rho_{air} \cdot A_r \cdot v \cdot dt \qquad [kg]$$

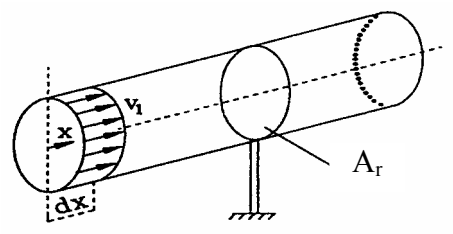


Figure 3.4: Mass flow through a surface area $A_r$. [GASCH (1996)]
*Massendurchsatz einer durchströmten Fläche $A_r$.*

With Equation (3.1.1) the kinetic energy dE follows to

$$dE = \frac{1}{2} \cdot \rho_{air} \cdot A_r \cdot v_1^3 \cdot dt \qquad [J = W.s] \tag{3.1.3}$$

The power $P_{v1}$ in undisturbed moving air is the kinetic energy per time unit. Therefore:

$$P_{v1} = \frac{dE}{dt} = \frac{1}{2} \cdot \rho_{air} \cdot A_r \cdot v_1^3 \qquad [W] \tag{3.1.4}$$

The wind power varies linearly with air density. The air density varies with pressure and temperature in accordance with the gas law [PFEIFER (1972)]:

$$\rho_{air} = \frac{P_{air}}{R_{air} \cdot T_{air}} \qquad [kg/m^3] \tag{3.1.5}$$

where $P_{air}$ is air pressure in [N/m²], $T_{air}$ is air temperature in Kelvin [K] and $R_{air}$ is the gas constant for the air [287 W s/kg K]. At sea level, with one atmospheric pressure [101,300 $N/m^2$] and a temperature of 288.12 K = 15.12 °C, dry air density is 1.225 kg/m³. Hence, dry air density is 1.127 kg/m³ at an air temperature of 40°C.

Figure 3.5 illustrates the theoretical wind power curve for the rotor swept area $A_r$ = 80 m² and air density $\rho_{air}$ = 1.225 kg/m³. The technically realized use of the wind energy takes place only in a limited range. The kind of surfaces which extract the energy from the wind determines the beginning and the end of the output power of the wind. Table 3.1 shows wind speed classification according to the Beaufort scale.

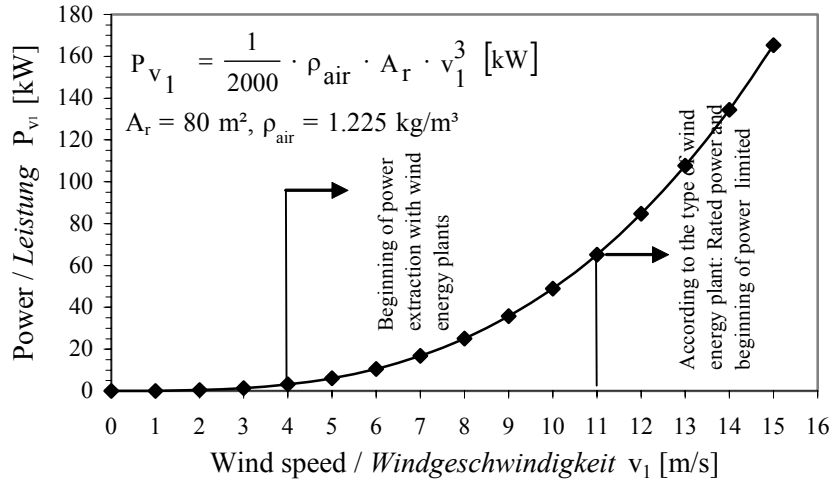


Figure 3.5: Theoretical wind power curve of an undisturbed air flow through a surface of 80 m². [after GASCH (1996)]
*Theoretische Windleistungskurve in der ungestörten Luftströmung durch eine Fläche von 80 m².*

Table 3.1: Beaufort wind scale. [GOURIERES (1982)]
*Beaufort Windskala.*

| Beaufort number | Wind speed | | | Descriptive terms |
|---|---|---|---|---|
| | knots | [m/s] | [km/h] | |
| 0 | 1 | 0.0 - 0.4 | <1 | Clam |
| 1 | 1 - 3 | 0.5 - 1.5 | 1 - 6 | Light air |
| 2 | 4 - 5 | 2.0 - 3.0 | 7 - 11 | Light breeze |
| 3 | 7 - 10 | 3.5 - 5.0 | 12 - 19 | Gentle breeze |
| 4 | 11 - 16 | 5.5 - 8.0 | 20 - 28 | Moderate breeze |
| 5 | 17 - 21 | 8.1 - 10.9 | 29 - 38 | Fresh breeze |
| 6 | 22 - 27 | 11.4 - 13.9 | 39 - 49 | Strong breeze |
| 7 | 28 - 33 | 14.1 - 16.9 | 50 - 61 | Near gale |
| 8 | 34 - 40 | 17.4 - 20.4 | 62 - 74 | Gale |
| 9 | 41 - 47 | 20.5 - 23.9 | 75 - 88 | Strong gale |
| 10 | 48 - 55 | 24.4 - 28.0 | 89 -102 | Storm |
| 11 | 56 - 63 | 28.4 - 32.5 | 103 -117 | Violent storm |
| 12 | 64 - 71 | 32.6 - 35.9 | 118 -133 | Hurricane |

### 3.1.2.2 Power extraction from the wind by wind power converter

The first complete mathematical study about the power extraction of wind energy was carried out by BETZ (1926) in Göttingen, Germany. Betz assumed that the wind rotor is ideal; that is to say, it has no hub passage of air through it. Thus it is a pure energy converter. Moreover, the conditions over the whole area swept by the rotor are supposed to be uniform and the speed of the air through and beyond the rotor is assumed to be axial. Thus let us consider an “ideal” wind rotor at rest, placed in a moving atmosphere (Figure 3.6).

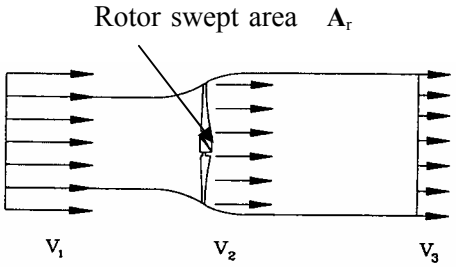


Figure 3.6: Flow through an idealised wind turbine. [GASCH (1996)]

*Aufweitung der Stromlinien infolge Abbremsung der Strömung durch den Rotor einer Windturbine.*

The actual power, which is extracted by the rotor blades, is the difference between the upstream and the downstream wind powers. That is, using Equation (3.1.4). The air velocity is discontinuous from $v_1$ to $v_3$ at the plane of rotor blades in the macroscopic sense. Then the actual power extracted by the blades is customarily expressed as a fraction of the upstream wind power as follows.

$$P_N = C_p \cdot \frac{1}{2} \cdot \rho_{air} \cdot A_r \cdot v_1^3 \qquad [W] \qquad (3.1.6)$$

where $P_N$ is actual mechanical power extracted by the rotor, i.e., the turbine output power and $A_r$ is the area swept by the rotor blades in m².

$C_p$ is the fraction of the upstream wind power, which is captured by the rotor blades. The remaining power is discharged or wasted in the downstream wind. The factor $C_p$ is called the power coefficient of the rotor. For a given upstream wind speed, the value of $C_p$ depends on the ratio of the downstream to the upstream wind speed. $C_p$ has the maximum value of 0.59 when $v_3 / v_1$ is one-third. In practical design, the maximum achievable $C_p$ is below 0.5 for high-speed, two or three-bladed turbines, and between 0.2 and 0.4 for slow speed turbines with more blades [PATEL (1999) and HEIER (2000)].

### 3.1.2.2.1 Power extracted with drag force rotors

The main element of the wind machine, whatever the type may be (horizontal or vertical-axis machine) is the blade. This may be considered as a rotating wing. The utilization of the aerodynamic drag represents the oldest form of extracting power from the wind. Each surface $A_r$, standing vertically in the flow, experiences a force which is equal to the drag of the surface opposite to that flow and which acts in the flow direction. This force is proportional to $A_r$, to the air density and to the square of the wind speed:

$$F_w = C_d \cdot \frac{1}{2} \cdot \rho_{air} \cdot A_r \cdot v_1^2 \qquad [N] \qquad (3.1.7)$$

The factor $C_d$ is called the **drag-coefficient** and quantifies the effects of the form of the resistance surface. Figure 3.7 shows the drag-coefficients of different bodies:

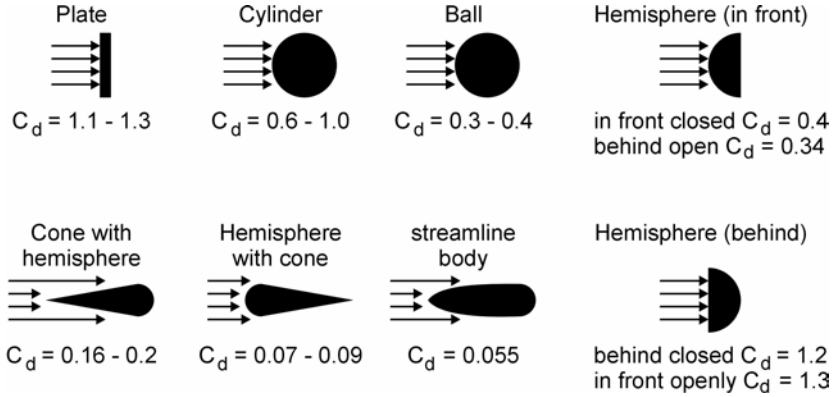


Figure 3.7: The drag-coefficients of different bodies. [after QUASCHNING (1999)]

*Widerstandsbeiwerte unterschiedlicher Körper.*

For a rotating system of resistance surfaces which are affected by the flow on one side only, an upwind speed results with:

$$v_r = v_1 - u = v_1 - \omega r \quad [m/s]$$

where u is the circumferential speed (m/s) of the outer parts of the resistance surface rotating with the angular velocity ω and an average radius r. For the drag force $F_d$ it can therefore be written as:

$$F_d = C_d \cdot \frac{1}{2} \cdot \rho_{air} \cdot A_r \cdot \left(v_1 - u\right)^2 \quad [N] \qquad (3.1.8)$$

The averaged actual power extracted by the rotor blades is:

$$P_N = C_d \cdot \frac{1}{2} \cdot \rho_{air} \cdot A_r \cdot \left(v_1 - u\right)^2 . u \quad [W] \qquad (3.1.9)$$

and $$C_p = C_d \cdot \left(1 - \frac{u}{v_1}\right)^2 . \frac{u}{v_1} \qquad (3.1.10)$$

The ratio between the rotor circumferential speed u and the wind speed $v_1$ is generally dimensionless and **called tip-speed-ratio λ:**

$$\lambda = \frac{u}{v_1} \qquad (3.1.11)$$

It is obvious that in rotors based on the aerodynamic drag principle this tip-speed-ratio must lie between zero and one. The optimal power-coefficient is given with $\lambda = \frac{1}{3}$, hence,

$$C_{p,max,d} = \frac{4}{27} C_d \qquad (3.1.12)$$

Assuming a maximum $C_d$ = 1.33 (open hemisphere in flow direction according (Figure 3.6), the maximum possible power coefficient amounts to $C_{p,\,max,\,d}$ = 0.197. But when considering real machines, the surfaces of the covered half side experience a drag force proportional to the rotational speed, the power-coefficient is reduced further, and it becomes clearly evident why this principle plays no current role in the exploitation of wind energy.

### 3.1.2.2.2 Power extracted with lift force rotors

If we suppose the wing to be at rest and air to be moving at the same speed (see Figure 3.8), but in the opposite direction, the aerodynamic force exerted on the wing does not change in value. The effort exerted only depends on upstream air speed $v_1$ and the angle of attack α. The pressure of the air on the external surface of the wing is not uniform: on the upper surface, there is a reduction and on the lower surface, an increase in pressure. The resultant of the different elementary forces acting on the wing is a force F, which is given by the expression:

$$F = C_r \cdot \frac{1}{2} \cdot \rho_{air} \cdot A_r \cdot v_1^2 \quad [N] \qquad (3.1.13)$$

where $C_r$ is the total aerodynamic coefficient

This force can be divided into two components. A component parallel to vector $\overline{v_1}$ : the drag $\overrightarrow{F_d}$ and a component perpendicular to vector $\overrightarrow{v_1}$ : the lift $\overrightarrow{F_L}$ . Each wing element has a depth $d_e$ and width b in m, so the $F_d$ and $F_L$ are given by the expressions:

$$F_d = C_d \cdot \frac{1}{2} \cdot \rho_{air} \cdot (d_e \cdot b) \cdot v_1^2 \qquad [N] \qquad (3.1.14)$$

$$F_L = C_L \cdot \frac{1}{2} \cdot \rho_{air} \cdot (d_e \cdot b) \cdot v_1^2 \qquad [N] \qquad (3.1.15)$$

where $C_d$ is the **drag-coefficient** and $C_L$ is the **lift coefficients.**

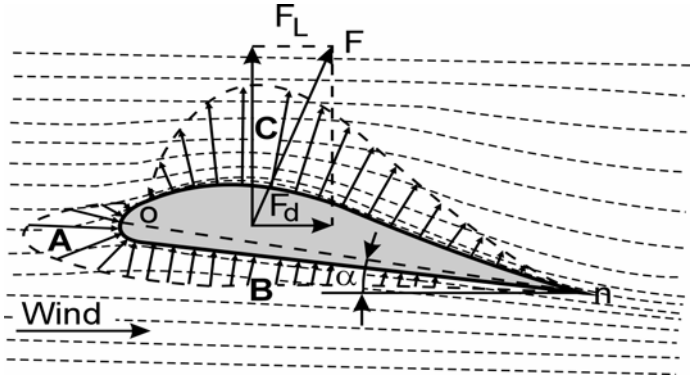


where:

**no** = profile chord
**$F_L$** = lift force
**$F_d$** = drag force
**A** = zone of higher positive pressure
**B** = zone of lower positive pressure
**C** = zone of higher negative pressure
**α** = angle of attack

Figure 3.8: Pressure distribution around a blade element, resulting lift and drag forces.
*Druckverteilung auf einem Flügelelement, resultierende Auftriebs- und Widerstandskraft.* [after HEYWANG (1999)]

The components of $C_d$ and $C_L$ are perpendicular. These coefficients also depend on the angle of attack α. Figure 3.9 illustrates the variation of $C_d$ and $C_L$ versus the angle of attack α for a known profile. Considering first the variation of the lift coefficient $C_L$, the representative curve is seen to consist of a straight-line curving over at the higher value of $C_{L\,max}$, at an angle of attack $\alpha_m$ known as the stalling point. The representative line is also curved for a negative angle of attack. Also the variation curve of drag coefficient $C_d$ is minimum for a certain value of the attack angle. The important results can be derived from the lift coefficient curve. In MoWEC (see section 3.1.7), any small changes in the angle of attack α will exert a significant influence on the energy extracted from the wind. The fast increase of $C_d$ with larger α values will also impair the stability of MoWEC. The sudden change in the coefficients is due to the flow separation from the suction side of the aerofoil; this is called the stall-effect.

In practice the profile of the rotor blades must turn. Thus, the lift and drag forces on the blades are transformed into a rotational torque and axial thrust force. The torque produces useful work whereas the thrust will try to overturn the turbine and must be resisted by the tower and foundations. The relative wind speed $v_{relative}$ is found from the triangle of velocities as a result of the rotational speed of the blade element $v_{rotational}$ and the wind speed $v_1$. The angle of attack α is optimal when $v_2 = \frac{2}{3} v_1$. The wind speeds and forces on the blade element during the rotation can be shown as in Figure 3.10.

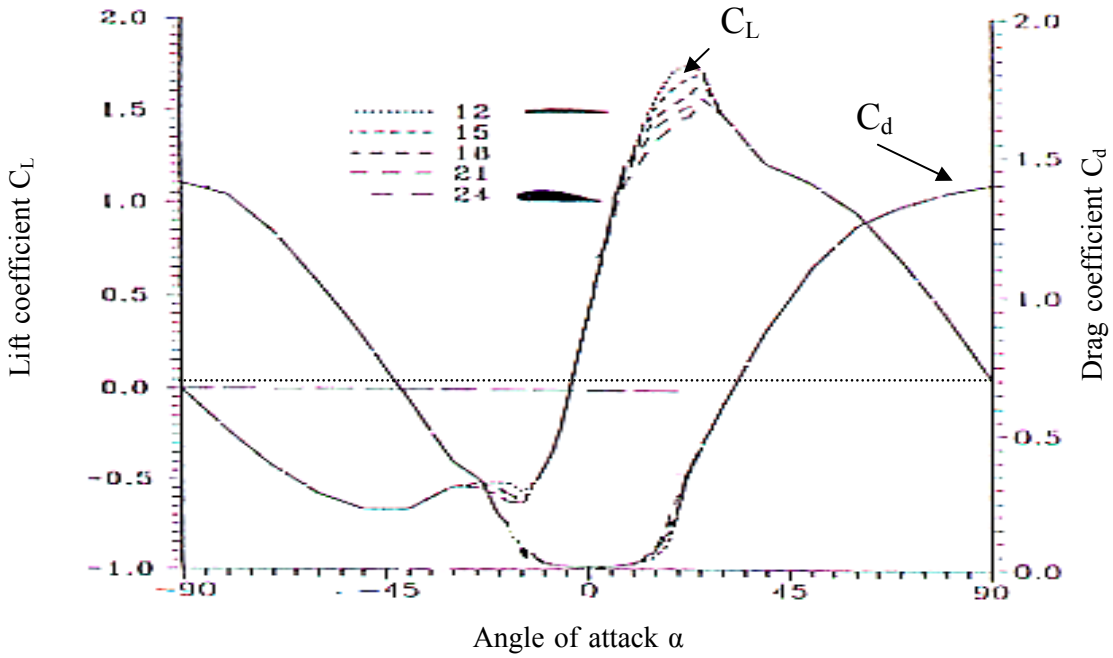


Figure 3.9: Corrected drag and lift coefficients as function of the angle of attack with the profiles NACA 4412 to 4424. Measurements in air channel. [GASCH (1996)]

*Korrigierte Auftriebs- und Widerstandskoeffizienten als Funktion der Anstellwinkel mit den Profilen NACA 4412 bis 4424. Messungen im Windkanal.*

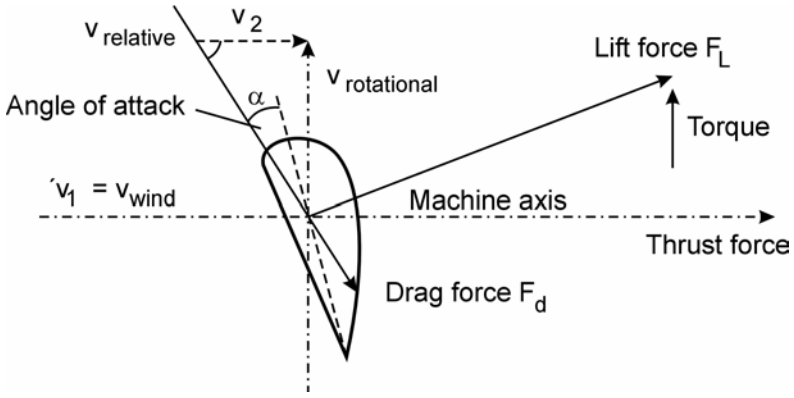


Figure 3.10: Simple representation of the forces on a blade element. [JOHN (1997)]

*Vereinfachte Darstellung der Kräfte an einem Rotorblattelement.*

The fast and slow wind horizontal-axis rotors in **fast wind rotors** have one, two or generally three or four blades today. At equal power, these types have a small starting torque; but large numbers of revolutions ($\lambda > 4$, it can reach 10) and use the lift forces optimally. For these types, a wind speed of at least 5 m/s is necessary to make them rotate. In our research with MoWEC, two three-bladed rotors are used. The power and torque coefficients are given by Equations (3.1.16) and (3.1.17) for slow and fast wind rotors types. Figure 3.11 illustrates the torque and power coefficients of fast wind turbines as a function of $\lambda$ for a two-bladed wind rotor [GOURIERES (1982)].

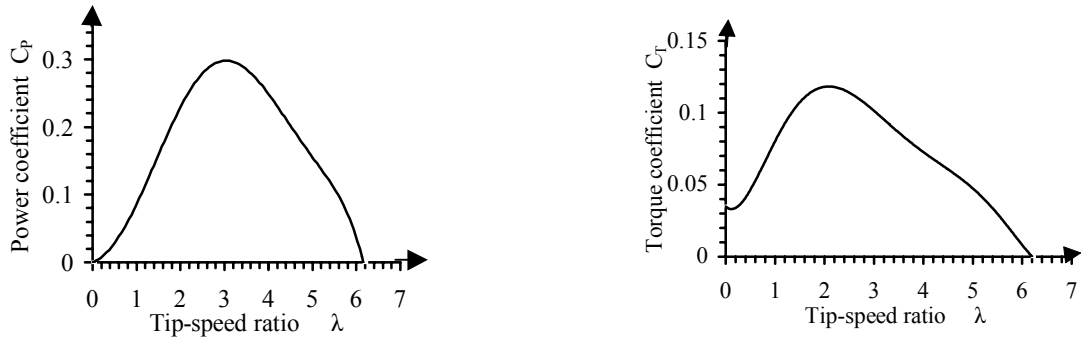


Figure 3.11: Torque and power coefficients of a fast wind turbine as a function of $\lambda$.

*Drehmoment- und Leistungskoeffizienten eines Schnellläufers als Funktion von $\lambda$.*

Slow wind rotors have multi-bladed rotors, varying from 8 to 24. These types can start freely with winds ranging from 2 to 3 m/s. At equal power, these types have a high starting torque, small numbers of revolutions ($\lambda < 4$) and mainly use the drag forces but also the lift force. In our research, a slow wind rotor (lee-wind wheel) is used as energy source for the MoWEC yaw drive system. Figure 3.12 shows the torque and power coefficients of slow wind rotors as a function of $\lambda$.

$$C_p = \frac{2\,P_N}{\rho_{air} \cdot \pi \cdot R^2 \cdot v_1^3} \tag{3.1.16}$$

$$C_T = \frac{2\,T_w}{\rho_{air} \cdot \pi \cdot R^3 \cdot v_1^2} \tag{3.1.17}$$

where: $C_p$ = power coefficient; $C_T$ = torque coefficient; R = rotor radius in [m]; $P_N$ = actual mechanical power extracted by the rotor in [W]; $T_w$ = actual torque extracted by the rotor in [Nm]

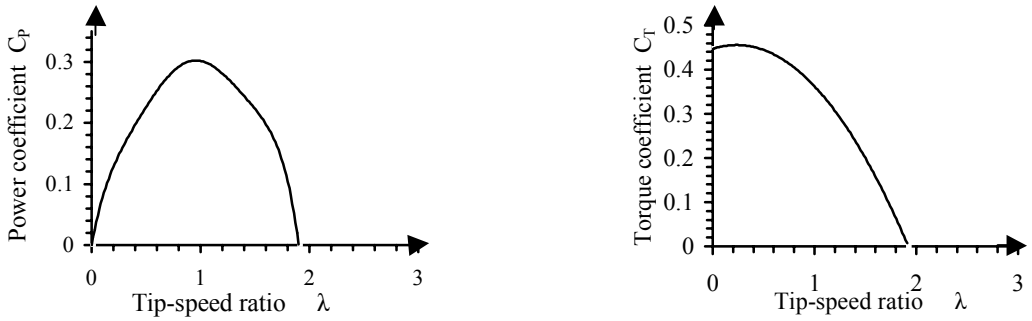


Figure 3.12: Torque and power coefficients of a slow wind rotor as a function of λ.

*Drehmoment- und Leistungskoeffizienten eines Langsamläufers als Funktion von λ.*

## 3.1.3 Conversion of rotational energy and wind power application

Since the mechanical energy of the rotor has only limited possibilities in direct applications (e.g. for grinding grain, water pumping) it is changed mostly into another energy form such as heat, electrical and potential energy. The conversion of rotational movement into electricity usually takes place with generators of various designs. The electrical energy is fed either into the existing electric grid or, independently of the grid, is directly used or accumulated in some kind of storage (island-solution = stand alone solution). Increasingly important, especially in the developing countries, is the conversion from wind energy into potential energy for pumping water. Several types of application can be distinguished: Drinking water supply, irrigation and drainage [CAHOON (1987) and CLARK (1988)].

Wind energy is one of the most flexible of all renewable energy sources. It can be used for different purposes, such as irrigation, electricity generation, crop drying, grain grinding and also many other purposes. The conquest of wind energy did not begin yesterday. In the third century B.C., in a study dealing with pneumatics, an Egyptian, Hero of Alexandria, designed a

four-bladed horizontal axis windmill, which provided compressed air to an organ. As early as 1000 B.C. simple windmills with vertical axis were found in Egypt, where they were used for irrigation [GOURIERES (1982)].

Current wind-powered pumping systems generally utilize bulky, slow-moving rotors and reciprocating pumps. These systems operate well in low-speed winds but reach peak water production in moderate winds around 7 to 8 m/s. Systems using a high-speed rotor coupled to a centrifugal pump could provide increased water production over a wide range of wind speeds and at reduced cost. Wind-powered reciprocating pumps have been adapted for domestic and irrigation water supply in developing countries [BRUSH (1987)].

As mentioned, the wind has been used for pumping water in many centuries. The main type of wind pump that has been used is the so-called American wind pump Figure 3.13. This system normally has steel, multi bladed, fan-like rotor, which drives a reciprocating pump linkage usually via reduction gearing that connects directly with a piston pump located in a borehole directly below. It should be noted that the so-called American Wind Pump is rarely used today for irrigation. Most pumps of this type are used for the purpose they were originally developed for, namely watering livestock and, to a lesser extent, for farm or community water supplies. They therefore tend to be applied at quite high heads by irrigation standards; typically in the 10 to 100 m range on boreholes. Large wind pumps are even in regular use on boreholes more than 200 m deep [PETER (1986)].

GOURIERES (1982) reported that the rotor diameter of this type ranges from 2 to 8 m and can start freely with winds ranging from 2 to 3 m/s. A power coefficient of 0.3 could be obtained at a tip-speed ratio of $\lambda = 1$. FARAHAT (1999) reported that Hassan et al (1994) carried out experiments on rotors with different numbers of blades and found that the multi bladed rotor was more efficient for low wind speeds. Figures 3.13 and 3.14 show the schematic diagram of the American wind pump components.

CLARK (1992) compared the performance of the American multi-bladed wind pump to that of a three blade electric generating wind turbine used for water lifting. They found that the discharge rate of the American wind pump was twice as large at low wind speed ranging from 3 to 4.5 m/s, but at high wind speeds greater than 5 m/s the wind electric system pumped more than twice as much water as the American wind pump.

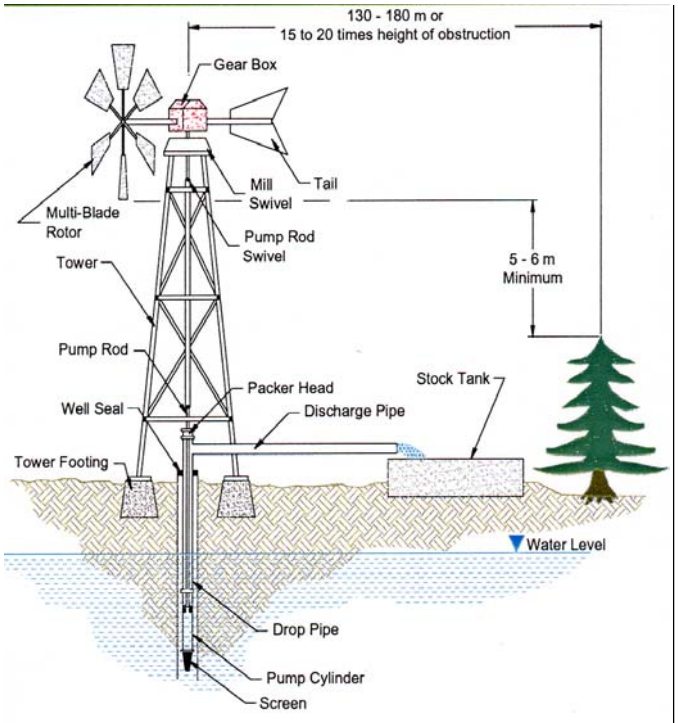


Figure 3.13: Typical American wind pump.

Typische amerikanische Windpumpe.

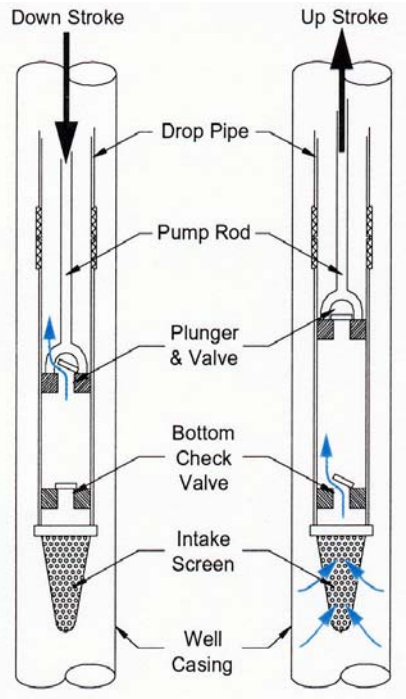


Figure 3.14: Typical wind pump cylinder

*Typischer Pumpenzylinder einer Windpumpe.*

### 3.1.4 Mobile wind energy converter (MoWEC)

MoWEC is a mobile wind energy converter with two three-blade rotors. This mobile can be used to capture wind energy at different locations. The first MoWEC-prototype has been designed and constructed by IRPS through the period from 1999 to 2001 at the German Federal Agricultural Research Center (FAL) in Braunschweig, Germany.

Up to now, the unsolved problem of this prototype has been the lack of an automatic drive control system to winding the main rotors at low wind speeds and provides automatic protection from damage caused by strong gusts of wind. For this reason, we began to solve this problem at the beginning of the year 2002 with the aid of a specialized lee wind wheel, which shall be used for yaw control at low and high wind velocities and the measurement of the MoWEC power curve in the field.

#### 3.1.4.1 Construction of the MoWEC- prototype

**Upwind and downwind construction**

MoWEC was designed with rotors at an upwind and downwind position from the towers. Operating the rotor upwind of the tower produces higher power as it eliminates the tower

shadow on the blades. This also results in less noise, lower blade fatigue, and smoother power output. The downwind blades, on the other hand, allow a free yaw system to be used. It also allows the blades to deflect away from the tower when loaded.

In contrast to the well known wind energy plants, this MoWEC system consists of the main construction elements: Downwind construction for simple and easy turning in the wind, upwind fastening of one or more wind rotors in front of the tower and a tower which can be folded up for transportation. For the latter the rotor blades must be screwed off the hub (or in the future quick action chucks). The use energy transformers are placed at the base of the tower. The rotational energy is transmitted by the prototype using a toothed gear and a chain. In this case, it is easier to change the transmission ratio in experiments. Figure 3.15 shows the construction details of MoWEC and an explanation of the Downwind and Upwind construction.

**Forces on the yaw drive system**

Wind energy plants with a horizontal axis need a yaw drive system that turns the rotor or the rotors (MoWEC prototype) into the wind according the actual wind direction. The rotor must also be yawed to reduce the power during high wind periods. Figure 3.16 explains in which direction the gyro forces work. The MoWEC prototype has two rotors where the rotations are in opposite direction. That is a contribution to the compensation for forces which could attack the frame and tower construction (see Figure 3.16).

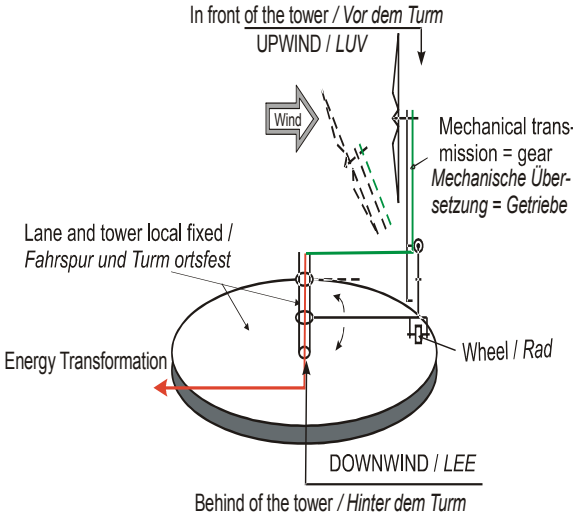


Figure 3.15: Construction details of MoWEC and explanation of the Downwind and Upwind construction.

*Konstruktionsdetails von MoWEC und Erklärung der LUV- und LEE-Konstruktion.*

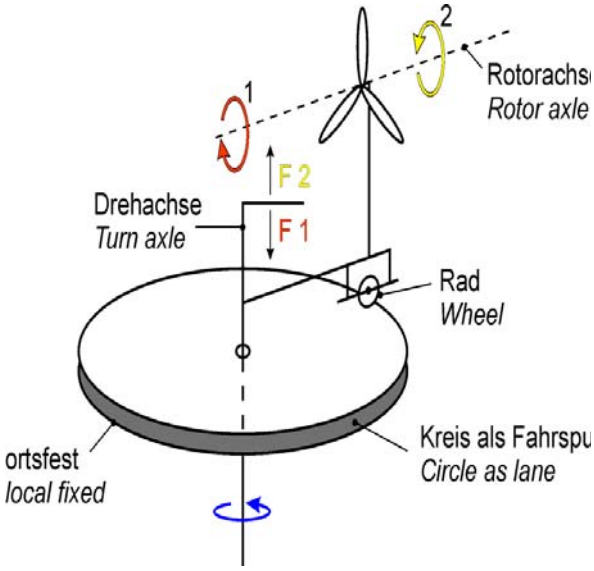


Figure 3.16: Yaw drive with forces F1 and F2 at the turn axis of MoWEC. [IRPS (2002b)]

*Windrichtungsnachführung mit den Kräften F1 und F2 an der Drehachse von MoWEC.*

**MoWEC construction drawing**

The MoWEC prototype has two rotors with horizontal axes and three bladed GFK (glass fiber reinforced plastic) rotor wings. The first place to use the rotational energy is the common shaft on top of the yaw drive frame. The second possible place for the use of rotational energy is the PTO shaft near the ground (Figure 3.17). Four jibs, to be folded for transportation, are used for the stability of the construction. The frame must have a horizontal position. Otherwise, the yaw drive and the rotor wings would hinder the correct operation of the mobile wind energy plant.

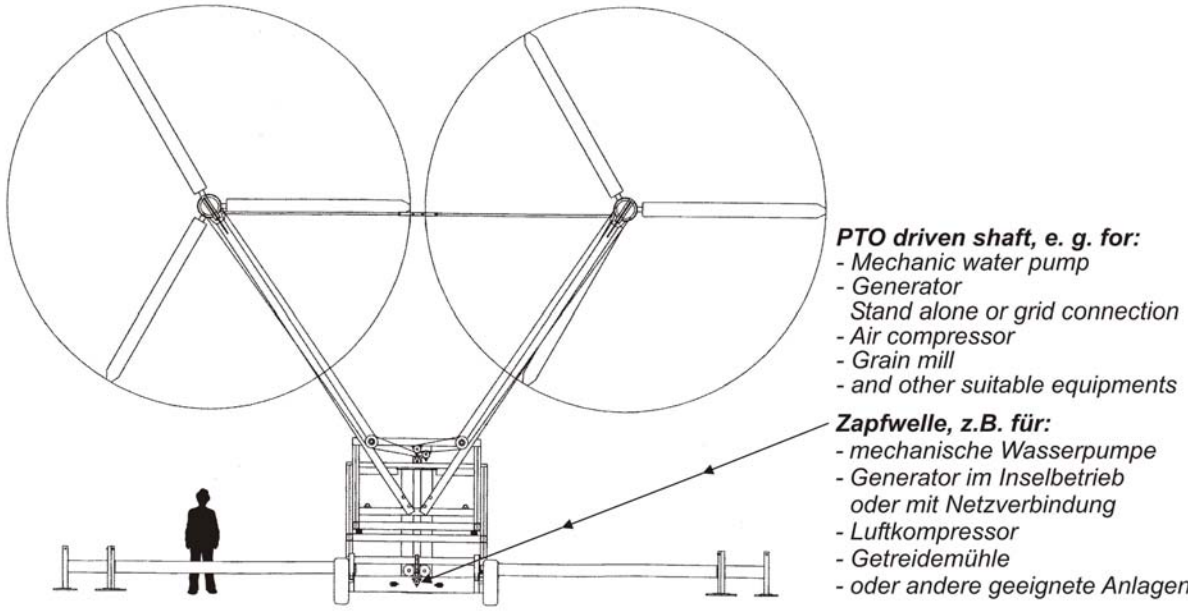


Figure 3.17: One of the construction drawings of the prototype MoWEC in the year 2001. [after IRPS (2002c)]

*Eine der Konstruktionszeichnungen des Prototyps MoWEC im Jahr 2001.*

**Barriers in the wind which influence the wind speed**

In contrast to wind energy plants featuring towers of about one hundred meters, which are well known today, the MoWEC concept shall also use the wind power at lower heights. Here, one should remember past experiences with the traditional windmills. Figure 3.18 shows basic knowledge about wind velocities near natural or man-made barriers. In the past, wind hills have guaranteed respectable wind velocities also at low heights. Given these considerations, the relation between the height and length of the wind hill is important.

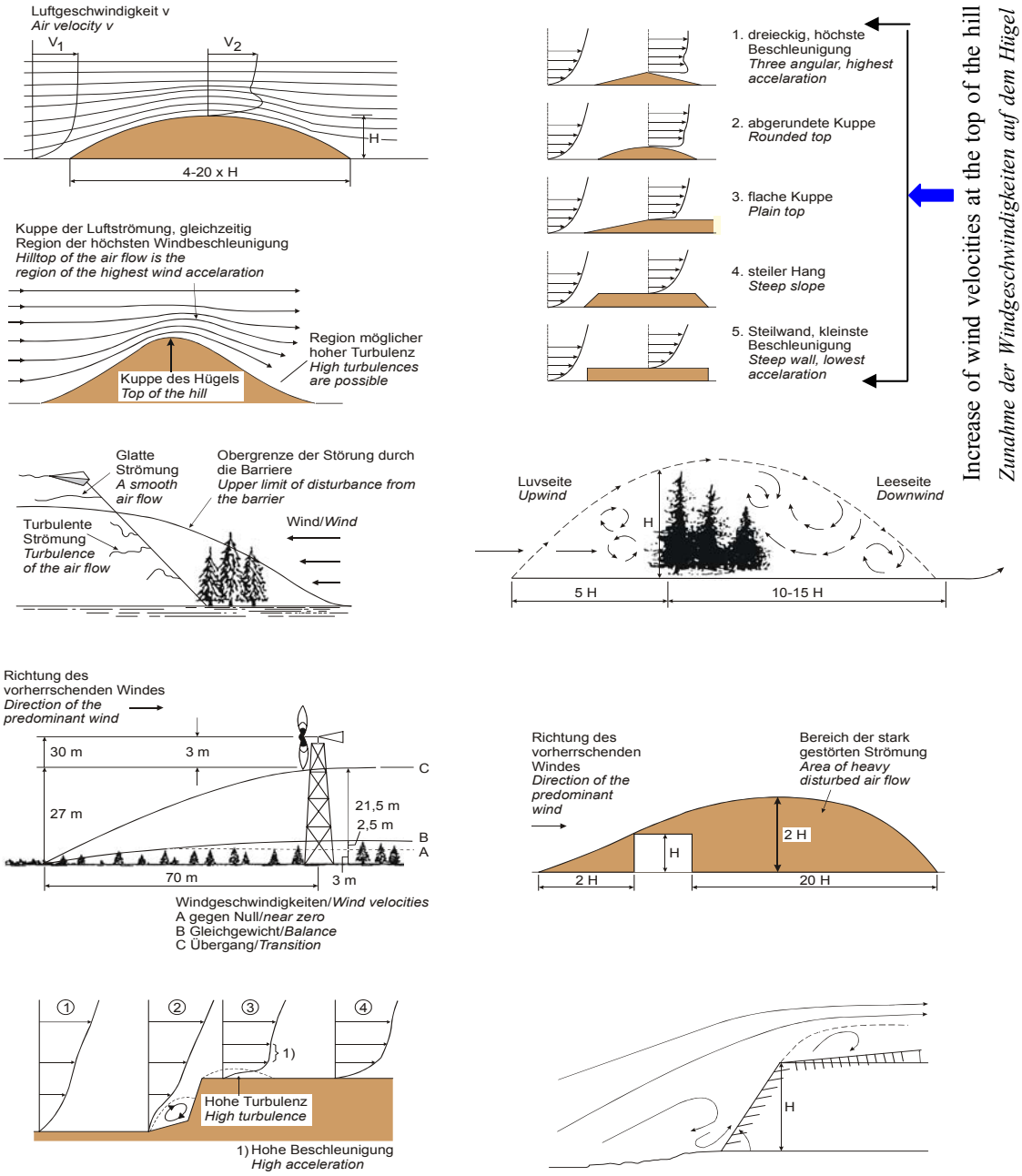


Figure 3.18: Barriers in the wind. [after GASCH (1996) and IRPS (2002a)]
*Barrieren im Wind.*

## 3.1.4.2 Energy track of the MoWEC prototype

### Rotors

Rotor blades have been manufactured from glass fiber reinforced plastic (GFK) with a metal core and a metal foot in a female form. During the production of the rotor blades, light glass fibers are placed into polyester resins or epoxy resins. Thus high-tension force is achieved.

A further benefit of this production process is that GFK enables sharp-edged products (e.g. rotor blades) to be manufactured. With the aid of computation methods, the profile of the rotor blades is calculated and illustrated in the female form. An alternative to glass fiber is carbon fiber (CFK). The MoWEC rotor blades are constructed from glass fiber reinforced plastic (GFK). It confers the highest stiffness and lowest weight, but unfortunately the material is expensive. There has been hope that carbon fiber will become cheaper as demand increases but currently the price is rising steadily and it will not be used frequently for blades until it becomes much cheaper.

For the construction of the MoWEC- prototype with two three-blade rotors, the rotor diameter was 7.1 m. From the technical data of the rotor the rated power for each rotor is expected to be 12.7 kW at a wind speed of 11 m/s. With two rotors, the rated power without an energy transmission system is 2 x 12.7 kW. The MoWEC prototype with two three-blade rotors features a different design than a conventional wind-powered plant with one rotor. The largest wing tip heights of the present MoWEC prototype was 10 m and the total rotor-swept area was 2 x 40 m² = 80 m². In order to increase the stability of the system, the rotors rotate in opposite directions. Thus two different female forms had to be manufactured for the production of the rotor blades.

Based on the MoWEC rotors data sheet, the rated rotational velocity of the rotors is expected to be 180 rpm. At three rotations per second divided by the wind speed of 11 m/s, this results in a calculated tip-speed ratio of $\lambda = 6.1$. A tip-speed ratio of $\lambda = 5.4$ would correspond to a rated rotor speed of 160 rpm. The rotor blades were prepared as fast runners according to the lift principle. Airflow regulation at the rotor blades also occurs according the stall effect.

**The hub and rotor brake system**

The metal feet of the rotor blade are firmly connected with the rotor hub by bolt connections. Each rotor hub is connected with a steel shaft (diameter 90 mm). At both rotor steel shafts a compressed air brake system was installed. Each air brake consists of a diaphragm cylinder; a pressure spring and a drum break system. By means of a manually controlled cylinder compressed air pump, the compressed air is pumped through compressed air hoses into the two diaphragm cylinders in order to clamp the compression spring. The strained compression spring will remove the brake disks from the brake drum. At sufficient wind velocity, the two MoWEC rotors will move. If the pressure hose is exhausted, then the brake assembly of both rotors comes into function. Figure 3.19 shows the arrangement of MoWEC's one-rotor tower components at the hub.

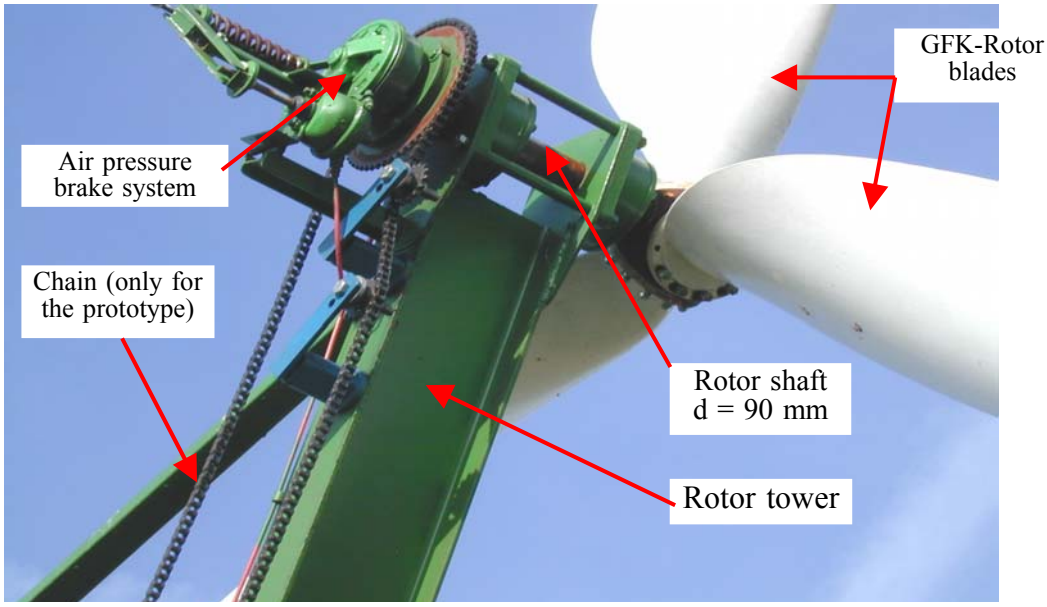


Figure 3.19: The MoWEC tower peak (prototype).
*Die Turmspitze von MoWEC (Prototyp).*

**MoWEC tower**

The MoWEC tower consists of two important parts: the stationary tower connected to a round iron foundation on the ground (inner diameter 2.60 m and outer diameter 2.80 m) in the middle. Second, two-rotor towers, one for each rotor, are connected to the wind-adjusting frame. This frame is mounted to a stationary tower and could be turned around it. This is necessary to turn the two rotors into the wind (see Figure 3.20). The towers were designed to withstand wind loads and gravity loads.

### 3.1.4.3 Transport of MoWEC

The prototype of this mobile wind-powered plant is developed for rural areas. When commercially available, it can be bought, rented or leased. The necessary installations are understandable and technically simple. For transportation purposes, the mobile wind energy converter MoWEC can be folded up. The towers and the transport wheels are moved with the help of a hydraulic system - alternatively also the use of a mechanical system is possible from the vertical position into the horizontal position and back. After the rotor blades have been dismantled and the towers have been folded, the permitted dimensions for road transport are met. Total width then amounts to 2.80 m, which means that the new machine can be transported on normal roads as an agricultural implement. Figure 3.21 shows the MoWEC-prototype while being transported by a tractor.

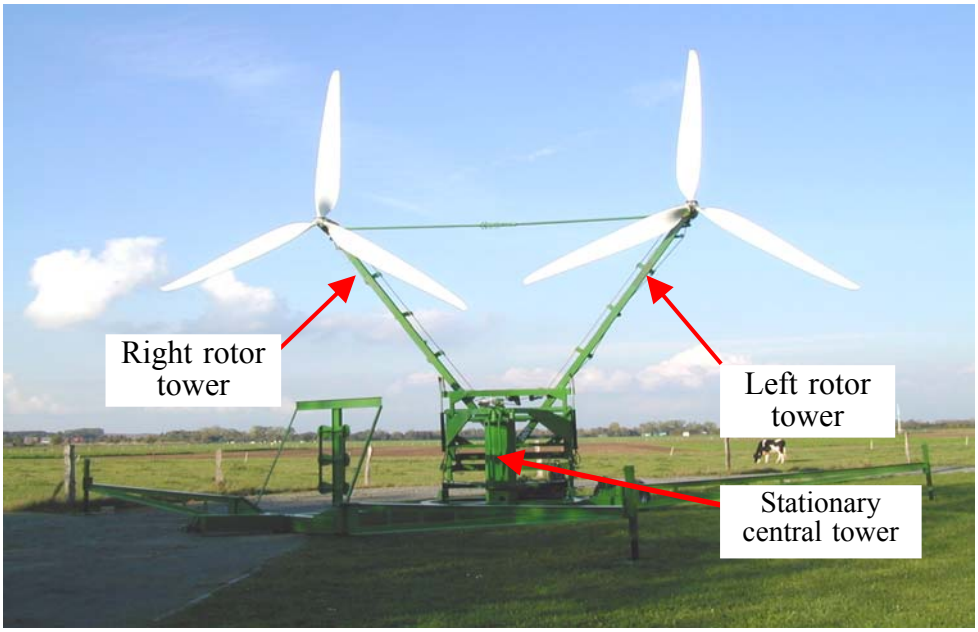


Figure 3.20: MoWEC in the field without the yaw drive control system.
*MoWEC im Feld ohne Windrichtungsnachführungssystem*

Figure 3.21: MoWEC during transportation.
*MoWEC während des Transportes.*

### 3.1.4.4 MoWEC energy transformation and use

MoWEC was designed as a prototype. The mechanical power generated by the rotor blades is transmitted to the bottom of the towers by a transmission system located at the back of the towers. In order to be able to realize different speeds economically in later tests, a chain drive system was used. Transmission ratio to a central shaft according Figure 3.17 was 1:3. Although the two rotors rotate in opposite directions, the central shaft adds the rotation energy (see Figure 3.22). At the central shaft, the preferred energy converter (e.g. electrical generator)

can be installed. The generator support is attached to the wind-adjusting frame. Generator and central shaft are connected to a horizontal cardan shaft. The stationary tower is used to run the electrical cable from the generator to the switchbox (see Figure 3.23).

The MoWEC concept also permits the stationary installation of the energy converter at ground level. In this position, for example without generating electricity a stationary mechanical water pump can also be driven directly. In addition, other energy converters can be installed at ground level according Figure 3.24. The rotational energy is conveyed through the central tower up to the stationary driving frame. For this purpose, two bevel gearboxes (speed ratio 1:1), two bearings of the shaft, two cardan shafts and a power-take-off (PTO) tap are used. The bevel gearbox at the tower head is connected with the upper MoWEC ball race of the wind-adjusting frame. Commercially, normal land technical gears and cardan shafts are used.

The rated speed at the central shaft and at the power-take-off shaft at the driving frame is calculated based on the rated speed of the rotors with 160 – 180 rpm multiplied by the speed ratio of 1:3. This results in a rated speed of 480 – 540 rpm. Thus the rated speed corresponds to the PTO speed of agricultural tractors.

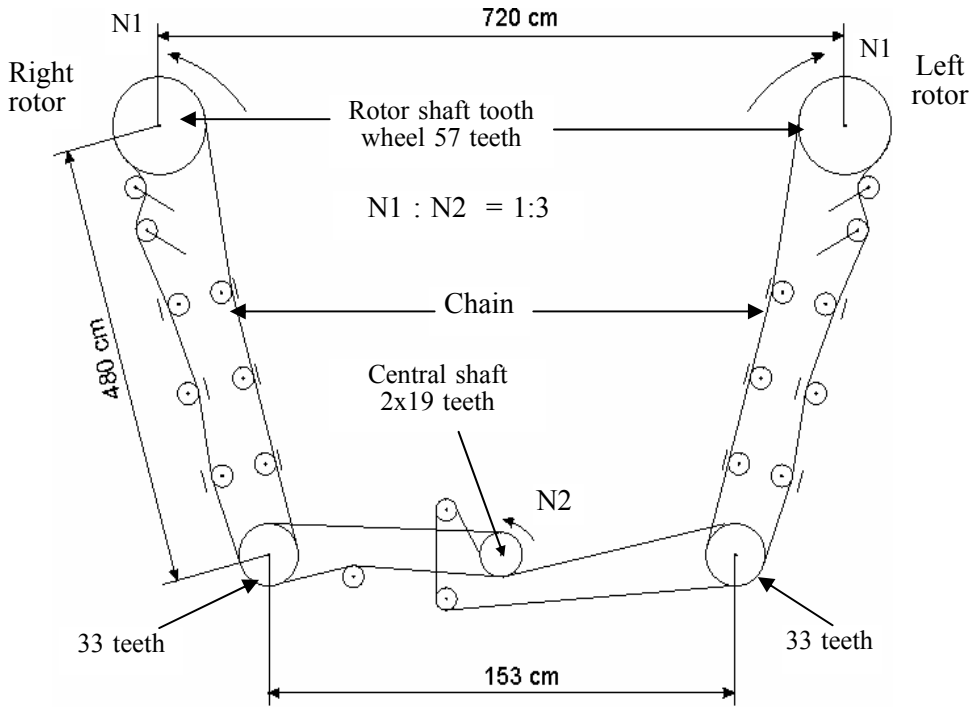


Figure 3.22: MoWEC energy transmission system from rotors to the first PTO-shaft. View to the backside of rotors, towers.

*MoWEC Energieübertragung von den Rotoren zur ersten PTO-Welle. Sicht auf die Rückseite der Rotoren, Türme.*

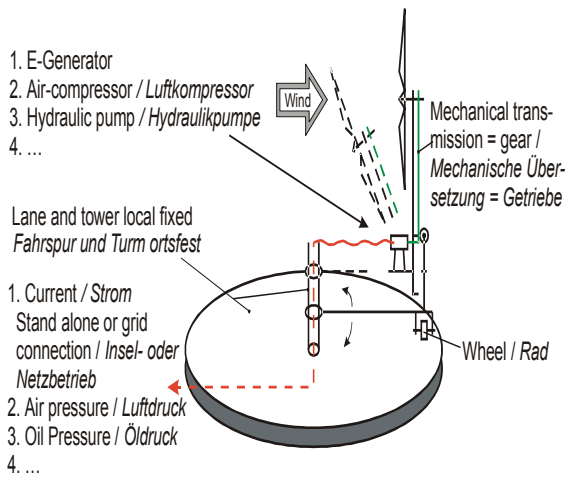


Figure 3.23: Construction details of MoWEC. The position of the energy transformer at the bottom of the tower.
*Konstruktionsdetails von MoWEC. Die Position des Energiewandlers unten am Turm.* [IRPS (2002c)]

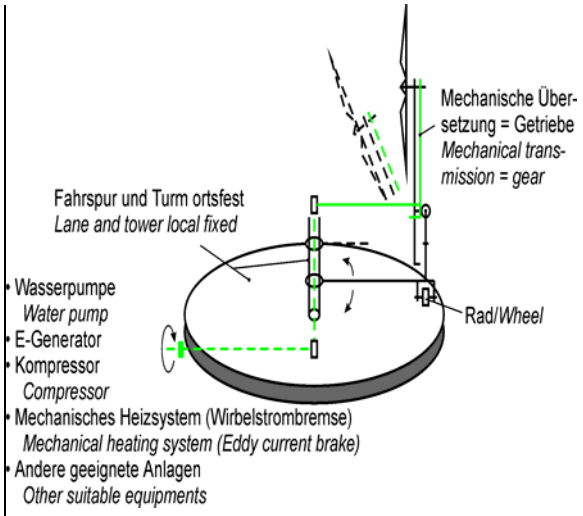


Figure 3.24: Construction details of MoWEC. The position of the use energy transformer direct on the fixed frame.
*Konstruktionsdetails von MoWEC. Position des Nutzenergiewandlers direkt am Rahmen.*

### 3.1.4.5 Winding the MoWEC

MoWEC is designed to work with its rotors facing the wind. If a MoWEC is to work as efficient as possible, its rotors plain must always face the wind squarely. For this purpose, some means of turning them into the wind, or winding the MoWEC (Yaw drive system), must be used. In addition, MoWEC does not have a regulating system for power limitation and for the reduction of the force acting on the blades when wind velocity is high (more than rated wind speed). With this in mind, the adaptation of the winding systems of historic windmills and yaw drive systems to modern wind energy converters are being discussed.

**Winding historical windmills**

As soon as a rotor yaws out of the main wind stream, performance deteriorates because the blades rotate in a cross-flow situation. Then in each revolution the angle at which the wind hits the blade will vary all the time, giving rise to unsteady flow over the blades, resulting in loss of power and in periodic dynamic variations. It is very difficult to calculate this deterioration but it is evident that a substantial amount of power can be lost through the wind changing direction slightly. Then greater stresses are imposed upon the blades themselves in addition to the normal reversal of forces, which occur through gravity as the blades rotate in each revolution. The incidence of such forces can be decreased both by keeping the mill facing the wind and to limit the body of windmill (wind shadow) [BENNETT (1898)].

Early post mills were winded by hand, the long beam or tail pole attached to the body of the mill being pushed round by brute force. In 1745 Edmund Lee invented the fantail as a device that ensured automatically that the wind blades were kept facing the wind. The fantail consisted of a set of vanes positioned at right angle to the blades. When the wind blades faced the wind directly, no force was exerted on the fantail vanes, but if the wind altered the fantail, it was set in motion and through a system of gears the windmill blades moved back into the wind. This was probably the earliest example of an automatic yaw drive control on windmills. The fantail blades (vanes) on early examples were set at an angle of 45° to the shaft on which they rotated but later this angle was about 35° or 22.5° [GREAVES (1969), RICHARD (1996), SCHNELLE (1999), MAYR (1970) and CLARK (1928-29)].

Post mills are normally winded from ground level, as the whole body of the mill goes round. To automate this process, the tail pole is mounted on a tandem carriage, with a big fantail above it. The fantail drive runs down to the wheels, and as the wind turns the fantail, the carriage moves one way or the other on a hard circular track round the mill, taking the body with it. Figure 3.25 and 3.26 show the ground-level fantail as well as the fantail fixed directly to the tail pole with wind dead head. The fact that this type of fantail is low down, and therefore screened to some extent from the wind by nearby buildings, tree and the mill itself might make it less effective than the cap fantail in Figure 3.27. The fantail will always catch enough wind for it to turn and bring the windmill blades into a 10° working arc according Figure 3.25 [SUZANNE (1975) and SCHOFIELD (1963)].

Some post windmills are winded by a fantail on the roof. Basically, a fantail is a secondary windmill set at right angles to the main blades of the windmill. It is geared through to a worm or a spur pinion so that it turns the cap of the windmill. Two thousand revolutions of the fantail might be necessary to rotate the cap of a tower mill in one complete circle, which may take as along as five minutes, but the response is normally quick enough for the safety of the windmill [DELITTLE (1972), SUZANNE (1975), WAILES (1945-47) and BUCKLAND (1987)].

Figure 3.27 shows the photo of a historical windmill in Peine, Germany, in the year 2002. The roof, in the shape of a truncated cone, which supports the revolving shaft, can turn above the building, which is made of stone. The cap is extended by a lee-wind wheel (fantail) which, when rotated, allows the blades of the mill to be oriented to the wind. Figure 3.28 illustrates the reduction ratio of the lee-wheel in this windmill. The total lee-wind wheel reduction ratio is $R_T = 1525:1$ [TOSTMANN (2002)].

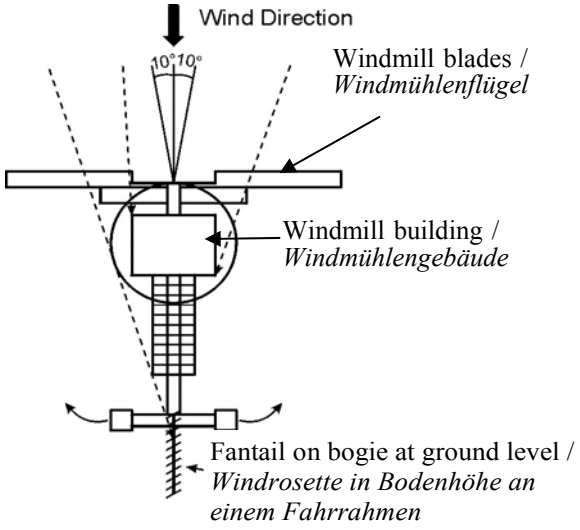


Figure 3.25: Ground-level fantails.

*Boden-Windrosette.*

Figure 3.26: An eight-bladed ground-level fantail attached to the tailpole.

*Boden-Windrosette mit acht Blättern angebracht am „Windmühlenstert".*


Figure 3.27: Historical windmill with a lee- wheel on the tower cap in the town Peine, Germany.

*Historische Windmühle mit einem Lee-Rad an der Turmhaube in der Stadt Peine, Deutschland.*

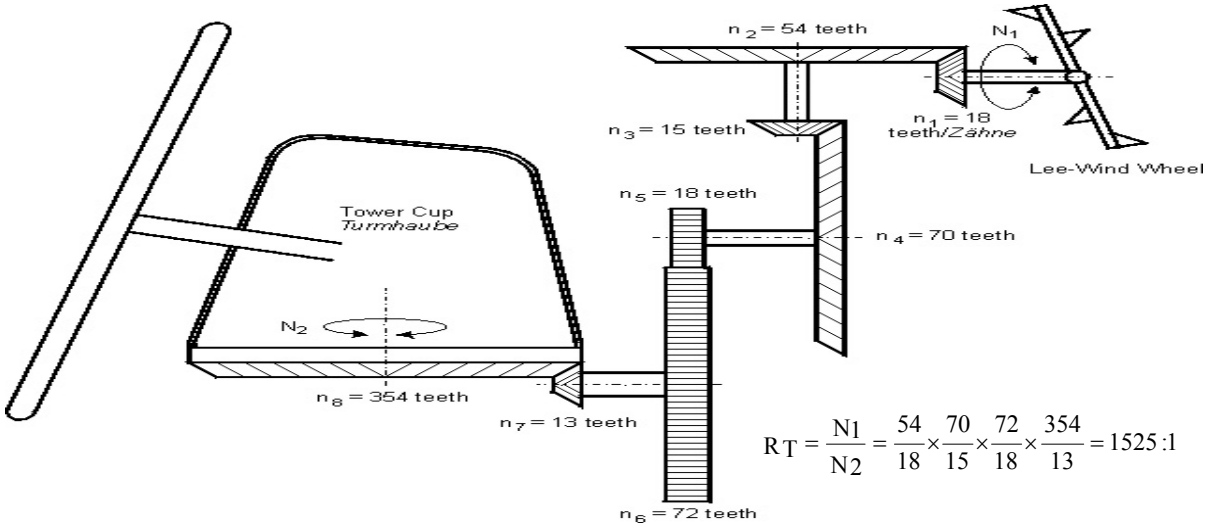


Figure 3.28: Lee-wheel reduction ratio.
*Lee-Windrad Untersetzungsverhältnis.*

**Yaw drive system of modern wind energy converters**

For the necessary limitation of power output from wind energy converters (WEC) beyond their rated performance (see Figure 3.5) different control systems are available, but the choice of pitch or stall control is still a matter of discussion. In small units, the tower head is often installed eccentrically in the front of the mast axis and held in the wind in the partial-load range by means of a spring. Above the rated wind speed, the wind thrust presses the rotor out of the wind and reduces the effective surface area for power generation. Bigger units which directly feed electricity into the grid often use only the effect of stalling at the rotor blades. For very big units and units with indirect feeding into the grid usually a blade-angle adjustment (pitch) is applied for power limitation. Through the variation of the angle of attack and the resulting tip-speed ratio the power and rotational speed are regulated. In stall-regulated units, the cut-out during storms is by means of aerodynamic brakes like adjustable blade tips or movable spoilers. Almost all WEC with stall- and pitch control have a secondary mechanical brake for emergencies.

The yaw drive of a WEC with horizontal axis is either passive or active. A passive yaw drive is affected by the attachment of the rotor in the lee of the tower, but for generators with high tip-speed ratio and low area coverage of the rotor-circle surface this principle only works for a moving rotor. Active yaw drive was achieved previously by a slower running wind wheel with high torque attached to the side of the nacelle that started to spin when crosswind components occurred and transferred this movement by a worm gear to the mounting ring of the tower connection. Nowadays the application of an electric support motor is commonly used, which is triggered by a small wind vane appropriately mounted at the nacelle [HAU (1996) and FRANQUESA (1989)].

### 3.1.5 Conclusions

Wind energy is one of the most flexible of all renewable energy sources. It can be used for different purposes such as irrigation, electricity generation, crop drying, grain grinding and many other purposes after the conversion of wind power into mechanical power by wind pumps. Current wind-powered pumping systems generally utilize bulky, slow-moving rotors and reciprocating pumps. These systems operate well in low-speed winds but reach peak water production in moderate winds around 7 to 8 m/s. Systems using a high-speed rotor coupled to a centrifugal pump could provide increased water production over a wide range of wind speeds and at a reduced cost.

**MoWEC** is the prototype of a **mobile wind energy converter** with two rotors, which can be used to capture wind energy at different locations. The rotational energy which is produced by the two three bladed rotors can use for a mechanical water pump, an electric generator for stand-alone use or with grid connection, an air-compressor for energy storage or for other suitable equipment. There are lots of different designs in terms of heights, width and rated power possibilities. In the present MoWEC prototype, wing heights amount to 10 m. The total rotor swept area is 80 m² and the theoretical rated power is 20 kW at a wind speed of 11 m/s

Up to now, the unsolved problem of the MoWEC prototype has been the lack of an automatic drive control system for the winding of the main rotors at low wind speeds and for automatic protection from damage caused by strong gusts of wind. After a literature review, it was decided that a wind driven lee-wind wheel should turn the two MoWEC-rotors depending on wind direction and wind velocity. Our own investigations pursue the goal of developing a yaw drive system for stand alone use with a lee-wind wheel, which shall be used for yaw control at low and high wind velocities.

The lee-wind wheel (fantail) was a device which ensured automatically that the MoWEC-rotors were kept facing the wind. The fantail consisted of a set of vanes positioned at right angle to the main rotor axes of the windmill. When the rotor directly faced the wind, no force was exerted on the fantail vanes, but if the wind altered the fantail was set in motion and through a system of gears brought the rotor back into the wind. This was probably the earliest example of the use of automatic control in machinery. The design and test of a lee-wind wheel and its installation in a MoWEC system is one of our work objectives. Another aim of this work is the measurement of the MoWEC power curve in the field in order to define MoWEC performance and its power coefficient value in particular along with studying the possibility of using this prototype equipped with a special low head pressure irrigation system for fruit tree watering on the North West Coast of Egypt.

## 3.2 Irrigation techniques for small orchard farms with a wind energy water pumping system

Combining a wind-electric system with an irrigation system for watering fruit trees may open up vast regions of land heretofore untapped due to no utility supplied electricity. So it is necessary to choose an irrigation system to enable energy source availability and reliability. There are many inherent advantages of using wind energy for water delivery in irrigation systems. Wind energy pumping offers high reliability, low maintenance, modularity, environmental acceptability, independence of central utility power, and a strong coincidence of water needs and water supply.

### 3.2.1 Irrigation techniques

Irrigation, which is generally defined as the application of water to soil through different types of systems for the purpose of supplying moisture for plant growth, plays a vital role in increasing crop yields and stabilising production. Irrigation systems fall into three categories: surface irrigation, micro irrigation and sprinkler irrigation (see Figure 3.29). Water-distribution systems that use closed conduits are potentially capable of higher irrigation uniformity than surface systems. A closed-conduit water distribution system makes it possible to apply water at a rate low enough that it does not pond on the soil surface. This transfers control of infiltration from the soil to the system. If during each irrigation water is delivered uniformly in increments sufficiently small that soil storage capacity is not exceeded, variations in soil properties from place to place in a field no longer cause differences in the quantity of water stored for crop use. Each plant can effectively receive its water supply directly. For sparsely planted crops, like orchards or vineyards, uniform irrigation can be achieved with a system that fills small basins with equal quantities of water [RAWLINS (1977)].

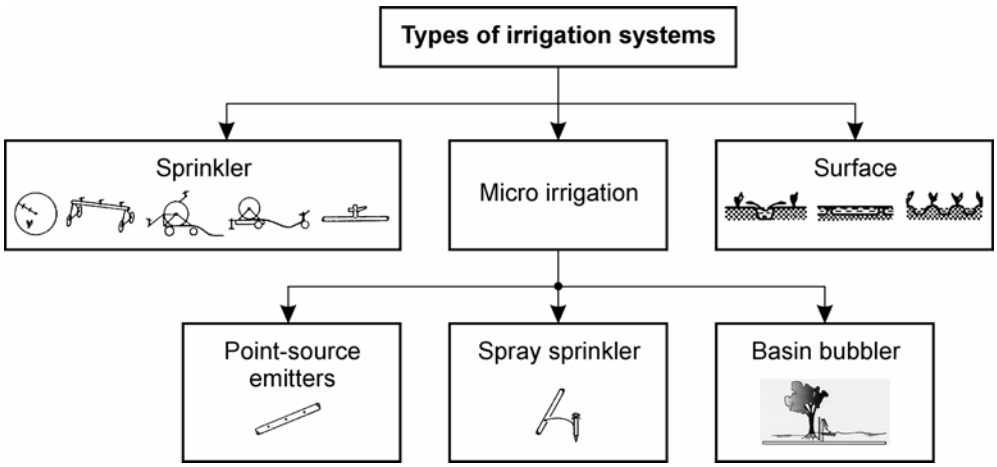


Figure 3.29: Irrigation systems. [OMARA (2004c), SOURELL (1998) and SPOFFORD (1997)]
*Bewässerungssysteme.*

SOURELL (1999) reported that the comparison of techniques initially related to the five techniques of irrigation used under central European climatic conditions, in other words not including surface irrigation. The comparison encompasses characteristic data relating to the requirements for energy, water, capital and labour. The capital and labour requirements of the irrigation techniques are specified for average operating conditions with five irrigation applications, each with an irrigation height of 30 mm (Figure 3.30 and 3.31).

Figure 3.30 shows that drip irrigation has the greatest capital requirements. For the other irrigation techniques, which are not installed enduringly, the investment per hectare depends on the area of use. In this case, semi-permanent pipe installation requires the lowest capital investment per hectare. In contrast, sprinkling machines for small areas of application require relatively high capital investment, and it is only when the areas of application are relatively large (above 30 ha) that the capital requirements become reasonable.

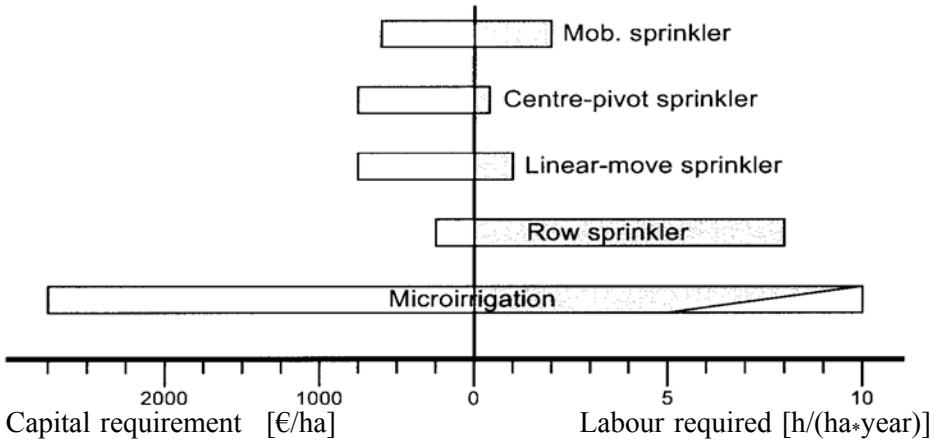


Figure 3.30: Capital and labour requirements for the most important irrigation techniques. [after SOURELL (1999)]

*Kapital- und Arbeitszeitbedarf für die wichtigsten Bewässerungstechniken.*

A completely different view of the individual techniques is presented with regard to the labour requirements, which are recorded per hectare and year. The longest labour is required for the movable application of pipe irrigation systems, at eight hours per hectare and year, while the shortest labour requirements are for stationary sprinkling machines. Drip irrigation has relatively high labour requirements where it is designed for area-wide coverage, but this work is not directly tied to particular timing and in some cases arises before or after the irrigation season. The shaded areas of the bars indicate the work on installation and removal, and the shaded areas the labour required for operating the system. In conclusion, it can be established that for medium-sized areas of application mobile sprinkling machines require the least labour with relatively high capital requirements, while the same is true of stationary sprinkling machines where the areas of application are larger.

Figure 3.31 illustrates that the energy and water requirements are highest for mobile sprinkling machines at 800 kWh per hectare and year - caused by the high water pressure required - and an assumed water volume of 1200 m³ per hectare and year. In the case of row sprinklers with pipes it is sufficient to have low water pressure. As a result, energy requirements drop to roughly 650 kWh per hectare and year. Further savings can be made using stationary sprinkling machines. When using drip irrigation, it is possible to reduce energy requirements to approximately 135 kWh per hectare and year because of low water requirements and low water pressure. Furthermore, as a result of the avoidance of any water losses due to the straight supply of water directly to the plant, water savings of up to 30% can be achieved without jeopardizing yields [MAYER (2001)].

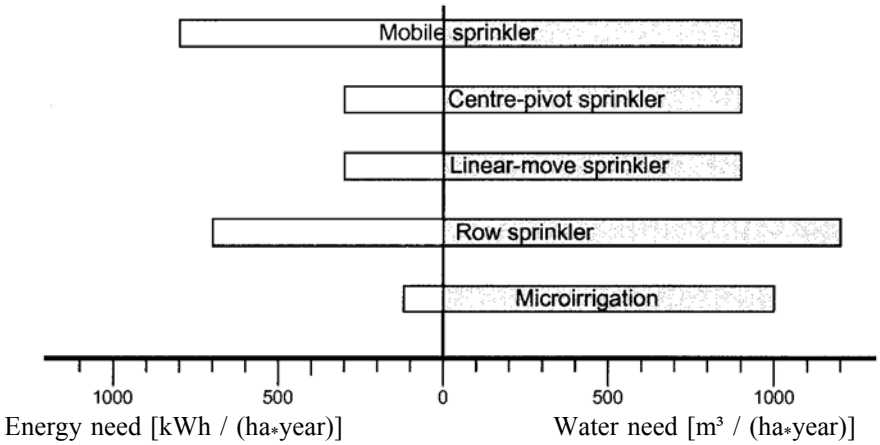


Figure 3.31: Energy and water requirements of various irrigation techniques. [after SOURELL (1999)]

*Energie- und Wasserbedarf der verschiedenen Bewässerungstechniken.*

The most significant features of the various methods of irrigation are shown in Table 3.2. In the case of low water consumption being of high priority and given the assumption that small farm sizes are the main application, micro-irrigation shows its predominance. On such farms, the argument of the labour requirements for system operation is of lower importance since often families and their members are involved in farming. Thus, maintenance will not be cost-intensive [MAYER (2001)].

According to the comparison of the irrigation methods and the characteristic data, the micro-irrigation technique is a suitable application for sparsely planted crops, like orchards or vineyards equipped with wind energy or photovoltaic water pumping systems. Any other methods (sprinkling) of irrigation either require excessively high operating pressures or are unsuitable for small farms because of the size of the machines or the output per unit area. In addition, gravity irrigation has lower application efficiency and is not suitable for automatic operation. Therefore, micro-irrigation systems will be discussed in the next section.

Table 3.2: Characteristics of irrigation methods.
*Charakteristik der Bewässerungsmethoden.*

| Characteristic | Methods | | |
|---|---|---|---|
| | **Surface irrigation** | **Sprinkler irrigation** | **Micro-irrigation** |
| Pressure demand [m] | low | 20-50 | 5-35 |
| Energy content (hyd.) [Wh/m³] | low | 100 - 150 | 40 - 100 |
| Autom. Water metering | none | good | very good |
| Water losses<br>Cause<br>Extent | high<br>seepage<br>up to 100% | moderate<br>evaporation<br>up to 60% | low<br>seepage<br>up to 35% |
| Application efficiency % | 40-60 | 70 | 85-90 |
| Erosion | low- moderate | high | low |
| Salt encrustation of emitters (not soil) | - | moderate | moderate-high |
| Handling | manual | automatic | automatic |
| Maintenance requirements | low | moderate | moderate- high |
| Costs | low | moderate- high | moderate- high |

### 3.2.2 Micro-irrigation systems

Micro-irrigation is the broad classification of frequent, low volume, low-pressure application of water on or beneath the soil surface by drippers, drip emitters, spaghetti tubes, subsurface or surface drip tubes, basin bubblers, and spray or mini sprinkler systems. It is also referred to as drip or trickle irrigation. Existing closed-conduit irrigation systems are capable of saving water by increasing application uniformity. But, because most of them require pumping to pressurize water for distribution, water is saved often at the expense of increased energy consumption [RAWLINS (1977) and SPOFFORD (1997)]. The types of micro irrigation can be classified as follows:

#### Point-source emitters

In the point-source form of micro irrigation, water is applied to the soil surface as discrete or continuous drops, tiny streams, or low volume fountains through small openings. Discharge rates typically range from 2 to nearly 114 l/h for individual drip emitters. Micro tubes (spaghetti tubing) are classed as point-source emitters even though they are actually tubes rather than emitters. Micro tubes consist of various lengths of flexible tubing that is small in diameter (0.5 to 1 mm). Typically, no other water control device is used. Discharge rates are adjusted by varying the length and diameter of the tubing. Longer tubes and smaller diameters cause greater friction loss, which decreases the discharge rate. Because discharge orifices are small, complete filtration of water is required. The discharge rates can also be adjusted by using compensated emitters. Another type of point-source emitter is the surface or subsurface line-source emitter system. This type of micro-irrigation uses surface or buried flexible tubing with uniformly spaced emitter points (or porous tubing). The tubing comes as lay flat tubing, flexible

tubing, or as semi rigid tubing that retains its shape. Generally, this system is used in permanent crops, but has been used successfully as either surface or buried lines with high value row crops, such as vegetables, cotton, and melons. Surface or subsurface line-source emitter systems have a uniform discharge in units of litres per minute per 100 m over a specified pressure range. Also because discharge orifices are small, complete filtration of water is required.

## Spray sprinkler

With spray or mini sprinkler micro irrigation systems, water is applied to the soil surface as spray droplets from small, low-pressure heads. The typical wetted diameter is 0.61 to 2.13 m. Discharge rates are generally less than 114 l/h. The wetted pattern is larger than that of typical drip emitter devices, and generally fewer application devices are needed per plant. Spray and mini sprinklers also have less plugging problems and less filtration is required than in point-source emitters (drippers). Many spray heads only require the replacement of the orifice to change the discharge rate. If an orifice becomes plugged, it is easily removed and cleaned or replaced. Spray or mini sprinkler head application patterns can be full, half circle, or partial circle (both sides).

## Basin bubblers

The basin bubbler (low-head bubbler) micro irrigation system applies water to the soil surface in small fountain type streams. The streams have a point discharge rate greater than that of a typical drip or line source system, but generally less than 227 l/h. The discharge rate normally exceeds the infiltration rate of the soil. Therefore, small basins are used to contain the water until infiltration occurs. Discharge is generally from a small diameter (6 to 13 mm) flexible tube that is attached to a buried or surface lateral and located at each plant vine or tree. The typical emitter device is not used, and discharge pressure heads are very low (< 3.5 m). Energy costs are more significant than water costs in most countries. These energy costs can be reduced in many cases if the bubbler technology is adopted, especially in areas where delivery canals for surface irrigation system exist and have more than a meter of a head available with respect to the field. Figure 3.32 displays a typical basin bubbler system.

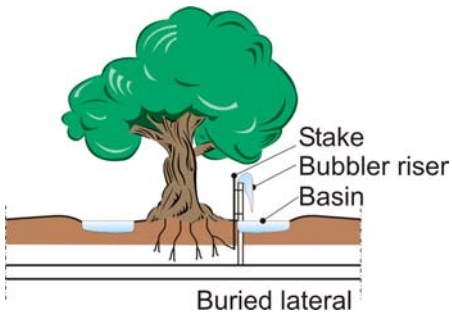


Figure 3.32: Basin bubbler system.
*Bassin Bubblersystem.*

Basin bubblers are used in orchards and landscaping and ornamental plantings. These systems are best used on medium to fine textured soils where lateral water movement can provide adequate soil moisture for the desirable plant root development area. On coarsely textured soils, bubbler discharge rates are increased and shorter time periods used, thereby providing more wetted area above the potential plant root zone.

The main objective of micro irrigation system design is to obtain suitable water application uniformity. The first low-head bubbler system was introduced by RAWLINS (1977). A low-head bubbler irrigation system consists of a mainline connected to a water source, a constant head device, manifolds, laterals, and small-diameter delivery hoses. The laterals are laid midway between two rows of trees or beside one row of trees, and small-diameter hoses (called delivery hoses, distributor hoses or tubes) are inserted into the laterals to deliver water to the trees. These hoses are anchored on a tree or stake, and hose heights or lengths are adjusted such that the water flows out from all hoses at equal rates. The name of the system, bubbler, is derived from the fountain of water streaming out from the hoses and from the bubbling noise made as air escapes from the pipelines when the system is turned on.

The distinguishing feature of a low-head bubbler system is the flexible delivery hoses which contrast with the small emitters commonly used in other micro-irrigation systems. These hoses allow greater rates of water to discharge into the small basins to be reached, and they do not require a filtration system because of their large orifice openings. The basins are usually circular or rectangular in shape and are bordered by low embankments or levees, so that water is uniformly distributed over the root zone [YITAYEW (1995)].

Motivated by RAWLINS´ (1977) work, others such as THORNTON (1980), CARR (1980) and HULL (1981) designed and installed similar low-head bubbler systems. All of these systems were similar in design to the ones described by RAWLINS (1977) in that the design head was 1 m; laterals of corrugated PE tubing were laid on fields with gradual slopes; delivery hoses were made of smooth 9.5 mm tubing; design flows ranged from 115 to 241 l/h; and both the Manning and Darcy-Weisbach equation were used to size the laterals and delivery hoses, respectively. Later in the 1980s, ROTH (1992) installed several bubbler systems in Arizona, and these systems differed from previous designs, as they were located on level fields and used rigid PVC pipes instead of corrugated PE tubing. Recently, REYNOLDS (1993); REYNOLDS (1995a); and REYNOLDS (1995b) did extensive work on the design of bubbler systems by providing a step-by-step design procedure and presenting a design solution to prevent air lock problems associated with systems located on level fields. Correspondingly, some of the management problems caused by air locks in the delivery hoses were solved.

Low-head bubbler irrigation systems are well suited for the irrigation of trees and orchard crops. The air lock problem for bubbler systems located on level fields is also addressed, and a solution which prevents air locks is provided to improve the operation and management of the system [YITAYEW (1995)]. KELLER (1990a) ranked bubbler systems in the same low-risk category as surface irrigation systems, as both systems are largely based on gravity flow and do not require mechanical pumps or filtration systems when compared with other micro irrigation systems.

The main objective of Low-Head Bubbler Irrigation System (LHBIS) design is to achieve suitable water application uniformity. Low uniformity is usually associated with poor efficiency and implies a reduced control of water use and therefore creates a possibility of aquifer degradation and/or pollution. The hydraulic analysis required for the simulation and design of low-head bubbler irrigation systems will now be discussed.

## 3.2.3 Hydraulic analysis of low-head bubbler irrigation systems

The analysis and design of low-head bubbler irrigation systems requires three equations, namely: energy equation, friction loss and flow rate.

### 3.2.3.1 Energy concepts

Fluids possess energy in three forms. The amount of energy depends upon the fluid's movement (kinetic energy), elevation (potential energy), and pressure (pressure energy). In a hydraulic system, a fluid can have all three types of energy associated with it simultaneously. The total energy associated with a fluid per unit weight of the fluid is called head. The energy equation, or Bernoulli equation, is the primary hydraulic equation used for basin bubbler irrigation system analysis [REYNOLDS (1995a)]:

$$\frac{P_1}{\gamma} + \frac{V_1^2}{2g} + Z_1 = \frac{P_2}{\gamma} + \frac{V_2^2}{2g} + Z_2 + \sum h_f + \sum h_{mc} \qquad (3.2.1)$$

where P is pressure within the pipe [N/m²]; V is the flow velocity of water in pipes [m/s]; Z is elevation of the pipe centreline with respect to a reference datum [m]; $h_f$ is friction head loss in pipes [m]; $h_{mc}$ is minor losses at pipe fittings [m]; $\gamma$ is specific weight of water [N/m³]; and g is the gravitational constant [9.81 m/s²]

The energy equation is useful to size the pipe diameters of a bubbler system by determining the piezometric heads for the upstream and downstream ends of the bubbler system. The piezometric heads at the upstream and downstream ends of the bubbler system are

determined from the elevation of water source and field layout. The difference between the upstream and downstream piezometric heads is the total allowable head loss caused by the system. The friction loss through each pipe component of the bubbler system will comprise a certain amount of the total allowable head loss.

To initially size the pipe diameter, the velocity head and minor losses are assumed zero, but they will be accounted for the manifold and lateral when calculating the distributor hose heights or lengths. The diameter of each pipe can be determined by substituting the assumed flow rate, known pipe length, and calculated allowable head loss for each pipe component into the friction loss equation and solving the terms of the diameter.

MORCOS (1994) observed that from the experimentally measured resultant pressure head tended to drop gradually in the first portion of the perforated tube, followed by a gradual increase in it the remaining length of the tube. The length of this portion and the value of the minimum and the maximum resultant pressure head depended on the number of outlets. As the number of outlets decreased, the length of this portion decreased and the values of the minimum and the maximum resultant pressure head increased.

A fundamental approach to the problem is to apply the first low of thermodynamics (conservation of energy) to the hose outlet in Figure 3.33 and 3.34. After some reorganization [according to MCNOWN (1954)], the resulting equation is:

$$\frac{P}{\rho g}+\frac{\alpha V^2}{2g}=\frac{P_c}{\rho g}+\frac{\alpha_c V_c^2}{2g}+\frac{q_{oh}}{Q}\left(\frac{\alpha_o V_o^2}{2g}-\frac{P_c}{\rho g}-\frac{\alpha_c V_c^2}{2g}\right) \tag{3.2.2}$$

Which can be reduced to:

$$\frac{P}{\rho g}+\frac{\alpha V^2}{2g}=\frac{P_c}{\rho g}+\frac{\alpha_c V_c^2}{2g}+\Delta h \tag{3.2.3}$$

where: P is the pressure [N/m²]; V is the average velocity in the pipeline [m/s]; $\alpha$ is the kinetic energy correction factor; $\rho$ is water density [kg/m³]; $q_{oh}$ is the distributor hose outflow [m³/s]; and $\Delta h$ is the head loss term in [m].

The equation (3.2.3) is equivalent to the (incorrect) application of Bernoulli's equation across the outlet of the hose and given the assumption of the head loss, $\Delta h$ occurs. This term actually represents the energy loss plus the energy removed as water exits from the hose. As expected, this term becomes small whenever the distributor hose flow $q_{oh}$ is small compared to Q.

If the pressure head recovery, $\frac{P - P_c}{\rho g}$ , is replaced by $\Delta hp$, and if $\frac{\alpha V^2}{2g}$ is replaced by $h_V$,

then: $$\frac{\Delta h_p}{h_v} = 1 - \frac{\alpha_c}{\alpha}\left(\frac{V_c}{V}\right)^2 - \frac{\Delta h}{h_v} \qquad (3.2.4)$$

If it could be assumed that $\alpha = \alpha_c = 1$ and $\Delta h = 0$, the equation (3.2.4) would reduce to:

$$\frac{\Delta h_p}{h_v} = 1 - \left(\frac{V_c}{V}\right)^2 \qquad (3.2.5)$$

where $\Delta h_p$ is the pressure head recovery across the hose inlet [m]; and V and $V_c$ are the flow velocities in the pipeline upstream and downstream of the hose respectively [m/s].

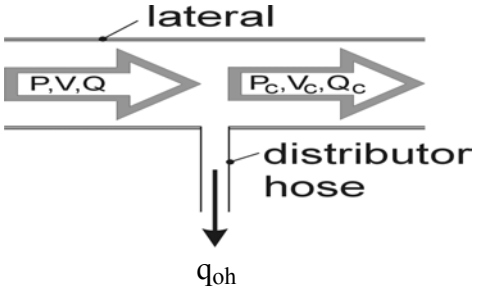


Figure 3.33: Definition of symbols. [after OMARA (1997)]
*Definition von Symbolen.*

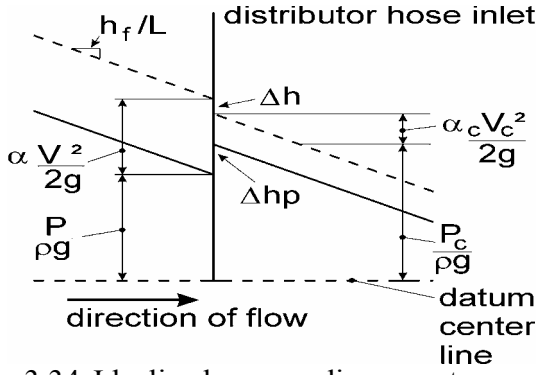


Figure 3.34: Idealized energy diagram at a distributor hose.[after OMARA (1997)]
*Idealisiertes Energiediagramm an einem Verteilerschlauch.*

### 3.2.3.2 Friction loss

There are many equations that approximate the friction losses associated with the flow of a liquid through a given section. Using dimensional analysis, the Darcy-Weisbach formula was developed. This equation is commonly used in the analysis of pressure pipe systems [THOMAS (2001) and WALSKI (2003)]:

$$h_f = f\frac{L}{D}\frac{V^2}{2g} \qquad (3.2.7)$$

where $h_f$ is friction head loss in pipes [m]; L is the length of pipeline [m]; D is the inside diameter of pipes [m]; V is flow velocity of water in pipes [m/s]; g is the gravitational constant [m/s²]; and f is the friction factor. For smooth plastic pipes, the friction factor (f) for laminar

flow Eq. (3.2.8), transitional flow Eq. (3.2.9) and turbulent flow Eq. (3.2.10) and (3.2.11), flow conditions are:

For $R_e < 2000$, $$f = \frac{64}{R_e} \quad (3.2.8)$$

For $2000 < R_e < 4000$, $$f = 3.42 \times 10^{-5} R_e^{0.85} \quad (3.2.9)$$

For $4000 < R_e < 10^5$, $$f = \frac{0.316}{R_e^{0.25}} \quad (3.2.10)$$

For $10^5 < R_e < 10^7$, $$f = \frac{0.13}{R_e^{0.172}} \quad (3.2.11)$$

KELLER (1990b) and BOSWELL (1984) recommend equations (3.2.8), (3.2.10), and (3.2.11) in micro irrigation design, with Eq. (3.2.10), the Blasius equation, having a Reynolds´ number lower limit of 2000. The Reynolds´ lower limit for the Blasius equation is typically 3000 to 4000, however, for desktop calculations. Eq. (3.2.9) as defined by WU (1974) can be ignored by setting the lower limit for the Blasius equation at 2000.

By combining the Darcy-Weisbach Eq. (3.2.7) and the Blasius relationship Eq. (3.2.10), an equation for the description of the energy loss $h_f$ for smooth pipes due to pipe friction at each length between the outlets, which similar in form to the Hazen-Williams equation, is obtained for $2000 < R_e < 10^5$. The Hazen-Williams equation is most frequently used for the design and the analysis of pressure pipe systems. The equation was developed experimentally, and therefore it should not be used for fluids other than water [ASCE (1992) and WALSKI (2002)]. The Hazen-Williams equation is:

$$h_f = \frac{1.22 \times 10^{10} L_o}{D^{4.87}} \left( \frac{Q}{C_{HW}} \right)^{1.852} \quad (3.2.12)$$

where $h_f$ is the friction loss along the pipeline [m]; $L_o$ is the length of the pipeline [m]; D is the inside diameter [mm]; Q is the total pipeline flow rate [l/s]; $C_{HW}$ is the Hazen-Williams coefficient.

The reason why the Hazen-Williams equation is used in low head bubbler irrigation calculations is that it is easier to use than the Darcy Weisbach equation. The Hazen-Williams equation is used to calculate the flow in a fully flowing pipe in order to convert pressure loss in a fully flowing pipe into pressure loss in a pipe with regular outlets. Applying the Christiansen reduction coefficient, F, is commonly used to calculate head losses in multiple outlet pipes and to initially size the diameters of mainlines, manifolds, and laterals [CHRISTENSEN (1942)].

The application of the Christiansen reduction to head loss Eq. (3.2.12) simplifies calculations for multiple outlet pipes because it estimates friction loss along the entire length of multiple-outlet pipes, such as the manifold and the lateral. When using the Christiansen coefficient, the total friction loss for multiple outlet pipes is expressed as:

$$h_{ac} = h_f \cdot F \tag{3.2.13}$$

where $h_{ac}$ is the actual pressure loss in the pipeline [m]; $h_f$ is the friction head loss between the upstream and downstream ends of a multiple outlet pipe [m]; F is the Christensens friction factor.

KRUSE (1980) assumed uniform outflows from the $N_o$ orifices along the pipeline, and also that the first orifice is at one space from the upstream end of the pipeline. In this case, F is given by:

$$F = \frac{1}{m_d + 1} + \frac{1}{2N_o} + \frac{(m_d + 1)^{0.5}}{6N_o^2} \tag{3.2.14}$$

where $N_o$ is the number of outlets along the pipeline; $m_d$ is the flow velocity exponent in the Darcy-Weisbach equation (3.2.7).

### 3.2.3.3 Flow rate

The flow in the immediate vicinity of an outlet is defined in Figure 3.33 and 3.34. Clearly, mass continuity must apply at each outlet such that:

$$Q = Q_c + q_{oh} \tag{3.2.15}$$

where Q is the discharge in the pipe upstream of the hose; $Q_c$ is the discharge continuing downstream in the pipeline; and $q_{oh}$ is the discharge from the distributor hose.

## 3.2.4 Conclusions

Energy costs are more significant than water costs in most countries. Combining a wind-electric system with an irrigation system for watering fruit trees may open up vast regions of land heretofore untapped due to no utility supplied electricity. According to the comparison of the irrigation methods and the characteristic data, the micro irrigation technique is a suitable application for sparsely planted crops, like orchards or vineyards with wind energy water pumping systems. Any other methods (sprinkling) of irrigation either require excessively high operating pressures or are unsuitable for small farms because of the size of the machines or the output per unit area. In addition, gravity irrigation has lower application efficiency and cannot operate automatically.

Micro irrigation is the broad classification of the frequent, low volume, low-pressure application of water on or beneath the soil surface by drippers, drip emitters, spaghetti tubes, subsurface or surface drip tubes, low-head bubblers, and spray or mini sprinkler systems.

Low-head bubbler irrigation enables water to be used economically, and its low operating pressure makes it particularly well-suited for combination with alternative energy such as wind energy water pumping systems. This irrigation system is particularly well suited for orchard crops and requires very low-pressure heads to distribute irrigation water to the trees. It is based on gravity flow and has large orifice openings to deliver water directly to the root zone, thus eliminating elaborate filtration systems and pumps required by other micro irrigation systems. Despite these advantages, bubbler systems have not been widely used.

The analysis and design of low-head bubbler irrigation systems require three equations, namely: energy equation, friction loss and flow rate. Moreover, this analysis will be used to design and write a computer program for the simulation of the outlet elevation of the distributor hoses or their length along the laterals in this irrigation system.

# 4 PRESENTATION OF OWN INVESTIGATIONS

## 4.1 Further development of the MoWEC yaw drive system

**MoWEC** is the prototype of a **mobile wind energy converter** with two rotors, which can be used to capture wind energy at different locations. There are lots of different designs in terms of heights, width and rated power possibilities (see section 3.1.5). The wing heights in the present MoWEC prototype amount to 10 m. The total rotor-swept area results in 80 m² because each of the two rotors has a diameter of 7.10 m. The theoretical rated power is 20 kW at a wind speed 11 m/s.

Horizontal axis wind rotors require a mechanism to swing them into the wind. Small units usually have a tail assembly. Larger rotors usually have a “servo mechanic” that orients them to the direction of maximum wind power. In addition, modern wind turbines are usually equipped with systems which prevent damage in excessively high winds. Large wind energy plants may have complex arrangements to shut down the generator at very high wind speeds. Smaller systems change the rotor area through a turn in order to have less square meters facing the wind. Normally brakes are used to stop rotor revolution. Systems having a rated power of up to 10 kW are normally called “smallest wind energy plants”. 10 kW to 70 kW plants are called “small wind energy plants”. According of this classification the investigated MoWEC is a “small wind energy converter”.

The MoWEC prototype requires an automatic yaw drive system without an energy store in stand-alone use to move the rotors into the wind at low wind speeds and to move the rotors out of the wind at wind velocities beyond rated power. To fulfil this demand, a lee- wind wheel yaw drive system was chosen.

### 4.1.1 Material and method

#### 4.1.1.1 Design of a lee-wind wheel yaw drive system for MoWEC

The energy required by the yaw drive system to turn the rotors is provided by a multi bladed wind wheel. This wind wheel installed on the yaw drive frame in a lee-position in relation to the central turn axle is called the **lee-wind wheel.** Figure 4.1 shows a diagram of the mechanical system of the lee-wind wheel designed by the author, which features two bevel gearboxes and one toothed gear connected to the driven roll wheel on the MoWEC ball race. It takes 942 or 1371 revolutions of the lee-wind wheel to turn the two MoWEC-rotors, which are fastened on the yaw drive frame, in one complete circle. Depending upon the wind velocities, nearly five minutes are required for a 360° turn.

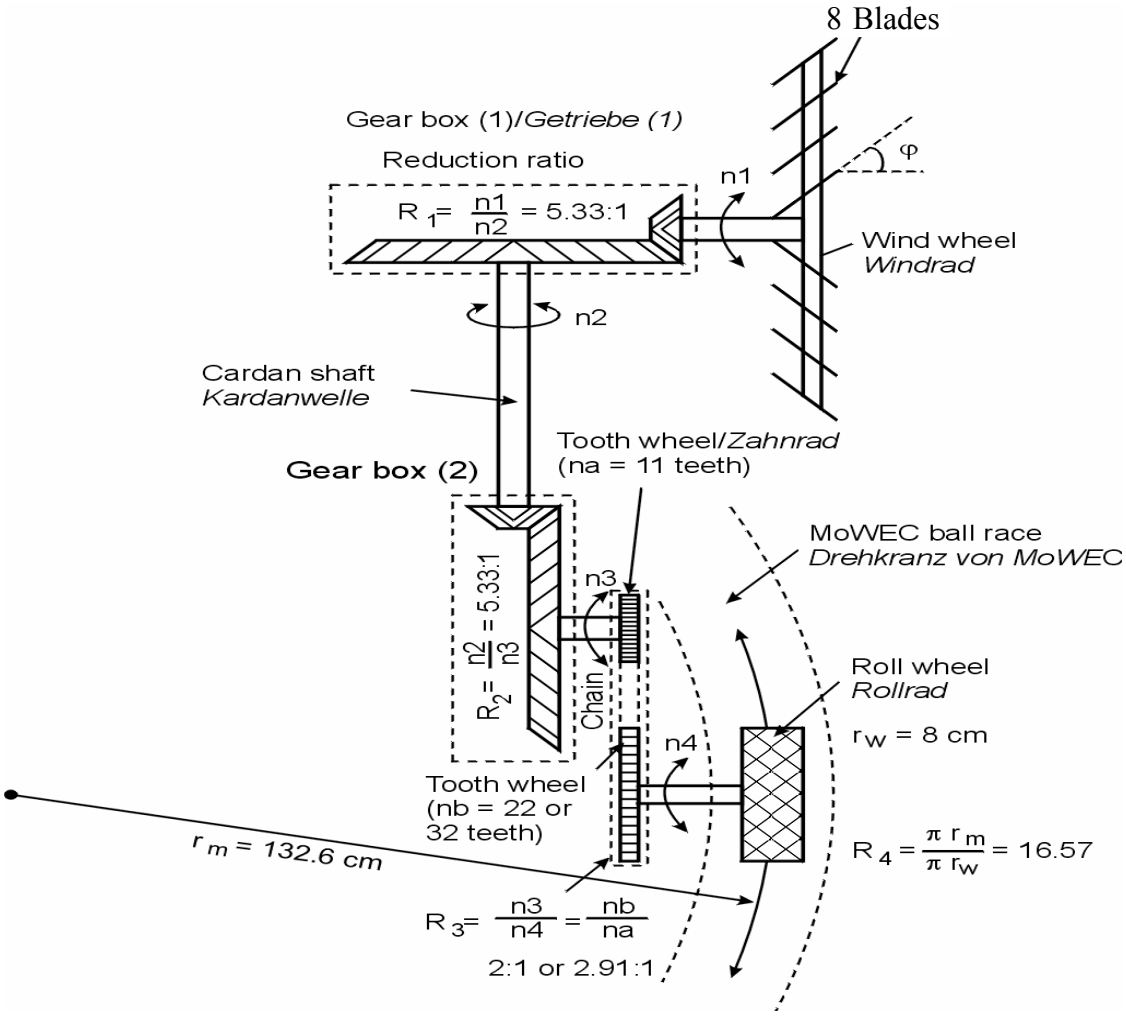


Figure 4.1: Lee-wind wheel with four gear stages.

*Lee-Windrad mit vier Getriebestufen.*

To obtain the total required reduction ratio ($R_T$) three reduction stages in the wind tunnel experiment would be necessary. According to Figure 4.1, four reduction stages are installed on the MoWEC. In a first step, the total reduction ratio ($R_T$) was similar to the reduction ratio in the traditional windmills described in chapter 3.1.6. These converters featured two bevel gearboxes, each with a reduction ratio of 5.33:1, followed by a toothed gear having a ratio of 2.91:1 or 2:1 depending on the wind tunnel experiment.

The friction roll wheel was 16 cm in diameter and 10 cm in width. This roll wheel became the driven wheel on the MoWEC ball race. The MoWEC ball race has had an average diameter of 265.2 cm. Therefore, the reduction ratio in this fourth stage $R_4$ was $R_4 = 265.2 / 16 = 16.58:1$. Hence, the total speed reduction ratio of the lee-wind wheel system ($R_T$), installed on MoWEC, is:

$$R_T = R_1 \times R_2 \times R_3 \times R_4 \quad \Rightarrow \quad R_T = 1371:1 \text{ or } 942:1$$

**Determination of the lee-wind wheel diameter**

To determine the torque required to turn the MoWEC towers around the stationary central tower, the tangential force ($F_T$) at MoWEC`s outer ball race diameter was measured using a spring balance. The average tangential force $F_T$ was 588.6 N in calm wind. Since the two MoWEC rotor towers are also standing in a lee-position, the needed $F_T$ is always reduced. The mean diameter of the MoWEC ball race $D_b$ was 2.652 m. Hence, the required torque $T_r$ is:

$$T_r = \frac{F_T \cdot D_b}{2} = \frac{588.6 \times 2.652}{2} = 780.48 \qquad [Nm]$$

Thus, the minimum tangential force at the last roll wheel ($F_{Tr}$) in the lee-wind wheel system must not be less than the required tangential force to turn the MoWEC tower ($F_T$). It was assumed that the value of $F_{Tr} = F_T = 588.6$ N. In this case the minimum required torque at the horizontal axis of the wind wheel $T_w$ is:

$$T_w = \frac{F_{Tr} \cdot r}{rw \cdot \eta_g} \qquad [Nm]$$

where:

$F_{Tr}$ is the required tangential force at outer diameter of roll wheel, 588.6 [N]

r is the radius of the roll wheel, r = 0.16/2 = 0.08 [m]

rw is the Speed reduction ratio between the wind wheel and the last tooth wheel in the transmission system according Figure 4.1. It is also assumed that the value of $R_3$ to design the lee-wind wheel diameter of 2:1. Hence, $rw = R_1 \times R_2 \times R_3 = 5.33 \times 5.33 \times 2 = 56.82{:}1$

$\eta_g$ is the transmission efficiency of the gearboxes, tooth wheels and bearings. It could be as high as 95% if good. Assume that this efficiency could be 65% at low speed. Then the required torque at the horizontal axis of the wind wheel $T_w$ would be,

$$T_w = \frac{588.6 \times 0.08}{56.82 \times 0.65} = 1.275 \qquad [Nm]$$

The horizontal-axis multi bladed rotor with diameter ranges between 2 and 8 m can start freely in wind speeds of 2 to 3 m/s. The maximum power coefficient $C_p$ of 0.3 (when the wind wheel is perpendicular to the wind direction) could be obtained at a tip-speed ratio $\lambda = 1$ and the maximum torque coefficient $C_T$ of 0.35 at a tip-speed ratio $\lambda = 1$ (Figure 3.12) [GOURIERES (1982)].

Using equation (3.1.17) and Figure 3.12, which presents the torque coefficient as a function of the tip- speed ratio of a slow wind machine and given the above considerations, the small wind wheel diameter can be calculated.

$$C_T = \frac{2\,T_w}{\rho_{air} \cdot \pi \cdot R_{wo}^3 \cdot \sin\theta \cdot v_1^2}$$

where:

$C_T$ = lee-wind wheel torque coefficient. It could be assumed that the tip-speed ratio for this lee-wind wheel is $\lambda$ =1. Then the value of $C_T$ in Figure 3.12 is 0.35 (when the wind wheel is perpendicular to the wind direction). In this case, it could be assumed that the value of $C_T$ is 0.20 when the angle between the wind wheel and the wind direction is less than 90°.

$\theta$ = Angle between the horizontal axis of the wind wheel and the wind direction [degree]. It was assumed that the wind wheel would catch enough wind to turn and to hold the MoWEC towers in a working position of $\theta$ = 20° [SUZANNE (1975)].

$\rho_{air}$ = Air density, 1.225 [kg/m³]

$R_{wo}$ = Wind wheel outer ring radius [m]

$v_1$ = Wind speed; assume that the lee-wind wheel can deliver enough power to turn the MoWEC yaw drive frame when the angle between the lee-wind wheel and wind direction is 20° and the wind speed $v_1$ = 5 m/s. Then the outer ring radius of the wind wheel can be calculated as follows:

$$T_w = 0.5 \cdot C_T \cdot \rho_{air} \cdot \pi \cdot R_{wo}^3 \cdot \sin\theta \cdot v_1^2$$

$$1.275 = 0.5 \cdot 0.20 \cdot 1.225 \cdot \pi \cdot R_{wo}^3 \cdot \sin 20° \cdot 5^2$$

This equation indicates that the minimum radius of the lee-wind wheel $R_{wo}$ should be 0.75 m. The outer ring diameter of the wind wheel is now determined to be $D_{wo}$ = 1.5 m. Eight blades having the dimensions shown in Figure 4.2 could be used. In the experiment, the wind wheel blades was able to be fastened at different angles $\varphi$ (15°, 22.5°, 35° and 45°) to the shaft on which it rotates (see Figure 4.3). These angles were tested in the wind tunnel experiment to find the best one, which provides the highest torque at the lowest wind speed. It was the goal of this test to produce a high torque moment at the driven roll wheel on the MoWEC ball race. This is also a function of the lee-wind wheel transmission ratio $R_T$.

### 4.1.1.2 Test of the lee-wind wheel system

An eight-bladed lee-wind wheel was constructed and tested in a wind tunnel in the configuration of Figure 4.1. The roll wheel was used as a rope barrel to measure the tangential force at various wind speeds (see Figure 4.2). The position of the lee-wind wheel inside the wind tunnel was changed depending on real use on the MoWEC yaw drive frame. In addition, the blade angle $\varphi$ would be changed in the wind tunnel experiment in order to optimize wind power transformation by the lee-wind wheel.

## Purpose of the test

The purpose of this experiment was the test of the above recommended eight bladed lee-wind wheel system in order to determine the optimal blade angle φ (15°, 22.5°, 35° or 45°) and to estimate which reduction speed ratio rw should be used for later installation on the MoWEC yaw drive frame (56.82:1 or 82.64:1). A wind tunnel was specially built for this test which allowed wind velocities from 2.0 m/s to 8.2 m/s to be simulated. These are the wind velocities where the MoWEC yaw drive frame is turned into the wind.

## Experimental design

The constants in the experiment were: (i) The described lee-wind wheel system with a 1.5 m outer ring diameter, two gearboxes (reduction ratio 5.33:1 each), (ii) the same number, shape, dimension and type of wind blades and (iii) the toothed gear at the third gear stage always starts with 11 teeth. Figure 4.2 and 4.3 show the components of the test.

The two variables were: (i) The wind wheel blade angle φ (15°, 22.5°, 35° or 45°), and (ii) the speed reduction ratio at the third toothed gear stage. Here it is a second wheel featuring 22 or 32 teeth. Therefore, all three gear stages had a reduction ratio rw = 56.82:1 or rw = 82.64:1. These variables should be tested at different lee-wind wheel position angles inside the wind tunnel at wind velocities ranging from 2.0 m/s to 8.2 m/s. The angle θ (10° to 90°) is the angle between the lee-wind wheel axle and the wind direction, here produced by 6 electric fans behind the lee-wind wheel. The air stream first passes the lee-wind wheel and then the fans, which produce low air pressure.

The responding variables were wind wheel velocity, output power and the power coefficient from each single test of the lee-wind wheel system. To calculate the responding variables, a steel rope was tied to the assigned MoWEC drive wheel (diameter 16 cm), which is now working as a rope drum in order to pull a weight of 588.6 N (mass 60 kg). Three trials were carried out during each single experiment to measure how long it took to pull the weight up to a height of 100.5 cm (two revolutions of the rope drum) depending on the adjusted wind speed. Wind wheel velocity is calculated using the distance, H =100.5 cm, divided by the circumference of the pulley (50.25 cm) and the average time. Then the result is multiplied by the amount of the total speed reduction ratio (rw). The work (W) equals the force ($F_T$ = weight = 588.6 N) multiplied by the distance (H = 100.5 cm). To determine the output power ($P_{mw}$), the amount of work (W) must be divided by the average time (t).

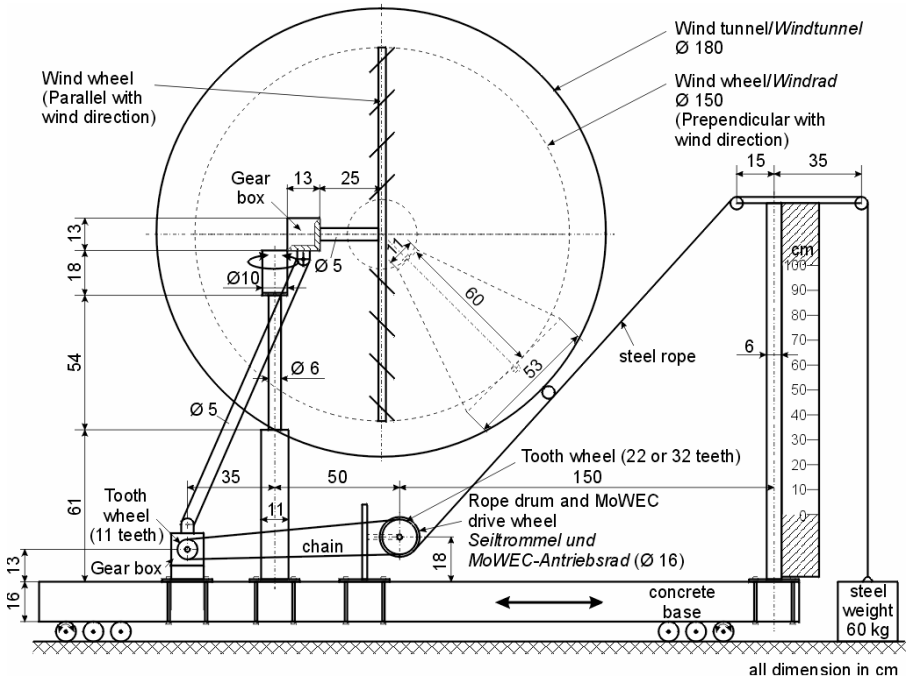


Figure 4.2: Components of the lee-wind wheel experiment.

*Komponenten des Lee-Windrad-Experiments.*

Wind tunnel opened View inside the wind tunnel with θ = 90°

Figure 4.3: Wind tunnel test of the MoWEC - lee - wheel. [OMARA (2003)]

*Windkanaltest des MoWEC - Leerades.*

**Experimental procedures**

1. Construction of the lee-wind wheel system and the wind tunnel according Figure 4.2 and Figure 4.3.
2. Adjust the lee-wind wheel system in the wind tunnel at reduction ratio rw of 56.28:1, using 22 teeth in the third gear stage.
3. Adjust the wind wheel blades at an angle φ of 15° to the shaft on which it rotates, using a protractor.

4. Operate the wind tunnel air system to achieve a constant wind speed and record it with a bowl anemometer. Watch the weight position and if there is a movement measure the time for the vertical distance of 100.5 cm, repeat this three times at the same wind speed and perform the mathematical calculation.
5. Compute the measured average time for the weight heights 100.5 cm.
6. Calculate the output power $P_{mw}$ of the lee-wind wheel system, use the power formula,

$$P_{mw} = \frac{F_T \cdot H}{100\ t} \qquad [W]$$

where:

$F_T$ = Force (weight), 588.6 [N ]

$H$ = Distance (height), 100.5 [cm]

$t$ = Measured time in sec

7. Calculate the pulley ( MoWEC drive wheel) rotational speed $n_4$,

$$n_4 = \frac{60\ H}{2\pi \cdot r_p \cdot t} \qquad [rpm]$$

where: $r_p$ is the pulley radius, 8 [cm]

8. Calculate the wind wheel rotational speed ($n_1$) by;

$n_1 = n_4 \cdot rw$ [rpm],

where: rw is the reduction ratio

9. Calculate the wind wheel measured power coefficient $C_{pm}$ by using the equation:

$$C_{pm} = \frac{2\ P_{mw}}{\rho_{air} \cdot \pi \cdot R_{wo}^2 \cdot v_1^3}$$

where:

$P_{mw}$ = Measured output power [W]

$R_{wo}$ = Wind wheel outer ring radius, 0.75 [m]

$\rho_{air}$ = Air density, 1.225 [kg/m³]

$v_1$ = Measured wind speed in front of the wind wheel [m/s]

10. Record the data at different wind speed levels from 2.0 to 8.2 m/s in steps of 0.5 m/s approximately.
11. Change the fixed position of the lee-wind wheel inside the wind tunnel to realize different angles ($\theta$ = 10°, 20°, 30°, 40°, 50°, 60°, 70°, 80° and 90°) between the wind direction and the lee-wind wheel.
12. Repeat the record at different wind speeds.
13. Change the reduction ratio rw to 82.64:1 at the third gear stage using 32 instead of 22 teeth.
14. Repeat the record at different wind speed levels.
15. Carry out the experiment at wind wheel blade angles $\varphi$ of 22.5°, 35° and 45° and repeat all records.

### 4.1.2 Result and Discussion

The main purpose of our own experiments was to design and to test the described wheel in order to give a technical recommendation for its use as a lee-wind wheel which shall be installed on the available MoWEC yaw drive system to hold the two MoWEC rotors reliably in the expected wind direction. The effect of different wind velocities and different angles θ and φ influences the driven force of the later driven wheel (rope drum in the test) on the MoWEC ball race. The question of which reduction ratio rw should be used has been answered as well. The variables were:

1. Angle φ = 15°, 22.5°, 35° or 45°
2. Angle θ = 10°, 20°, 30°, 40°, 50°, 60°, 70°, 80° and 90°
3. Change wind velocity from 2.0 to 8.2 m/s
4. Use the reduction ratio rw = 56.82:1 and 82.64:1

The presented results will be arranged and discussed depending on the purpose. Figures 4.4 to 4.11 show the data measured during the wind wheel experiment. The wind speed $v_1$ [m/s] was measured at the center of the wind tunnel; and the time t [min] required to lift the weight 588.6 N over a vertical distance of 100.5 cm was measured with the aid of a stopwatch.

All Figures 4.4 to 4.11 show the time required to lift the weight of 588.6 N over a vertical distance of 100.5 cm at various wind speeds, measured in the center of the wind tunnel when changing the angle between the lee-wind wheel and the wind direction θ from 90° (wind wheel stands perpendicular to the wind direction) to zero degree (wind wheel stands parallel to the wind direction). The two following Figures have the same blade angle φ but a different reduction ratio 56.82:1 or 82.64:1.

**Figure 4.4 and Figure 4.5 at a blade angle φ = 15°**: These curves illustrate the beginning of the wind wheel turn (called **cut-in speed** below), depending on the angles θ and φ. As expected, the cut-in speed begins early in position θ = 90° at $v_1$ = 2.6 m/s in Figure 4.4 (rw = 56.82:1) and a little bit earlier at $v_1$ = 2.3 m/s in Figure 4.5 (rw = 82.64:1). At vertical heights of 100.5 cm, it needs 7.5 min in Figure 4.4 or 17.8 min in Figure 4.5. Cut-in speed was measured up to θ = 30° with $v_1$ = 6.5 m/s in Figure 4.4 and up to θ = 20° at $v_1$ = 8.0 m/s in Figure 4.5.

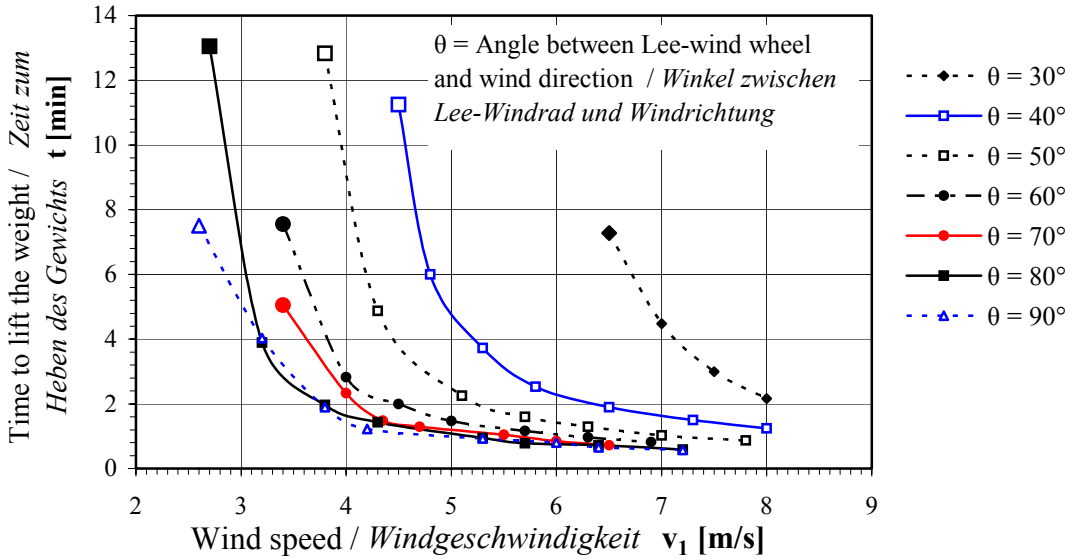


Figure 4.4: Time required to lift 588.6 N over a vertical distance of 100.5 cm. Blade angle φ = 15° and reduction ratio 56.82:1.

*Zeitbedarf zum Heben von 588,6 N über eine vertikale Höhe von 100,5 cm. Blattwinkel φ = 15° und Untersetzungsverhältnis 56,82:1.*

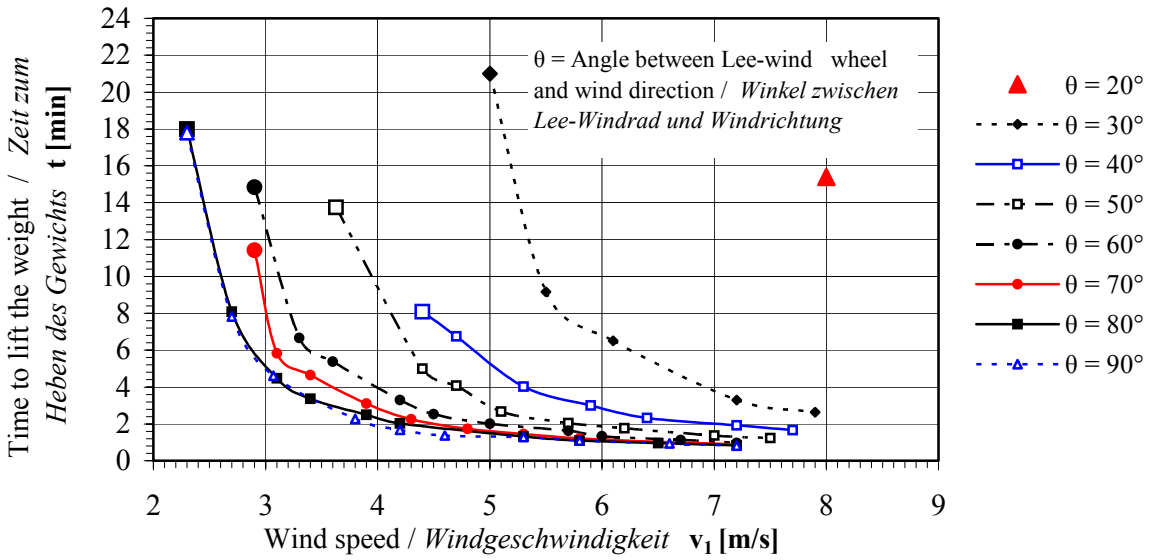


Figure 4.5: Time required to lift 588.6 N over a vertical distance of 100.5 cm. Blade angle φ = 15° and reduction ratio 82.64:1.

*Zeitbedarf zum Heben von 588,6 N über eine vertikale Höhe von 100,5 cm. Blattwinkel φ = 15° und Untersetzungsverhältnis* 82,64:1.

**Figure 4.6 and 4.7 at a blade angle φ = 22.5°:** As expected, the cut-in speed begins early in position θ = 90° at $v_1$ = 2.6 m/s in both Figures 4.6 and 4.7 (rw = 56.82:1 and 82.64:1). For the vertical heights of 100.5 cm, it needs 12.33 min in Figure 4.6 or 8.50 min in Figure 4.7.

Cut-in speed was measured up to θ = 20° at $v_1$ = 7.5 m/s in Figure 4.6 and up to θ = 10° at $v_1$ = 8.2 m/s in Figure 4.7.

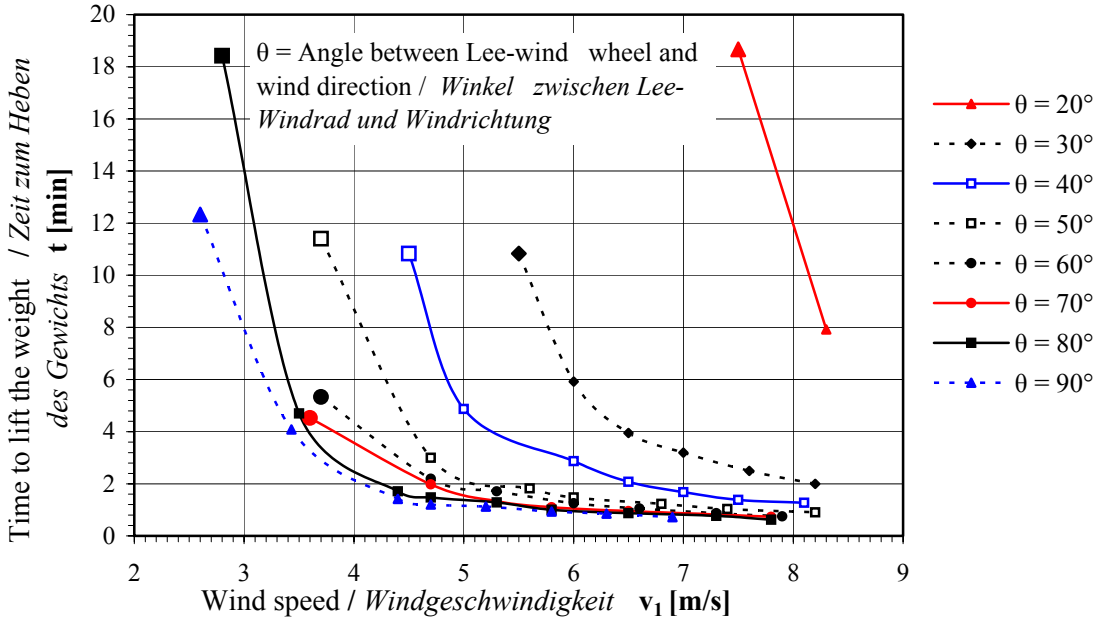


Figure 4.6: Time required to lift 588.6 N over a vertical distance of 100.5 cm. Blade angle φ = 22.5° and reduction ratio 56.82:1.

*Zeitbedarf zum Heben von 588,6 N über eine vertikale Höhe von 100,5 cm. Blattwinkel φ = 22,5° und Untersetzungsverhältnis 56,82:1.*

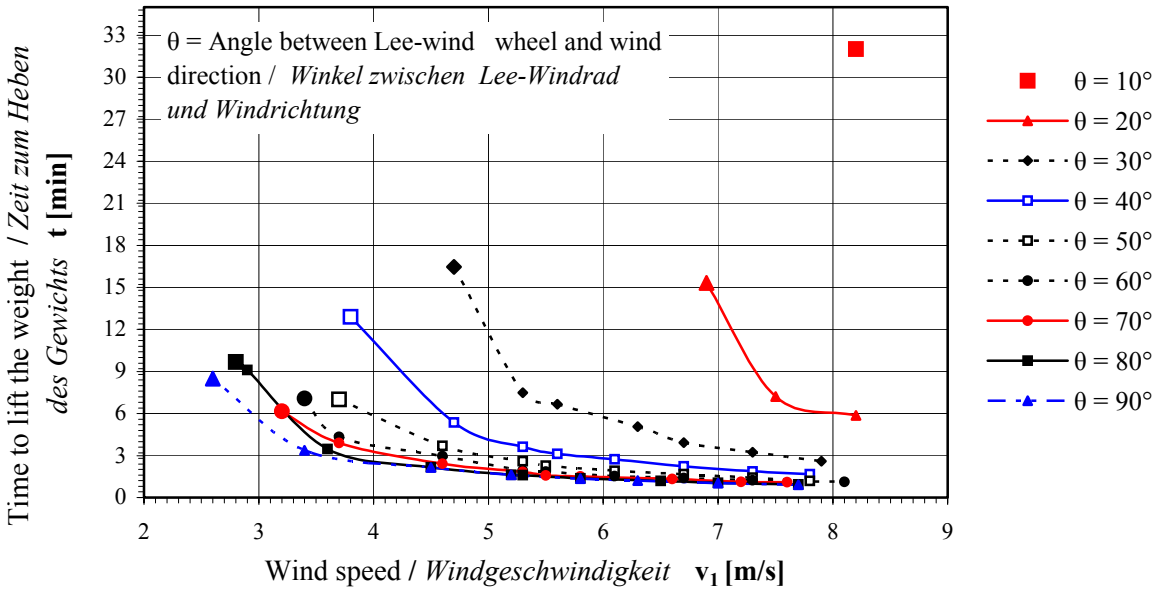


Figure 4.7: Time required to lift 588.6 N over a vertical distance of 100.5 cm. Blade angle φ = 22.5° and reduction ratio 82.64:1.

*Zeitbedarf zum Heben von 588,6 N über eine vertikale Höhe von 100,5 cm. Blattwinkel φ = 22,5° und Untersetzungsverhältnis 82,64:1.*

**Figure 4.8 and Figure 4.9 at a blade angle φ = 35°**: These curves illustrate that the cut-in speed begins early in position θ = 90° at $v_1$ = 2.6 m/s in Figure 4.8 (rw = 56.82:1) and a little bit later at $v_1$ = 2.7 m/s in Figure 4.9 (rw = 82.64:1). For the vertical heights of 100.5 cm, it needs 12.48 min in Figure 4.8 or 12.3 min in Figure 4.9. Cut-in speed was measured up to θ = 20° at both reduction ratios (rw = 56.82:1 or 82.64) at $v_1$ = 7.9 m/s in Figure 4.8 and $v_1$ = 6.9 m/s in Figure 4.9.

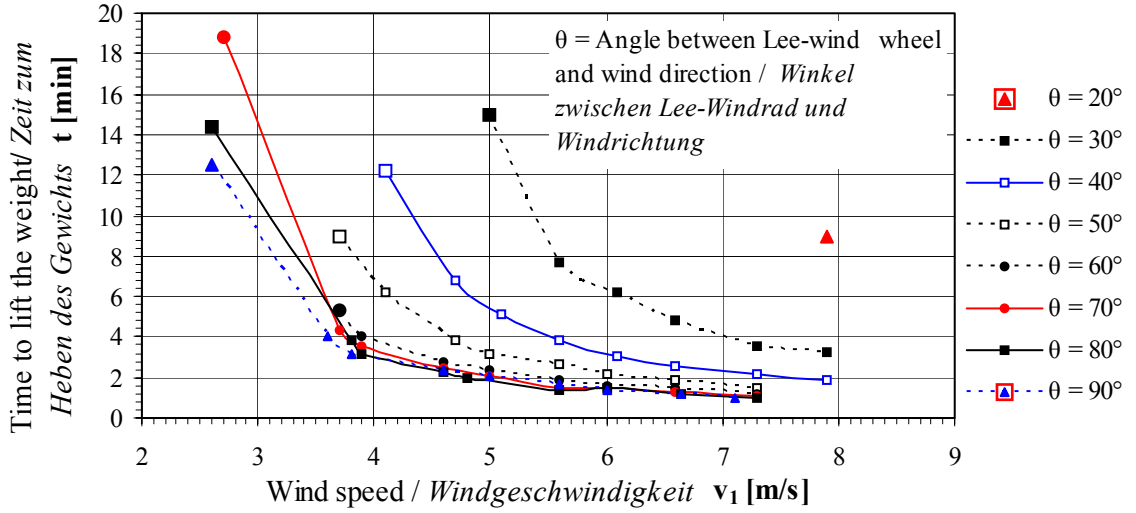


Figure 4.8: Time required to lift 588.6 N over a vertical distance of 100.5 cm.
Blade angle φ = 35° and reduction ratio 56.82:1.
*Zeitbedarf zum Heben von 588,6 N über eine vertikale Höhe von 100,5 cm.*
*Blattwinkel φ = 35° und Untersetzungsverhältnis 56,82:1.*

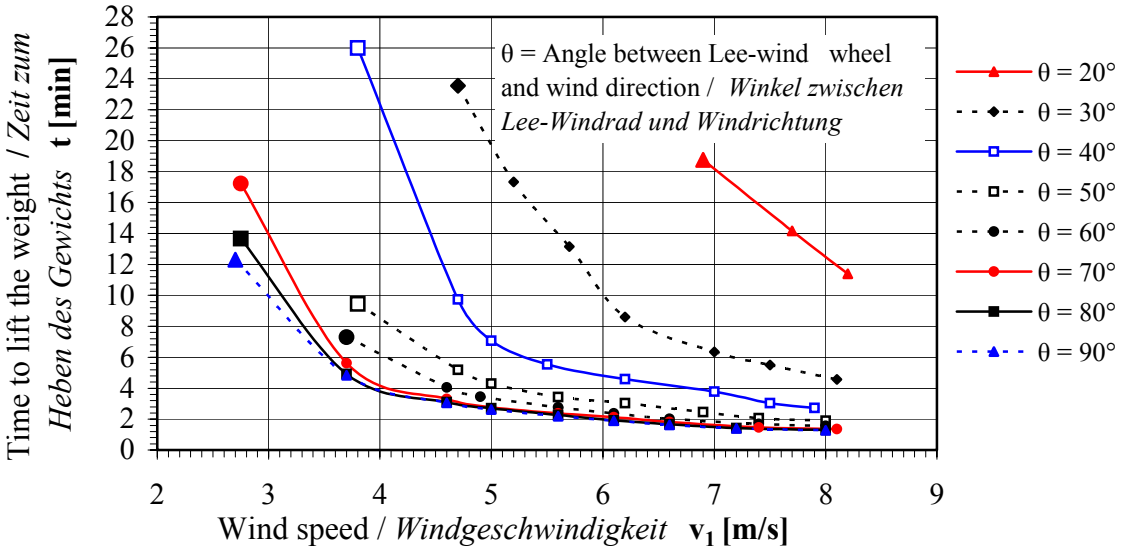


Figure 4.9: Time required to lift 588.6 N over a vertical distance of 100.5 cm.
Blade angle φ = 35° and reduction ratio 82.64:1.
*Zeitbedarf zum Heben von 588,6 N über eine vertikale Höhe von 100,5 cm.*
*Blattwinkel φ = 35° und Untersetzungsverhältnis* 82,64:1.

**Figure 4.10 and Figure 4.11 at a blade angle φ = 45°**: These curves show that the cut-in speed begins early in position θ = 90 at $v_1$ = 3.3 m/s in Figure 4.10 (rw = 56.82:1) and a little bit earlier at $v_1$ = 2.9 m/s in Figure 4.11 (rw = 82.64:1). For vertical heights of 100.5 cm, it needs 8.07 min in Figure 4.10 or 13.53 min in Figure 4.11. Cut-in speed was measured up to θ = 20° at both reduction ratios (rw = 56.82:1 or 82.64) at $v_1$ = 7.96 m/s in Figure 4.10 and $v_1$ = 7.0 m/s in Figure 4.11.

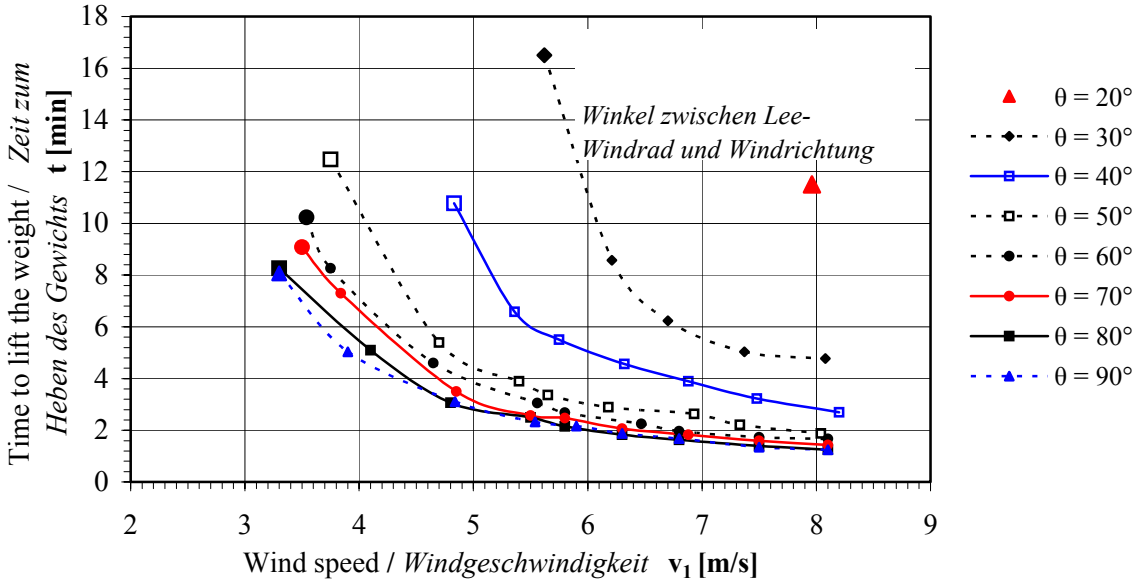


Figure 4.10: Time required to lift 588.6 N over a vertical distance of 100.5 cm. Blade angle φ = 45° and reduction ratio 56.82:1.

*Zeitbedarf zum Heben von 588,6 N über eine vertikale Höhe von 100,5 cm. Blattwinkel φ = 45° und Untersetzungsverhältnis 56,82:1.*

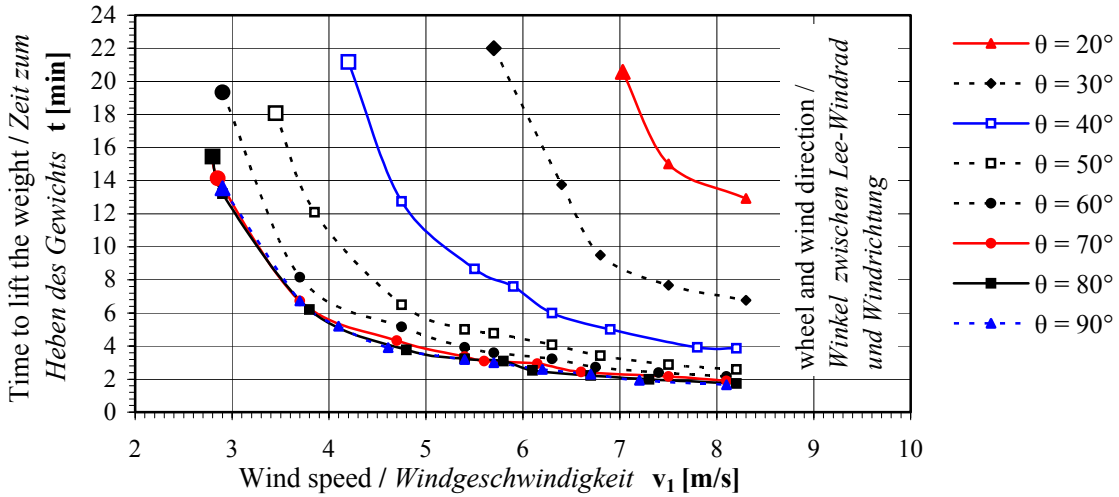


Figure 4.11: Time required to lift 588.6 N over a vertical distance of 100.5 cm. Blade angle φ = 45° and reduction ratio 82.64:1.

*Zeit zum Heben von 588,6 N über eine vertikale Höhe von 100,5 cm. Blattwinkel φ = 45° und Untersetzungsverhältnis 82,64:1.*

The wind tunnel data of the lee-wind wheel experiments were analysed with the aid of an SAS statistic program. The statistical analysis indicated that the effect of the wind wheel blade angle φ on the time required by the lee-wind wheel to lift 588.6 N, the power coefficient and the cut-in wind speed at wheel position angles of less than θ = 70° was highly significant. However, it was not significant if the wheel position angles were larger than lift 588.6 N, the power coefficient and the cut-in wind speed at wheel position angles of less than θ = 70°. In addition, it is indicated that the wind wheel blade angle φ = 22.5° is the optimal angle with all speed reduction ratios 56.82:1 and 82.64:1.

Table 4.1 shows the summary of the wind tunnel results. The results are that a blade angle φ = 22.5° is optimal and that the reduction ratio rw = 82.64:1 allows the cut-in wind speed to be reached even at wind wheel position angles of less than θ = 20°. Then the lee-wind wheel system transforms enough energy to lift 588.6 N even at the position θ = 10°. Therefore the measured power coefficient of the lee-wind wheel is 0.1 % at φ = 22.5° in position θ = 10° with rw = 82.64:1. But this power coefficient value equals zero when the blade angle was 15°, 35° or 45°. Installed on MoWEC with rw = 82.64:1, the wind wheel would have a total reduction ratio of 1371:1. The results in Figure 4.1 also show that with the total reduction ratio and with the choice of another diameter of the lee-wind wheel the demands of energy of different MoWEC yaw drive systems can be fulfilled [OMARA and IRPS (2003)].

Another question is what will happen in practice if this lee-wind wheel system is installed on the present MoWEC wind energy plant, which has two fast- running rotors having a diameter of 7.10 m each. The measured mass of the construction at the position of the MoWEC ball race was 2950 kg but it can be expected that future designs will not be so heavy. This provides the advantage that instead of 588.6 N the force delivered by the lee- wind wheel system can be lower. The towers of MoWEC also stand in a lee-position. And therefore the installed lee-wind wheel system gets support from the wind power because the wind attacks the rotor wings and the towers. If the two rotors start to turn, the rotor area increases to a total of 2 x 40 m² = 80 m², which results in the rotor being to rotate and hold the MoWEC in the correct wind position. The installed lee-wind wheel system has a function which allows it to stop if quick changes of the wind direction occur.

An important description of the rotor area in the wind can be found in Figure 4.12 through the function $A_{ef} = A \times \cos \theta$ [m²], where $A_{ef}$ is the MoWEC-rotors effective area, A is the MoWEC-rotors´ swept area (80 m²) and θ is the angle between the MoWEC-rotor axles and the wind direction. If the wind direction is parallel to the rotor axle, then cos θ = cos 0° = 1. Therefore $A_{ef} = A = 80$ m², and 100% of the rotor area stands rectangular to the wind. If wind direction and rotor axles are at an angle of 20°, for example, the resulting values are $A_{ef} = A \times \cos 20° = 75.18$ m² and 93.97% if the rotor area stands rectangular to the wind. If

the angle is 30°, for example, the results are $A_{ef}$ = 69.28 m² and 86.60 %. If the angle is 60° the value is $A_{ef}$ = 40 % and 50 % of the total rotor area. These results indicated that with the lee-wind wheel system installed on the MoWEC yaw drive frame, the correct position is not always found at speeds below the MoWEC cut-in wind speed. The loss of area measured in square metres is in minimal. On the other hand, Figure 4.12 shows that for storm safety at least 60° to 90° must be reached in order to reduce the rotor area $A_{ef}$ significantly.

Table 4.1: Summary of wind tunnel results.
*Zusammenfassung der Windkanalergebnisse.*

| Angle between wind wheel and wind direction **θ** | Cut-in wind speed, required time and power coefficient **$v_1$ , t , $C_{pm}$** | | Wind wheel blades angle φ | | | | | | | |
|---|---|---|---|---|---|---|---|---|---|---|
| | | | φ = 15° | | **φ = 22.5°** | | φ = 35° | | φ = 45° | |
| | | | **rw** 56.82:1 | **rw** 82.64:1 | **rw** 56.82:1 | **rw** **82.64:1** | **rw** 56.82:1 | **rw** 82.64:1 | **rw** 56.82:1 | **rw** 82.64:1 |
| θ = 90° | **$v_1$** | [m/s] | 2.60 | 2.30 | 2.60 | **2.60** | 2.60 | 2.70 | 3.30 | 2.90 |
| | **t** | [min] | 7.50 | 17.80 | 12.33 | **8.50** | 12.48 | 12.30 | 8.07 | 13.53 |
| | **$C_{pm}$** | [%] | 6.90 | 4.20 | 4.20 | **6.10** | 4.20 | 3.80 | 3.10 | 2.80 |
| θ = 30° | **$v_1$** | [m/s] | 6.50 | 5.0 | 5.50 | **4.70** | 5.0 | 4.70 | 5.62 | 5.70 |
| | **t** | [min] | 7.28 | 21.0 | 10.83 | **16.47** | 15.0 | 23.55 | 16.50 | 22.0 |
| | **$C_{pm}$** | [%] | 0.50 | 0.3 | 0.50 | **0.50** | 0.5 | 0.40 | 0.30 | 0.20 |
| θ = 20° | **$v_1$** | [m/s] | - | 8.00 | 7.50 | **6.90** | 7.90 | 6.90 | 7.96 | 7.00 |
| | **t** | [min] | - | 16.05 | 18.67 | **15.33** | 8.92 | 18.75 | 11.50 | 20.58 |
| | **$C_{pm}$** | [%] | - | 0.10 | 0.10 | **0.20** | 0.20 | 0.10 | 0.10 | 0.10 |
| θ = 10° | **$v_1$** | [m/s] | - | - | - | **8.20** | - | - | - | - |
| | **t** | [min] | - | - | - | **32.00** | - | - | - | - |
| | **$C_{pm}$** | [%] | - | - | - | **0.10** | - | - | - | - |

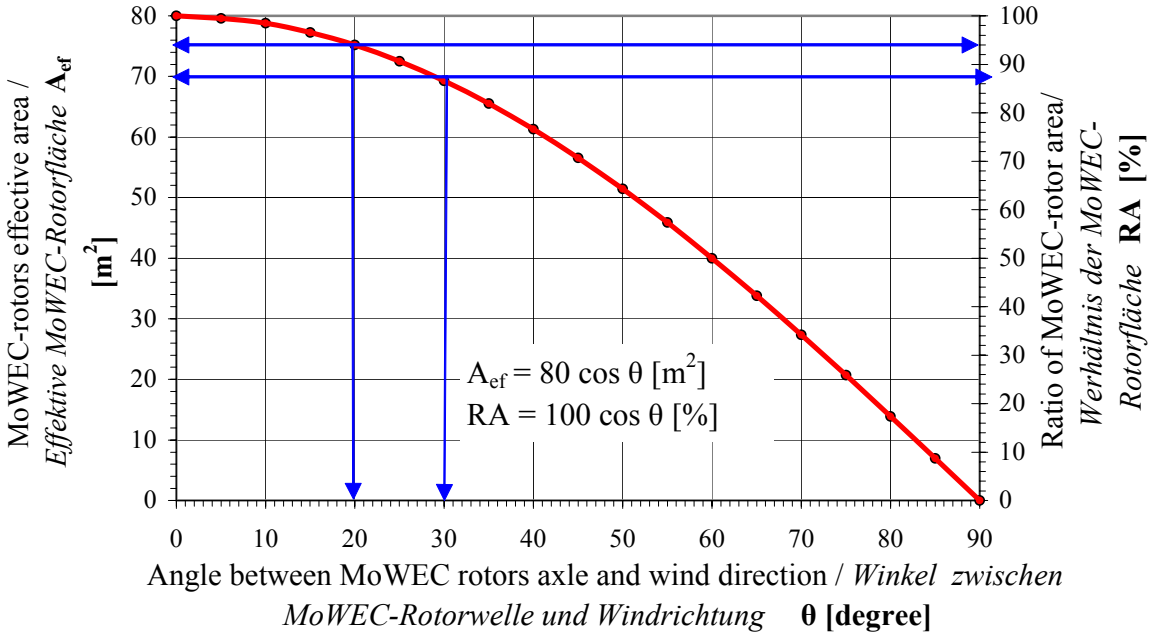


Figure 4.12: MoWEC-rotors effective area as a function of the angle to the wind direction.
*Effektive Fläche der MoWEC-Rotoren als Funktion des Winkels zur Windrichtung.*

Figure 4.1 shows the lee-wind wheel system, installed on the yaw drive frame. The wind wheel drives the roll wheel which rotates on a circular rack (MoWEC ball race) anchored on the ground. If the MoWEC rotors are not facing the wind, the wind will strike the lee-wind wheel, causing it to rotate, slowly turning the rotor towers of the MoWEC into the wind. The motion will stop when the wind wheel stands parallel to the wind.

The data obtained from the lee-wind wheel tests in the wind tunnel were used as the database for the development of a yaw drive system for MoWEC. Figures 4.13 and 4.14 show photos of the lee-wind yaw drive system after construction and installation in the year 2002. This configuration was used to measure the power curve.

Figure 4.13: Installed lee-wind wheel on the MoWEC yaw drive system.
*Installiertes Lee-Windrad am MoWEC-Windnachführungsrahmen.*

Figure 4.14: Drive roll wheel of the yaw drive system.
*Antriebsrad des Windnachführungsrahmens.*

Figure 4.15 shows a diagram for the MoWEC operation position. The lee-wind wheel is installed like in Figure 4.16 with its axle rectangular to the wind direction and shows no motion in that position. If the wind direction changes, the lee-wind wheel blades get wind power and the yaw drive system can turn back into the correct wind position [OMARA (2004d)].

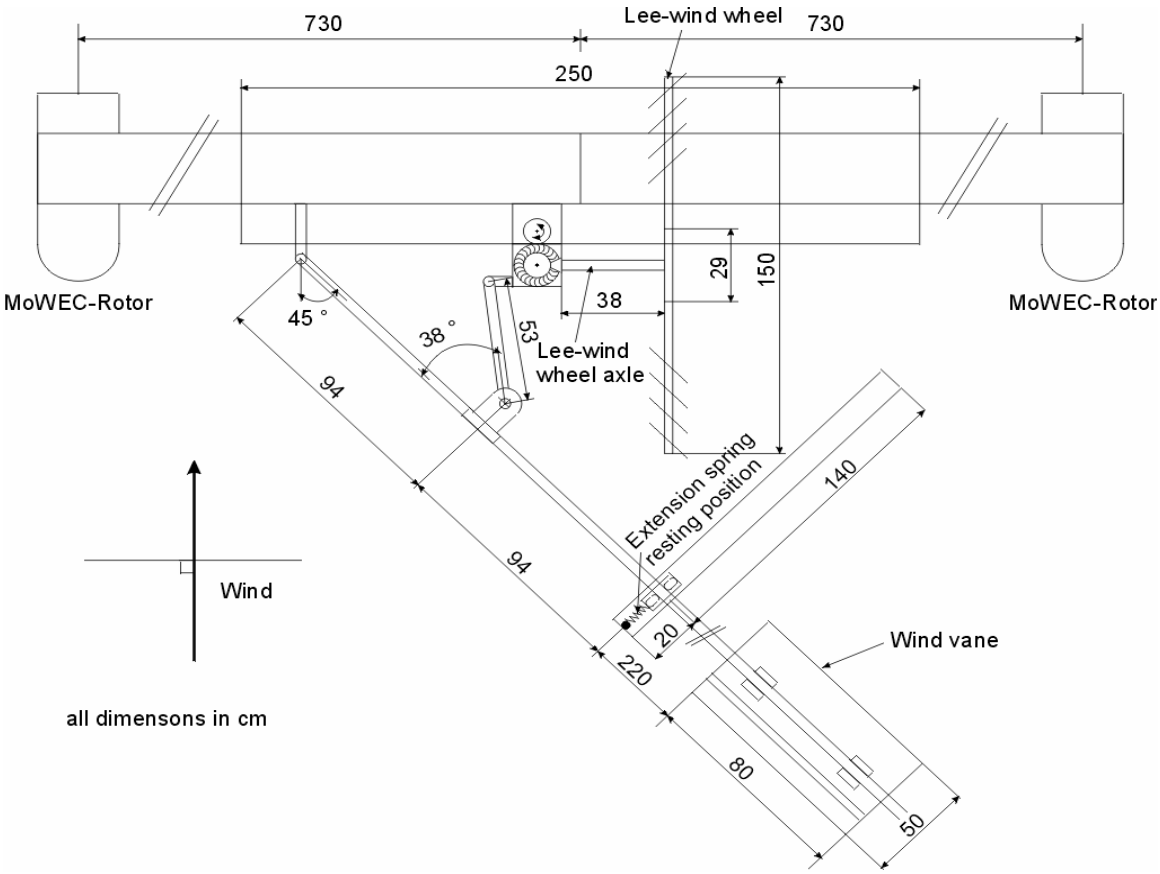


Figure 4.15: Installation of a wind vane which turns the lee-wind wheel out of the basic position.

*Installation einer Windfahne, um das Lee-Windrad aus der Basisposition drehen zu können*

Figure 4.16: Lee-wind wheel in basic position up to the rated power.

*Lee-Windrad in der Basisposition bis zur Nennleistung.*

Figures 4.17 and 4.18 show the storm position, changed as compared with Figure 4.15 through the force of the wind wheel (wind vane). The number of square meters of the wind wheel is a function of the wind velocity and the spring force. This part of construction depends on the other safety systems of the MoWEC system.

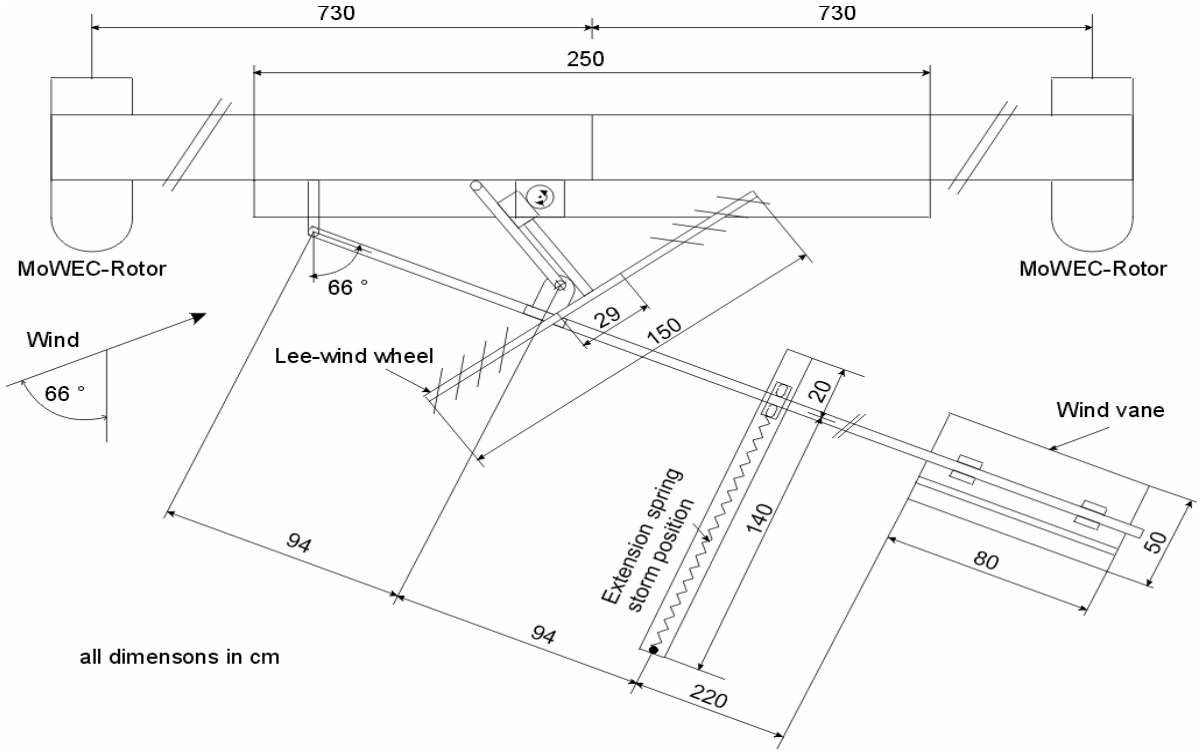


Figure 4.17: Wind vane in the storm position.
*Windfahne in der Sturmposition.*

Figure 4.18: Lee-wind wheel in storm position for MoWEC safety.
*Lee-Windrad in der Sturmposition zur Sicherheit von MoWEC.*

### 4.1.3 Conclusions

**MoWEC** is the prototype of a **mobile wind energy converter** with two rotors, which can be used to capture wind energy at different locations. This MoWEC prototype requires an automatic yaw drive system without an energy store in stand-alone use to move the rotors into the wind at low wind velocities and to move the rotors out of the wind at wind velocities beyond the rated power. To fulfil this demand, a lee-wind wheel yaw drive system was chosen.

Theoretical studies result in a lee-wind wheel featuring eight blades and an outer diameter of $D_{wo} \geq 1.50$ m. This lee-wind wheel was constructed and then tested at different blade angles φ [15°, 22.5°, 35° and 45°] and two-gear reduction ratios rw (56.82:1 or 82.64:1) inside a specially built wind tunnel at different angle positions θ between the lee-wind wheel and the air stream. The different angle positions θ between the lee-wind wheel and the direction of the air stream in the wind tunnel should reflect the field application of the MoWEC yaw drive frame.

The main results of the lee-wind wheel wind tunnel experiments indicated that the blade angle φ should be 22.5 degrees and that the reduction ratio should be rw = 82.64:1. At these values, the lee-wind wheel is able to work well even at angle positions below θ = 20°, which are required to lift a weight of 588.6 N in position θ = 10°, for example. This weight stands for the tangential force needed to move the MoWEC yaw drive frame with its two rotors. At this position, the measured power coefficient was $C_{pm}$ = 0.1 %, but this power coefficient value equalled zero when the blade angles were 15°, 35° or 45°.

The installation of the lee- wind wheel system with rw = 82.64:1 on the MoWEC yaw drive frame results in a total reduction ratio of 1371:1. The field test proved that a modern wind energy converter works well with a lee-wheel yaw drive system in stand alone use and that this technique can also be recommended for the reduction of the effective rotor area at very high wind velocities. When the MoWEC rotors are facing the wind, the lee-wind wheel does not rotate. In this case, the theoretical angle θ is zero. At this position, no power is needed for the yaw drive system.

## 4.2 Measurement of the MoWEC power curve

To forecast the energy yield of a MoWEC-prototype, the power curve is used as the technical characteristic for the evaluation of the available power output depending on the wind speed at hub height and other relevant meteorological parameters. In addition, these measurements are necessary to define the performance of the prototype, in particular the power coefficient value.

### 4.2.1 Material and method

#### 4.2.1.1 Experimental conditions

First power measurements MoWEC were carried out under stand-alone conditions with a permanent-magnet synchronous generator. The current is converted into heat over heating elements, Figure 4.19. A benefit of this application is that one needs no special requirements to guarantee the stability of frequency and voltage. The transformation of electricity into heating energy provided by the MoWEC generator is substantially more economical in relation to the network power supply and can preferably be used where users requires heating energy. However, if the electricity is to be fed into the public electricity mains, the variable voltages and frequencies must be converted before into net quality by a three-phase inverter with fully controlled thyristor bridge connection.

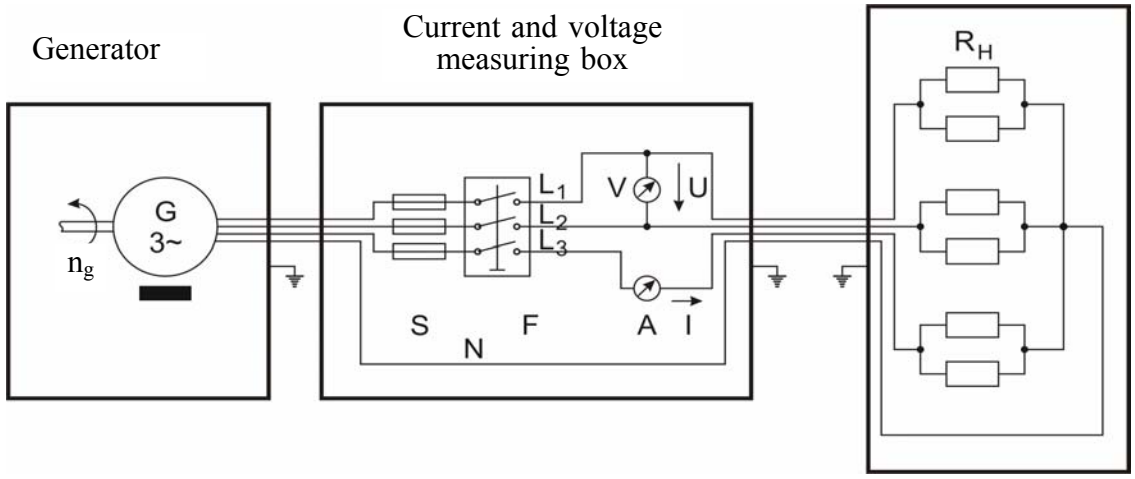


G = three-phase generator / *Drehstromgenerator*
$n_g$ = rotational speed / *Drehzahl*
S = fuse / *Sicherung*
F = main switch / *Hauptschalter*
$L_1$, $L_2$, $L_3$ = three-phase current lines / *Drehstromleitungen*
N = neutral conductor / *Neutralleitung*
V = voltmeter / *Voltmeter*
A = ammeter / *Amperemeter*
$R_H$ = six heating elements / *6 Heizwiderstände*

Figure 4.19: Electric circuit diagram (Generator and electrical consumer in star-connection). *Elektrischer Schaltplan ( Generator und Verbraucher in Sternschaltung).*

### 4.2.1.2 Experiment components

#### 4.2.1.2.1 Electrical generator

The electrical generator used fulfills the international safety class system IP 55 (dust and water protected). This speed-variable generator has its own air-cooling. It is a 10-pole (5 pairs of poles) generator, which achieves a frequency of 50 Hz at the rotational speed of 600 rpm.

The MoWEC synchronous generator achieves the rated power (9 kW) at a speed of 540 rpm. Measured voltage during rated power generation was 400 V. Under the condition of sufficient air cooling, the speed of the generator can be increased to up to 700 rpm with a voltage under load ($U_L$) of 505.5 V. Figures 4.20 to 4.23 show the generator characteristics of the 10-pole permanent magnet three phase current synchronous generator DSG P 160.20-145 [manufacturer: Hübner, Fabrik elektrischer Maschinen, Giessen, Germany (2002)].

This synchronous generator is calculated only for one MoWEC rotor, which has a diameter of 7.10 m. But the generator was still installed on the MoWEC prototype with two rotors in order to determine the average power coefficient for MoWEC and to test the MoWEC components at moderate wind velocities. The total weight of the generator is about 137 kg, heavier than other generator types.

During the calibration of this generator in the laboratory, the rotational speed of the generator, current, voltage, torque and power were measured. Figure 4.20 shows the generator current as a function of the rotational speed. The curve equation is

$$I_g = 0.023\ n_g \quad [\text{Ampere}] \tag{4.2.1}$$

where $I_g$ is the generator output current in [Ampere] and $n_g$ is the generator's rotational speed in [rpm]. From equation (4.2.1), the rotational speed $n_g$ can also be calculated as a function of the current using equation (4.2.2),

$$n_g = 43.5\ I_g \quad [\text{rpm}] \tag{4.2.2}$$

Figure 4.21 and 4.22 show the output generator power and torque as a function of the rotational speed. The curve equations are:

$$P_g = 2 \times 10^{-5}\ n_g^2 + 0.0034\ n_g \quad [\text{kW}] \tag{4.2.3}$$

$$T_g = -9 \times 10^{-5}\ n_g^2 + 0.367\ n_g \quad [\text{Nm}] \tag{4.2.4}$$

where $P_g$ is the generator output power in [kW] and $T_g$ is the generator torque in [Nm].

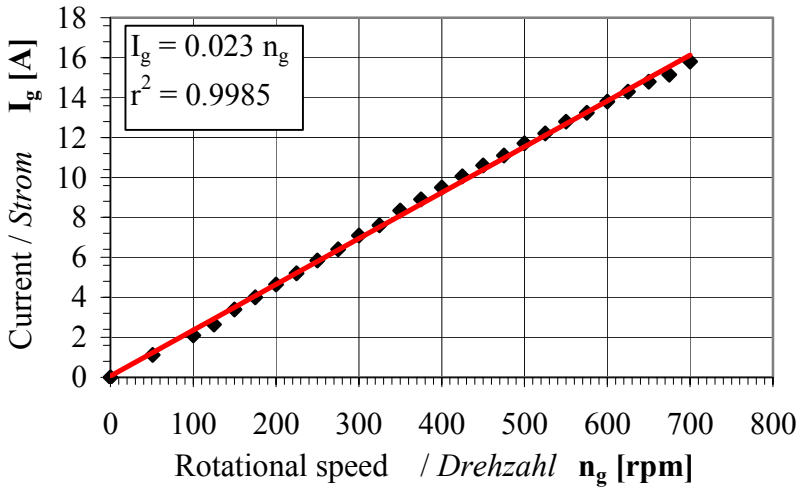


Figure 4.20: Synchronous Generator: Current as function of the rotational speed.
*Synchron-Generator: Strom als Funktion der Drehzahl.*

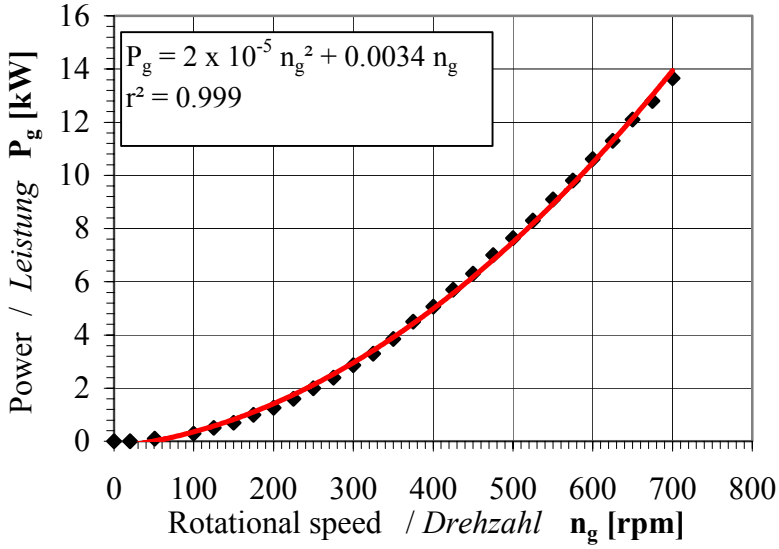


Figure 4.21: Synchronous Generator: Power as function of the rotational speed.
*Synchron-Generator: Leistung als Funktion der Drehzahl.*

As described in chapter 3.1.5, MoWEC was equipped with rotor blades according to the stall principle. Technically, a pitch regulation would have been too expensive. Due to the rigid rotor blade position, the rotor speed thus rises proportionally with the wind velocity. Wind power is proportional to the third power of the wind velocity. An ideal generator would have to be able to follow this increase in output power over all wind velocities if the tip-speed ratio of the rotors remained constant. Figure 4.24 shows a photo of the generator at ground level during the measurement of the MoWEC power curve.

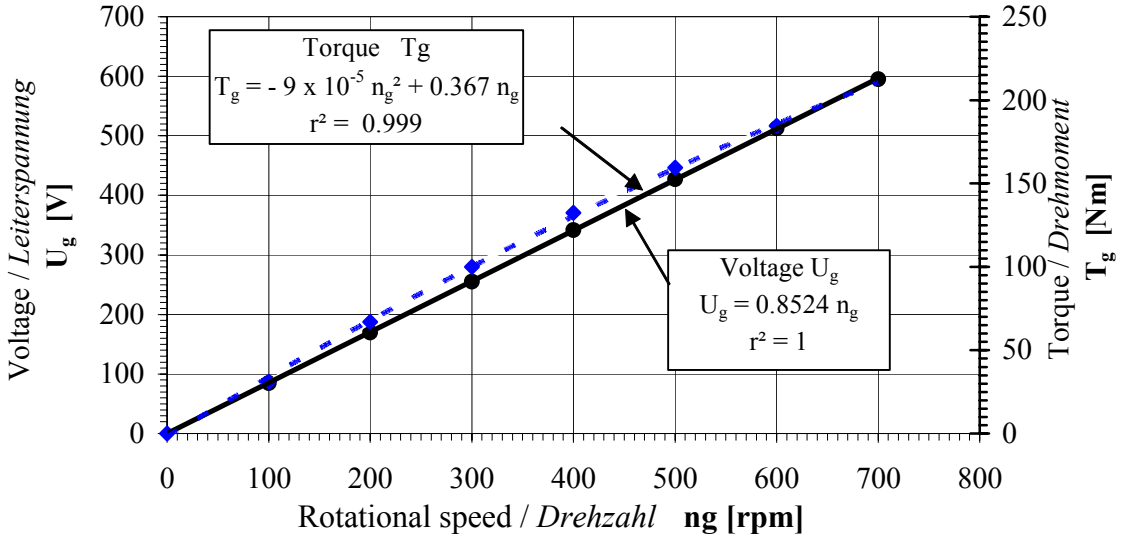


Figure 4.22: Synchronous Generator: Voltage and torque as function of the rotational speed. *Synchron-Generator: Spannung und Drehmoment als Funktion der Drehzahl.*

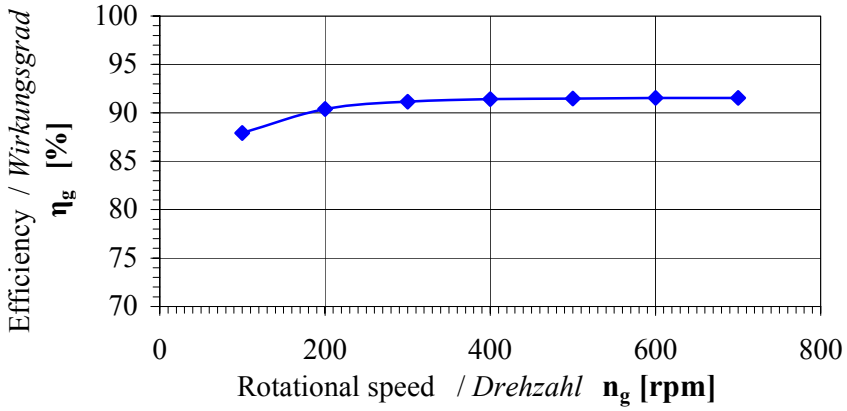


Figure 4.23: Synchronous Generator: Efficiency as function of the rotational speed. *Synchron-Generator: Wirkungsgrad als Funktion der Drehzahl.*

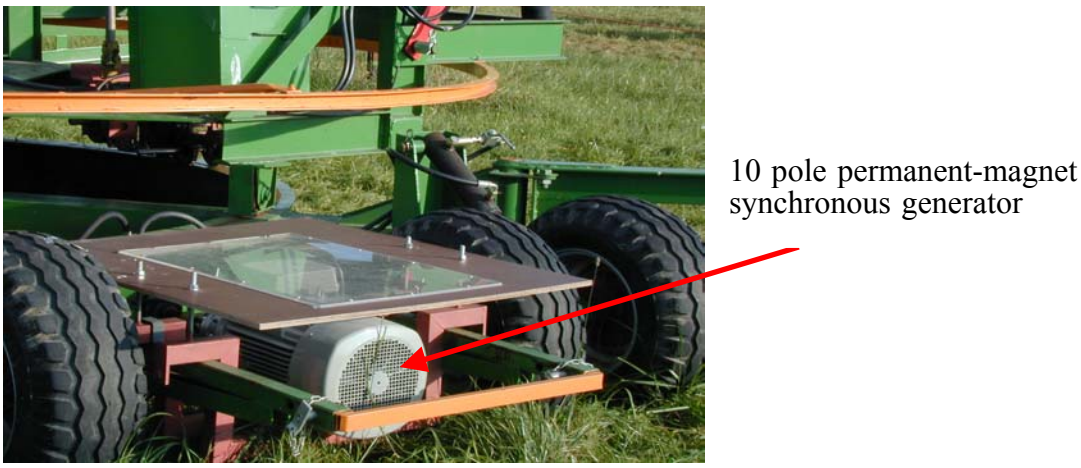


Figure 4.24: Testing the MoWEC power curve with an electrical generator at ground level. *Prüfung der MoWEC Leistungskurve mit einem elektrischen Generator auf Bodenhöhe.*

In reality, compromises must be made, and the technical requirements as well as the financial expenditure must be justifiable. As already mentioned, the generator installed in the MoWEC prototype is particularly suitable for stand alone use, but it can also be used for grid feeding. These arguments speak in favour of the permanent-magnet synchronous generator. The high magnetic field density with relatively small dimensions is created by Samarium-Cobalt-magnets (SmCo). The smallest movement of the magnets will already induce a voltage into the generator, which makes a current flow into the connected heating elements. The connection of the generator results in a star connection at $L_1$, $L_2$, $L_3$ and N. The benefit of this simply built machine is justified by the power, which can be delivered over a large rotational speed range. The life of wearing parts is limited only by the ball bearings of the generator. In addition, this generator design ensures a nearly constant efficiency at high rotational speeds (see Figure 4.23).

#### 4.2.1.2.2 Current and voltage measurement

Fuse and measuring instruments are accommodated in a normal, commercially available switchbox. Figure 4.19 shows the construction of the electrical circuit diagram. The complete fuse box is grounded by a ground rod. The fuse box contains three phases $L_1$, $L_2$ and $L_3$ of the three-phase current, before the main switch S becomes secured by a 16 Ampere fuse. Between two conductors, $L_1$ and $L_2$, a voltmeter measures the voltage U and within the conductors $L_3$ an ammeter measures the current I. The protective conductor N features a simple design and is connected to the resistance heater via the neutral point. Figure 4.25 shows a photo of the fuse and measuring instruments for current and voltage.

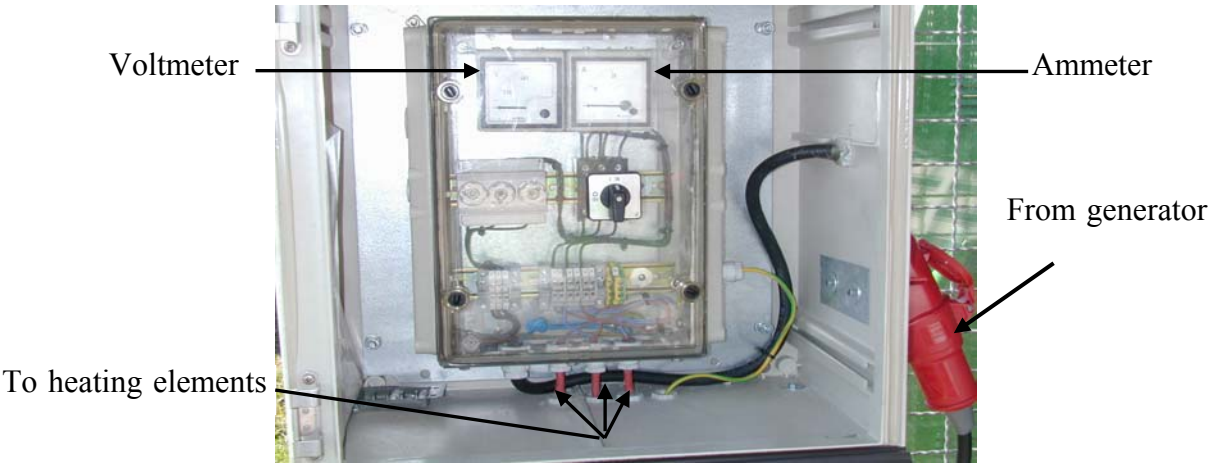


Figure 4.25: Fuse and measuring instruments for current and voltage.
*Sicherung und Messinstrumente für Strom- und Spannungsmessung.*

In addition, a calibrated current clamp VC – 605 [CONRAD (2002)] was used to measure the current I on $L_1$, $L_2$ or $L_3$ (Figure 4.26). A second current measurement, though not calibrated, could take place on $L_3$ according Figure 4.19.

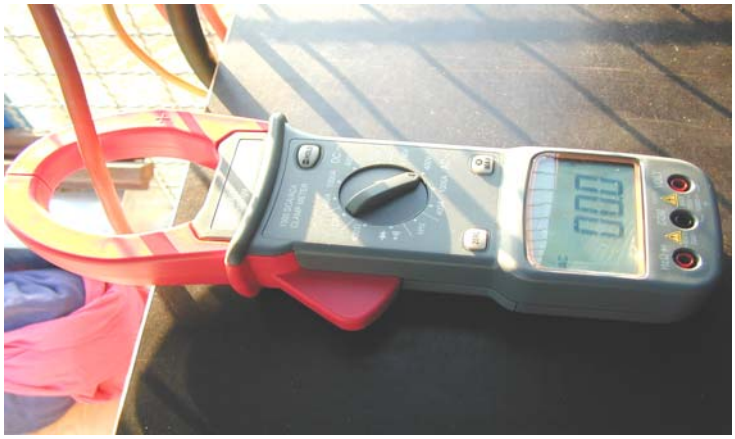

Figure 4.26: Current clamp VC–605.
*Stromzange VC – 605.*

### 4.2.1.2.3 Heating elements

The heating elements are arranged in three phases in parallel connection corresponding to two single ones according to Figure 4.19. The heating elements are made by the company Vulcanic Czepek GmbH, Brown-Boveri-Str. 30, 63457 Hanau, Germany. Each of the six heating elements has a resistance of $R_H$ = 35.2 Ω, providing a heat power of about 1500 W. Figure 4.27 illustrates the geometrical dimension of an individual heating element. The functional diagram is still being prepared by the company Vulcanic Czepek GmbH, Germany (2002). Figure 4.28 shows the housing of the heating elements. The neutral point of the circuit is connected to the protective conductor N (see Figure 4.29). The heating rods are accommodated in a grounded metal housing. The cooling effect is achieved through air convection.

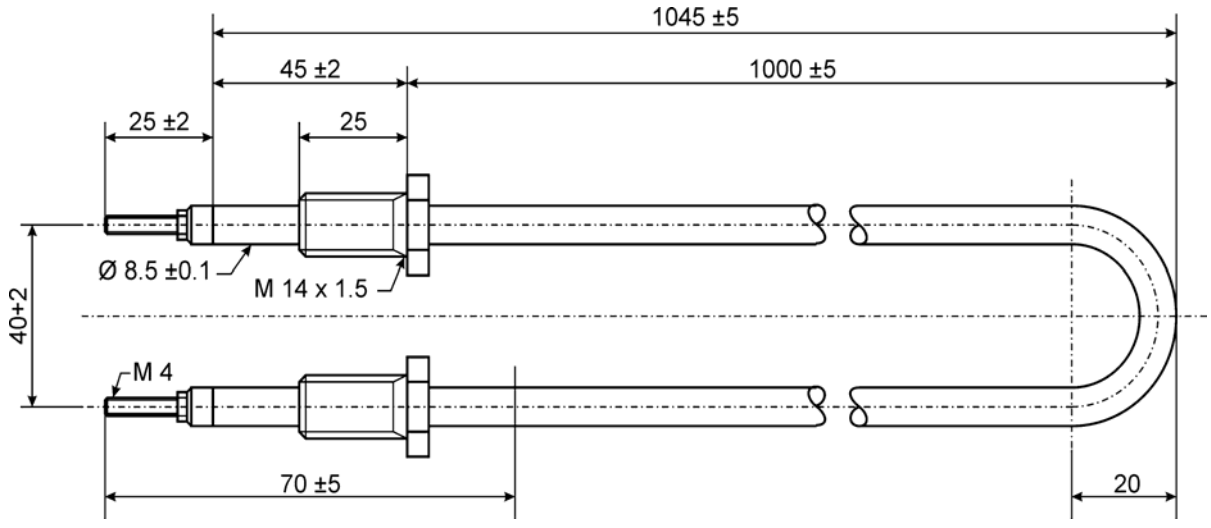


Figure 4.27: Geometrical dimensions of the heating element.
*Geometrische Abmessungen des Heizelementes.*

Figure 4.28: The housing of the heating elements

*Gehäuse für die Heizelemente.*

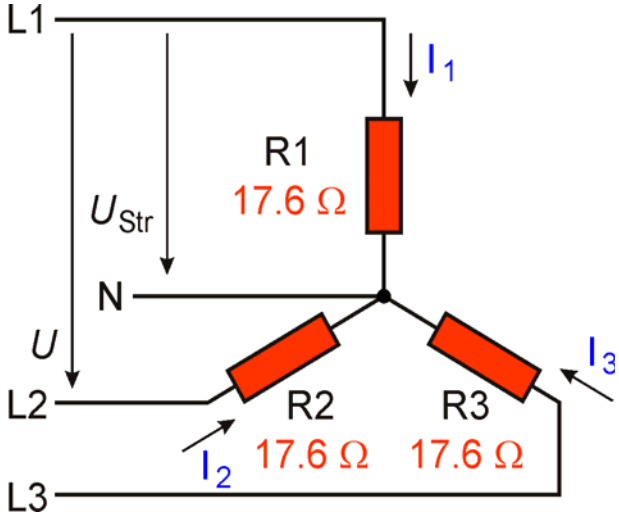


Figure 4.29: Three-phase-current: Star-connected circuit with heating elements.

*Drehstrom-Schaltung von Heizelementen in Sternschaltung.*

The active power in the three-phase current supply is calculated under symmetrical load (Figure 4.29) identically for the y-connection and triangle circuit - according to the formula:

$$P = \sqrt{3} \cdot U \cdot I \cdot \cos \varphi_c \qquad [W]$$

where:

P = active power [W]

U = voltage between two conductors [V], $U = \sqrt{3} \cdot U_{str}$

I = current [A]

$\varphi_c$ = current phase angle [degree]

$\cos \varphi_c$ = power factor (active power)

If a symmetric load on the three heating elements (three same resistors) is present in the circuit, $\cos \varphi_c$ is one ($\cos \varphi_c = 1$). In three-phase current, it is easier to measure the line-to-line voltage than the voltage between one conductor and the neutral point. For current measurement, the ammeter is shifted into the $L_3$ conductor. If the voltage between one conductor and the neutral point is measured, the power in the three-phase current supply is calculated with symmetrical Ohm's load using the formula:

$$P = 3 \cdot P_{phase} = 3 \cdot U_{str} \cdot I \qquad [W]$$

where $U_{Str}$ is the voltage between one conductor and the neutral point (see Figure 4.29). Both equation results have identical values. Under the symmetrical load of a three-phase current supply through heating elements in a star-connection, for example, the neutral conductor N leads no current.

If the generator current is fed into a public grid, one must take voltage in the individual country into account, e.g. according to [SPRINGER (1993)]:

| | | | |
|---|---|---|---|
| Germany | 230/400 Volt, 50 Hz; | Egypt | 220/380 Volt, 50 Hz |
| UK | 240/415 Volt, 50 Hz; | USA | 120/240 Volt, 60 Hz |

#### 4.2.1.2.4 Wind speed measurement

Wind speeds are measured by using a digital three-cup anemometer (made in Germany, type: Wilog 306). This anemometer is fixed on a vertical shaft at the same level as the MoWEC hub (10 m above ground level). The technical data of the anemometer are:

Measuring range: 0.3 to 50 m/s
Accuracy: ± 0.3 m/s ± 2% of measure value
Resolution: 0.3 m/s
Measuring principle: optoelectronic (slotted disk)

### 4.2.1.3 Realization of the experiment

MoWEC was installed on the field on the FAL farm, Braunschweig, Germany, and tested to determine the power curve, the total power coefficient $C_{pt}$ and the rotational speed versus the wind speed. The wind speed was measured every 5 sec by a digital three-cup anemometer. And at each wind speed the electric current output from the generator was measured by a calibrated current clamp.

Data are taken when winds are available. For this reason, a test may be a few minutes long or extend past an hour. These tests were performed on a day-to-day basis. The end result was a large amount of data taken for a wide range of wind conditions over many days. These data for a given generator output current can be combined with the generator performance curves or equations and thus allow the performance of the MoWEC-prototype (output power, total power coefficient $C_{pt}$ and rotational speed) to be computed. The results of the summarized data records are presented in the form of MoWEC output power as a function of wind speed and MoWEC-PTO rotational speed as a function of wind speed. The MoWEC average power coefficient $C_{pt}$ can be calculated from output power and wind power.

### 4.2.2 Results and Discussion

The testing of MoWEC in the field causes problems not usually encountered in wind tunnel tests. In particular, although a special wind wheel enables rotors´s rotational speed to be held when the wind speed exceeds 11 m/s, the atmospheric wind speed seldom remains constant for any appreciable length of time. Consequently, it is difficult to assign an appropriate wind velocity corresponding to a given electric voltage or current measurement from the generator. Consequently, large amounts of data are taken for a wide range of wind conditions over many days.

#### 4.2.2.1 MoWEC-Generator electric current

The directly measured data from field tests of MoWEC were the output electric current from the generator, which was measured by a calibrated current clamp VC – 605 (see Figure 4.26) for each actual wind speed value, which was measured by a digital three-cup anemometer at the level of the MoWEC hub. Figure 4.30 illustrates the typical MoWEC generator electric current as a function of wind speed in field tests. The maximum average current observed was 14.6 Ampere at the rated wind speed of 11 m/s.

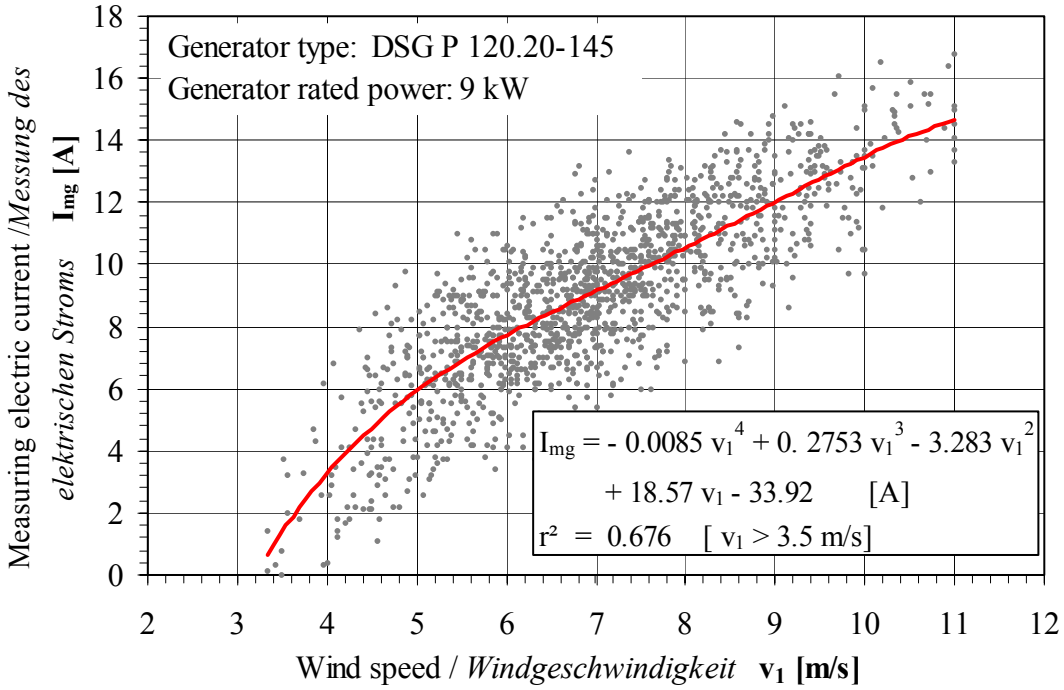


Figure 4.30: Measured MoWEC - Generator current as a function of the measured wind speed. Generator linked with two rotors.
*Gemessener MoWEC - Generatorstrom als Funktion der gemessenen Windgeschwindigkeit. Generator mit zwei Rotoren verbunden.*

### 4.2.2.2 MoWEC rotational speed

Using equation (4.2.2), the MoWEC-PTO rotational speed was calculated at each measuring point of the MoWEC field test (current versus wind speed) in Figure 4.30. Figure 4.31 shows the PTO rotational speed as a function of wind speed based on measured data and the theoretical speed when the tip-speed ratio for MoWEC rotors is 6. The maximum theoretical value of PTO rotational speed at rated wind speed 11 m/s was 540 rpm. However, based on measurement data, the maximum value of PTO rotational speed at rated wind speed 11 m/s was 640 rpm. The rotor's rotational speed could be calculated by dividing the PTO rotational speed by 3 (speed ratio of rotor and PTO = 1:3). In the first case, the rotor speed at rated wind speed was 180 rpm, whereas in the second case it was 213.3 rpm. The difference between the theoretical and measured PTO speed is very small in the low wind speed range from 3.5 to 6.4 m/s and this difference increases at higher wind speeds. This difference is caused by the difference between the generator's rated power (9 kW) and the rated system power of MoWEC (20 kW). In the MoWEC calculation carried out to determine the power coefficient of this generator, which was too small, the wind speed range between 3.5 and 6.4 m/s was considered in our analysis. The developed MoWEC-prototype system would work better if only one rotor was connected with this generator (9 kW rated power). It is therefore recommended to increase the MoWEC rated output power from 9 kW to at least 20 kW. In the future, after the completion of MoWEC development, the MoWEC should work better if one bigger generator set having a rated power of 25 kW is used together with the two rotors to test the MoWEC.

### 4.2.2.3 Power curve and power coefficient of MoWEC

By using the calculated MoWEC-PTO rotational speed, which was determined based on measuring data and equation (4.2.3), one can determine the MoWEC power curve. The power curve for a MoWEC indicates the net power output from a MoWEC as a function of wind speed at hub height. To forecast the energy yield from a MoWEC, the power curve is used as the technical characteristic for the evaluation of the available power depending on the wind speed and other relevant meteorological parameters. Since the working machine, including tooth wheels, chains, gears and bearings has a certain resistance against rotation. WEC units with high tip-speed ratio like the MoWEC rotors used show a low moment-coefficient when still. The data obtained from tests of two three-blade rotors from MoWEC- prototype rotors in the field are presented in the form of generator output power as a function of wind speed in Figure 4.32. MoWEC begins to operate at a certain minimum wind speed, the so-called cut-in wind speed. This speed is defined by the technical design and is 3.5 m/sec but it is 4 m/sec in MoWEC field tests. The power increase slows down up to the rated wind speed ($v_{rated}$) at which the rated power is reached. The typical value of $v_{rated}$ due to the technical design of the rotor and field tests of MoWEC is 11 m/sec. Based on the MoWEC power curve, the nominal rated

power at the rated wind speed ($v_{rated}$) is 10.4 kW for two rotors with small generator (9 kW rated power).

Figure 4.32 shows the measured MoWEC power curve and the theoretical MoWEC power curve which was calculated using equation (3.1.6) based on the MoWEC total power coefficient $C_{Pt} = 0.32$ (which contains the normal wind power coefficient $C_P$, generator efficiency, chain efficiency and gear box/bearing efficiency), the MoWEC-rotor-swept area of 80 m² and the air density of 1.225 kg/m³ (standard density, sea level at 15 °C). Based on the measured power curve, the reactive power varied from 0.4 kW at cut-in wind speed (3.5 m/s) to 10.4 kW at rated wind speed (11 m/s). In addition, these curves show that at low wind speeds ranging from 3.5 to 6.4 m/s the difference between measured power $P_{mg}$ and theoretical power $P_N$ is very small (i.e. $P_{mg} \approx P_N$). But at high wind speed (11 m/s), the theoretical power is two times the measured power and this return to theoretical MoWEC rated power (20 kW) is approximately two times the rated power of the generator (9 kW) at rated wind speed (11 m/s). These curves show that the MoWEC total power coefficient $C_{Pt}$ is 0.32 [IRPS and OMARA (2003)]. The maximum theoretical value of $C_P$ is 0.59, but in practice the maximum value is 0.5 for three-bladed turbines [PATEL (1999)].

MoWEC is a variable-speed wind turbine. There are several advantages of operating wind turbines at variable speed. The most obvious one is an increase in aerodynamic efficiency. This can be seen clearly if the power coefficient, $C_p$, of the rotor is plotted against the tip-speed ratio $\lambda$. Notice that the maximum value of $C_p$ is only achieved at a particular tip-speed ratio of approximately 6.1, which corresponds to a rotor rotational speed 180 rpm.

For a fixed-speed wind turbine, where the angular velocity $\omega$ was constant, this corresponds to a particular wind speed. At all other wind speeds, the efficiency of the rotor is reduced. Thus, it would be desirable to operate the rotor at a constant tip-speed ratio, which given varying wind speeds implies that the rotor's rotational speed must also vary. In practice, the increase in energy capture possible through variable-speed operation is quite small and often exceeded by the electrical losses incurred in the variable-frequency conversion equipment.

The decrease of the MoWEC power coefficient value ($C_{Pt} = 0.32$) is return to some factors in the MoWEC-prototype structure. 1) The rotor blades´s angle of attack at the point where the blades are attached to the rotor hub by 10 bolts. In the experiment, it was impossible to adjust the blades at exactly the right angle of attack. For this reason, the MoWEC will be built with a new hub in the future, which allows the angle of attack to be changed. 2) The MoWEC transmission system (chain) in the future MoWEC will be built with a cardan shaft to transmit the energy from rotors to the stationary central shaft. 3) The generator should be attached to the central shaft (Figures 3.22 and 3.23) if maximum energy transformation is to be achieved.

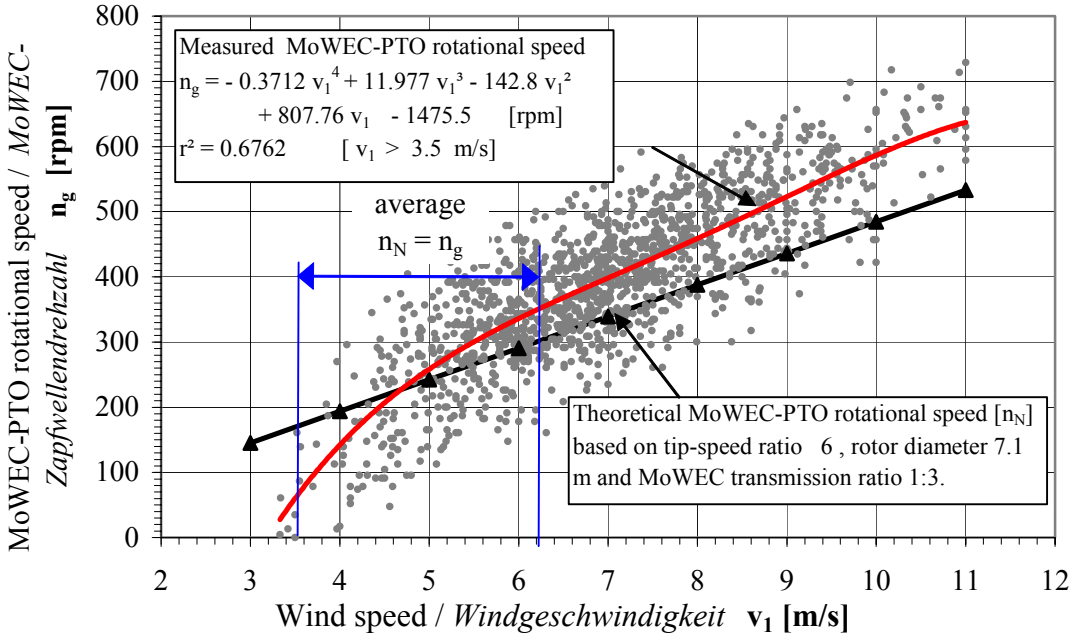


Figure 4.31: Measured MoWEC-PTO rotational speed as a function of the measured wind speed. Generator linked with two rotors.

*Gemessene MoWEC-Zapfwellendrehzahl als Funktion der gemessenen Windgeschwindigkeit. Generator mit zwei Rotoren verbunden.*

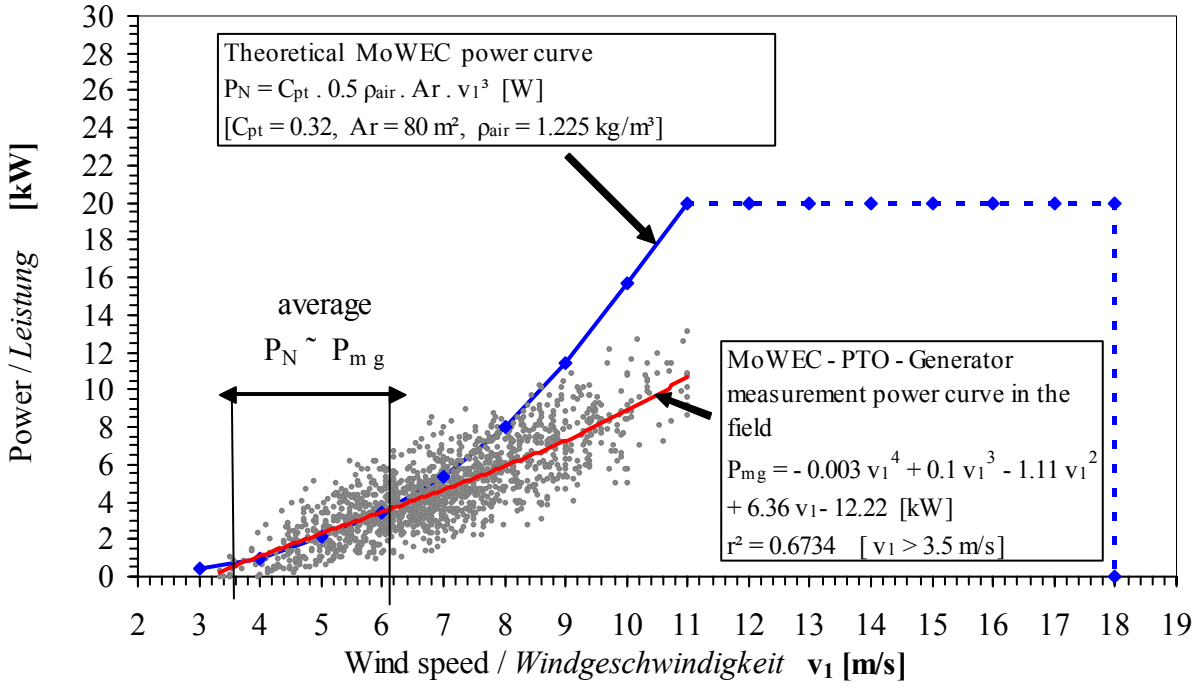


Figure 4.32: Measured and theoretical MoWEC-Generator output power as a function of the measured wind speed. Generator linked with two rotors.

*Gemessene und theoretische MoWEC-Generator-Ausgangleistung als Funktion der gemessenen Windgeschwindigkeit. Generator mit zwei Rotoren verbunden.*

### 4.2.2.4 MoWEC output torque

Using the calculated MoWEC-PTO rotational speed, which determined from measuring data and equation (4.2.4), one can determine the output torque of the MoWEC-PTO. Figure 4.33 shows the measured MoWEC-PTO torque curve and the theoretical curve as a function of wind velocity at hub height given a MoWEC power coefficient of 0.32. This figure illustrate that at low wind speeds ranging from 3.5 to 6.4 m/s the difference between the measured torque $T_{mg}$ and the theoretical torque $T_N$ is very small (i.e. $T_{mg} \approx T_N$). But at high wind speeds (11 m/s) the theoretical torque is two times the measured torque. These differences are due to the generator's rated torque of 180 Nm, while the MoWEC rated torque was 360 Nm at a wind speed of 11 m/s. These curves also show that the MoWEC power coefficient is 0.32.

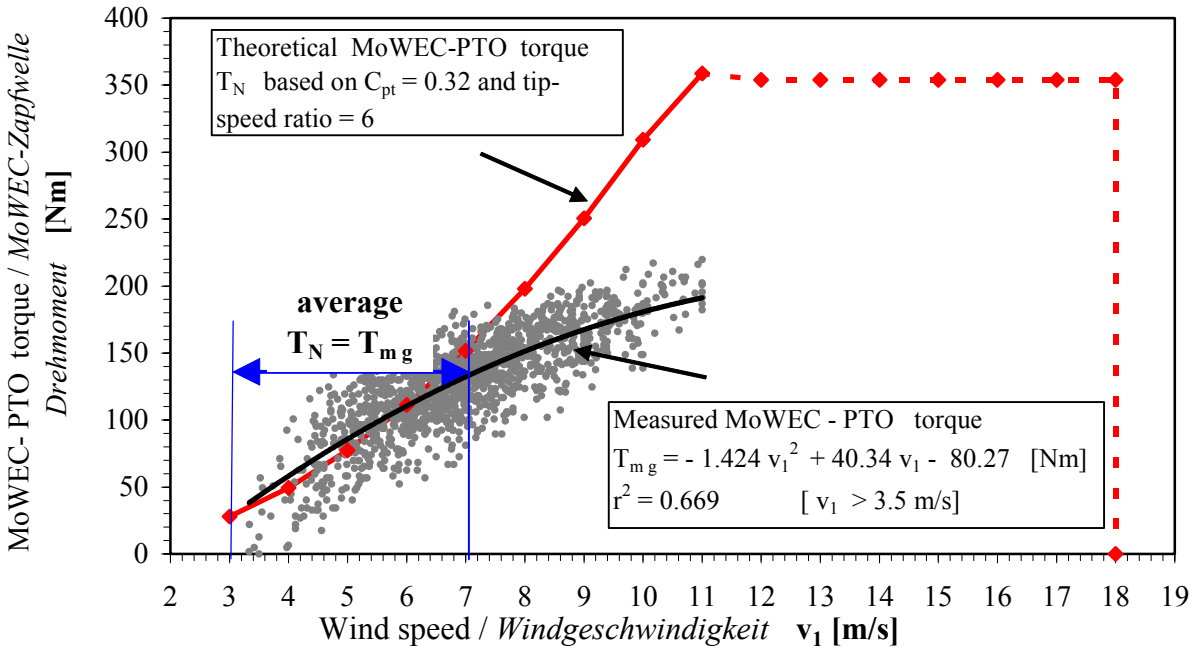


Figure 4.33: Measured and theoretical MoWEC-PTO torque as a function of the measured wind speed. Generator linked with two rotors.
*Gemessenes und theoretisches MoWEC-Zapfwellen-Drehmoment als Funktion der gemessenen Windgeschwindigkeit. Generator mit zwei Rotoren verbunden.*

### 4.2.2.5 Power curve and power coefficient of MoWEC (only one rotor)

For a reliable measurement of the MoWEC power coefficient ($C_{Pt}$ = 0.32), the output power was tested with one rotor in action. The other rotor and the yaw drive system (lee-wind wheel) were blocked. This experiment was carried out on days characterized by approximately laminar wind flow and in particular a nearly constant wind direction. Under these experimental conditions, the yaw drive system did not work, and unsymmetrical forces hit the MoWEC-system. That was the reason for the short measuring period.

The directly measured MoWEC data with one rotor were the output electric current from the same generator and the wind speed. Figure 4.34 illustrates the typical MoWEC electric current from the generator as a function of wind speed in field tests with one rotor.

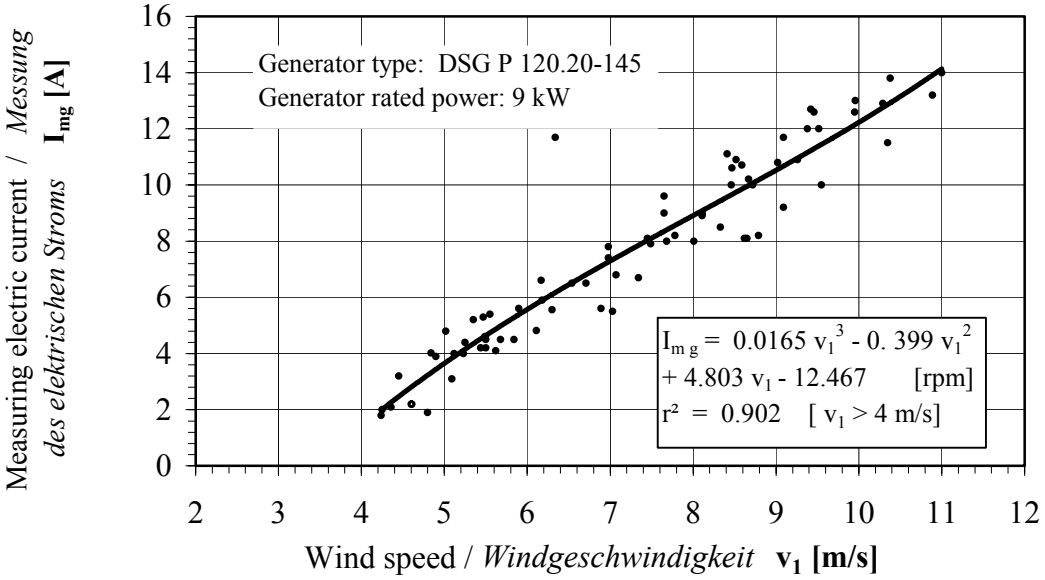


Figure 4.34: Measured MoWEC - Generator current as a function of the measured wind speed. Generator linked with one rotor.
*Gemessener MoWEC - Generatorstrom als Funktion der gemessenen Windgeschwindigkeit. Generator mit einem Rotor verbunden.*

MoWEC-PTO rotational speed was calculated at each measuring point from the field test data using equation (4.2.2). Figure 4.35 shows the PTO rotational speed as a function of wind speed from measured data and the theoretical speed when the tip-speed ratio for the MoWEC rotor used is six. The theoretical PTO rotational speed was higher than the measured value when the wind speed was less than 8.3 m/s, but when the wind speed was more than 8.3 m/s the measured speed was more than the theoretical PTO speed.

In order to determine the MoWEC power curve based on the calculated MoWEC one rotor PTO rotational speed, which was determined from measuring data and equation (4.2.3), one can determine the MoWEC one rotor power curve. In Figure 4.36, the data obtained from tests of one three-blade rotor from a MoWEC- prototype in the field are presented in the form of generator output power as a function of wind speed. MoWEC begins to operate at a certain minimum wind speed, the so-called cut-in wind speed. This speed was 4 m/s during the MoWEC two rotor tests. However, in this test it was 4.4 m/s. MoWEC´s measured maximum one rotor PTO output power was 9 kW at a wind speed of 11 m/s. Figure 4.36 shows the measured MoWEC power curve and the theoretical power curve calculated using equation (3.1.6) based on the power coefficient $C_{Pt}$ = 0.32 and a rotor swept area of 40 m². This figure illustrates that the total power coefficient value of $C_{Pt}$ = 0.32 for MoWEC is correct.

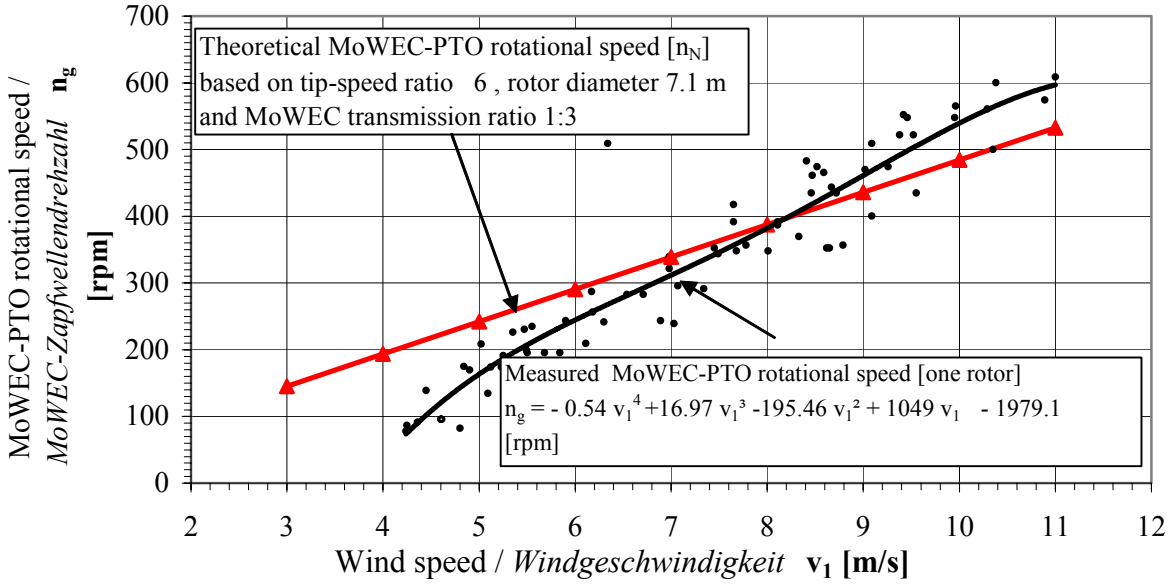


Figure 4.35: Measured MoWEC-PTO rotational speed as a function of the measured wind speed. Generator linked with one rotor.

*Gemessene MoWEC-Zapfwellendrehzahl als Funktion der gemessenen Windgeschwindigkeit. Generator mit einem Rotor verbunden.*

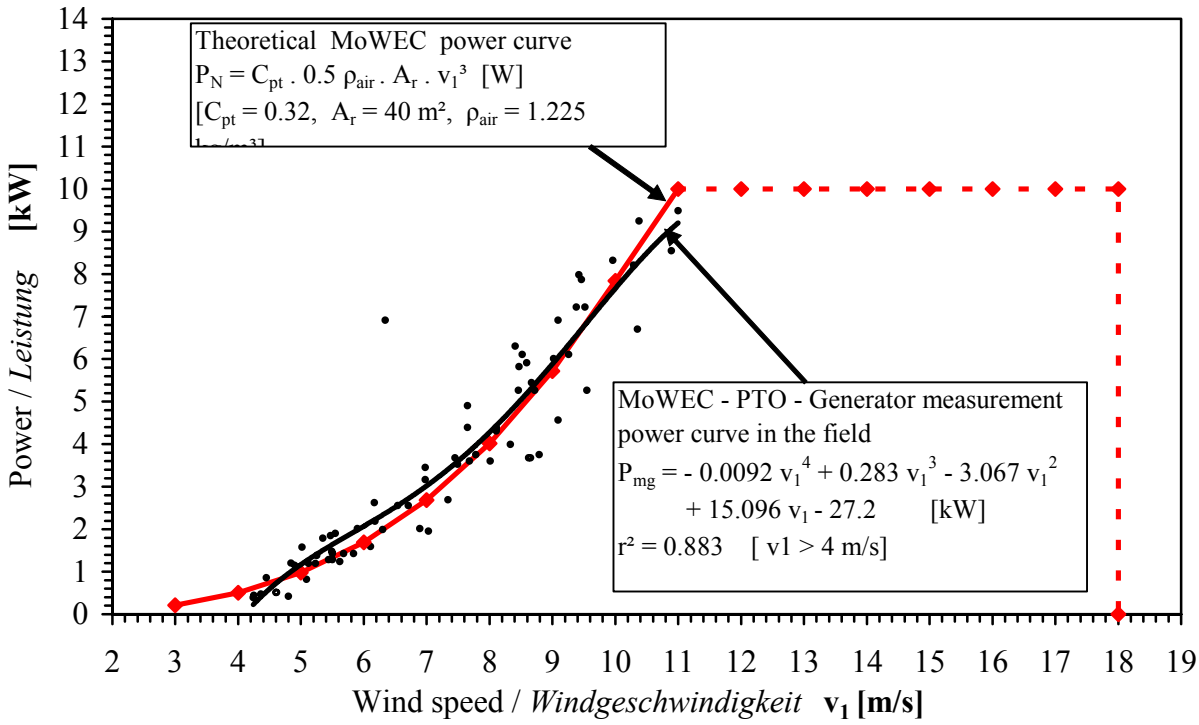


Figure 4.36: Measured and theoretical MoWEC-Generator output power as a function of the measured wind speed. Generator linked with one rotor.

*Gemessene und theoretische MoWEC-Generator-Ausgangleistung als Funktion der gemessenen Windgeschwindigkeit. Generator mit einem Rotor verbunden.*

Figure 4.37 shows MoWEC´s measured one rotor PTO torque curve and the theoretical curve as a function of wind velocity at hub height given a MoWEC power coefficient of 0.32. The measured torque curve was calculated over the rotational speed of the MoWEC-PTO, which was determined from measurement data, and equation (4.2.4). These curves illustrate that the measured torque was higher than the theoretical torque at all wind speeds. This was a result of the rotor blades´s angle of attack at the point where the blades were attached to the rotor hub by 10 bolts. In the experiment, it was impossible to adjust the blades at exactly the right angle of attack. In the future the MoWEC will be built with a new hub, which allows the angle of attack to be changed.

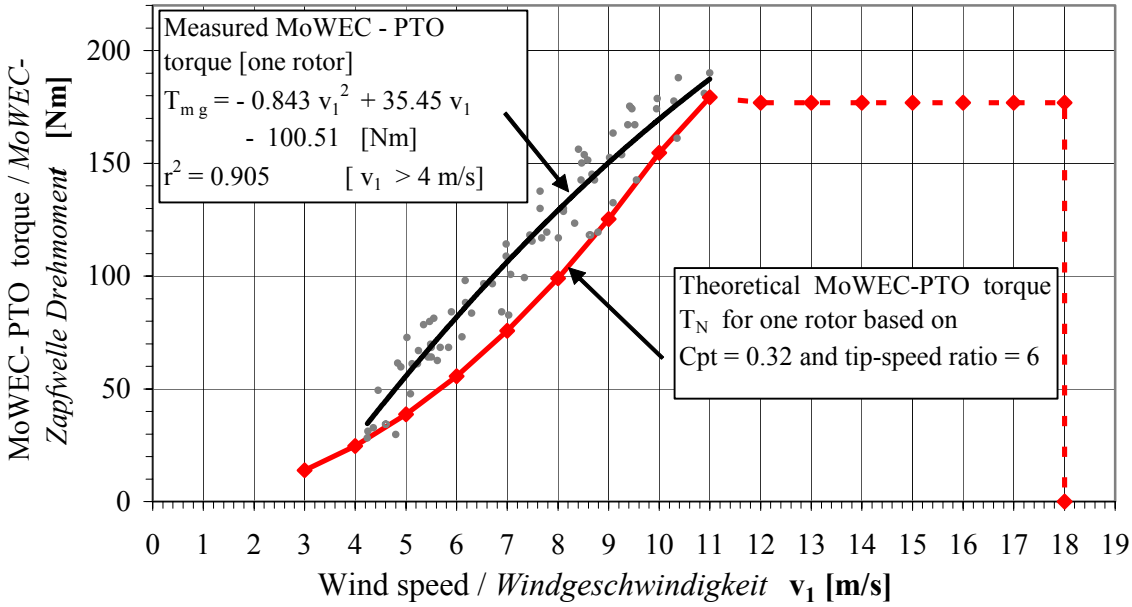


Figure 4.37: Measured and theoretical MoWEC-PTO torque as a function of the measured wind speed. Generator linked with one rotor.

*Gemessenes und theoretisches MoWEC-Zapfwellen-Drehmoment als Funktion der gemessenen Windgeschwindigkeit. Generator mit einem Rotor verbunden.*

### 4.2.2.6 MoWEC energy generation on the N.W. coast of Egypt

MoWEC power curve measurements are used as input for wind plant energy yield predictions in order to evaluate the project economics. Egypt is located in the north-eastern corner of the African continent, and the northwest coast of Egypt extends about 550 km from Alexandria to Al-Salloum and about 10-20 km south of the Mediterranean Sea shore.

**Mean wind speed and duration**

To assess the case for a wind pump it is important to consider not only the mean wind speed, but also the way the actual values develop over a period of time. Perhaps it is rather unlikely that the statistically determined annual mean wind speed prevails in reality. Statistical data will give a first-guess idea of the viability of the site, but by no means are they a sufficient criterion. Although the variation in the annual mean from year to year may be fairly small, the seasonal variation within the year is likely to be large. A more useful statistic is the mean monthly wind speed. This will take account of seasonal changes and is the quantity most often used for sitting studies. However, it should be realized that the fluctuation in mean monthly wind speed for a certain month between different years could be quite large. For periods of less than a month there is too much fluctuation for mean statistics to be of great use, but it is still necessary to know the way the wind will change. The number of consecutive wind-less or low-wind days in each month is of particular relevance. It is important to size the wind pump and the storage tank so that there is sufficient water to last for the longest likely lull period.

Tables in appendix A illustrate the daily average wind speed and duration on the N.W. coast of Egypt in Alexandria (location, 30° 12´ N / 29° 51`E, elevation above sea level 10 m) and Mersa Matruh (location, 31° 20`N / 27° 13`E, elevation above sea level 10 m) when wind speed ranges between 3.5 to 20 m/s [according NWSTOC (2002)]. Winds, whose speed is less than 3.5 m /s (cut-in wind speed), are not considered as they are not productive. Strong winds exceeding 20 m/s (cut-out wind speed), which endanger the installation, and during which the MoWEC is stopped, are also discarded. In winds which exceed the rated wind speed (11 m/s) and for which regulating devices come into play, the MoWEC does not produce more energy than at rated wind speed. These higher wind speeds have to be counted, therefore, as having a value of 11 m/s. Then the available wind speed data from the N.W. coast of Egypt, from the years 1984 to 2002 was used. Figure 4.38 and 4.39 shows the mean monthly wind speed and duration based on a wind speed range between 3.5 and 20 m/s, which corresponds to the cut-in and cut-out wind speed of MoWEC respectively.

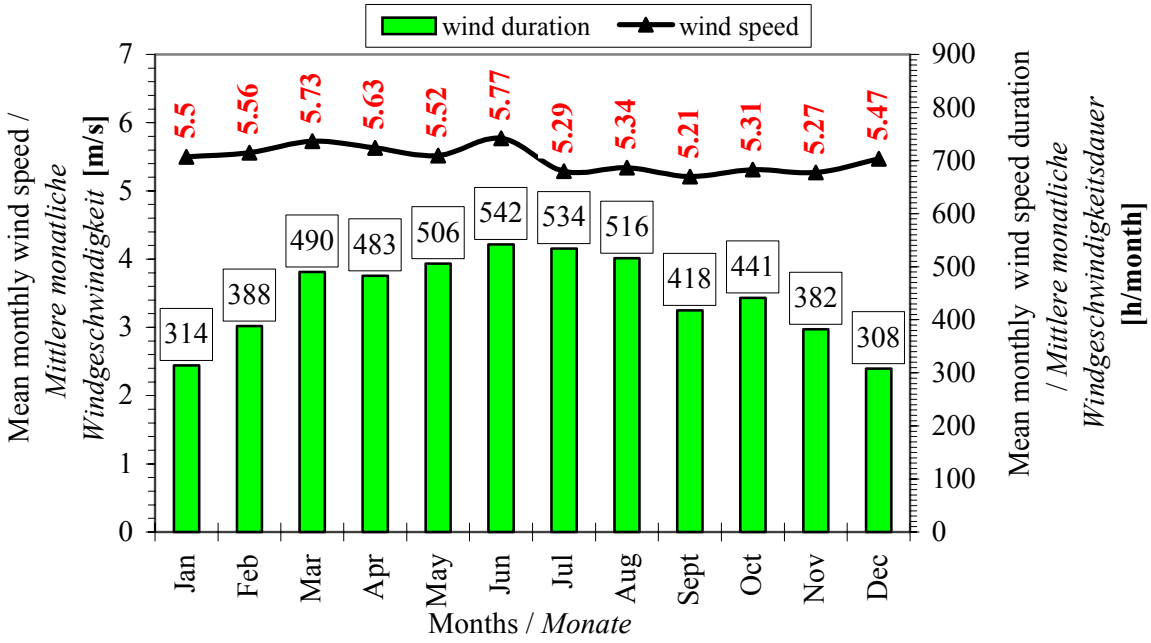


Figure 4.38: Mean monthly wind speed and duration in Alexandria on the N.W. coast of Egypt with the wind speed ranging between 3.5 and 20 m/s; data from the years 1984 to 2002. [according to NWSTOC (2002)]
*Mittlere monatliche Windgeschwindigkeit und- dauer in Alexandria an der N.W. Küste von Ägypten im Windgeschwindigkeitsbereich von 3,5 bis 20 m/s; Daten der Jahre 1984 bis 2002.*

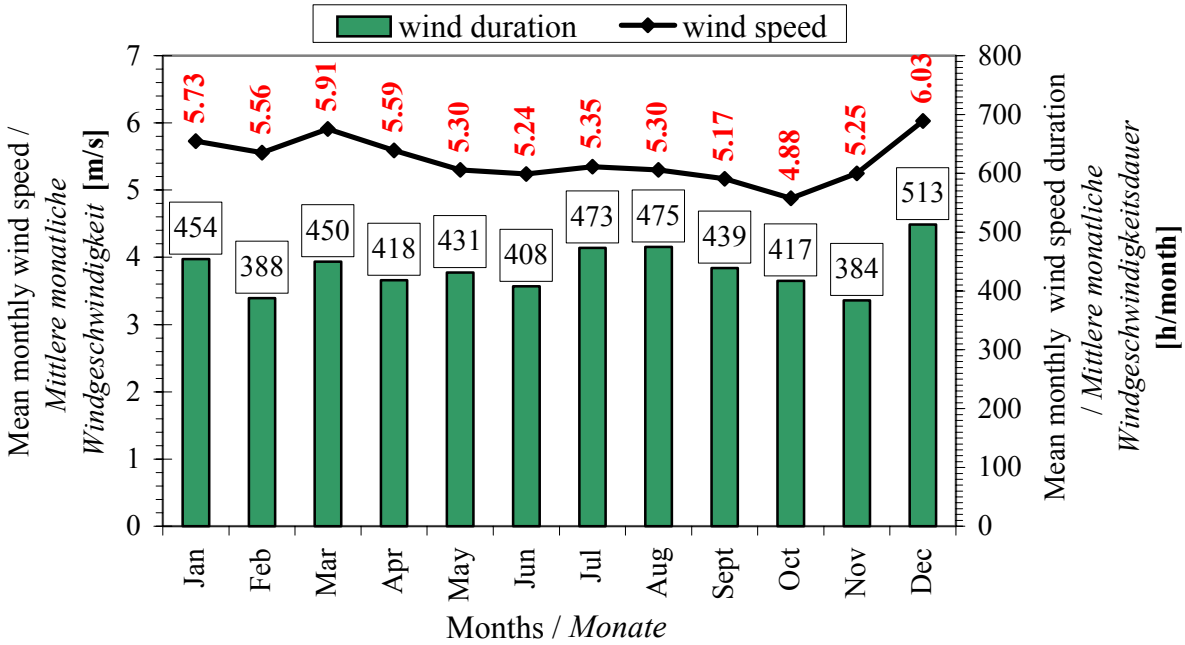


Figure 4.39: Mean monthly wind speed and duration in Mersa Matruh on the N.W. coast of Egypt with the wind speed ranging between 3.5 and 20 m/s; data from the years 1984 to 2002. [according to NWSTOC (2002)]
*Mittlere monatliche Windgeschwindigkeit und- dauer in Mersa Matruh an der N.W. Küste von Ägypten im Windgeschwindigkeitsbereich von 3,5 bis 20 m/s; Daten der Jahre 1984 bis 2002.*

**MoWEC mean monthly energy production**

The mean monthly wind speed and duration at Alexandria and Mersa Matruh in Egypt, which are presented in Figures 4.38 and 4.39, were used to determine the mean monthly energy production (MEP) from MoWEC at each location based on MoWEC´s total power coefficient of 0.32 using the following equation:

$$MEP = MWD \times \frac{C_{pt} \cdot \rho_{air} \cdot A_r \cdot (MWS)^3}{2 \times 1000} \quad [kWh/month]$$

where:

MWD = Mean monthly wind speed duration, Figure 4.38 and 4.39 [h/month]
MWS = Mean monthly wind speed, Figure 4.28 and 4.29 [m/s]
$A_r$ = MoWEC rotor swept area, 80 [$m^2$]
$C_{Pt}$ = MoWEC power coefficient, 0.32
$\rho_{air}$ = air density, 1.225 [$kg/m^3$]

Table 4.2 shows the mean monthly MoWEC energy production at Alexandria and Mersa Matruh in Egypt.

**MoWEC actual mean monthly energy production**

Some care must be exercised when using mean wind speed data, as the same wind pump at two different sites, which have the same wind speed, will not necessarily produce the same power output. This is because the mean power (and so the mean quantity of water lifted) over a period of time depends on the wind speed distribution; in other words, on the frequency of occurrence of different wind speeds. The reason for this is that the mean power depends on the mean of the cubes of the wind speeds over that time, which is different from the cube of the mean wind speed. This can be a confusing concept, but in general it can be said that the actual power produced will be larger than that calculated from the mean wind speed. This is because a disproportionately large amount of power will be produced at those times when the wind speed is higher compared to when the winds are lighter. So the real power available will be greater than that calculated from the mean wind speed by a factor ranging anywhere from 1.2 to 4. This factor is called the Energy Pattern factor, and for most localities it has a value of about 2 [FRAENKEL (1993)].

Table 4.2 shows the actual mean monthly energy production **(AMEP)** from MoWEC. The method used to calculate the energy production at different wind speeds takes account of the likely wind speed distribution, and assumes an Energy Pattern factor of 2. This makes it possible to work with the mean wind speed, and still get a realistic answer for most sites.
Then, **AMEP = 2 × MEP.**

Table 4.2: Mean monthly MoWEC energy production on the N.W. coast of Egypt.
*Mittlere monatliche MoWEC Energieproduktion an der N.W. Küste von Ägypten.*

| **Months** | **Alexandria** | | | | **Mersa Matruh** | | | | **AAMEP** |
|---|---|---|---|---|---|---|---|---|---|
| | MWS $\left[\frac{m}{s}\right]$ | MWD $\left[\frac{h}{month}\right]$ | MEP $\left[\frac{kWh}{month}\right]$ | AMEP $\left[\frac{kWh}{month}\right]$ | MWS $\left[\frac{m}{s}\right]$ | MWD $\left[\frac{h}{month}\right]$ | MEP $\left[\frac{kWh}{month}\right]$ | AMEP $\left[\frac{kWh}{month}\right]$ | $\left[\frac{kWh}{month}\right]$ |
| January | 5.5 | 314 | 819.15 | 1638.30 | 5.73 | 454 | 1339.26 | 2678.53 | 2158.41 |
| February | 5.56 | 388 | 1045.69 | 2091.38 | 5.56 | 388 | 1045.69 | 2091.38 | 2091.38 |
| March | 5.73 | 490 | 1445.46 | 2890.92 | 5.91 | 450 | 1456.54 | 2913.07 | 2902.00 |
| April | 5.63 | 483 | 1351.51 | 2703.01 | 5.59 | 418 | 1144.87 | 2289.75 | 2496.38 |
| May | 5.52 | 506 | 1334.49 | 2668.97 | 5.30 | 431 | 1006.12 | 2012.25 | 2340.61 |
| June | 5.77 | 542 | 1632.57 | 3265.15 | 5.24 | 408 | 920.45 | 1840.90 | 2553.02 |
| July | 5.29 | 534 | 1239.52 | 2479.04 | 5.35 | 473 | 1135.71 | 2271.43 | 2375.24 |
| August | 5.34 | 516 | 1232.03 | 2464.05 | 5.30 | 475 | 1108.84 | 2217.67 | 2340.86 |
| September | 5.21 | 418 | 926.91 | 1853.81 | 5.17 | 439 | 951.22 | 1902.45 | 1878.13 |
| October | 5.31 | 441 | 1035.30 | 2070.61 | 4.88 | 417 | 759.87 | 1519.75 | 1795.18 |
| November | 5.27 | 382 | 876.68 | 1753.36 | 5.25 | 384 | 871.27 | 1742.55 | 1747.96 |
| December | 5.47 | 308 | 790.42 | 1580.84 | 6.03 | 513 | 1763.66 | 3527.32 | 2554.08 |
| **Total** | - | 5322 | 13729.7 | 27459.45 | - | 5250 | 13503.5 | 27007.03 | 27233.24 |

where **AAMEP** is the average actual mean monthly energy production on the N.W. coast of Egypt, which is calculated as follows:

$$\text{AAMEP} = \frac{\text{AMEP of Alexandria} + \text{AMEP of Marsa Matruh}}{2} \qquad \text{[kWh/month]}$$

In addition, Table 4.2 illustrates the actual mean annual energy production **(AMAEP)** by MoWEC in Alexandria (27459.45 kWh/year) and in Mersa Matruh (27007.03 kWh/year). The difference between AMAEP in Alexandria and Mersa Matruh is very small because each station is situated in Northern Egypt direct at the Mediterranean Sea and the difference in the degree of longitude is very small 1° 08` N. Therefore, actual mean annual energy production by the MoWEC prototype on the N.W. coast of Egypt is

$$\text{AMAEP} = \frac{27459.45 + 27007.03}{2} = 27233.24 \qquad \text{[kWh/year]}$$

### 4.2.2.7 Economics of the MoWEC-prototype

The economics of collecting energy from the wind is dependent on several factors, which can fluctuate depending on the specific application. The cost of energy produced from the MoWEC was calculated using the following equation [RAMLER (1979)]:

$$\text{COE} = \frac{[(\text{IC}) \cdot (\text{FCR})] + \text{AOM}}{\text{AMAEP}} \qquad \text{[€ cent/kWh]}$$

where:

COE = the cost of energy, [€ cent/kWh]

IC = the initial installed cost, [€]

FCR = the fixed charge rate, [% year]

AOM = annual operation and maintenance, [% of IC/year]

AMAEP = actual mean annual energy production [kWh/year]

The total initial cost of the MoWEC-prototype was 26,000 €, with an additional 4,000 € for the generator and water pump. A payback period of 10 years was selected with an annual rate of interest of 8%, which results in a fixed charged rate of 14%. Annual operation and maintenance was assumed to be 2% of the initial cost, which is 600 €. An actual mean annual energy production of 27233.24 kWh/year on the N.W. coast of Egypt was used as the basis of the calculation. The cost of energy based on the mentioned data was calculated to be 15.44 € cents /kWh.

Sensitivity curves are helpful in locating the areas most responsive to the cost of energy (see Figure 4.40). Two of the most critical factors were initial cost and energy production. The initial cost is a function of mass production, government credits, and several design features. Energy production is directly affected by wind speed and air density at specific locations and the power coefficient and the availability of MoWEC. A 10 % decrease in the initial cost or increase in energy production would result in a drop of 1.20 € cents/ kWh in the cost of energy.

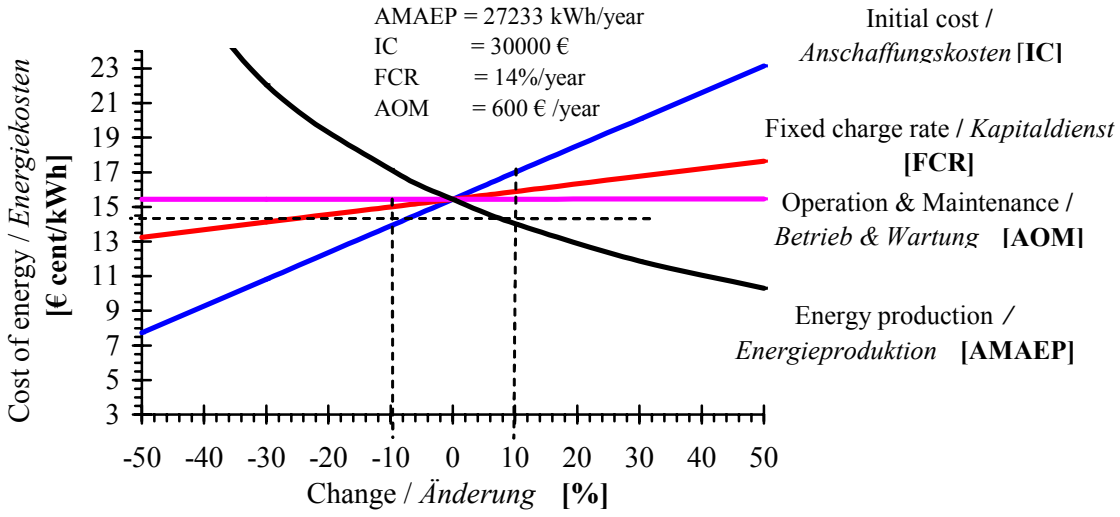


Figure 4.40: Sensitivity diagram for the cost of energy of the MoWEC-prototype for possible use on the N.W. coast of Egypt.

*Sensibilitätsdiagramm für die Energiekosten des MoWEC-Prototypen kalkuliert für den möglichen Einsatz an der N.W. Küste von Ägypten.*

### 4.2.3 Conclusions

The power performance measurements of the MoWEC are focused on the determination of the turbine power output versus the wind speed characteristics, potential annual energy production, and wind turbine efficiency.

The first power curve of the MoWEC- prototype was tested in the field at the FAL research station in Braunschweig, Germany. The wind speed and power output from MoWEC were measured over a long period during the test. MoWEC´s total power coefficient value $C_{Pt}$ determined on the basis of the measurement data was 0.32, which contains the normal wind power coefficient, the generator efficiency, chain efficiency and gear box/bearing efficiency.

The N.W. coast of Egypt extends about 550 km from Alexandria to Al-Salloum and about 10-20 km south of the Mediterranean Sea shore. The mean monthly wind speed and duration range from 5.17 to 6.03 m/s for wind speed and from 308 h/month to 614 h/month for duration.

The MoWEC actual mean annual energy production of 27,233 kWh/year on the N.W. coast of Egypt was calculated based one the average available wind data and the MoWEC total power coefficient of 0.32.

The total initial costs of the MoWEC-prototype was 26,000 € with an additional 4,000 € for the generator or the pump. The cost of the MoWEC output energy was calculated to be 15.44 € cent/kWh based over a payback period of 10 years given an annual rate of interest of 8% and annual operation and maintenance of 2% of the initial costs.

## 4.3 Wind powered low-head bubbler irrigation system

Irrigation is a major energy user in on-farm agricultural production. Combining a wind-electric system with an irrigation system for watering fruit and nut trees may open up vast regions of land heretofore untapped due to no utility supplied electricity. Therefore, it is necessary to choose, design and test an irrigation system to ensure energy source availability and reliability. A literature review showed that low-head bubbler irrigation enables water to be used economically, and its low operating pressure makes it particularly well-suited for combination with alternative energy such as wind energy. It has large orifice openings which deliver water directly to the root zone, eliminating elaborate filtration systems and pumps required by other micro irrigation systems. One of the objectives of this study is the design and validation of a computer model of a low-head bubbler irrigation system.

### 4.3.1 Computer modelling and simulation of the low-head bubbler irrigation systems

#### 4.3.1.1 Mathematical model

A computer program called LHBIS (Low-Head Bubbler Irrigation System) was written for the exact analysis of a low-head bubbler irrigation system with different elevations or lengths of the distributor hoses. The program was written for IBM compatible PCs using the Microsoft QuickBasic language. The program requires DOS 3.3 or higher and 640 Kbytes RAM memory. The program uses menus and submenus for data input, output, file manipulation, and to access the rest of the program functionality. The main components for low-head bubbler irrigation systems include the distributor hoses, laterals, the manifold, the mainline and the constant head device. Figure A in appendix C illustrates the flow chart of the LHBIS computer program.The following main equations have been used for the calculation of the LHBIS program hydraulic parameters:

- The energy equation (3.2.3) with $\alpha = \alpha_c = 1.1$ and $\Delta h = 0$
- The Hazen-Williams equation (3.2.12)
- The flow rate equation (3.2.15).

This approach is used to calculate the elevation or lengths of the distributor hoses in order to obtain an equal outflow from all hoses in the irrigation system, the total discharge of the irrigation system, pressure head at each lateral inlet, required pressure head at each manifold inlet (by constant head device) and total required pressure head at the mainline inlet (by the tank). Figure 4.41 shows the data flow diagram of the computer program. The main elements of the data flow diagram, such as input data; calculation process and the output data for this approach, were described in more detail in the next sections.

**Computer program input data:** Data input has been organized in 5 blocks:

**System shape:** Shape of low-head bubbler irrigation system with Different Distributor Hoses Elevation (DDHE) or with Different Distributor Hoses Length (DDHL).

**Distributor hoses:** Hoses position from lateral on one lateral side (S = 1) or on two lateral sides (S = 2), outflow ($q_{oh}$), inner diameter ($d_{oh}$), minimum length ($L_{oh}$), minimum hose outlet elevation ($E_{fh}$), Hazen-William's coefficient ($C_{Hwh}$) and hose number per lateral side ($n_{oh}$).

**Lateral:** Lateral position from manifold on one manifold side (SS = 1) or on two manifold sides (SS = 2), inner diameter ($D_L$), distributor hoses spacing along the lateral ($S_L$), length (L), slope ($S_{oL}$), Hazen-William's coefficient ($C_{HwL}$) and number of laterals per manifold side ($N_L$).

**Manifold:** Inner diameter ($D_{mf}$), laterals spacing along the manifold ($S_m$), length ($L_{mf}$), slope ($S_{omf}$), Hazen - William's coefficient ($C_{Hwmf}$) and number of manifolds used for irrigation at the same time per mainline ($n_{mf}$).

**Mainline:** Inner diameter ($D_m$), length ($L_m$), slope ($S_{om}$) and Hazen-William's coefficient ($C_{Hwm}$).

**Calculation process:** First note that given the shape of the low-head bubbler irrigation system with different distributor hose elevation (DDHE), the program will calculate the hose outlet elevation. Given a LHBIS with different distributor hose length (DDHL), however, the program will calculate the length of the hoses.

We will begin with the minimum distributor hose outlet elevation or minimum hose length of the first distributor hose at the closed end of the last lateral from the manifold inlet. The friction loss of each hose is obtained using the Hazen-Williams equation (3.2.12) and the values $V_{oh}^2/2g$ and $0.5\ V_{oh}^2/2g$ to calculate the outlet and inlet energy loss for each hose in the irrigation system respectively. The program determined the pressure head recovery across the inlet of this hose based on equation (3.2.3). The summation of minimum hose outlet elevation, hose friction loss, hose outlet and inlet loss, and head recovery was the total required pressure head just before the inlet of this distributor hose (first hose).

From the distributor hose outflow, the program calculated the discharge from each of the two hoses along the lateral by using equation (3.2.15), and using equation (3.2.12) to compute the friction loss in this part of the lateral. It computed the pressure head recovery across the inlet of the next hose using equation (3.2.3). The program calculated the total pressure head at the inlet of this hose. The difference between the pressure head at the first hose inlet and the pressure head at the next hose inlet is a hose outlet elevation in the DDHE system. In the DDHL system, however, the program computed the new hose length at this position. The program repeats this calculation for each of the two hoses along the first lateral to determine the outlet elevation or length at each hose.

The program also computed the total flow rate and pressure head at the inlet of the first lateral from the manifold´s closed end. Then the program computed the friction loss in the manifold between each two laterals by using equation (3.2.12) and also calculated the pressure head recovery at each lateral inlet by using equation (3.2.15). From these values the program computed the pressure head at the inlet of the next lateral. From this point, the program started to calculate the elevation or length of the hoses along the laterals from the lateral´s open end. The program repeated this calculation for each of the two laterals along the manifold to determine the outlet elevation or length at each hose along the laterals.

After having determined the required pressure head for the manifold and using the input data for the mainline and for the calculation of how many manifolds will be irrigated at the same time, the program computed the friction loss in the mainline and then calculated the total required pressure head at the mainline inlet (in the tank). In all calculations, the program required the slope of the lateral, the manifold and the mainline.

**Computer program output data:**

- The distributor hoses outlet elevations or lengths in the irrigation system
- The required pressure head at each lateral inlet
- The required pressure head at each manifold inlet (delivered by a constant head device)
- The total required head for the irrigation system at the mainline inlet (in the tank)
- The total discharge of the irrigation system.

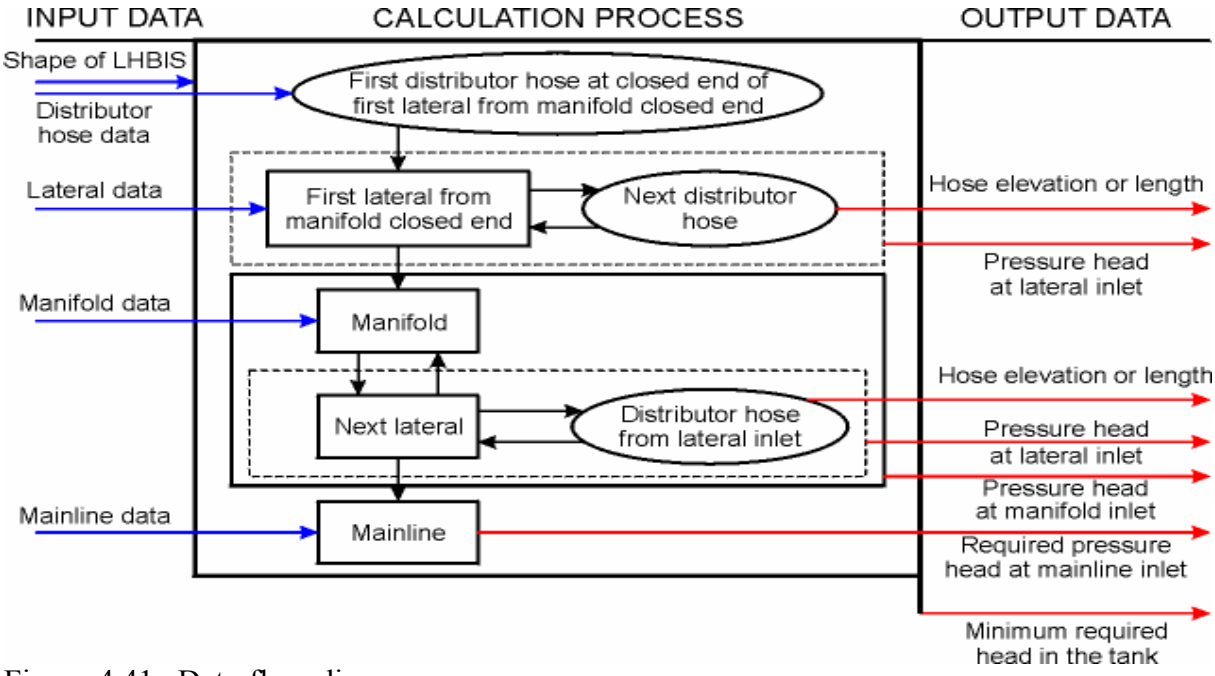


Figure 4.41: Data flow diagram.
*Datenflussdiagramm.*

### 4.3.1.2 Laboratory tests for the validation of the LHBIS computer program

In the development of a new water distribution system, water distribution measurements are very important. When using low-head bubbler irrigation systems, we must know how the distributor hoses outlet heights (or lengths) are distributed along the lateral and also how the water is distributed and how much water can be obtained from the distributor hoses at different operating pressures. The hoses´s discharge and height (or length) are dependent on the hoses´s diameter, friction coefficient and the operating pressure.

#### 4.3.1.2.1 Material and method

**Experimental design**

In the low-head bubbler irrigation system, one lateral equipped with a 32 mm inner diameter polyethylene (PE) pipeline was tested. The pipeline was available at a length of 50 m. One pipeline end was connected to an elevated tank, which would have required constant head itself, while a gate valve closed the other pipeline end (Figure 4.42). After the experiments which investigated the characteristics of lateral pipeline friction had been completed, the 13 circular outlets were drilled only along one horizontal side (horizontal direction) of the lateral pipeline (during the simulation of the LHBIS computer program with DDHL), Figure 4.43. After the completion of the last experiments, 13 circular outlets were drilled along two-horizontal sides of the lateral pipeline (during the simulation of the LHBIS computer program with DDHE), Figure 4.44 and 4.45. The outlets were spaced 4 m apart and had an inner diameter of 4 mm. The first outlet was located 2 m from the lateral inlet. Just before and after each outlet, two circular outlets were drilled in the upper side of the pipeline to measure the pressure head using a manometer tube at each outlet. The outlets were connected to a the silicon tube of a distributor hose having an inner diameter of 6 mm by a stainless steel nipple featuring an outer diameter of 6 mm, an inner diameter of 4 mm and a length of 1 cm. In addition, one manometer tube was connected to an upper side of the lateral pipeline at an inlet to adjust the required pressure head for each experiment. Water was supplied to the test pipe from an elevated constant head tank as shown in Figure 4.42. The pressure in the pipe was controlled by installing a gate valve on the outlet of the tank and a ball valve in the tank, as well as a bend, spigot and faucet rubber ring jointing system.

In order to obtain a straight pipeline, a metal part which was 52 m long and 0.1 m wide was used, and the pipeline was fixed above this metal part. To obtain the pipeline slopes (Level, Uphill or Downhill) and designed elevation for the delivery hoses at all outlets, the 40 metal risers were constructed as shown in Figure 4.45. The experimental work was conducted in the irrigation laboratory at the Institute for Production Engineering and Building Research, Federal Agricultural Research Center (FAL), Braunschweig, Germany.

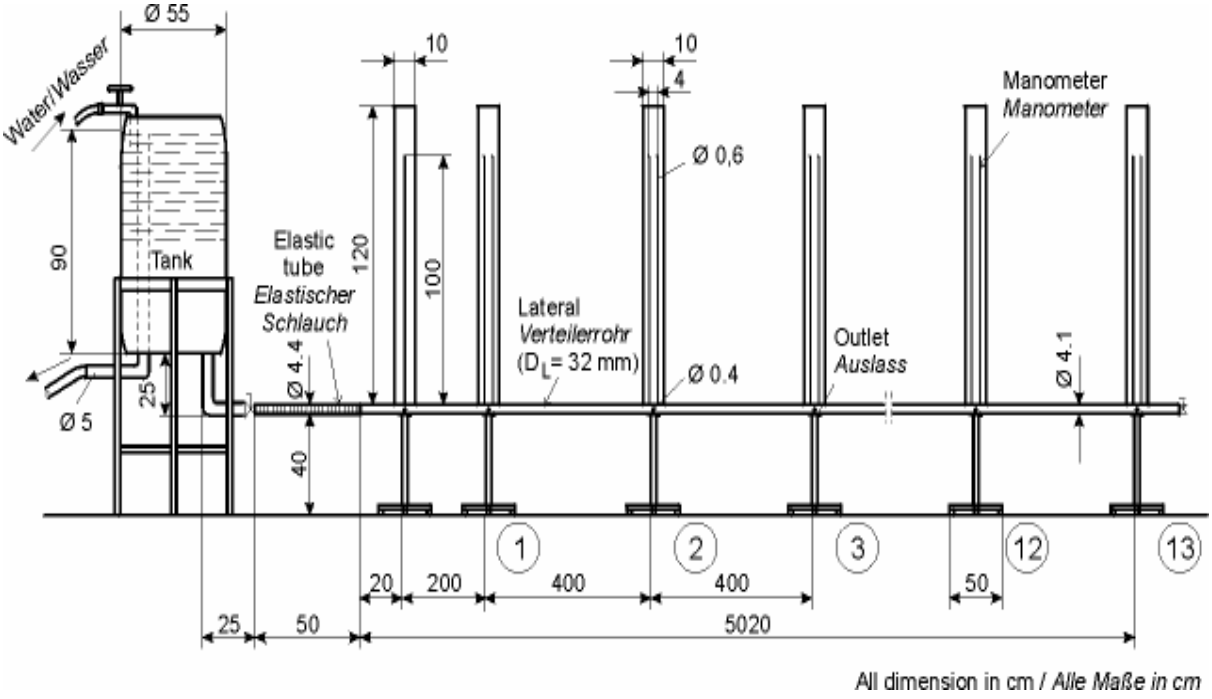


Figure 4.42: Test assembly for the verification of a LHBIS computer program.
*Versuchsaufbau zur Überprüfung des LHBIS Computerprogramms.*

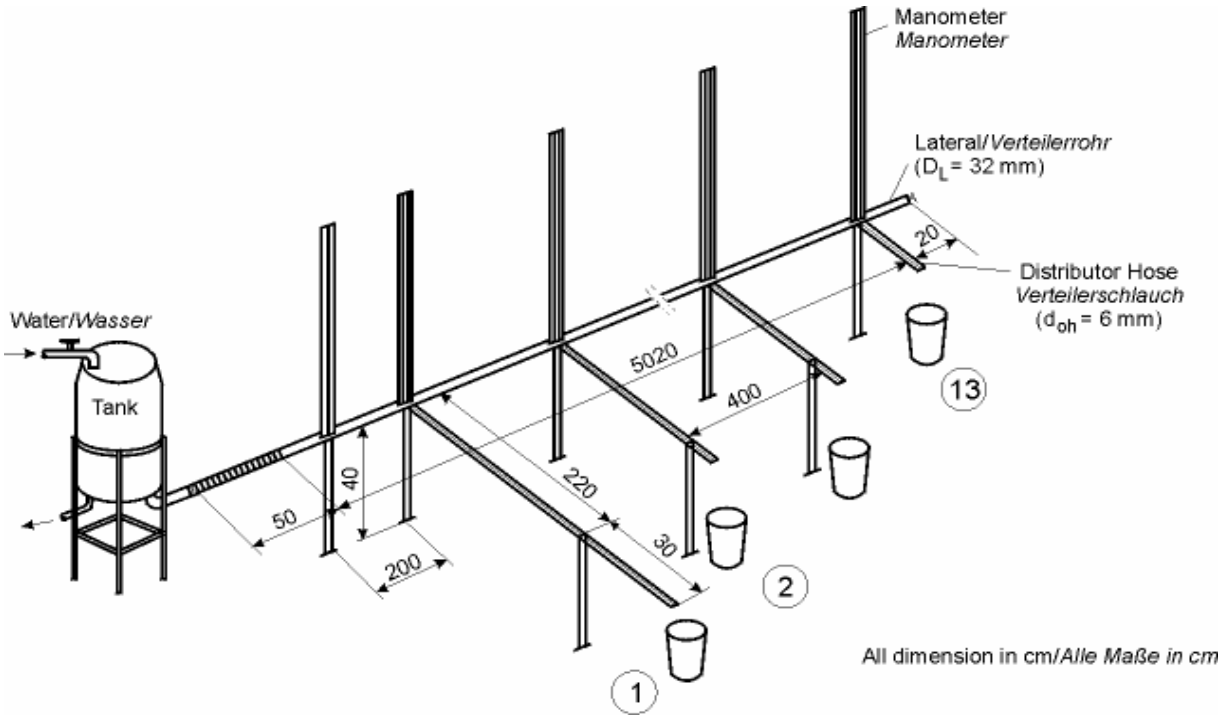


Figure 4.43: Test assembly for the verification of a LHBIS computer program at different lengths of the distributor hoses.
*Versuchsaufbau zur Überprüfung des LHBIS Computerprogramms mit unterschiedlichen Längen des Verteilerschlauches.*

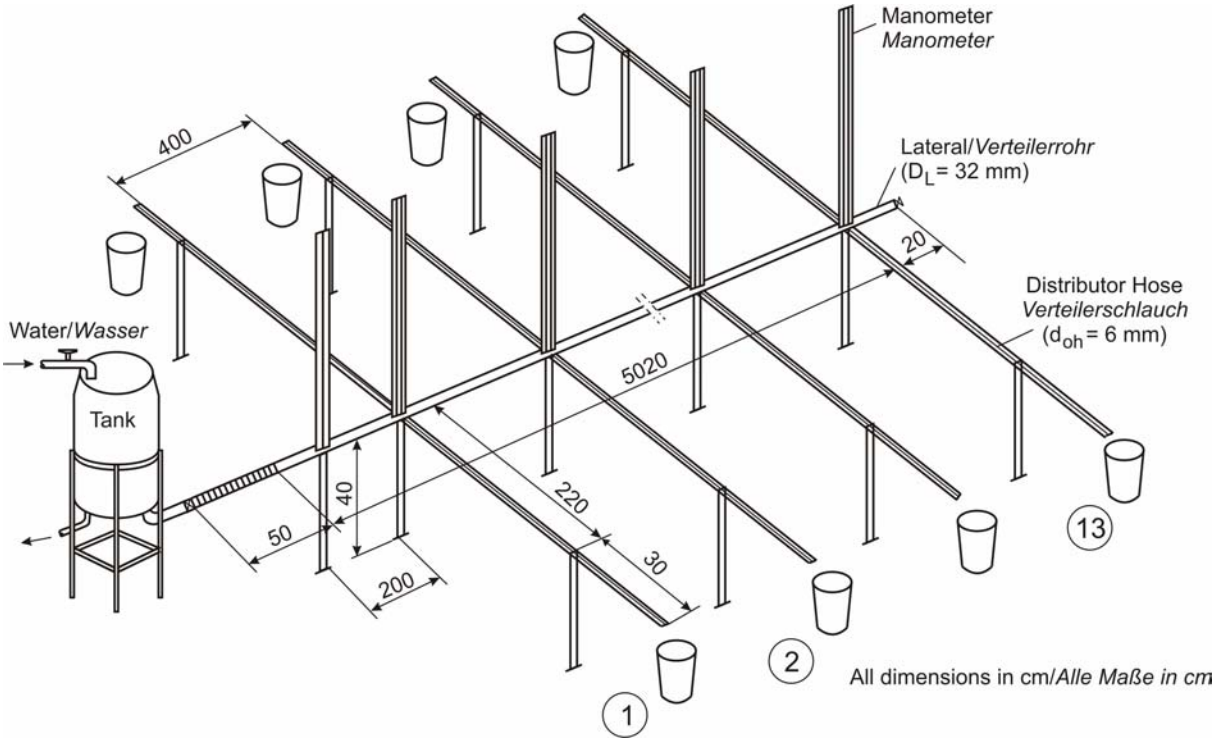


Figure 4.44: Test assembly for the verification of a LHBIS computer program at different elevations of the distributor hoses.

*Versuchsaufbau zur Überprüfung des LHBIS Computerprogramms mit unterschiedlicher Auslasshöhe des Verteilerschlauches.*

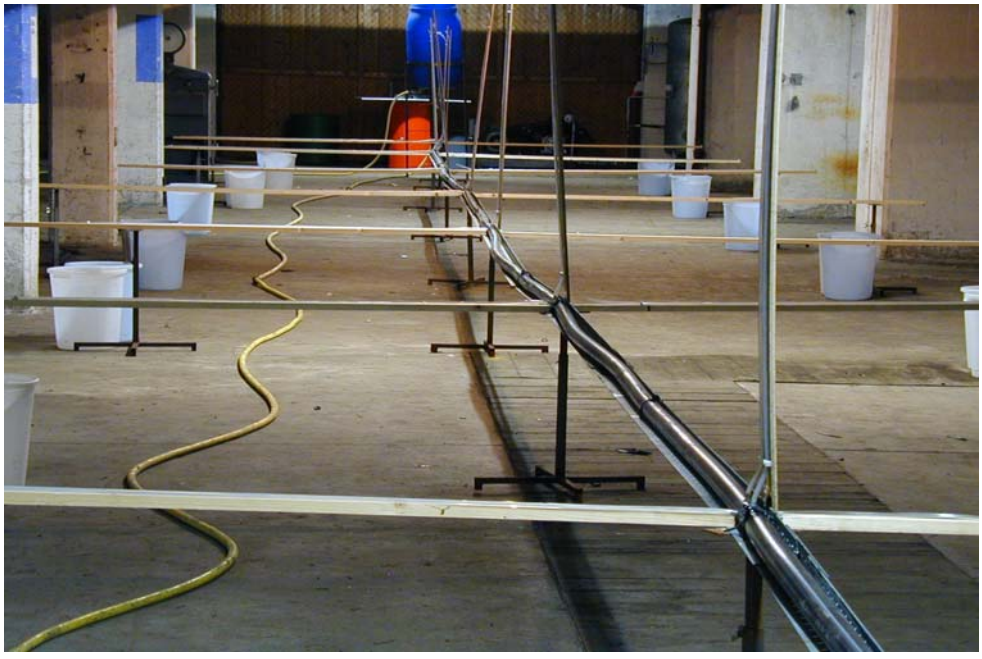

Figure 4.45: Experimental irrigation plant for the verification of the computer program.

*Versuchsanlage zur Überprüfung des Computerprogramms.*

**Experimental procedure**

Three separate groups of tests were undertaken. **Firstly**, to determine the friction characteristics of the lateral and the distributor hoses. For the lateral, steady uniform flow tests at discharges ranging from 270.36 l/h to 1854 l/h are carried out over full lateral length of 50 m. Before the outlets were drilled, the inner diameter was 32 mm. For the distributor hoses, steady uniform flow tests at discharges ranging from 33.73 l/h to 100 l/h are carried out over the hose length of 3.5 m hose length at an inner diameter of 6 mm. Besides the flow rate, the pressure head upstream and downstream of the lateral and the hose were measured.

**Secondly,** to simulate the elevation of the distributor hoses along two sides of one lateral, the outflow from the hoses and the pressure head in the lateral just before and after each hose were measured. In this case, it could be applied that the calculated required pressure head in the tank for each discharge and each lateral slope; here all distributor hoses had an elevation of zero from the lateral level. The outflow and pressure head were then measured at each hose along the lateral in order to compare the two cases, see this Table.

| Laterals location from manifold | Theoretical distributor hose outflow $q_{oh}$ [l/h] | Lateral slope $So_L$ | | |
|---|---|---|---|---|
| | | Uphill + 0.5% | Level 0.0 % | Downhill - 0.5% |
| One-sided connection, (SS =1) | 20, 40 and 60 [l/h] | 1. Calculation of the elevation of the distributor hoses along the lateral and head in the tank by the computer program and their application in the laboratory experimental system.<br>2. Measuring outflow from each distributor hose and pressure head in the lateral at each hose | | |
| Two-sided connection: one side Uphill and another side Level or Downhill, (SS =2) | 20, 40 and 60 [l/h] | | | |

**Third,** to simulate the length of the distributor hoses along one side of one lateral, the outflow from the hoses and pressure head in the lateral just before and after each hose were measured, see this Table.

| Laterals location from manifold | Theoretical distributor hose outflow $q_{oh}$ [l/h] | Lateral slope $So_L$ | | |
|---|---|---|---|---|
| | | Uphill + 0.5% | Level 0.0 % | Downhill - 0.5% |
| One-sided connection (SS =1) | 60 and 80 [l/h] | 1. Calculation of the lengths of the distributor hoses along the lateral and head in the tank by a computer program and their application in the laboratory experimental system.<br>2. Measurement of the outflow from each distributor hose and pressure head in the lateral at each hose | | |
| Two-sided connection: one side Uphill and another side Level or Downhill, (SS =2) | 60 and 80 [l/h] | | | |

**Emission uniformity of distributor hoses**

KELLER and KARMELI (1974) have suggested two parameters to define the uniformity of application of a micro irrigation system such as low-head bubbler system. Their emission uniformity involves the relationship between minimum and average distributor hose discharge rates within the system. They noted that this relationship is the most important factor for the uniformity of application, since a primary objective of irrigation system design is to ensure enough system capacity to adequately irrigate the least watered area. They recommended that EU values of 94% or more are desirable, and in no case should the designed EU be below 90%. The emission uniformity was calculated by Keller (1974) as follows:

$$EU = \left( q_{ohL} \,/\, q_{ohA} \right) \times 100 \qquad (4.3.1)$$

where:

EU = the emission uniformity of distributor hoses, in %

$q_{ohL}$ = average discharge from hoses in the lowest 25% of the discharge range, in l/h

$q_{ohA}$ = average discharge of all distributor hoses, in l/h.

**Distributor hoses flow variation**

The distributor hoses flow variations indicate the relationship between the maximum and minimum flow variation in percent of the maximum flow value. Distributor hoses flow variation was expressed by WU (1983) as follows:

$$q_{oh\,var} = \frac{q_{oh\,max} - q_{oh\,min}}{q_{oh\,max}} \times 100 \qquad [\%] \qquad (4.3.2)$$

where:

$q_{oh\,var}$ = distributor hoses flow variation, in %,

$q_{oh\,max}$ = maximum distributor hoses discharge, in l/h, and

$q_{oh\,min}$ = minimum distributor hoses discharge, in l/h.

### 4.3.2 Results and Discussion

The laboratory experiments were conducted to investigate the friction coefficient of the lateral and the distributor hose. In addition, they were used to validate our computer program for different heights or lengths of the distributor hoses.

#### 4.3.2.1 Lateral friction loss

The average rate of energy loss for each steady, uniform flow tests was obtained by using the formula:

$$MLF = \frac{h1 - h2}{L_L} \quad [m/m]$$

where: MLF is the measured friction loss of the lateral in [m/m], $L_L$ is the length of the lateral in [m], h1 is the pressure head at the lateral inlet (upstream) in [m] and h2 is the pressure head at the lateral outlet (downstream) in [m].

Table 4.3 illustrates an analysis of the lateral PE pipeline friction loss at various discharge rates based on laboratory work and the Hazen- William's equation given an inside diameter ($D_L$) of 32 mm and a lateral length of 50 m ($L_L$), which is the spacing between the upstream and the downstream of the pipeline.

The Hazen- William's coefficient ($C_{HwL}$) was calculated at each lateral discharge by using Eq. (3.2.12). The results showed that a value of 140 for $C_{HwL}$ was better. Figure 4.46 shows the relationship between the lateral pipeline friction loss and the discharge. Adopting the Hazen- Williams formula Eq. (3.2.12) with a value of 140 for $C_{HwL}$ reasonably accounts for the experimental data. Based on LAMONT (1981), THOMAS (2001) reported that the Hazen-William's coefficient ($C_{HwL}$) of a pipe should vary with the pipe materials. The $C_{HwL}$ value was 140 and 147 when the pipe material was smooth pipe polyethylene (PE) and the pipe diameters were 25 mm and 76 mm respectively.

Table 4.3: Lateral friction loss. [$D_L$ = 32 mm, $L_L$ = 50 m]
*Reibungsverlust im Verteilerrohr.*

| Exp. Nr. | h1 [cm] | h2 [cm] | Q [l/s] | V [m/s] | MLF [m/m] | FLHW [m/m] |
|---|---|---|---|---|---|---|
| 1 | 0.0 | 0.0 | 0.0 | 0.0 | 0.0 | 0.0 |
| 2 | 94 | 91.5 | 0.0751 | 0.09338 | 0.0005 | 0.0005 |
| 3 | 94 | 85.5 | 0.148 | 0.18402 | 0.00171 | 0.00176 |
| 4 | 94 | 73.0 | 0.230 | 0.2860 | 0.00422 | 0.00400 |
| 5 | 94 | 59.5 | 0.300 | 0.37302 | 0.00693 | 0.00651 |
| 6 | 94 | 45.5 | 0.365 | 0.45384 | 0.00974 | 0.00935 |
| 7 | 94 | 22.1 | 0.454 | 0.5645 | 0.01444 | 0.01400 |
| 8 | 94 | 10.5 | 0.495 | 0.61548 | 0.01677 | 0.01650 |
| 9 | 94 | 5.5 | 0.515 | 0.64035 | 0.01777 | 0.01770 |

where $D_L$ is the lateral inner diameter, $L_L$ is the lateral length, h1 is the pressure head at the lateral inlet, h2 is the pressure head at the lateral outlet, MLF is the measured friction loss of the lateral, Q is the measured lateral discharge, V is the lateral water velocity and FLHW is the lateral theoretical friction loss based on a value of 140 for $C_{HwL}$.

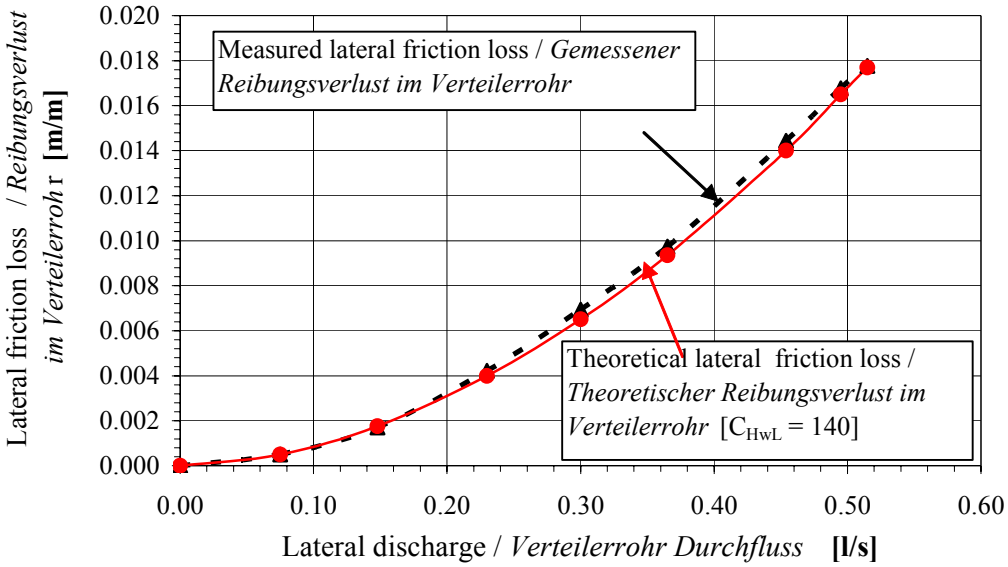


Figure 4.46: Lateral friction loss. [$D_L$ = 32 mm, $L_L$ = 50 m]
*Reibungsverlust im Verteilerrohr.*

### 4.3.2.2 Distributor hose friction loss

The average rate of energy loss for each steady, uniform flow test was obtained by using the formula:

$$MDF = \frac{Dh1 - Dh2}{L_{oh}} \qquad [m/m]$$

where: MDF is the measured friction loss of the distributor hose in [m/m], $L_{oh}$ is the length of the hose in [m], Dh1 is the pressure head at the hose inlet (upstream) in [m] and Dh2 is the pressure head at the hose outlet (downstream) in [m].

Table 4.4 illustrates an analysis of the distributor hose friction loss at various discharge rates based on laboratory work and the Hazen- William's equation given an inside diameter ($d_{oh}$) of 6 mm and a hose length of 3.5 m ($L_{oh}$).

The Hazen- William's coefficient ($C_{Hwh}$) was calculated for each hose discharge using Eq. (3.2.12). The results showed that a value of 115 for $C_{Hwh}$ was better. Figure 4.47 shows the relationship between the friction loss of the distributor hose and the discharge. Adopting the Hazen- Williams formula Eq. (3.2.12) with a value of 115 for $C_{Hwh}$ reasonably accounts for the experimental data.

Table 4.4: Distributor hose friction loss. [$d_{oh}$ = 6 mm, $L_{oh}$ = 3.5 m]
*Reibungsverlust im Verteilerschlauch.*

| Exp. Nr. | Dh1 [cm] | Dh2 [cm] | $q_{oh}$ [l/s] | $V_{oh}$ [m/s] | MDF [m/m] | FDHW [m/m] |
|---|---|---|---|---|---|---|
| 1 | 0.0 | 0.0 | 0.0 | 0.0 | 0.0 | 0.0 |
| 2 | 24.5 | 6.5 | 0.00937 | 0.3314 | 0.05143 | 0.0530 |
| 3 | 37.0 | 8.5 | 0.01193 | 0.42194 | 0.08143 | 0.0829 |
| 4 | 50.8 | 10.5 | 0.01410 | 0.4983 | 0.11514 | 0.1129 |
| 5 | 65.5 | 13.0 | 0.01597 | 0.56483 | 0.1500 | 0.1422 |
| 6 | 88.2 | 18.0 | 0.01958 | 0.69251 | 0.2006 | 0.2070 |

where $d_{oh}$ is the inner diameter of the distributor hose, $L_{oh}$ is the distributor hose length, Dh1 is the pressure head at the inlet of the distributor hose, Dh2 is the pressure head at the outlet of the distributor hose, MDF is the measured distributor hose friction loss, $q_{oh}$ is the measured distributor hose discharge, $V_{oh}$ is the distributor hose water velocity and FDHW is the theoretical friction loss of the distributor hose based on a value of 115 for $C_{Hwh}$.

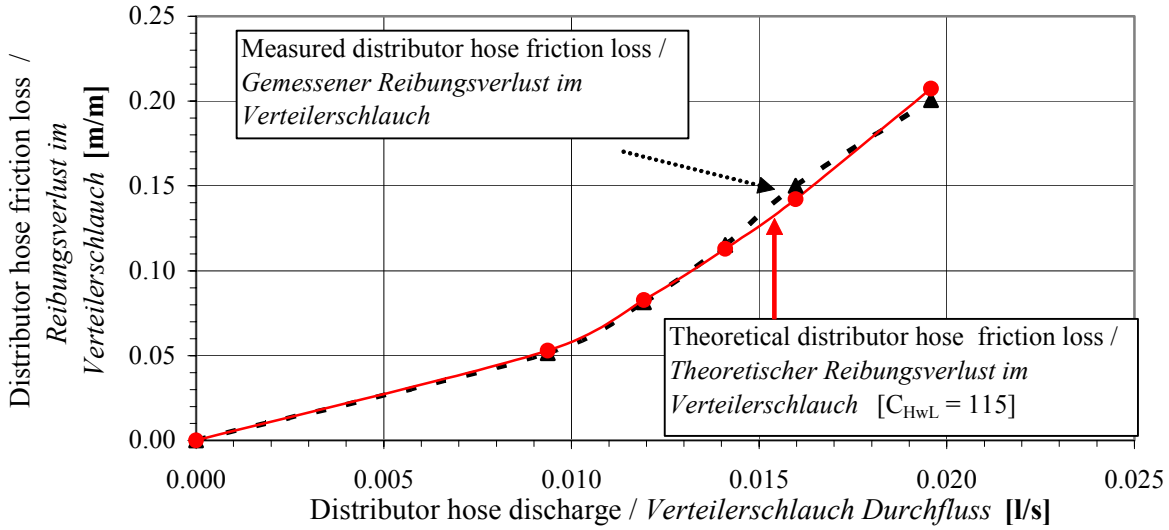


Figure 4.47: Distributor hose friction loss. [$L_{oh}$ = 3.50 m, $d_{oh}$ = 6 mm]
*Reibungsverlust im Verteilerschlauch.*

### 4.3.2.3 Model validation

To achieve a uniform distribution of water, it is necessary to analyse the water pressure distribution in the system. Because the discharge from the distributor hose is a function of water pressure, it is important to know the pressure distribution along the lateral and manifold pipelines. Many methods have been developed to analyse pressure distribution. Our computer program was written for the exact analysis of low-head bubbler irrigation systems at different distributor hose elevation or different distributor hose length. Data specific to the particular laboratory experiments described in the previous section was used.

**System 1:** low-head bubbler irrigation at ***Different Distributor Hose Elevation (DDHE)***

- Lateral number, $N_L = 1$
- Hose position from lateral on two lateral sides, S = 2
- Diameter of the lateral pipeline, $D_L = 32$ mm
- Diameter of the distributor hose, $d_{oh} = 6$ mm
- Distributor hose spacing, $S_L = 4$ m
- Distributor hose length, $L_{oh} = 2.5$ m
- Number of the distributor hoses per lateral side, $n_{oh} = 13$
- Hazen-William's coefficient of the lateral pipeline, $C_{HwL} = 140$
- Hazen-William's coefficient of the distributor hoses, $C_{Hwh} = 115$
- Longitudinal slope of the lateral pipeline (lateral), $So_L = 0.0\%$, + 0.5% and - 0.5%
- Distributor hose discharge, $q_{oh} = 20$, 40 and 60 l/h

The distributor hose elevation and required pressure head at the lateral inlet were calculated by the computer program and these data were applied in two variants in a laboratory experimental system at three lateral slopes and three hose discharge rates. **Firstly,** the laterals were located on two manifold sides (SS = 2). The theoretical and the measured data for this variant are presented in Tables 4.5 and 4.6 and Tables B-1 to B-4 in appendix B. The data presented in the Tables 4.5 and 4.6 are also illustrated in Figures 4.48 and 4.49. **Secondly,** the laterals located one manifold side only (SS = 1). The theoretical and measured data are presented in Tables 4.7 and 4.8 and Tables B-5 to B-8 in appendix B. In addition, the data presented in the Tables 4.7 and 4.8 are illustrated in Figures 4.50 and 4.51.

Distributor hose emission uniformity and flow variation were calculated from the laboratory experiments data by using equations 4.3.1 and 4.3.2, in two variants: a low-head bubbler irrigation system with different distributor hose elevation or different distributor hose length along one lateral. In the case of irrigation systems with different distributor hose elevation, the distributor hose emission uniformity and flow variation are presented in Tables 4.5 to 4.8 and Tables B-1 to B-8 in appendix B. The emission uniformity values were higher than 97% at all distributor hose discharge rates (20, 40 and 60 l/h). This is extremely high as compared with commercial irrigation systems. This is a consequence of the fact that the hose outlets are simply and individually adjustable. On the other hand, the flow variation values were lower than 5% when the theoretical hoses discharge were 40 l/h and 60 l/h but it was 5% to 7% when the theoretical hoses discharge was 20 l/h. At the same time when all distributor hose outlets were at the level of the lateral and applied the same operation pressure head, emission uniformity values were 62% to 98% and flow variation values were 4.7% to 63.4%. These results are presented in Tables 4.5 to 4.8 and Tables B-1 to B-8 in appendix B.

Table 4.5: Measured distributor hose outflow at different distributor hose elevation along one lateral. **[S = 2, SS = 2 and $q_{oh}$ = 60 l/h]**

*Gemessener Verteilerschlauchdurchfluss entlang eines Verteilerrohres mit unterschiedlich hohen Auslässen am Verteilerschlauch.*

| Nr. of DH | MDHO [l/h] at DDHE | | | MDHO [l/h] at DHEZ | | |
|---|---|---|---|---|---|---|
| | $So_L$ = + 0.5% | $So_L$ = - 0.5% | $So_L$ = 0.0% | $So_L$ = + 0.5% | $So_L$ = - 0.5% | $So_L$ = 0.0% |
| 1 | 60.01 | 60.06 | 61.80 | 80.82 | 76.27 | 79.02 |
| 2 | 60.98 | 60.30 | 61.78 | 79.08 | 76.53 | 78.90 |
| 3 | 59.92 | 60.12 | 61.20 | 77.40 | 74.07 | 77.34 |
| 4 | 59.71 | 60.96 | 60.83 | 75.36 | 74.20 | 76.44 |
| 5 | 60.39 | 61.44 | 60.55 | 72.72 | 73.40 | 73.62 |
| 6 | 61.72 | 60.60 | 60.92 | 70.44 | 73.67 | 72.30 |
| 7 | 60.97 | 60.66 | 61.39 | 69.84 | 73.80 | 72.18 |
| 8 | 60.49 | 61.56 | 60.28 | 67.26 | 72.93 | 72.12 |
| 9 | 60.38 | 59.76 | 59.82 | 65.04 | 73.13 | 69.48 |
| 10 | 60.74 | 60.96 | 60.28 | 62.94 | 73.40 | 69.42 |
| 11 | 60.88 | 60.60 | 61.14 | 61.68 | 74.70 | 69.12 |
| 12 | 61.23 | 61.26 | 60.05 | 60.24 | 75.13 | 68.82 |
| 13 | 61.37 | 61.20 | 59.70 | 59.82 | 76.47 | 69.24 |
| **EU %** | **98.68** | **98.78** | **98.53** | **87.25** | **98.25** | **94.71** |
| **$q_{oh\ var}$ %** | **3.26** | **2.92** | **3.40** | **25.98** | **4.70** | **12.91** |

where **DH** is the distributor hose, **$So_L$** is the lateral slope, **MDHO** is the measured distributor hoses outflow, **DDHE** is different distributor hose outlet elevation (calculated by computer program), **DHEZ** is the outlet elevation of the distributor hoses (zero from lateral level), **S = 2** is the hose position on two lateral sides, **SS = 2** is the laterals on two manifold sides, **$q_{oh}$** is the theoretical discharge of the distributor hose, **EU** is the emission uniformity of distributor hoses and **$q_{oh\ var}$** is distributor hoses flow variation, in %,

Table 4.6: Measured and calculated pressure head just before each distributor hose inlet and calculated hose outlet elevation along one lateral. **[S = 2, SS = 2 and $q_{oh}$ = 60 l/h]**

*Gemessene und berechnete Druckhöhen am Übergang vom Verteilerrohr zum Verteilerschlauch und berechnete Auslasshöhen der Verteilerschläuche.*

| Nr. of DH | $So_L$ = + 0.5% , Hf = 99.6 cm | | | $So_L$ = - 0.5% , Hf = 99.6 cm | | | $So_L$ = 0.0% , Hf = 99.6 cm | | |
|---|---|---|---|---|---|---|---|---|---|
| | MPH [cm] | TPH [cm] | DHE [cm] | MPH [cm] | TPH [cm] | DHE [cm] | MPH [cm] | TPH [cm] | DHE [cm] |
| 1 | 96.70 | 96.10 | 44.37 | 98.80 | 98.06 | 46.37 | 97.20 | 97.06 | 45.37 |
| 2 | 89.20 | 89.70 | 38.00 | 96.10 | 95.67 | 44.00 | 92.40 | 92.69 | 41.00 |
| 3 | 83.30 | 84.00 | 32.29 | 94.00 | 93.97 | 42.29 | 88.20 | 88.97 | 37.29 |
| 4 | 78.00 | 78.87 | 27.18 | 92.10 | 92.87 | 41.18 | 85.00 | 85.87 | 34.18 |
| 5 | 73.30 | 74.33 | 22.64 | 91.30 | 92.32 | 40.64 | 82.20 | 83.33 | 31.64 |
| 6 | 68.90 | 70.29 | 18.61 | 91.10 | 92.29 | 40.61 | 79.30 | 81.29 | 29.61 |
| 7 | 65.70 | 66.71 | 15.03 | 90.80 | 92.71 | 41.03 | 77.50 | 79.71 | 28.03 |
| 8 | 63.20 | 63.53 | 11.85 | 91.40 | 93.53 | 41.85 | 75.20 | 78.53 | 26.85 |
| 9 | 59.30 | 60.70 | 9.01 | 92.40 | 94.70 | 43.01 | 74.20 | 77.70 | 26.01 |
| 10 | 56.50 | 58.16 | 6.47 | 94.00 | 96.16 | 44.47 | 73.60 | 77.16 | 25.47 |
| 11 | 54.60 | 55.85 | 4.17 | 95.30 | 97.85 | 46.17 | 72.40 | 76.85 | 25.17 |
| 12 | 52.00 | 53.71 | 2.03 | 97.10 | 99.72 | 48.03 | 72.60 | 76.72 | 25.03 |
| 13 | 50.10 | 51.69 | 0.00 | 99.70 | 102.00 | 50.00 | 73.00 | 76.69 | 25.00 |

where **Hf** is the pressure head at lateral inlet, **MPH** is the measure pressure head just before each distributor hose inlet, **TPH** is the theoretical pressure head calculated by the computer program and **DHE** is the distributor hose outlet elevation.

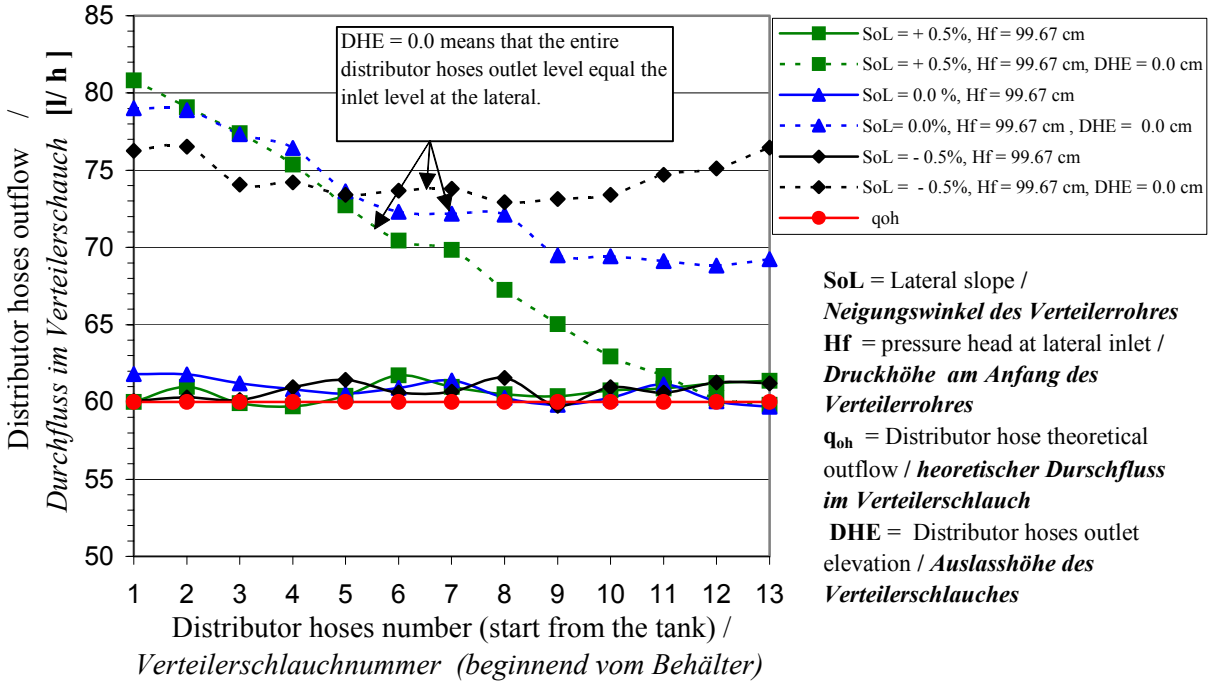


Figure 4.48: Measured and theoretical distributor hose outflow along one lateral at different distributor hose outlet elevation. **[S = 2, SS = 2 and $q_{oh}$ = 60 l/h]**
*Gemessener und theoretisch Durchfluss entlang eines Verteilerrohres mit unterschiedlich hohen Auslässen am Verteilerschlauch.*

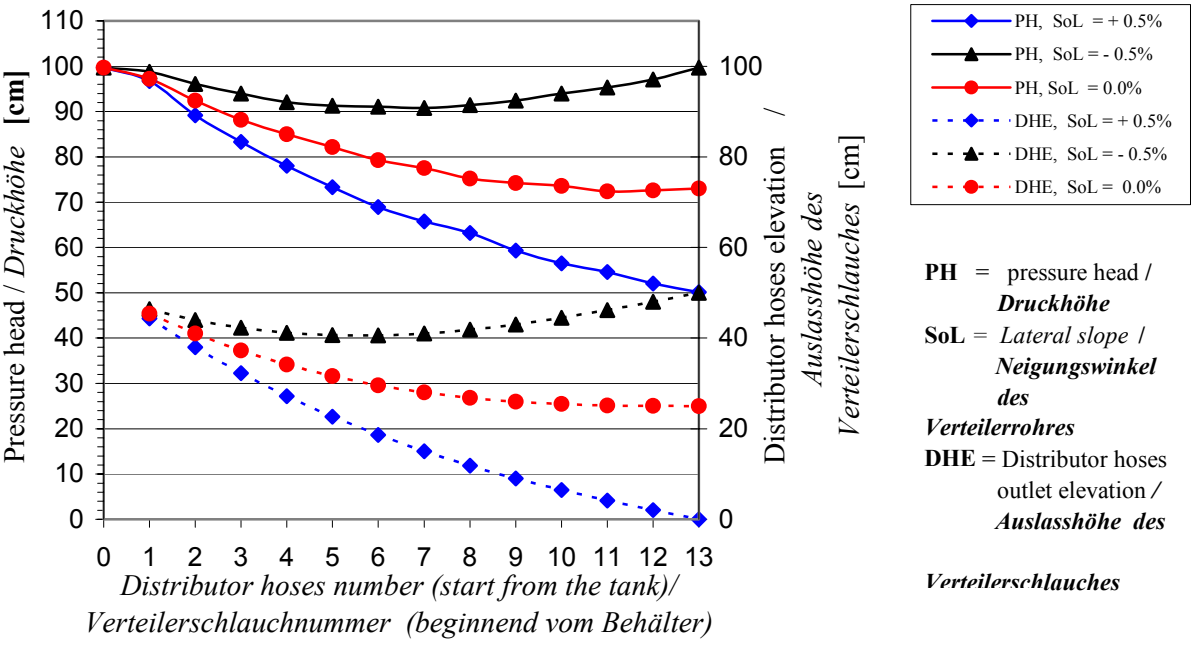


Figure 4.49: Measured pressure head just before the distributor hoses and calculated distributor hose outlet elevation along one lateral.**[S = 2, SS = 2 and $q_{oh}$ = 60 l/h]**
*Gemessene Druckhöhen am Übergang vom Verteilerrohr zum Verteilerschlauch und berechnete Auslasshöhen der Verteilerschlauche entlang eines Verteilerrohres.*

Table 4.7: Measured distributor hose outflow at different distributor hose elevation along one lateral. **[S = 2, SS = 1 and $q_{oh}$ = 60 l/h]**

*Gemessener Verteilerschlauchdurchfluss entlang eines Verteilerrohres mit unterschiedlich hohen Auslässen am Verteilerschlauch.*

| Nr. of DH | MDHO [l/h] at DDHE | | | MDHO [l/h] at DHEZ | | |
|---|---|---|---|---|---|---|
| | $So_L$ = + 0.5% | $So_L$ = - 0.5% | $So_L$ = 0.0% | $So_L$ = + 0.5% | $So_L$ = - 0.5% | $So_L$ = 0.0% |
| 1 | 60.23 | 60.01 | 60.59 | 71.23 | 80.82 | 69.10 |
| 2 | 60.16 | 60.98 | 60.93 | 69.36 | 79.08 | 67.34 |
| 3 | 60.32 | 59.92 | 60.54 | 69.41 | 77.4 | 67.39 |
| 4 | 60.60 | 59.71 | 60.68 | 68.35 | 75.36 | 66.38 |
| 5 | 60.55 | 60.39 | 60.68 | 67.10 | 72.72 | 65.16 |
| 6 | 60.92 | 61.72 | 60.93 | 65.33 | 70.44 | 63.43 |
| 7 | 61.39 | 60.97 | 60.88 | 64.94 | 69.84 | 63.07 |
| 8 | 60.28 | 60.49 | 60.93 | 62.82 | 67.26 | 61.01 |
| 9 | 59.82 | 60.38 | 60.30 | 62.11 | 65.04 | 60.29 |
| 10 | 60.28 | 60.74 | 60.54 | 60.38 | 62.94 | 58.61 |
| 11 | 60.88 | 60.88 | 60.44 | 61.54 | 61.68 | 59.76 |
| 12 | 60.37 | 61.23 | 60.89 | 61.78 | 60.24 | 60.00 |
| 13 | 61.10 | 61.37 | 61.10 | 62.30 | 59.82 | 60.48 |
| **EU %** | **98.69** | **99.51** | **99.49** | **87.25** | **97.87** | **94.03** |
| **$q_{oh\ var}$ %** | **2.92** | **1.31** | **2.56** | **25.98** | **7.88** | **15.18** |

where: **DH** is the distributor hose, **$So_L$** is the lateral slope, **MDHO** is the measured distributor hose outflow, **DDHE** is different distributor hose outlet elevation (calculated by computer program), **DHEZ** is the outlet elevation of the distributor hoses (zero from lateral level), **S = 2** is the hose position on two lateral sides, **SS = 1** is the laterals on two manifold sides, **$q_{oh}$** is the theoretical discharge of the distributor hose, **EU** is the emission uniformity of distributor hoses and **$q_{oh\ var}$** is distributor hose flow variation.

Table 4.8: Measured and calculated pressure head just before each distributor hose inlet and calculated hose outlet elevation along one lateral.**[S = 2, SS = 1 and $q_{oh}$ = 60 l/h]**

*Gemessene und berechnete Druckhöhen am Übergang vom Verteilerrohr zum Verteilerschlauch und berechnete Auslasshöhen der Verteilerschläuche.*

| Nr. of DH | $So_L$ = + 0.5% , Hf = 99.6 cm | | | $So_L$ = - 0.5% , Hf = 70.5 cm | | | $So_L$ = 0.0% , Hf = 74.7 cm | | |
|---|---|---|---|---|---|---|---|---|---|
| | MPH [cm] | TPH [cm] | DHE [cm] | MPH [cm] | TPH [cm] | DHE [cm] | MPH [cm] | TPH [cm] | DHE [cm] |
| 1 | 96.70 | 96.10 | 44.40 | 68.40 | 68.88 | 17.20 | 73.60 | 72.06 | 20.37 |
| 2 | 89.20 | 89.70 | 38.00 | 66.30 | 66.51 | 14.18 | 67.90 | 67.67 | 15.99 |
| 3 | 83.30 | 84.00 | 32.30 | 64.10 | 64.40 | 13.10 | 63.70 | 63.98 | 12.29 |
| 4 | 78.00 | 78.87 | 27.18 | 62.20 | 63.70 | 12.00 | 60.50 | 60.87 | 9.18 |
| 5 | 73.30 | 74.33 | 22.64 | 61.50 | 63.15 | 11.50 | 57.70 | 58.33 | 6.65 |
| 6 | 68.90 | 70.29 | 18.61 | 61.10 | 63.12 | 11.40 | 54.80 | 56.29 | 4.61 |
| 7 | 65.70 | 66.71 | 15.03 | 61.00 | 63.54 | 11.90 | 53.00 | 54.70 | 3.04 |
| 8 | 63.20 | 63.53 | 11.85 | 61.30 | 64.36 | 12.70 | 50.70 | 53.53 | 1.85 |
| 9 | 59.30 | 60.70 | 9.01 | 62.20 | 65.53 | 13.80 | 49.70 | 52.70 | 1.01 |
| 10 | 56.50 | 58.16 | 6.47 | 64.00 | 66.99 | 15.30 | 49.10 | 52.16 | 0.47 |
| 11 | 54.60 | 55.85 | 4.17 | 65.30 | 68.68 | 17.00 | 47.90 | 51.85 | 0.17 |
| 12 | 52.00 | 53.71 | 2.03 | 67.00 | 70.54 | 18.90 | 48.10 | 51.72 | 0.03 |
| 13 | 50.10 | 51.69 | 0.00 | 89.80 | 72.51 | 20.80 | 48.50 | 51.69 | 0.00 |

where: **Hf** is the pressure head at lateral inlet, **MPH** is the measure pressure head just before each distributor hose inlet, **TPH** is the theoretical pressure head calculated by the computer program and **DHE** is the distributor hose outlet elevation.

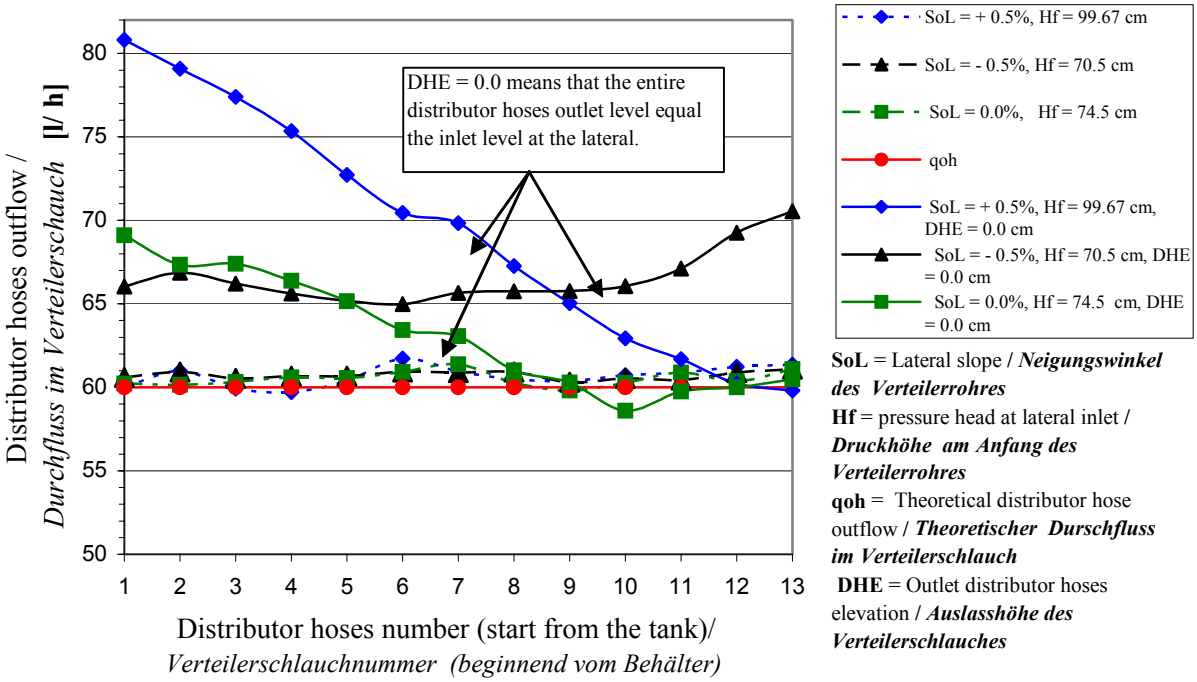


Figure 4.50: Measured and theoretical distributor hose outflow along one lateral at different distributor hose outlet elevation. **[S = 2, SS = 1 and $q_{oh}$ = 60 l/h]**
*Gemessener und theoretischer Durchfluss entlang eines Verteilerrohres mit unterschiedlich hohen Auslässen am Verteilerschlauch.*

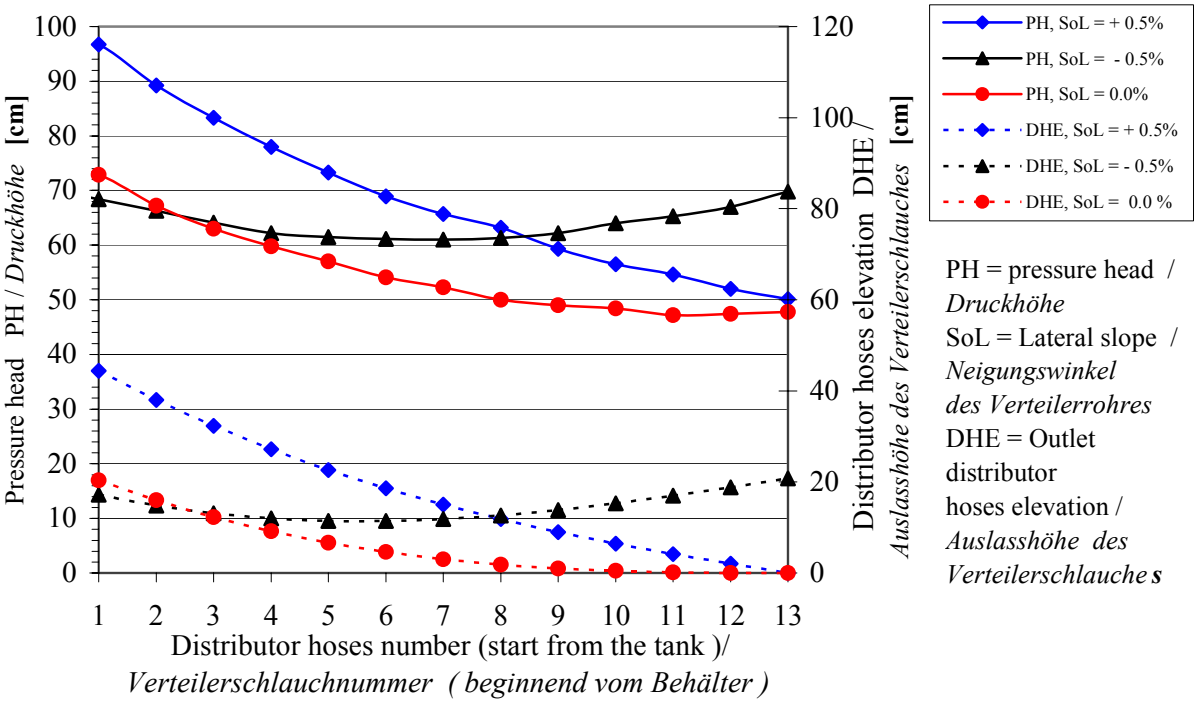


Figure 4.51: Measured pressure head just before the distributor hoses and calculated distributor hose outlet elevation along one lateral.**[S = 2, SS = 1 and $q_{oh}$ = 60 l/h]**
*Gemessene Druckhöhen am Übergang vom Verteilerrohr zum Verteilerschlauch und berechnete Auslasshöhen der Verteilerschlauche entlang eines Verteilerrohres.*

**System 2:** low-head bubbler irrigation at ***Different Distributor Hose Length (DDHL)***

- Lateral number, $N_L = 1$
- Hose position from lateral on one lateral side, S = 1
- Diameter of the lateral pipeline, $D_L = 32$ mm
- Diameter of the distributor hose, $d_{oh} = 6$ mm
- Distributor hose spacing, $S_L = 4$ m
- Number of the distributor hoses per lateral side, $n_{oh} = 13$
- Hazen-William's coefficient of the lateral pipeline, $C_{HwL} = 140$
- Hazen-William's coefficient of the distributor hoses, $C_{Hwh} = 115$
- Longitudinal slope of the lateral pipeline (lateral), $So_L = 0.0\%$ , + 0.5% and - 0.5%
- Distributor hose discharge, $q_{oh} = 60$ and 80 l/h

Distributor hose length and required pressure head at the lateral inlet were calculated by the computer program, and these data were applied in a laboratory experimental system at three lateral slopes and two hose discharge rates in two variants. **Firstly,** the laterals located on two manifold sides (SS = 2). The theoretical and measured data for this variant are presented in Tables 4.9 and 4.10 and Tables B-9 and B-10 in appendix B. The data presented in Tables 4.9 and 4.10 are also shown in Figures 4.52 and 4.53. **Secondly,** the laterals located on one manifold side (SS = 1) only. The theoretical and measured data are presented in Tables 4.11 and 4.12 and Tables B-11 and B-12 in appendix B. The data presented in Tables 4.11 and 4.12 are also shown in Figures 4.54 and 4.55.

Distributor hose emission uniformity and flow variation were also calculated based on the data provided by the laboratory experiments using equations 4.3.1 and 4.3.2 for low-head bubbler irrigation systems at different distributor hose length along one lateral. Distributor hose emission uniformity and flow variation for these variants are presented in Tables 4.9 to 4.12 and Tables B-9 to B-12 in appendix B. The emission uniformity values were higher than 97% at all distributor hose discharge rates (60 l/h and 80 l/h). At the same time, the flow variation values were lower than 5%. On the other hand, a low-head bubbler irrigation system featuring different distributor hose lengths could not be used in practice at all lateral slopes (in particular downhill) and when the distributor hose discharge was less than 60 l/h.

Table 4.9: Measured and theoretical distributor hose outflow along one lateral at different distributor hose length. **[S = 1, SS = 2 and $q_{oh}$ = 60 l/h]**

*Gemessener und theoretischer Durchfluß entlang eines Verteilerrohres mit unterschiedlicher Länge des Verteilerschlauches.*

| Nr. of DH from tank | MDHO [l/h] at DDHL | | $q_{oh}$ [l/h] |
|---|---|---|---|
| | $So_L$ = + 0.5 % | $So_L$ = 0.0 % | |
| 1 | 60.88 | 60.00 | 60 |
| 2 | 60.56 | 60.60 | 60 |
| 3 | 59.52 | 61.10 | 60 |
| 4 | 62.32 | 61.80 | 60 |
| 5 | 60.96 | 61.30 | 60 |
| 6 | 62.16 | 61.50 | 60 |
| 7 | 59.76 | 61.10 | 60 |
| 8 | 61.76 | 61.80 | 60 |
| 9 | 60.88 | 60.00 | 60 |
| 10 | 61.28 | 61.50 | 60 |
| 11 | 59.84 | 60.60 | 60 |
| 12 | 60.56 | 60.40 | 60 |
| 13 | 61.84 | 60.60 | 60 |
| **EU %** | **97.97** | **98.99** | |
| **$q_{oh\ var}$ %** | **4.49** | **2.91** | |

Where **DH** is the distributor hose, **$So_L$** is the lateral slope, **MDHO** is the measured distributor hoses outflow, **DDHL** is different distributor hose length (calculated by computer program), **S = 1** is the hose position on one lateral side only, **SS = 2** is the laterals on both manifold sides, **$q_{oh}$** is the distributor hose theoretical discharge, **EU** is the emission uniformity of distributor hoses and **$q_{oh\ var}$** is distributor hose flow variation.

Table 4.10: Measured and calculated pressure head just before each hose inlet and calculated hose length along one lateral. **[S = 1, SS = 2 and $q_{oh}$ = 60 l/h]**

*Gemessene und berechnete Druckhöhen am Übergang vom Verteilerrohr zum Verteilerschlauch und berechnete unterschiedliche Länge des Verteilerschlauches entlang eines Verteilerrohres.*

| Nr. of DH from the tank | $So_L$ = + 0.5% , Hf = 52.5 cm | | | $So_L$ = 0.0 % , Hf = 52.5 cm | | |
|---|---|---|---|---|---|---|
| | MPH [cm] | TPH [cm] | DHL [cm] | MPH [cm] | TPH [cm] | DHL [cm] |
| 1 | 50.00 | 50.76 | 243.90 | 51.20 | 51.75 | 250.50 |
| 2 | 46.40 | 47.54 | 222.90 | 49.90 | 50.54 | 242.50 |
| 3 | 44.10 | 44.51 | 203.10 | 48.90 | 49.51 | 235.80 |
| 4 | 40.90 | 41.65 | 184.40 | 48.00 | 48.65 | 230.10 |
| 5 | 38.30 | 38.94 | 166.70 | 47.10 | 47.94 | 225.50 |
| 6 | 35.70 | 36.37 | 149.90 | 46.60 | 47.37 | 221.80 |
| 7 | 33.60 | 33.93 | 134.00 | 45.80 | 46.93 | 218.90 |
| 8 | 30.80 | 31.60 | 118.70 | 45.20 | 46.60 | 216.80 |
| 9 | 28.40 | 29.37 | 104.20 | 44.80 | 46.37 | 215.30 |
| 10 | 25.90 | 27.22 | 90.10 | 44.50 | 46.22 | 214.30 |
| 11 | 23.60 | 25.14 | 76.50 | 44.20 | 46.14 | 213.70 |
| 12 | 21.60 | 23.10 | 63.10 | 44.50 | 46.10 | 213.50 |
| 13 | 19.60 | 21.10 | 50.00 | 44.60 | 46.10 | 213.40 |

where **Hf** is the pressure head at the lateral inlet, **MPH** is the measured pressure head just before each distributor hose inlet, **TPH** is the theoretical pressure head calculated by the computer program and **DHL** is the distributor hose length.

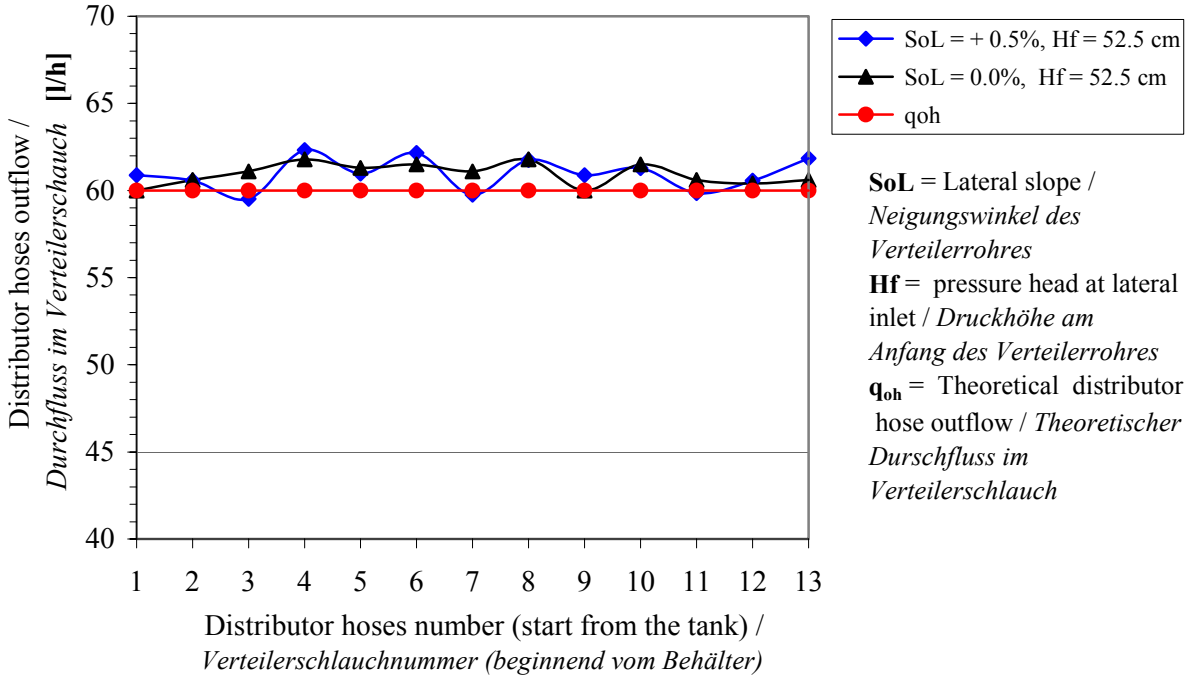


Figure 4.52: Measured and theoretical distributor hose outflow along one lateral at different hose length. **[S = 1, SS = 2 and $q_{oh}$ = 60 l/h]**
*Gemessener und theoretischer Durchfluss entlang eines Verteilerrohres mit unterschiedlicher Länge des Verteilerschlauches..*

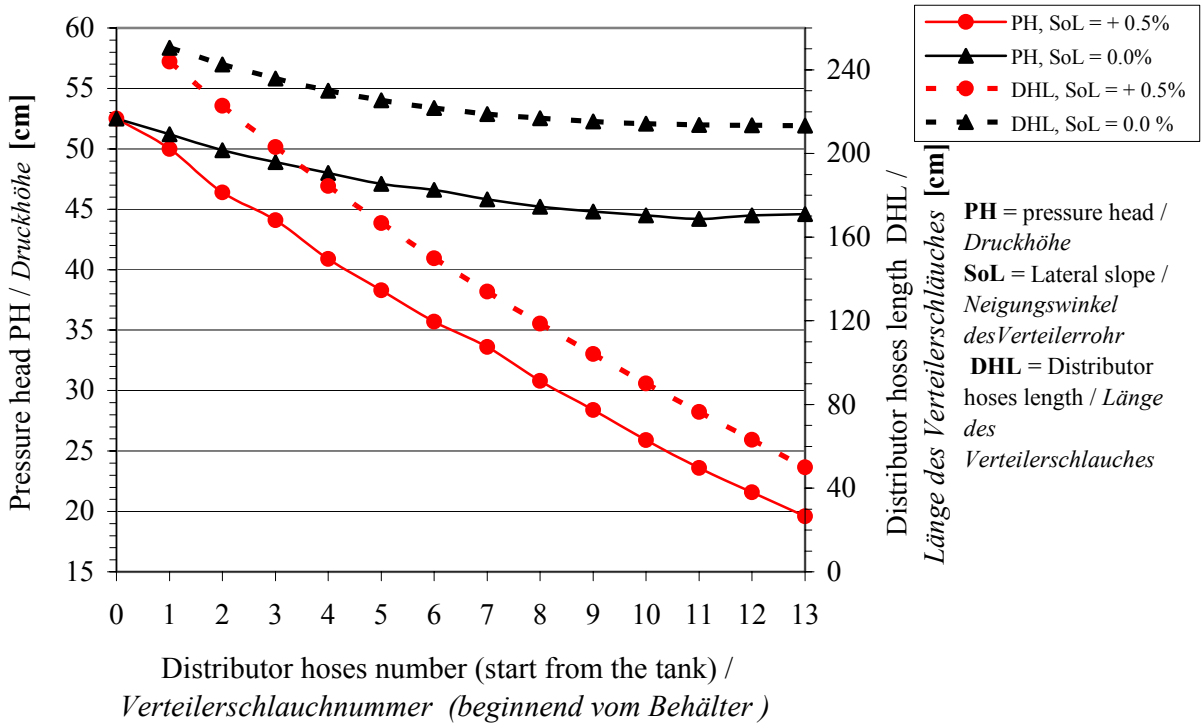


Figure 4.53: Measured pressure head just before each distributor hose inlet and calculated hose length along one lateral**. [S = 1, SS = 2 and $q_{oh}$ = 60 l/h]**
*Gemessene Druckhöhe am Übergang vom Verteilerrohr zum Verteilerschlauch und berechnete unterschiedliche Länge eines Verteilerschlauches.*

Table 4.11: Measured and theoretical distributor hoses outflow along one lateral at different distributor hose length. **[S = 1, SS = 1 and $q_{oh}$ = 60 l/h]**

*Gemessener und theoretischer Durchfluß entlang eines Verteilerrohres mit unterschiedlicher Länge des Verteilerschlauches.*

| Nr. of DH from the tank | MDHO [l/h] at DDHL | | | $q_{oh}$ [l/h] |
|---|---|---|---|---|
| | $So_L$ = + 0.5 % | $So_L$ = - 0.5 % | $So_L$ = 0.0 % | |
| 1 | 60.88 | 59.80 | 62.30 | 60 |
| 2 | 60.56 | 60.00 | 60.60 | 60 |
| 3 | 59.52 | 60.30 | 61.60 | 60 |
| 4 | 62.32 | 62.10 | 62.70 | 60 |
| 5 | 60.96 | 62.80 | 60.90 | 60 |
| 6 | 62.16 | 61.00 | 61.80 | 60 |
| 7 | 59.76 | 60.30 | 61.20 | 60 |
| 8 | 61.76 | 62.30 | 62.40 | 60 |
| 9 | 60.88 | 60.60 | 61.50 | 60 |
| 10 | 61.28 | 60.80 | 62.50 | 60 |
| 11 | 59.84 | 61.10 | 63.20 | 60 |
| 12 | 60.56 | 60.70 | 62.10 | 60 |
| 13 | 61.84 | 60.80 | 62.40 | 60 |
| **EU %** | **97.97** | **98.62** | **98.32** | |
| **$q_{oh\ var}$ %** | **4.49** | **4.78** | **3.35** | |

where **DH** is the distributor hose, **$So_L$** is the lateral slope, **MDHO** is the measured distributor hose outflow, **DDHL** is different distributor hose length (calculated by computer program), **S = 1** is the hose position only on one lateral side, **SS = 1** is the laterals only on one manifold side, **$q_{oh}$** is the distributor hose theoretical discharge, **EU** is the emission uniformity of the distributor hoses and **$q_{oh\ var}$** is distributor hose flow variation.

Table 4.12: Measured and calculated pressure head just before each hose inlet and calculated hose length along one lateral. **[S = 1, SS = 1 and $q_{oh}$ = 60 l/h]**

*Gemessene und berechnete Druckhöhen am Übergang vom Verteilerrohr zum Verteilerschlauch und berechnete unterschiedliche Länge des Verteilerschlauches entlang eines Verteilerrohres.*

| Nr. of DH | $So_L$ = + 0.5% , Hf = 52.5 cm | | | $So_L$ = - 0.5% , Hf = 16.8 cm | | | $So_L$ = 0.0 % , Hf = 27.5 cm | | |
|---|---|---|---|---|---|---|---|---|---|
| | MPH [cm] | TPH [cm] | DHL [cm] | MPH [cm] | TPH [cm] | DHL [cm] | MPH [cm] | TPH [cm] | DHL [cm] |
| 1 | 50.00 | 50.76 | 243.90 | 17.00 | 17.07 | 23.70 | 26.50 | 26.76 | 87.00 |
| 2 | 46.40 | 47.54 | 222.90 | 17.30 | 17.85 | 28.90 | 25.30 | 25.54 | 79.10 |
| 3 | 44.10 | 44.51 | 203.10 | 18.20 | 18.82 | 35.20 | 24.20 | 24.51 | 72.40 |
| 4 | 40.90 | 41.65 | 184.40 | 19.20 | 19.96 | 42.60 | 23.50 | 23.65 | 66.70 |
| 5 | 38.30 | 38.94 | 166.70 | 20.30 | 21.25 | 51.10 | 22.60 | 22.94 | 62.10 |
| 6 | 35.70 | 36.37 | 149.90 | 21.50 | 22.69 | 60.40 | 21.70 | 22.37 | 58.40 |
| 7 | 33.60 | 33.93 | 134.00 | 23.10 | 24.25 | 70.60 | 21.10 | 21.93 | 55.50 |
| 8 | 30.80 | 31.60 | 118.70 | 24.70 | 25.92 | 81.60 | 20.60 | 21.60 | 53.40 |
| 9 | 28.40 | 29.37 | 104.20 | 26.60 | 27.69 | 93.10 | 20.30 | 21.37 | 51.90 |
| 10 | 25.90 | 27.22 | 90.10 | 28.10 | 29.53 | 105.20 | 20.00 | 21.22 | 50.90 |
| 11 | 23.60 | 25.14 | 6.50 | 30.00 | 31.40 | 117.70 | 19.60 | 21.14 | 50.30 |
| 12 | 21.60 | 23.10 | 63.10 | 32.00 | 33.40 | 130.50 | 19.50 | 21.10 | 50.10 |
| 13 | 19.60 | 21.10 | 50.00 | 34.00 | 35.40 | 143.60 | 19.50 | 21.10 | 50.00 |

where **Hf** is the pressure head at lateral inlet, **MPH** is the measure pressure head just before each distributor hose inlet, **TPH** is the theoretical pressure head calculated by the computer program and **DHL** is the distributor hose length.

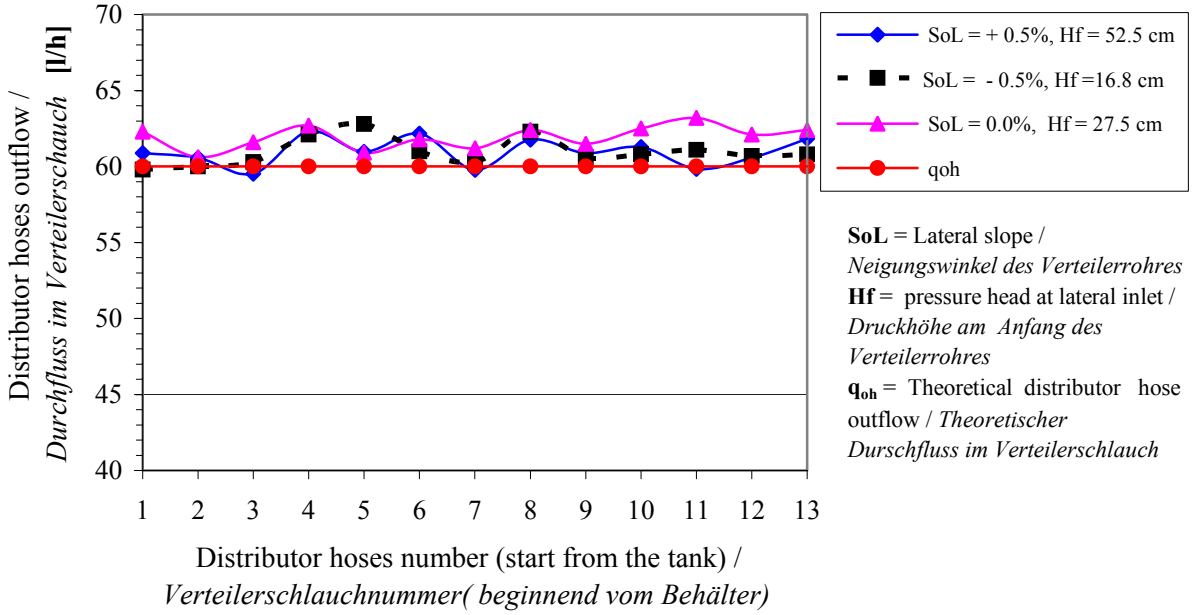


Figure 4.54: Measured and theoretical distributor hose outflow along one lateral at different hose length. **[S = 1, SS = 1 and $q_{oh}$ = 60 l/h]**
*Gemessener und theoretischer Durchfluss entlang eines Verteilerrohres mit unterschiedlicher Länge des Verteilerschlauches.*

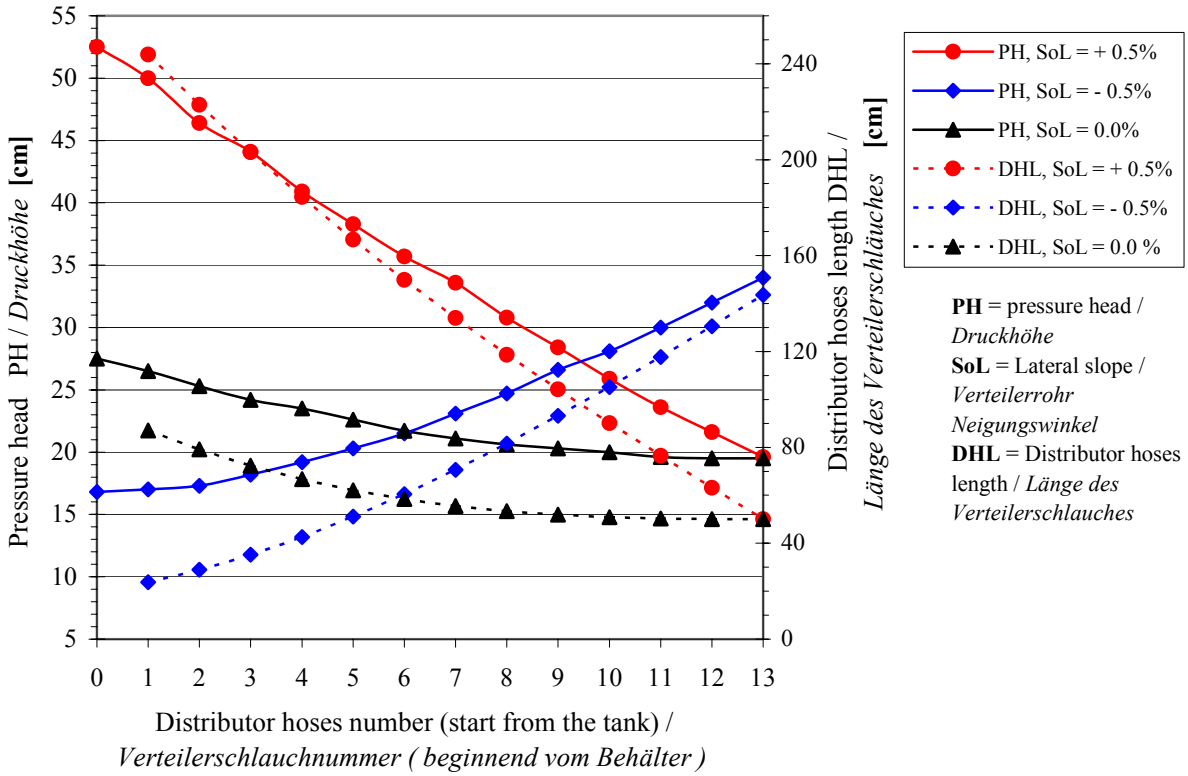


Figure 4.55: Measured pressure head just before each distributor hose inlet and calculated hose length along one lateral. **[S = 1, SS = 1 and $q_{oh}$ = 60 l/h]**
*Gemessene Druckhöhe am Übergang vom Verteilerrohr zum Verteilerschlauch mit berechneter unterschiedlicher Länge eines Verteilerschlauches.*

In order to determine whether the mathematical model is an accurate representation of the real bubbler irrigation systems at different distributor hose outlet elevation or different distributor hose length, the results of the laboratory tests were compared with the results obtained from the mathematical model. The theoretical and measured hose outflow, the theoretical and measured pressure head at each hose inlet and distributor hose outlet elevation or distributor hose length are presented in Tables 4.5 to 4.12 and B-1 to B-12 in appendix B. The data presented in Tables 4.5 to 4.12, are also shown in Figures 4.48 to 4.55. Within the limits of experimental accuracy, these Figures demonstrate the ability of the mathematical model to predict hose elevation or hose length in bubbler irrigation systems correctly.

### 4.3.2.4 Comparison of low-head bubbler irrigation systems

The slope of the land is most critical when selecting an irrigation method. If the land has a surface slope between ± 1.5%, bubbler irrigation systems can be used. But if the land slope exceeds the range of ± 1.5%, it may be better to use other irrigation methods.

By running the computer program and laboratory experiments of low-head bubbler irrigation systems (at different distributor hose outlet elevation DDHE or at different distributor hose length DDHL), one can decide whether the use of low-head bubbler irrigation systems at different distributor hose outlet elevation is more practical than the system which features different hose lengths for the irrigation of tree crops such as orchards in particular when the land is not level (land surface slope between ± 1.5%), because the maximum increase of the pressure head at the hose inlet in the irrigation system (one manifold) must be lost by increase the hoses length to obtain equal outflow from all hoses in the irrigation system. Assume that 0.3 m and 1 m are the minimum and maximum hose outlet elevation respectively in bubbler irrigation systems with different distributor hose outlet elevation. To use the bubbler system with different distributor hose length, the head $(h_f)_h = 1 - 0.3 = 0.7$ m is lost by friction in the hose. If, for example, hose discharge $q_{oh} = 60$ l/h, the Hazen-William's coefficient of the distributor hoses $C_{Hwh} = 115$, hose diameter $d_{oh} = 6$ mm and the minimum length of hoses in irrigation systems equals 0.5 m, the maximum increase of hose lengths ($L_{ih}$) can be calculated using Hazen-William's equation:

$$(h_f)_h = \frac{1.22 \times 10^{10} \times L_{ih}}{d_{oh}^{4.87}} \left( \frac{q_{oh}}{C_{Hwh}} \right)^{1.852} \quad \Rightarrow \quad 0.70 = \frac{1.22 \times 10^{10} \times L_{ih}}{6^{4.87}} \left( \frac{60}{3600 \times 115} \right)^{1.852}$$

then, $L_{ih} = 4.55$ m and the maximum hose length will be = 0.5 + 4.55 = 5.05 m.

Given these considerations, it becomes evident that the bubbler system with different distributor hose length is not practical and causes greater expenses than a system with different distributor hose outlet elevation. But if the land is level, the bubbler system with different distributor hoses length can be used because the difference between maximum and minimum pressure head at hose inlets in irrigation systems equals the friction loss in irrigation pipelines (lateral and manifold). In this case, the maximum increase of hose length depends on lateral and manifold diameter.

In bubbler systems with different hoses outlet elevation the hose discharge rate can be altered by changing the hose outlet elevation, but different hoses length requires new hoses having new lengths. It must also be noted that any small error in hose outlet elevation in the bubbler system significantly affects the uniformity of water distribution from hoses, but a small error in hoses length has little impact on the uniformity of water distribution from hoses.

### 4.3.2.5 Simulation studies

Simulation studies for low-head bubbler irrigation systems with different distributor hose outlet elevation have been carried out. The computer program was used to investigate certain factors which influence maximum distributor hose outlet elevation in the bubbler irrigation system. A minimum hose outlet elevation of 0.3 m was used as input for the computer program when the laterals slope was uphill or level and the hoses were on two sides of the lateral (one lateral per two tree rows). The laterals were placed only on one side of the manifold, and the field sloped only in the direction of the laterals (manifold was level). The following values were determined:

1. Longitudinal slope of the lateral ($So_L$)
2. Diameter of, distributor hose ($d_{oh}$), lateral ($D_L$) and manifold ($D_{mf}$)
3. Distributor hose discharge ($q_{oh}$)
4. Number of distributor hoses for each lateral side ($n_{oh}$)
5. Number of laterals on the manifold ($N_L$)

Table 4.13 illustrates the range of different factors which influence the distributor hose outlet elevation in the bubbler irrigation system within a longitudinal slope of the lateral ranging from uphill + 2 % to downhill – 2%. The Hazen-William's coefficient for the lateral and the manifold is 140, and for the distributor hose it is 115. Distributor hoses spacing $S_L$ = 4 m along the lateral. The lateral spacing $S_m$ = 2 × trees spacing = 8 m and the hose length of 2.5 m along the manifold.

Table 4.13: Factors influencing the maximum distributor hose elevation along the laterals.
*Faktoren, die die maximale Verteilerschlauchhöhe entlang des Verteilerrohres beeinflussen.*

| | Hoses discharge $q_{oh}$ [l/h] | Hoses number $n_{oh}$ | Lateral diameter $D_L$ [mm] | Laterals number $N_L$ | Manifold diameter $D_{mf}$ [mm] | Hose diameter $d_{oh}$ [mm] |
|---|---|---|---|---|---|---|
| Figure 4.56 | **20, 40, 60, 80** | **13** | **32** | **7** | **75** | **6** |
| Figure 4.57 | **60** | **6, 13, 17** | **32** | **7** | **75** | **6** |
| Figure 4.58 | **60** | **13** | **25, 32, 42,52** | **7** | **75** | **6** |
| Figure 4.59 | **60** | **13** | **32** | **4, 7, 9** | **75** | **6** |
| Figure 4.60 | **60** | **13** | **32** | **7** | **52, 75, 85, 95** | **6** |
| Figure 4.61 | **60** | **13** | **32** | **7** | **75** | **4, 6, 8, 10** |

Figure 4.56 shows the maximum simulated distributor hose outlet elevation at different distributor hose outflows. The optimum slope for a given lateral pipeline is level. Maximum distributor hose outlet elevation increases when distributor hoses outflow grows on any lateral slope. For uphill lateral slopes, a small hose outflow should be used. The range of positive slopes over which acceptable maximum hose elevation is achieved increases rapidly as hose outflow decreases. When downhill lateral slope can be used, the outflow of the hoses is larger than the outflow on uphill lateral slopes at the same absolute slope value. Maximum and minimum hose elevation cannot be simielar on any lateral slope (uphill or level) but on lateral downhill slopes minimum hose elevation may be equal zero.

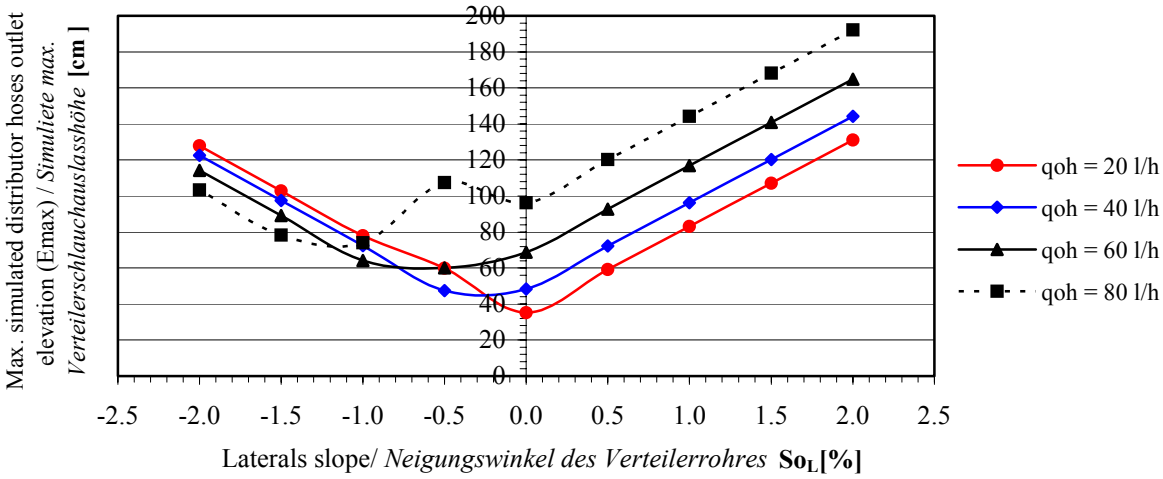


Figure 4.56: Maximum simulated distributor hose outlet elevation (Emax) at different hose outflows ($q_{oh}$).
*Simulierte maximale Auslasshöhe am Verteilerschlauch (Emax) bei unterschiedlichem Verteilerschlauchdurchfluss*($q_{oh}$).

Figure 4.57 shows the maximum simulated distributor hose outlet elevation for different hoses per lateral sides. The optimum slope for a given lateral pipeline is level. The maximum hose outlet elevation increases when the number of hoses increases on any lateral slope. For uphill lateral slopes, a small number of hoses should be used. The range of positive slopes over

which acceptable maximum hose elevation is achieved increases rapidly as the number of hoses decreases. In case of downhill lateral slopes, it could be use a hoses number more than if uphill lateral slope at the same absolute slope value. The maximum and minimum hose elevation cannot be reached on any lateral slope (uphill or level) or given any number of hoses, but on lateral downhill slopes minimum hose elevation may be equall zero.

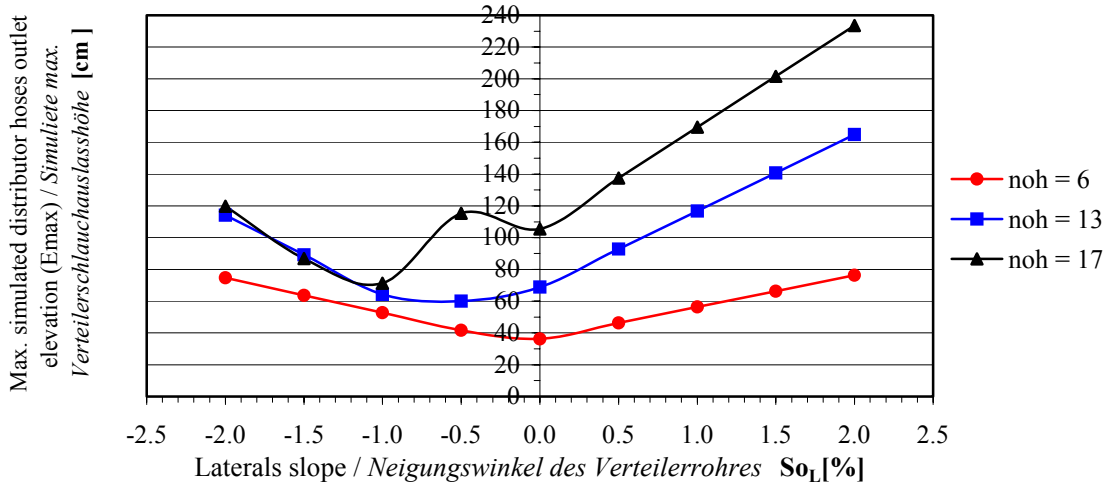


Figure 4.57: Maximum simulated distributor hose outlet elevation (Emax) for different hose numbers on the lateral ($n_{oh}$).
*Simulierte maximale Auslasshöhe am Verteilerschlauch (Emax) bei unterschiedlicher Zahl von Verteilerschläuchen am Verteilerrohr ($n_{oh}$).*

Figure 4.58 shows the maximum simulated distributor hose outlet elevation at different lateral diameters. The optimum slope for a given lateral pipeline is level. The maximum distributor hose outlet elevation increases when the lateral diameter decreases on any lateral slope. For uphill lateral slopes, large lateral diameters should be used. The range of positive slopes over which acceptable maximum hoses elevation is achieved increases rapidly as lateral diameters decrease. On downhill lateral slopes, the lateral diameter can be less than the lateral diameter on uphill lateral slopes if the absolute slope value is the same value. The maximum and minimum hose elevation cannot be reached on any lateral slope (uphill or level) or given any lateral diameters, but on lateral downhill slopes minimum hose elevation may be equall zero.

Figure 4.59 shows the maximum simulated distributor hose outlet elevation for different lateral numbers per manifold. The optimum slope for a given lateral pipeline is level. The maximum distributor hose outlet elevation increases when the lateral number per manifold increases on any lateral slope. For uphill lateral slopes, a small number of laterals per manifold should be used. The range of positive slopes over which acceptable maximum hose elevation is achieved increase rapidly as the lateral number per manifold decreases. On downhill lateral slopes, the lateral number per manifold can be larger than the number of laterals on uphill

lateral slopes if the absolute slope value is the same value. The maximum and minimum hose elevation cannot be reached on any lateral slope (uphill or level) or given any lateral number per manifold, but on lateral downhill slopes minimum hose elevation may be equall zero.

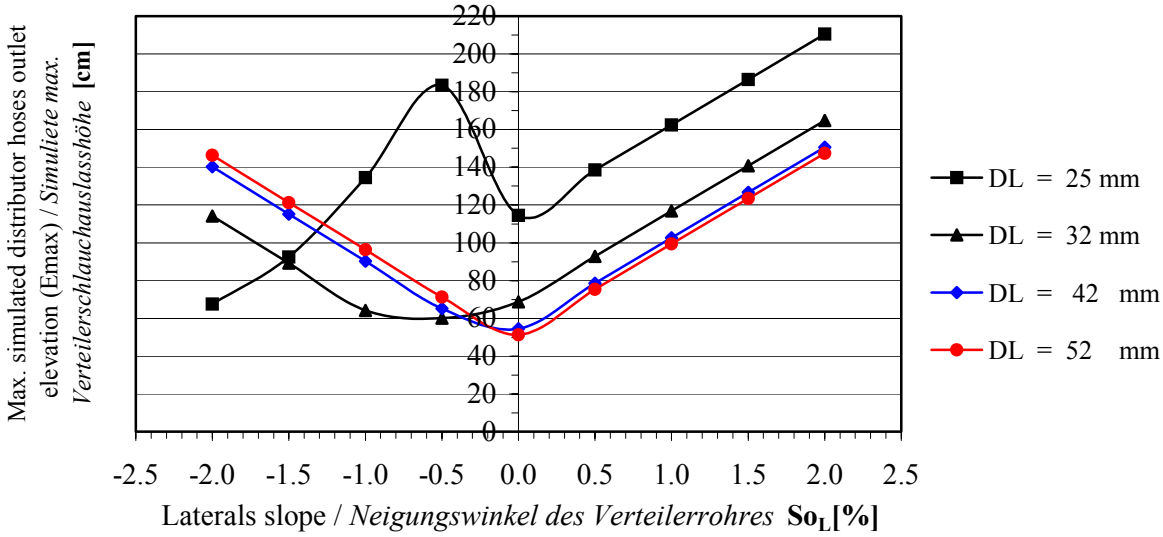


Figure 4.58: Maximum simulated distributor hose outlet elevation (Emax) at different lateral diameters ($D_L$).
*Simulierte maximale Auslasshöhe am Verteilerschlauch (Emax) bei unterschiedlichem Verteilerrohrdurchmesser ($D_L$).*

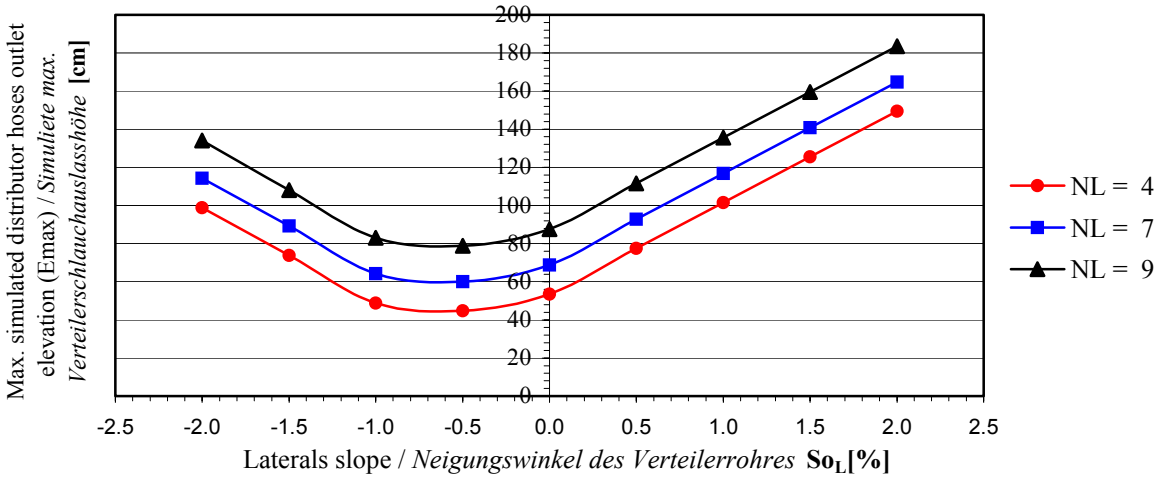


Figure 4.59: Maximum simulated distributor hose outlet elevation (Emax) at different lateral numbers on the manifold ($N_L$).
*Simulierte maximale Auslasshöhe an dem Verteilerschlauch (Emax) bei unterschiedlicher Zahl von Verteilerrohren am Feldzuleitung ($N_L$).*

Figure 4.60 shows the maximum simulated distributor hoses outlet elevation at different manifold diameters. The optimum slope for a given lateral pipeline is level. The maximum hose outlet elevation increases when the manifold diameter decreases on any lateral slope. For uphill or level lateral slopes, large manifold diameters should be used. The range of positive slopes

over which acceptable maximum hoses elevation is achieved increases rapidly as manifold diameters decrease. On downhill lateral slopes, the absolute slope value can be larger than on uphill lateral slopes if the manifold diameter is the same. The maximum and minimum hose elevation cannot be reached on any lateral slope (uphill or level) or given any manifold diameters, but on lateral downhill slopes hose elevation may be equall zero.

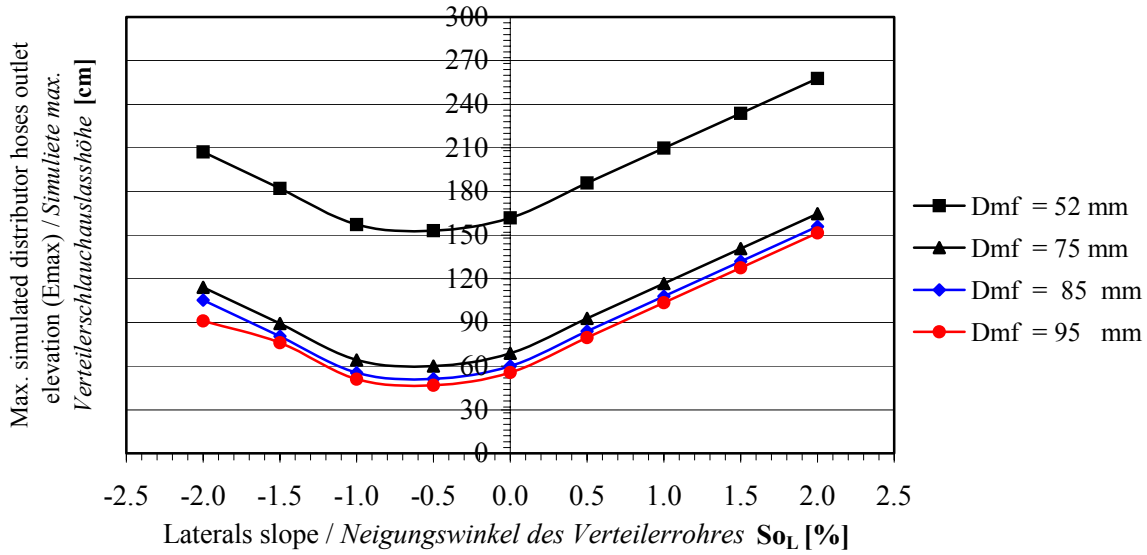


Figure 4.60: Maximum simulated distributor hose outlet elevation (Emax) at different manifold diameters ($D_{mf}$).
*Simulierte maximale Auslasshöhe am Verteilerschlauch (Emax) bei unterschiedlichem Feldzuleitungsdurchmesser ($D_{mf}$).*

The computer program is again used to study the effects of hose diameters on the hose outlet elevation and the required pressure head at each manifold inlet. The computer program was run at different distributor hose diameters while all other factors in the irrigation system were constant. It was shown that the change of hose diameters did not affect the hose outlet elevation, but that it had an effect on the required pressure head at the manifold inlet. Figure 4.61 shows the simulated pressure head at the manifold inlet at different distributor hoses diameters. Downhill, the optimum slope for a given lateral pipeline is > 0.5 % (from the lateral inlet). The pressure head increased rapidly as hose diameters decreased < 4 mm. Hose diameters of more than 8 mm had a small effect on the required pressure head at the manifold inlet. Air locks may occur in pipelines of low head bubbler irrigation systems located on level fields and with design heads as low as one meter. Air locks in bubbler systems can partially or entirely block the flow of water and thereby significantly decrease the uniformity of water application from distributor hoses. Therefore, distributor hose diameters of less than 6 mm and greater than 10 mm are not recommended for low-head bubbler irrigation systems due to excessive friction losses and poor water distribution uniformity, respectively [CURT (1994)].

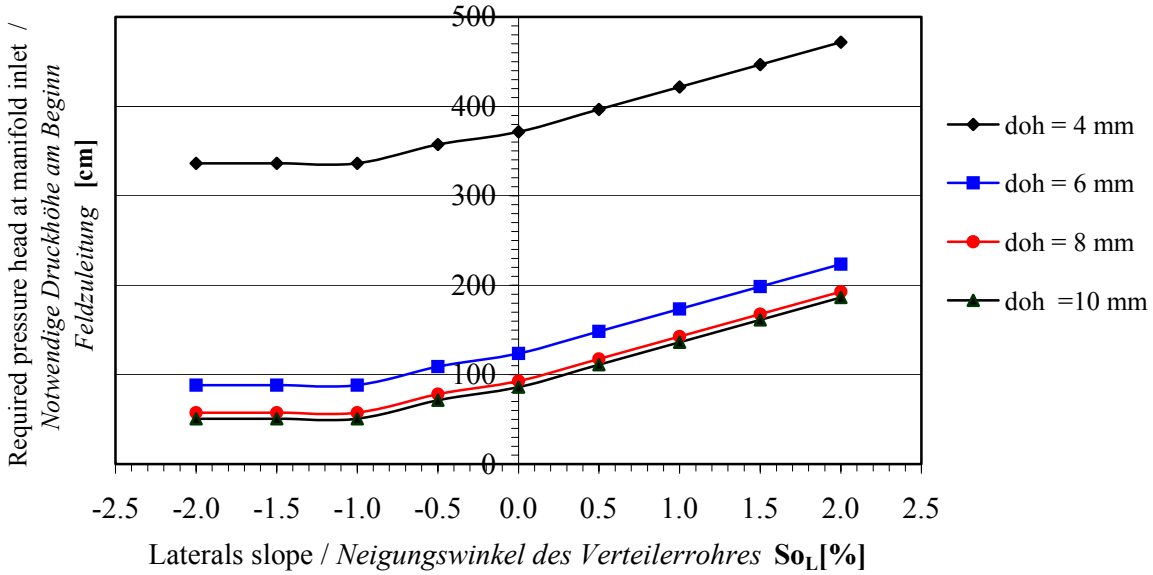


Figure 4.61: Maximum simulated required pressure head at manifold inlets at different hose diameters ($d_{oh}$).

*Simulierte maximal notwendige Druckhöhe am Beginn der Feldzuleitung mit unterschiedlichem Verteilerschlauchdurchmesser ($d_{oh}$).*

### 4.3.2.6 Low-head bubbler irrigation systems layout

After the hydraulic analysis of low-head bubbler irrigation systems with the aid of computer modelling and laboratory experiments, it can noted that the main component for low-head bubbler irrigation systems include the constant head device, mainline, manifold, laterals and distributor hoses. The most important factors are the design and position of the constant head device and the relation between this position and the field slope. Figure 4.62 shows a sketch of a constant head device when the water level in the tank is constant [REYNOLDS (1995a)]. When using the wind energy water pumping system, the water level in the tank may be not constant during the entire operation time. In this case, one may suggest a new constant head device to obtain the constant manifold design pressure head during the entire operation time Figure 4.63. Figures 4.64 to 4.68 also illustrate some simple field layout examples of low-head bubbler irrigation systems and constant head device positions based on the field dimensions and elevations (slopes) of each field direction.

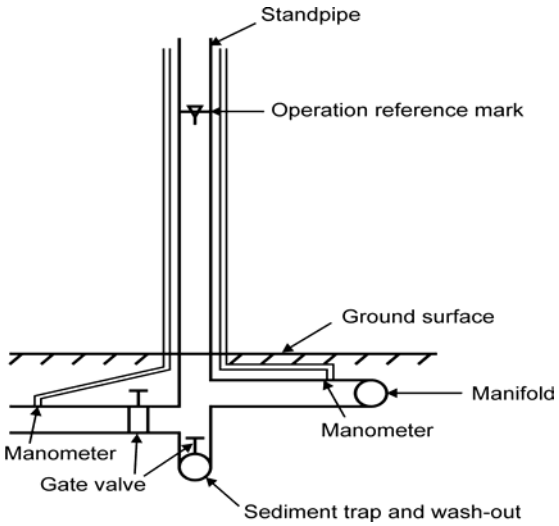


Figure 4.62: Sketch of a constant head device.
[REYNOLDS (1995a)]

*Skizze einer Vorrichtung für konstanten Druck.*

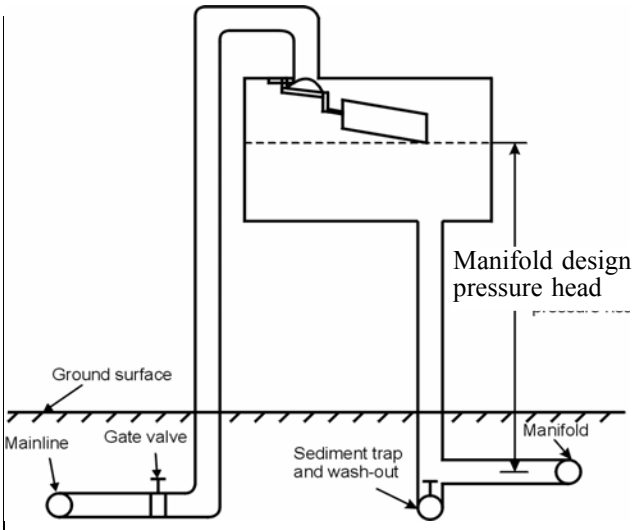


Figure 4.63: Sketch of a constant head device. The water level in the tank is variable.

*Skizze einer Vorrichtung für konstanten Druck. Der Wasserspiegel im Behälter ist variabel.*

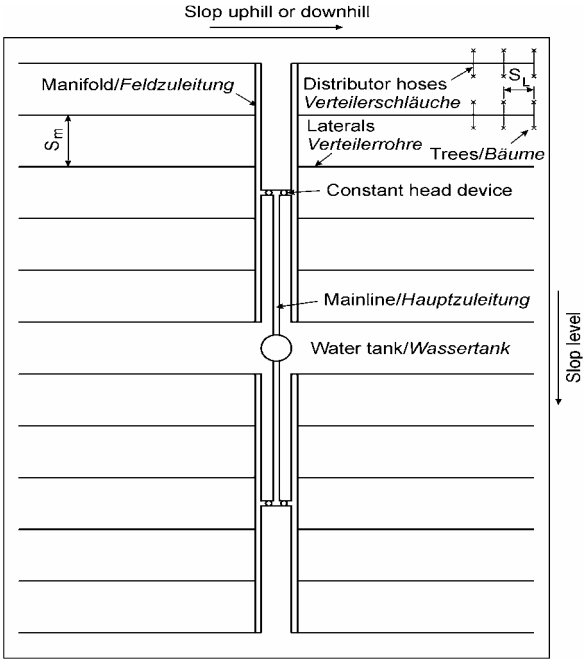


Figure 4.64: LHBIS layout, field slope is uphill or downhill in one direction and level in the other direction.
*LHBIS Layout, Neigungswinkel des Feldes ist "uphill or downhill" in eine Richtung und waagerecht in der anderen Richtung.*

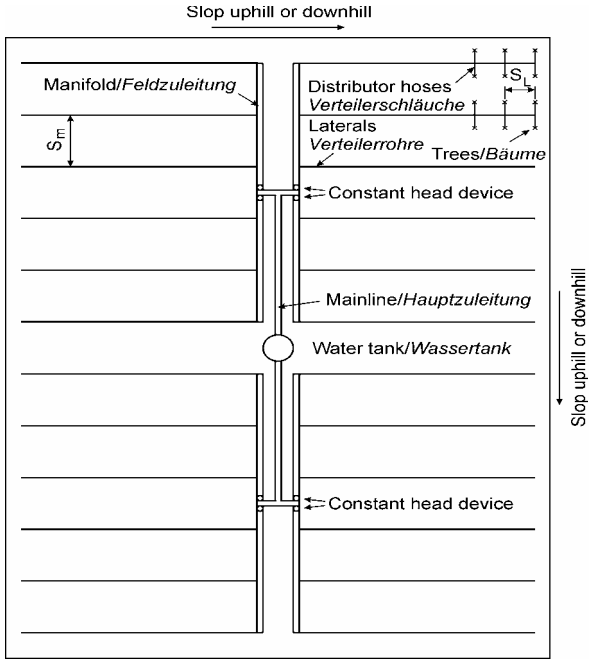


Figure 4.65: LHBIS layout, field slope is uphill or downhill in both directions.

*LHBIS Layout, Neigungswinkel des Feldes ist in beiden Richtungen "*uphill or downhill".

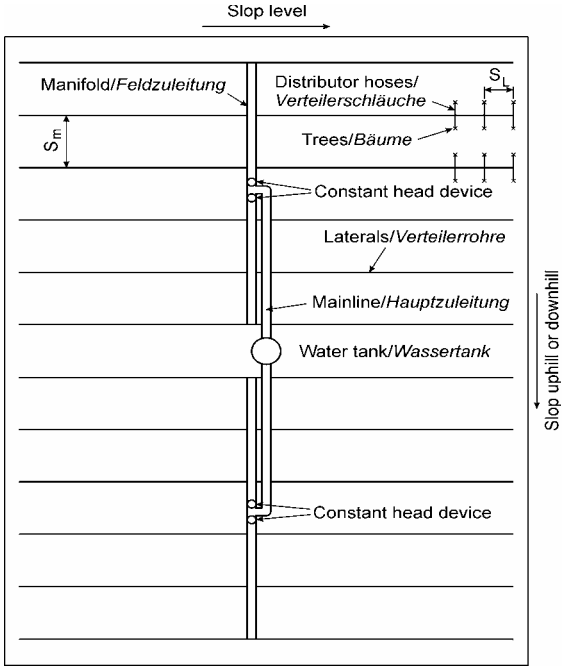


Figure 4.66: LHBIS layout, field slope is level in one direction and uphill or downhill in the other direction.

*LHBIS Layout, Neigungswinkel des Feldes ist waagerecht in eine Richtung und "uphill or downhill" in der anderen Richtung.*

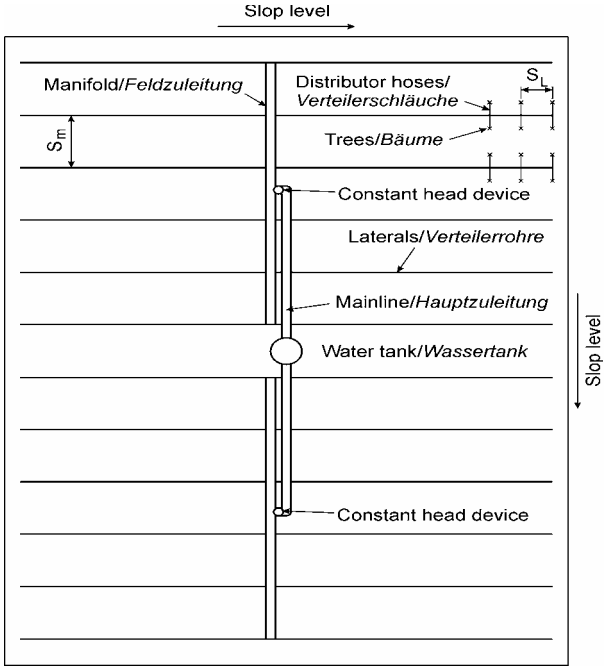


Figure 4.67: LHBIS layout, field slope is level in both directions.

*LHBIS Layout, Neigungswinkel des Feldes ist waagerecht in beiden Richtungen.*

### 4.3.3 Conclusions

Low-head bubbler irrigation systems differ from other micro-irrigation systems because they are based on gravity-flow. They can also operate at pressure heads as low as 1 m and do not require highly elaborate filtration systems. In addition, the low-head bubbler irrigation system enables water to be used economically, and its low operating pressure makes it particularly well suited for combination with alternative energy such as wind energy.

The computer program LHBIS was written to make low-head bubbler irrigation design simpler and faster than the traditional way of using charts and calculators. It allows a user to determine the distributor hose outlet elevation or distributor hose length and the required head at at the constant head device for a given discharge under certain tree and field conditions.

Laboratory experiments were conducted to determine the pipes (lateral and distributor hose) friction characteristics. The Hazen- William's coefficient was 140 for the lateral and 115 for the distributor hose. The laboratory experiments were also used to validate the LHBIS

computer program on three lateral slopes (level, uphill and downhill) by measuring the hose flow rate, the pressure head upstream and downstream at each hose inlet.

The uniformity of distributor hoses emission and flow variation were calculated based on the data from the laboratory experiments, in two variants: a low-head bubbler irrigation system with different distributor hose elevation or a system with different distributor hose length along one lateral. The emission uniformity values were higher than 97% at all distributor hose discharge rates. On the other hand, the flow variation values were 5% to 7%.

By running the computer program and laboratory experiments of low-head bubbler irrigation systems with different distributor hose outlet elevation or different distributor hoses length, one can decide whether the use of irrigation systems with different distributor hose outlet elevation is more practical than the application of a system with different hose length for the irrigation of tree crops such as orchards in particular if the land is not level (land surface slope between ± 1.5%). But if the land is level, the irrigation system with different distributor hoses length can be used, because the difference between maximum and minimum pressure head at hose inlets in irrigation systems is the friction loss in irrigation pipelines (lateral and manifold).

The computer program was used to investigate certain factors which influence the distributor hose elevation along the laterals and the required pressure head at each manifold inlet of the irrigation system. The results of the analysis of a large range of bubbler irrigation systems indicate that the minimum distributor hoses elevation is achieved on a small lateral downhill slope of - 0.5%. The hose elevation can be decreased by using a moderate hose discharge of 40 to 60 l/h, short laterals with a small number of hoses (≤ 13 hose per lateral side), large lateral diameters ≥ 32 mm, large manifold diameters ≥ 75 mm and small number of the lateral (≤ 9 lateral per manifold side).

The hose diameter does not affect the hose elevation, but it has a large effect on the required pressure head of the irrigation system. The pressure head increases rapidly as hoses diameters decrease < 4 mm. Hose diameters of more than 8 mm only have a small effect on the required pressure head at the manifold inlet. Air locks may occur in pipelines of low head bubbler irrigation systems located on level fields and at design heads as low one meter. Air locks in bubbler systems can partially or entirely block the flow of water and thereby significantly decrease the uniformity of water application from distributor hoses. Therefore, distributor hose diameters of less than 6 mm and greater than 10 mm are not recommended for low-head bubbler irrigation systems due to excessive friction losses and poor water distribution uniformity, respectively.

## 4.4 MoWEC-application with water storage: low-head bubbler irrigation system for fruit trees on the N.W. coast of Egypt

The agricultural land base of Egypt totals about 3.25 million hectares [ABDEL- MONEM (1998)]. The total fruit tree and orchard area in Egypt is 13.07% of the agricultural land [PETER (2000)]. The low-head bubbler irrigation system is well suited for the irrigation of fruit trees and orchard crops. In addition, this irrigation system enables water to be used economically, and its low operating pressure makes it particularly well suited for combination with alternative energy resources such as wind energy. The ground water is adequate and accessible along most parts of the N.W. coast of Egypt at a depth ranging from 5 to 50 m [BALBA (1981) and EL-MALLAH (1991)]. A report by UNDP/FAO (1970) indicated that an area of 137,460 ha in this region is suitable for fruit trees.

### 4.4.1 Irrigation requirement

The amount of water the crop needs depends on the rate of water transpired by the plant and the evaporation rate from the soil surface. The combined rate of these two processes, transpiration and evaporation, is known as “crop evapotranspiration rate” and commonly referred to as $ET_c$. It is expressed in units of mm per day. The magnitude of ET varies with the type of crop and the stages of growth. It is also influenced by climatic variables such as solar radiation, air temperature, relative humidity and wind speed. The influence of these climatic variables on the magnitude of crop $ET_c$ is integrated into a parameter known as reference evapotranspiration symbolized by $Et_o$ and also expressed in mm per day.

Different crops vary in their growth habits and sensitivity to water stress. The effect of a certain crop on the value of $ET_c$ is termed crop coefficient (Kc). The value of Kc varies with the type of crop and the stage of growth. The crop coefficients for most crops are available in several publications. The relation between $ET_c$, Eto and Kc is expressed quantitatively as: $ET_c = Kc \times Et_o$. Evidently, Kc is a dimensionless quantity. Table 4.14 illustrates the historical (28 years) average values of $Et_o$ in mm per day on the N.W. coast (Alexandria and Mersa Matruh) of Egypt [GEORGE (1986) and FAO (1977)].

Table 4.14: Long-term average values of potential $Et_o$ in mm per day on the N.W. coast of Egypt
*Langjährige Durchschnittswerte der möglichen $Et_o$ in mm pro Tag an der N.W. Küste von Ägypten.*

| | Jan | Feb | Mar | Apr | May | Jun | Jul | Aug | Sept | Oct | Nov | Dec |
|---|---|---|---|---|---|---|---|---|---|---|---|---|
| Alexandria | 2.10 | 2.86 | 3.71 | 4.63 | 5.81 | 6.67 | 6.87 | 6.63 | 5.06 | 4.03 | 2.73 | 2.06 |
| Mersa Matruh | 1.90 | 2.61 | 3.71 | 4.57 | 5.52 | 6.17 | 6.94 | 6.23 | 4.81 | 3.39 | 2.50 | 1.90 |

Perennial crops, such as trees and vines, take several years to reach maturity. They also go through several stages of growth and development each season. Immature crops use less water than fully-grown trees. The value of the crop coefficient, Kc, for orchards and vineyards varies with both the degree of maturity and the seasonal stage of growth [FAROUK (1998) and FAO (1977)]. Table 4.15 illustrates the average seasonal development coefficient for each stage, which is $Kc_1$ for the rapid growth stage, $Kc_2$ for the midseason stage and $Kc_3$ for the late season stage.

Table 4.15: Development coefficients for deciduous orchards, citrus, olives and vine. *Entwicklungskoeffizienten für Obstplantagen, Zitrusfrüchte, Oliven und Weinreben.* [FAROUK (1998)]

| **Crops** | **$Kc_1$** | **$Kc_2$** | **$Kc_3$** |
|---|---|---|---|
| Deciduous orchards | 0.5 | 1.0 | 0.7 |
| Grapes | 0.3 | 0.8 | 0.3 |
| Olives | 0.5 | 0.8 | 0.5 |
| Citrus | 0.7 | 0.7 | 0.7 |

The above listed crop coefficients are the coefficients for fields without cover crop (i.e. clean cultivation). Orchards and vineyards with active cover crop consume more water, and the crop factor is adjusted upward by multiplying it by a factor of 1.3. This coefficient will be referred to as the cover crop coefficient ($K_{cover}$). A cover crop coefficient which equals one is used for cleanly cultivated fields.

The degree of maturity is expressed subjectively as the percentage of ground shaded by the crop canopy at midday during midseason. Table 4.16 illustrates the percentages of ground shade (or maturity) and canopy coefficient ($K_{canopy}$) for deciduous orchards, citrus, olives and vineyards

Table 4.16: Canopy coefficients for deciduous orchards, citrus, olives and vineyards. *Bedeckungskoeffizienten für laubwechselnde Obstplantagen, Zitrusfrüchte, Oliven und Weinreben.* [FAROUK (1998)]

| Ground shaded (%) | 10 | 25 | 50 | 60 |
|---|---|---|---|---|
| Canopy coefficient | 0.3 | 0.6 | 0.9 | 1.0 |

**Then the crop water requirement can be calculated "$ET_c$"**

$ET_c$ = Development coefficient x Cover crop coefficient x Canopy coefficient x Eto [mm/day] [mm/day]

**Water use rate "WU"**

WU = $ET_c$ [mm/day] x Tree spacing [m] x Row spacing [m] [liter/(tree.day)]

**Irrigation requirement "IR"**

IR = 100 x Water use rate / Irrigation efficiency [%] [liter/(tree.day)]

The maximum root depth and typical plant spacing of some crops, which are commonly grown under low-head bubbler irrigation, are listed in Table 4.17 [DAVID (1975)].

Table 4.17: Rooting depths and row spacing for the design of an irrigation system.
*Wurzeltiefen und Reihenabstand für die Auslegung eines Bewässerungssystems.*

| **Crop** | **Root depth [m]** | **Plant spacing $S_L$ [m]** | **Row spacing $S_m$ [m]** |
|---|---|---|---|
| Citrus | 1.0 to 1.2 | 3 to 6 | 4 to 7 |
| Deciduous orchards | 1.0 to 2.0 | 2 to 8 | 4 to 8 |
| Grapes | 1.0 to 3.0 | 2 to 3 | 2 to 4 |
| Olives | 1.0 to 2.0 | 3 to 6 | 4 to 7 |

It could be assumed that the water pumped by MoWEC may be sufficient for 10 ha of orchards, olives or citrus trees on the N.W. coast of Egypt (see Figures 4.68 and 4.69). In this case, the mean monthly irrigation requirement **"MIR"** for this area on the N.W. coast of Egypt is given by

$$MIR = \frac{100 \cdot IR \cdot MDN}{S_L \cdot S_m} \qquad [m^3/(10ha \ . \ month)]$$

where:
MDN is the number of days in each month [day/month]
IR is the irrigation requirement [liters/(tree.day)]
$S_L$ and $S_m$ are the tree spacing [$m^2$]

Table 4.18 gives the average irrigation requirements (IR) and mean monthly irrigation requirement (MIR) for mature deciduous orchards, olives or citrus trees on the N.W. coast of Egypt. These values are calculated based on the long-term average $Et_o$ value in Alexandria and Mersa Matruh with a maximum seasonal development coefficient of 1.0 for orchards, 0.7 for citrus and 0.8 for olives, and a cover crop coefficient of 1.0, a canopy coefficient equalling 1.0 and an irrigation efficiency of 90 %. Tree spacing and row spacing are assumed to be 4 m [FAROUK (1998) and DAVID (1975)].

## 4.4.2 Design of a low-head bubbler irrigation systems

### 4.4.2.1 Example of field layout

Bubbler irrigation is an application of water to flood the soil surface using a small stream or fountain. The discharge rates for point-source bubbler hoses are greater than for drip or subsurface emitters but generally less than 3.785 liter per minute. A small basin is usually required to contain or control the water. It could be assumed that the total field area is approximately 10 ha. The field has 400 m length and 250 m width. The field shall be divided into four large plots; each plot is 100 m long and 250 m wide. The water storage tank is

constructed individually for each plot in the middle of the area. The main water source for the total area is in the middle field when using the wind energy water pumping system, but when using the photovoltaic water pumping system an individual photovoltaic water pumping plant for each plot area beside the storage tank is suggested. Figure 4.68 shows the description of the field layout with a water pumping system.

Table 4.18: Average irrigation requirements on the N.W. coast of Egypt.
*Durchschnittliche Bewässerungsanforderungen an der N.W. Küste von Ägypten.*

| **Month** | **Citrus** | | **Olives** | | **Orchards** | |
|---|---|---|---|---|---|---|
| | IR $\left[\frac{\text{liter}}{\text{tree}\cdot\text{day}}\right]$ | MIR $\left[\frac{\text{m}^3}{10\,\text{ha}\cdot\text{month}}\right]$ | IR $\left[\frac{\text{liter}}{\text{tree}\cdot\text{day}}\right]$ | MIR $\left[\frac{\text{m}^3}{10\,\text{ha}\cdot\text{month}}\right]$ | IR $\left[\frac{\text{liter}}{\text{tree}\cdot\text{day}}\right]$ | MIR $\left[\frac{\text{m}^3}{10\,\text{ha}\cdot\text{month}}\right]$ |
| January | 24.89 | 4821.47 | 33.50 | 6489.66 | 35.54 | 6885.88 |
| February | 34.04 | 5956.13 | 46.72 | 8175.13 | 48.62 | 8508.50 |
| March | 46.17 | 8945.44 | 58.88 | 11408.00 | 65.96 | 12779.75 |
| April | 57.24 | 10732.50 | 72.18 | 13533.75 | 81.78 | 15332.81 |
| May | 70.50 | 13658.41 | 85.19 | 16505.56 | 100.71 | 19511.59 |
| June | 79.89 | 14979.38 | 96.50 | 18092.81 | 114.14 | 21400.31 |
| July | 85.93 | 16647.97 | 93.15 | 18047.81 | 122.76 | 23783.78 |
| August | 80.02 | 15003.75 | 81.35 | 15253.13 | 114.32 | 21434.06 |
| September | 61.42 | 11899.16 | 60.09 | 11641.47 | 87.74 | 16998.66 |
| October | 46.17 | 8945.44 | 46.44 | 8997.75 | 65.96 | 12778.78 |
| November | 32.54 | 6101.25 | 32.93 | 6173.44 | 46.49 | 8715.94 |
| December | 24.64 | 4773.03 | 14.65 | 2838.44 | 35.20 | 6820.00 |

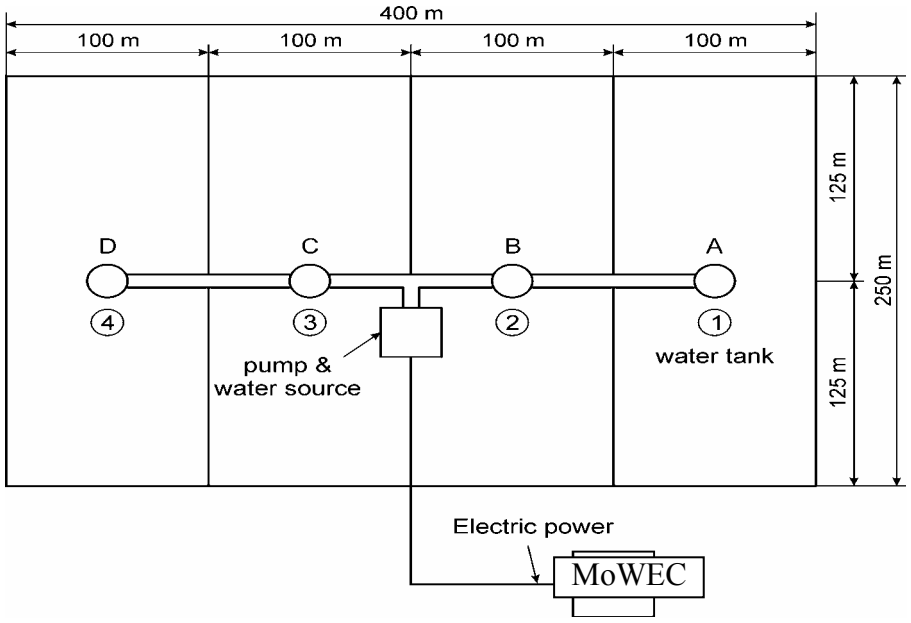


Figure 4.68: Layout of the irrigation field.
*Layout des Bewässerungsfeldes.*

### 4.4.2.2 The computer program input and output data

Figure 4.69 illustrates the field layout as an example of a low-head bubbler irrigation system (LHBIS) for fruit trees with different distributor hose outlet elevation and constant head device positions. The field elevation in both directions is level. The necessary data input for the computer program are the hose position of a lateral on both sides of the lateral (S =2) and the lateral position of a manifold on both sides of the manifold (SS = 2). The field dimensions and elevation of each field direction should be surveyed accurately. Elevation surveys with an error of centimeters will affect distributor hose elevation by a few centimeters, which in turn will affect the uniformity of flow though the irrigation system. Table 4.19 shows the input data for LHBIS computer program. In addition to these data, the required discharge from each distributor hose, maximum and minimum hose elevation and tree spacing must be input. In this case assume the hose discharge is 40 liter per hour, maximum and minimum hoses elevation are 1 m and 0.3 m respectively and tree spacing $S_L \times S_m = 4 \times 4$ m². Table 4.20 illustrates the computer program output data for this example (see Figure 4.69).

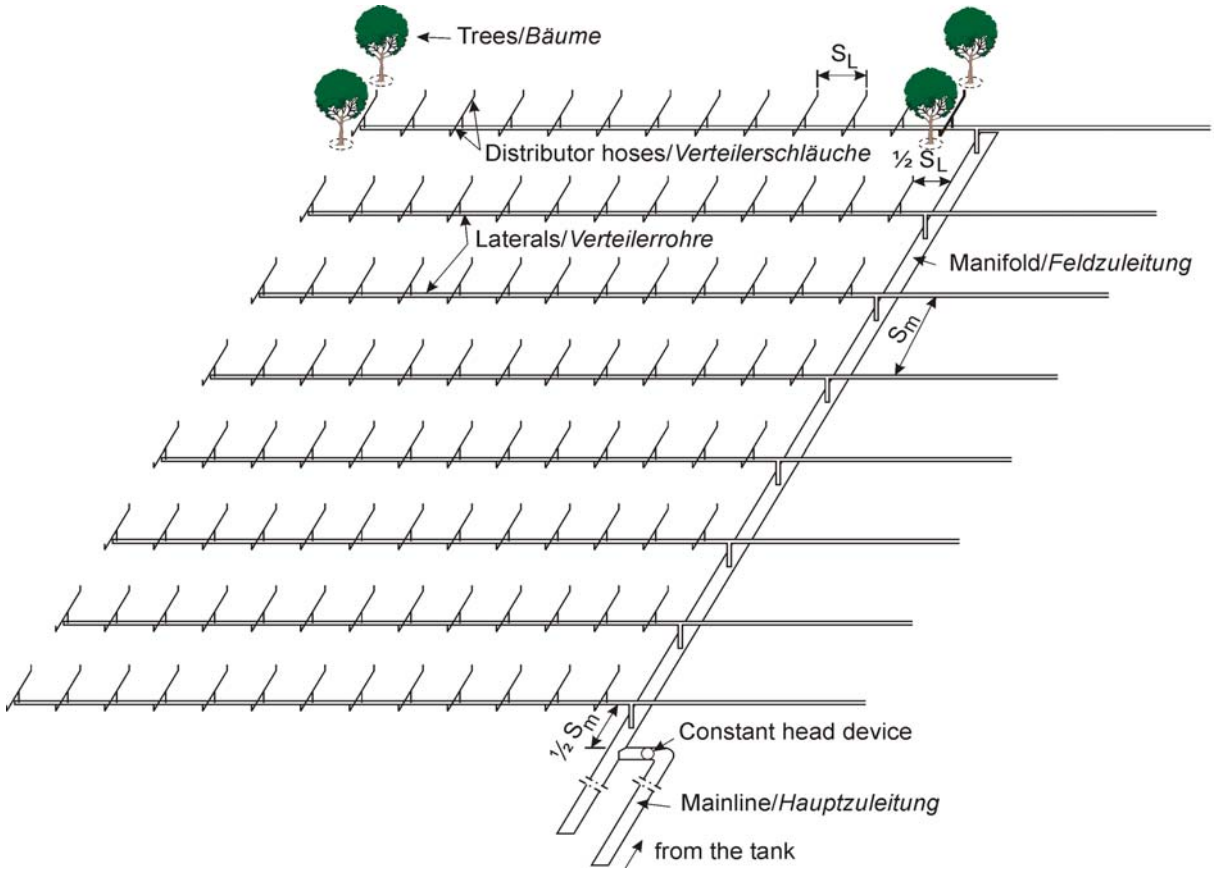


Figure 4.69: Typical layout of the orchard low-head bubbler irrigation system.

*Typisches Layout eines Obstgarten für ein Niedrigdruck-Bubbler-Bewässerungssystems.* [OMARA (2004a)]

Table 4.19: Computer program input data.
*Computerprogramm Eingabedaten.*

| | Distributor hose | Lateral | Manifold | Mainline |
|---|---|---|---|---|
| Diameter [mm] | 6 | 32 | 75 | 125 |
| Length [m] | 2.5 | 50 | 60 | 64 |
| $C_{HW}$ | 115 | 140 | 150 | 150 |
| Slope [%] | Level | Level | Level | Level |
| Number | 13 per lateral side | 8 per manifold side | 2 per mainline side | 2 per tank |

Table 4.20: Computer program output data.
*Computerprogramm Ausgabedaten.*

| **Distributor hoses number from lateral inlet** | **Lateral number from manifold closed end** | | | | | | | |
|---|---|---|---|---|---|---|---|---|
| | 1 | 2 | 3 | 4 | 5 | 6 | 7 | 8 |
| | **Distributor hoses elevation [m]** | | | | | | | |
| 1 | 0.391 | 0.396 | 0.420 | 0.458 | 0.514 | 0.591 | 0.693 | 0.821 |
| 2 | 0.355 | 0.377 | 0.400 | 0.438 | 0.494 | 0.572 | 0. 673 | 0.801 |
| 3 | 0.341 | 0.359 | 0.383 | 0.421 | 0.478 | 0.555 | 0.656 | 0.784 |
| 4 | 0.329 | 0.346 | 0.369 | 0.407 | 0.464 | 0.541 | 0.642 | 0.770 |
| 5 | 0.320 | 0.335 | 0.358 | 0.396 | 0.452 | 0.530 | 0.631 | 0.759 |
| 6 | 0.313 | 0.325 | 0.349 | 0.387 | 0.443 | 0.520 | 0.622 | 0.750 |
| 7 | 0.308 | 0.318 | 0.342 | 0.380 | 0.436 | 0.513 | 0.615 | 0.743 |
| 8 | 0.304 | 0.313 | 0.337 | 0.375 | 0.431 | 0.508 | 0.610 | 0.738 |
| 9 | 0.302 | 0.310 | 0.333 | 0.371 | 0.427 | 0.505 | 0.606 | 0.734 |
| 10 | 0.301 | 0.307 | 0.331 | 0.369 | 0.425 | 0.502 | 0.604 | 0.732 |
| 11 | 0.300 | 0.306 | 0.329 | 0.368 | 0.424 | 0.501 | 0.602 | 0.730 |
| 12 | 0.300 | 0.306 | 0.329 | 0.367 | 0.423 | 0.500 | 0.602 | 0.730 |
| 13 | **0.300** | 0.305 | 0.329 | 0.367 | 0.423 | 0.500 | 0.602 | 0.730 |
| **RHL** | 0.595 | 0.601 | 0.624 | 0.662 | 0.718 | 0.796 | 0.897 | 1.00 |
| **RHMF** | **1.240 m** | | | | | | | |
| **IRH** | **1.510 m** | | | | | | | |
| **RD** | **8.320 m³/h** | | | | | | | |

where: **RHL** is the required pressure head at the inlet of each lateral [m], **RHMF** is the required pressure head at the inlet of each manifold (by constant head device), **RD** is the required discharge for an area of 64 m x 52 m = 3328 m² and **IRH** is the required pressure head at the mainline inlet (minimum head from the tank = bottom tank level from ground level) of 1.51 m.

The total area irrigated by one mainline = hoses number per lateral x lateral number per manifold x manifold number per mainline x hose spacing = (13 x 2) x (8 x 2) x 2 x (4 x 4)

= 13312 m²

Hence, the total discharge required for each mainline (area = 2.66 ha) is:

$$TRD = 4 \times RD = 33.280 \text{ m}^3/\text{h}$$

### 4.4.3 Pumping of water by MoWEC

Wind pumping is a well-established technology that offers an alternative to diesel and electric pump sets in windy areas. Most wind pumps can operate under fairly low wind conditions and are especially appropriate for the modest water needs of small farming establishments. The wind-electric water pumping system consists of a wind turbine with a permanent magnet generator that produces 3-phase variable-frequency electricity. The system performs efficiently at low winds if the right size compensating capacitance is used. At high winds, when the frequency reaches a certain level (60-85 Hz), the system tends to lose synchronization especially under gusty wind conditions [LING (2000)]. Most small wind turbines like MoWEC have a mechanical furling mechanism (lee-wind wheel) to turn the rotors out of the wind and slow down the rotor speed. However, furling generally does not occur until synchronization has been lost, so system efficiency is quite low at high wind speed.

#### 4.4.3.1 Selecting a water pump for MoWEC

Due to their low starting torques and high speed, MoWEC is not suitable for driving piston pumps directly. Such an arrangement would not function correctly without an electric transmission between the MoWEC and the pump, or a centrifugal clutch to allow the MoWEC to come up to speed before being connected to the load. This would result in mechanical complications and in an increase in weight for the installation. It is better to associate a MoWEC with a centrifugal pump or with a helical pump having a fixed or variable pitch. The starting torque required by these pumps is quite low. Their rotational speed, on the other hand, is relatively high. As a result, they are well suited for coupling to MoWEC.

Figure 4.70 shows an arrangement according to the hoisting depths and symbols indicating the suitable combinations of wind turbine and pump designs, which result from the past remarks. Every one of the wind pumps shown in Figure 4.70 has a limited area of application, in which it works with good efficiency.

The single-stage centrifugal pump, D in Figure 4.70, is used as a radial or semi axial centrifugal pump, which extracts ground waters from dug wells or surface water from intake structures. The hoisting depth range is limited for the mechanically coupled single-stage centrifugal pump by the impeller diameters and the transmission translation on 10 m. Like the mechanical coupling, the electrical coupling of wind turbines with single-stage centrifugal pumps is possible, even though it has been rarely used so far. Generally the advantages of the centrifugal pump reside in its insensitivity to dirty water and the good starting behavior, which result from the agreement of the torque characteristics of the wind turbine and the centrifugal pump.

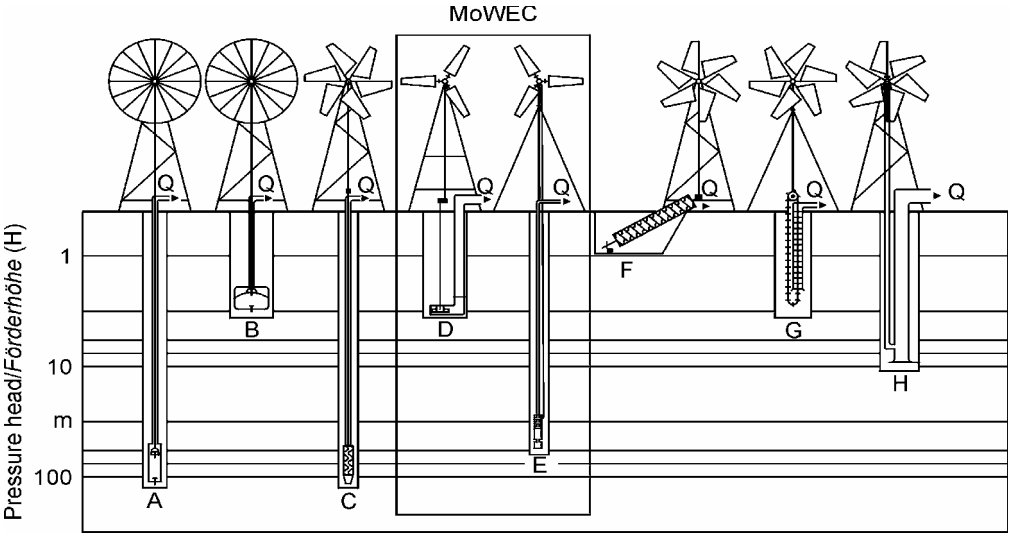


A: Piston pump
B: Diaphragm pump
C: Eccentric spiral pump
D: Single-stage centrifugal pump
E: Multi-stage centrifugal pump
F: Sanif trough pump
G: Kitten pump
H: Air-lift pump

Figure 4.70: Appropriate combinations of wind turbines and pumps. [after GASCH (1996)]
*Sinnvolle Kombinationen von Windturbinen und Pumpen.*

Multi-stage centrifugal pumps, E in Figure 4.70, are propelled so far exclusively through electrical power transmission and a dipping motor driven by a wind turbine. In multi-stage centrifugal pumps, the hoisting depth range, which depends on the stage number, extends the application of centrifugal pumps of this design. The electrical power transmission offers the advantages of the free choice of the location of the wind turbine independent of the well and the possibility of being able to use the electricity also for other applications. The disadvantage of electrical power transmission is the additional loss in relation to the mechanical coupling. The advantages and disadvantages of the multi-stage centrifugal pump correspond to those of the single-stage centrifugal pump.

A pump running at optimum head and speed has an efficiency of between 40% and 80% [KAY (1992)]. Many pumps, which receive the power from a wind energy converter, are not run at optimum head and speed, which may result in far lower efficiency. In this study, it was assumed that pump efficiency equaled 60%.

### 4.4.3.2 Water resources on the N.W. coast of Egypt

The N.W. coast of Egypt extends about 550 km from Alexandria to Al-Salloum and about 10-20 km south of the Mediterranean Sea shore. According to [BALBA (1981)], the ground water is adequate and accessible along most parts of the N.W. coast at a depth ranging from 5 to 50 m. FARAHT (1999) decided that well depth ranged from 5 to 25 m in a region

from km 21 to km 100 west of Alexandria and to a depth of about 3 km south of the Mediterranean Sea shore. It could be assumed that the water source is shallow groundwater with a sum of well depth and draw down (SSH) of about 12 m (the vertical distance from ground level to water surface in the well during the operation).

It has to be remembered that the required pressure head (RHM = IRH) for low-head bubbler irrigation systems at the inlet of a mainline of IRH = 1.51 m (minimum head from the tank = bottom tank level from ground level), which was designed by the computer program (see Table 4.20). It was also assumed that the storage tank height (TH) for each plot area in Figure 4.68 was 2 m, see Figure 4.71, which is a typical motor pump unit and water storage installation. When the suction and delivery pipelines are level, the total static head (TSH) can be calculated as follows:

$$TSH = SSH + IRH + TH = 12 + 1.51 + 2 = 15.51 \text{ m}$$

It was also assumed that the maximum friction loss in a suction and delivery pipeline was 4 m/100 m and that the minor losses amounted to 20% of the friction loss. Thus, the total loss (TL) in the pumping system is given by [SMITH (1986)],

$$TL = 1.2 \times 4 \times \frac{L_s + L_d}{100} \qquad [\text{m}]$$

where $L_S$ is the suction pipe length in [m] and $L_d$ is the delivery pipe length in [m]. Based on Figure 4.68, the total length of the suction and delivery pipeline is approximately 170 m. Hence, TL = 8.16 m and the total dynamic head (TDH) for the pump given by,

$$TDH = TSH + TL = 15.51 + 8.16 = 23.67 \text{ m}$$

### 4.4.3.3 Mean monthly quantity of water pumped by MoWEC on the N.W. coast of Egypt

The two main parameters that are needed to calculate the mean quantity of water pumped by MoWEC every month ($Q_M$) on the N.W. coast of Egypt are the average actual mean monthly energy production (AAMEP) by MoWEC on the N.W. coast of Egypt and the pumped total dynamic head TDH, which was discussed in the previous chapter.

$$Q_M = \frac{AMEP \cdot 3600 \cdot \eta_p}{TDH \cdot \gamma_w \cdot 100} \qquad [\text{m}^3/\text{month}]$$

where:

AAMEP is the average actual mean monthly energy production (AAMEP) by MoWEC on the N.W. coast of Egypt (see Table 4.2), [kWh/year]

TDH is total dynamic head, 23.67 [m]

$\eta_p$ is the pump efficiency, 60 [%]
$\gamma_w$ is the specific gravity of the water, 9.81 [kN/m³].

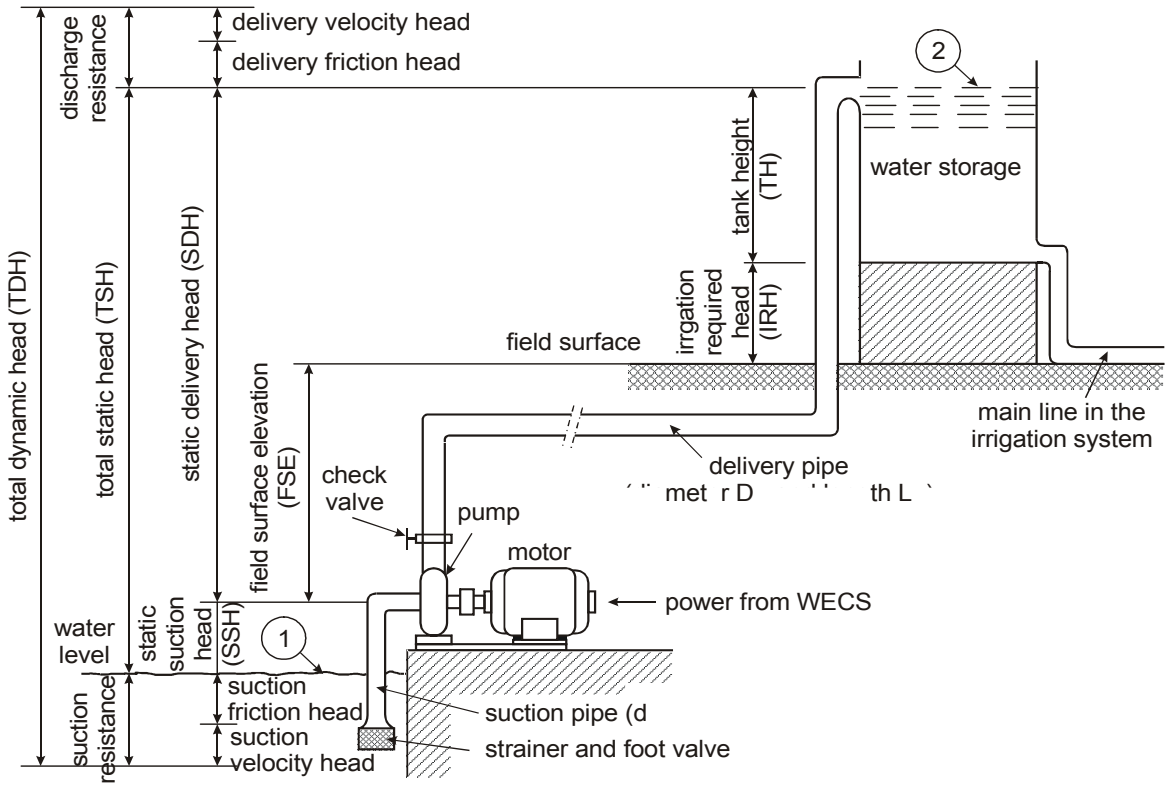


Figure 4.71: Typical motor pump unit and water storage installation. [OMARA (2004b)]
*Typische Motorpumpeneinheit und die Installation des Wasserspeichers.*

Figure 4.72 shows the mean monthly irrigation requirement (MIR) for 10 hectares of orchards, olives or citrus trees on the N.W. coast of Egypt (Alexandria and Mersa Matruh), which are presented in Table 4.18, and the mean monthly water quantity pumped by MoWEC ($Q_M$) on N.W. coast of Egypt, which is calculated using the equation given above. Figure 4.72 illustrates that the mean monthly quantity of water pumped by MoWEC ($Q_M$) can meet the monthly irrigation requirement (MIR) for 10 ha of orchards, olives or citrus trees in all months on the N.W. coast of Egypt. Only on orchard fields may external power supply be needed in July in order to pump the missing quantity of water (1688.83 m³ of water) in this month.

If MoWEC is used only to pump the water required to irrigate 10 ha of mature deciduous orchards, olives or citrus trees on the N.W. coast of Egypt, the cost per m³ of water given a total dynamic head of 23.67 m would be € cents 2.77, 3.92 or 3.5 per m³ of water for orchards, olives or citrus respectively based on the economics of the MoWEC-prototype (see section 4.2.4.7)

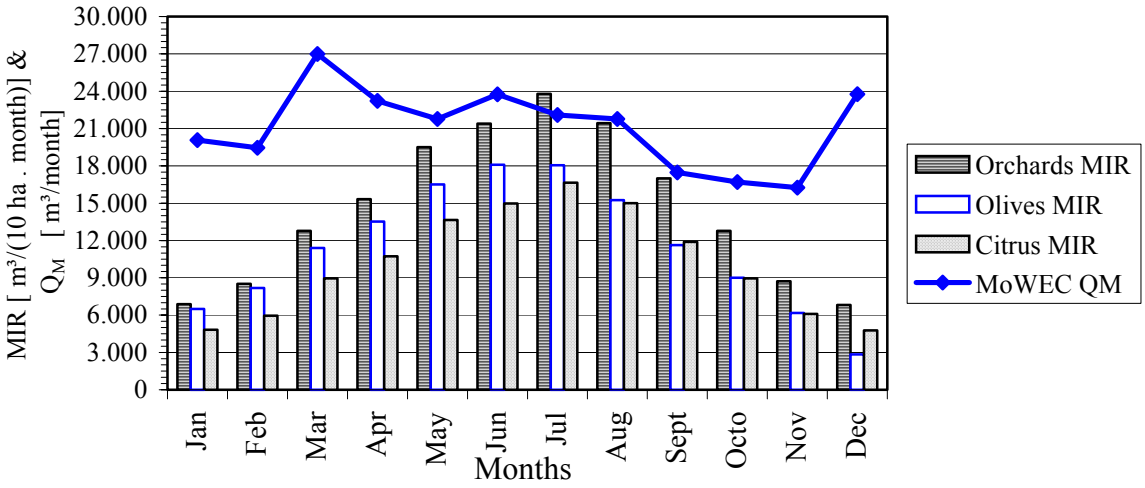


Figure 4.72: Mean monthly irrigation requirement (MIR) and the water quantity pumped by MoWEC ($Q_M$) on the N.W. coast of Egypt. [OMARA (2004b)]
*Mittlerer monatliche Bewässerungsbedarf (MIR) und das von MoWEC gepumpte Wassermenge ($Q_M$) an der N.W. Küste von Ägypten.*

### 4.4.4 Conclusions

Low-head bubbler irrigation systems with different distributor hose outlet elevation are well suited for the irrigation of fruit trees and orchard crops. In addition, this irrigation system enables water to be used economically, and its low operating pressure makes it particularly well suited for combination with alternative energy such as wind energy.

The agricultural land base of Egypt totals about 3.25 million hectares. The total orchard area in Egypt is 13.07% of the agricultural land. The N.W. coast of Egypt extends about 550 km from Alexandria to Al-Salloum and about 10-20 km south of the Mediterranean Sea shore. The ground water is adequate and accessible along most parts of the N.W. coast of Egypt at a depth ranging from 5 to 50 m. An area of 137,460 ha in this region is suitable for fruit trees.

The amount of water which the crop needs depends on the rate of water transpired by the plant and the evaporation rate of the soil surface. The maximum monthly irrigation requirements for 10 ha of orchards, olives or citrus trees on the N.W. coast of Egypt were reached in July and amounted to 16648, 18093 or 23784 m³/(10 ha. month) respectively.

The average mean monthly quantity of water pumped by MoWEC on the N.W. coast of Egypt is 21,111 m³/month when the total dynamic head amounts to 23.67 m. If MoWEC is used only to pump the water required for the irrigation of 10 ha of orchards, olives or citrus trees on the N.W. coast of Egypt, the cost per m³ of water given a total dynamic head of 23.67 m would be € cents 2.77, 3.92 or 3.5 per m³ of water for orchards, olives or citrus respectively based on the economics of the MoWEC-prototype.

# 5 CONCLUSIONS

## "Further development of a mobile wind energy plant for a low-pressure irrigation system"

The world energy demand is continually increasing due to the increase in the world's population, economic growth, and energy usage. At today's rate of increase, the sources of fossil energy, which meet the majority of the current world energy demand, will not be sufficient in the centuries to come. Energy use has been growing even faster than the world population growth. From 1970 to 1995 energy use was increasing at a rate of 2.5% per year (doubling every 30 years) and the world population at a rate of 1.7% per year (doubling about 40 years). From 1995 to 2015, energy use is projected to increase at a rate of 2.2% per year (doubling every 32 years) compared with a population growth rate of 1.5% per year (doubling every 47 years) [DOE (1995), IEA (1995) and PRB (1996)]. The world supply of oil is projected to last approximately 50 years at current production rates. Worldwide, the natural gas supply is adequate for about 50 years and coal for about 100 years [BP (1994), IVANHOE (1995), BARTLETT (1995), CAMPBELL (1997), DUNCAN (1997) and YOUNGQUIST (1997)]. These projections, however, are based on current consumption rates and current population numbers. Because of these short periods we should find solutions today for tomorrow. In order for sufficient energy to be available in future centuries, it is essential to develop the use of renewable energy sources further.

Renewable energy resources can be defined as energy that is replaced rapidly by natural processes. Renewable energy is beginning to grow out of its initial status and has experienced exponential growth in usage over recent years. Wind energy is one of the most flexible of all renewable energy resources. It can be used for different purposes such as irrigation, electricity generation, crop drying, grain grinding and also many other purposes through a wind energy converter system.

In Egypt, the use of electricity is increasing. Therefore the Ministry of Electricity and Energy has formulated a national strategy for the use and application of renewable energy and for energy conservation measures in the year 1980. The strategy targets a 10% saving of the projected 2005 primary energy consumption through energy conservation measures and a 5% contribution by renewable energies, primarily using solar, biomass and wind technologies.

**MoWEC** is the prototype of a **mobile wind energy converter** with two rotors, which can be used to capture wind energy at different locations, if necessary. The rotational energy can be transmitted to two selected positions of a shaft for power take off (PTO) , e.g. for a

mechanical water pump, a permanent magnet generator for stand alone use or a grid connection, an air-compressor for energy storage or other suitable equipment. There are lots of different designs in terms of heights, width and rated power possibilities. In the present MoWEC prototype, the wing heights amount to 10 m. The total rotor swept area is 80 m², because each of the two three-bladed rotors has a diameter of 7.10 meters. The theoretical rated power is 20 kW at a wind speed of 11 m/s. The MoWEC concept has been implemented in the Federal Agricultural Research Center (FAL) in Braunschweig, Federal Republic of Germany since the year 2002. This dissertation is based on work on this project.

The present MoWEC-prototype has had no yaw drive system in stand alone use for low wind velocities, which can also be used for very high wind velocities to reduce the rotor surface facing the wind. In addition, the performance of MoWEC has not yet been measured in a field experiment. This dissertation focuses on the yaw drive system as well as the power curve. As an example of an application of wind energy use, a gravity low head micro irrigation system was examined and designed for the watering of fruit trees based on the MoWEC power curve on the northwest coast of Egypt.

**The objectives of this study were:**

1. Further development of the mobile wind energy converter (MoWEC) with the goal of allowing a yaw drive control system to be realized without external energy storage in particular for stand-alone use.
2. Measurement of the MoWEC power curve in stand alone use (prototype).
3. Selection, simulation and laboratory test of a water- and energy saving irrigation technique for small orchard farms which are suitable for wind energy use.
4. Layout of an orchard farm in Egypt with this irrigation system and water provision by MoWEC.

In order to achieve these objectives, the study was divided in four steps:

## 1. Completion of the MoWEC yaw drive frame with a lee-wind wheel

The MoWEC prototype requires an automatic yaw drive system without an energy store in stand-alone use to move the rotors into the wind at low wind velocities and to move the rotors out of the wind at wind velocities beyond the rated power. To fulfill this demand, a lee-wind wheel yaw drive system was chosen, designed, tested inside a wind tunnel and fastened on MoWEC.

Theoretical studies resulted in a lee-wind wheel with eight blades and an outer diameter of $D_{wo} \geq 1.50$ m. This lee-wind wheel was constructed and then tested with different blade angles φ (15°, 22.5°, 35° and 45°) and two-gear reduction ratios rw (56.82:1 or 82.64:1) inside of a specially built wind tunnel in different angle positions θ between the lee-wind wheel and the air stream. The angle positions θ between the lee-wind wheel and the direction of the wind tunnel air stream should reflect the field application of the wheel after installation on the MoWEC yaw drive frame.

The main results of the lee-wind wheel wind tunnel experiments have indicated that the blade angle φ should be 22.5 degrees and that the reduction ratio should be rw = 82.64:1. At these values, the lee-wind wheel is able to work well also in angle positions below θ = 20°, e.g. for lifting a weight of 588.6 N (60 kg x 9.81 m/sec²) in position θ = 10°. This weight stands for the tangential force needed to move the MoWEC yaw drive frame with two rotors. At this position, the measured power coefficient was $C_{pm}$ = 0.1 %, but this power coefficient value equalled zero when the blade angles were 15°, 35° or 45°.

The installation of the lee- wind wheel system with rw = 82.64:1 on the MoWEC yaw drive frame results in a total reduction ratio of 1371:1. The field test proved that a modern wind energy converter works well in stand alone use with a lee-wheel yaw drive system and that this technique can also be recommended for the reduction of the effective rotor area at very high wind velocities. . If the MoWEC rotors face the wind, the lee-wind wheel does not rotate. In this case, the theoretical angle θ is zero. In that position, no power is needed for the yaw drive system. Gale displacement is caused by a wind vane. .

The relation between the MoWEC-rotor area and the angle of wind direction shows that in order to reduce by storm the effective rotor area the yaw drive frame must be moved entirely out of the wind. At the angle of θ = 60°, for example, the effective area must be reduced by 50%. . If wind velocities exceed the rated power, the lee-wind wheel must start in a cross position to move the yaw drive frame out of the wind. In the field test showed that the designed lee-wind wheel system could produce enough power forts the yaw drive frame to reduce the area of the main MoWEC-rotors which face the wind. The field test has also shown that the forces from the MoWEC-rotor areas work in a handshake manner with the forces of the roll wheel so that it is not allowed to install a worm gear inside the lee-wind wheel system.

## 2. The measurement of the MoWEC power curve

After the examinations of the lee-wind wheel had been completed, the first power curve of the MoWEC-prototype was tested in the field. For this purpose, a 10-pole permanent-magnet synchronous generator with 9 kW rated power (max. 14 kW) was used along with measuring

facilities for current and voltage, heating elements as load and a digital three-cup anemometer for the wind velocity. The wind speed and the electric current in one phase were measured twice over a long period during the test: first in normal operation with two rotors and the designed lee-wind wheel yaw drive system and second with only one rotor fastened in the wind position (lee-wind wheel out of function). These measurements allowed the MoWEC performance and the power coefficient value to be determined. The generator used was dimensioned for one rotor for future MoWEC developments in the FAL-Institute.

Based on the measurement data from these two applications, the MoWEC total power coefficient $C_{Pt}$ value was 0.32, which contains the normal wind power coefficient $C_P$, generator efficiency, chain efficiency and gear box/bearing efficiency. This value $C_{Pt} = 0.32$ shall be increased by further development of some factors of this first MoWEC prototype, e.g. the chain will be replaced by a drive shaft and the generator could be installed in a better position. A new hub also enables the blades to be fastened in a better wind angle of attack position. After these experiments, we can recommend that this MoWEC prototype should have an electric generator having at least 20 kW of rated power. A rated power of 25 kW would have the advantage that at wind velocities above 11 m /s the generator could deliver sufficient counter torque for more storm safety.

A wind energy converter system (MoWEC) allows wind energy to be used for different purposes such as irrigation, electricity generation, crop drying, grain grinding and many other purposes. In Egypt, like in most other developing countries, there is an increasing demand for energy. Wind energy can be very useful for lifting water and generating electricity on the N.W. coast of Egypt. The land used for agriculture on the N.W. coast of Egypt extends about 550 km from Alexandria to Al-Salloum and about 10-20 km south of the Mediterranean Sea shore. The mean monthly wind speed and duration range from 5.17 to 6.03 m/s (wind speed) and from 308 h/month to 614 h/month (duration). MoWEC´s actual mean annual energy production of 27,233.-- kWh/year on the N.W. coast of Egypt was calculated based one the average available wind data and MoWEC´s total power coefficient of 0.32. The total initial cost of the MoWEC-prototype, based on a small batch, was 26,000.-- € with an additional 4,000.-- € for the generator and for water pump facilities. The cost of the MoWEC output energy was calculated to be 15.44 € cents per kWh based on a payback period of 10 years, an annual rate of interest of 8% and annual operation and maintenance expenses of 2% of the initial cost.

## 3. Wind powered gravity-low-head bubbler irrigation system for fruit trees and orchards

Irrigation is one of the main energy consumers in agriculture. The combination of a wind-electric system with suitable irrigation equipment for the watering of fruit trees may also provide electricity for common applications in regions without a public electrical grid. For this

study, a gravity low-head bubble irrigation system was chosen because the needed water tank allows the transformed potential water energy to be stored.

Low-head bubbler irrigation differs from other micro-irrigation systems because they are based on gravity-flow with water pressure heights of nearly 1 m and do not require highly elaborate filtration systems. Their outlet diameters are at least 4 mm. This irrigation system enables water to be used economically. The low operating pressure makes it particularly well suited for combination with the MoWEC wind energy.

The computer program LHBIS was written to make low-head bubbler irrigation design simpler and faster than the traditional way of using charts and calculators. It allows a user to determine the distributor hose outlet elevation or distributor hose length and the required head at the constant head device for a given discharge per tree and field condition.

Laboratory experiments were conducted to determine the pipes (lateral and distributor hose) friction characteristics. The Hazen-William's coefficient was 140 for the lateral and 115 for the distributor hose. The laboratory experiments were also used for the validation of the LHBIS computer program on three lateral slopes (level, uphill and downhill) by measuring the flow rate in the hose and the upstream and downstream pressure head at each hose inlet.

The emission uniformity of the distributor hoses and flow variation were calculated based on the data of the laboratory experiments for two variants of a low-head bubbler irrigation system with different distributor hose elevation or different distributor hose length along one lateral. The emission uniformity values were higher than 97% at all distributor hose discharge outlets. On the other hand, flow variation values were 5% to 7%.

By running the computer program and laboratory experiments of low-head bubbler irrigation systems with different distributor hose outlet elevation or with different distributor hose length, it can be determined that the use of low-head bubbler irrigation systems with different distributor hose outlet elevation is more practical than the system with different hose length for the irrigation of tree crops such as orchards, especially when the land is not level (land surface slope between ± 1.5 %). If the soil surface is level, the irrigation system with different distributor hose length can be used because the difference between the maximum and minimum pressure head at the distributor hose inlet of the irrigation system is the friction loss inside the irrigation pipeline (lateral and manifold).

The computer program was used to investigate certain factors which influence the distributor hose elevation along the laterals and the required pressure head at each manifold inlet of the irrigation system. The results of the analysis of a large range of bubbler irrigation

systems indicate that the minimum distributor hose outlet elevation is achieved at a small lateral downhill slope of minus 0.5 %. The distributor hose outlet elevation can be decreased by using moderate hose discharges of 40 to 60 l/h, short laterals with small numbers of hoses (≤ 13 hose per lateral side), large lateral diameter (≥ 32 mm), large manifold diameter (≥ 75 mm) and a small number of laterals (≤ 9 lateral per manifold side).

The distributor hose diameter does not have any effect on the hose outlet elevation, but it has a large effect on the required pressure head of the irrigation system. The pressure head increased quickly at hose diameters of < 4 mm. Hose diameters of more than 8 mm only have a small effect on the required pressure head at the manifold inlet. Air locks may occur in pipelines of irrigation systems located on level fields and with design pressure heads lower than one meter. Air locks in bubbler systems can partially or entirely block the flow of water, and thereby significantly decrease the uniformity of water application from distributor hoses. Therefore, distributor hose diameters of less than 6 mm and greater than 10 mm are not recommended for low-head bubbler irrigation systems due to excessive friction losses and poor water distribution uniformity, respectively.

The examined low-head bubbler irrigation system can be combined with a water tank, which differs in volume and in water pressure heights. Therefore this irrigation system is suitable for combined operation with the wind energy converter MoWEC.

## 4. MoWEC-application for water storage: Low-head bubbler irrigation system for fruit trees and orchards on the N.W. Coast of Egypt

Low-head bubbler irrigation systems are well suited for the irrigation of fruit trees and orchard crops. This irrigation system enables water to be used economically, and its low operating pressure makes it particularly well suited for combination with renewable energy, such as wind energy. The agricultural land base of Egypt totals about 3.25 million hectares. The total orchard area in Egypt is 13.07 % of the agricultural land. The ground water is adequate and accessible along most parts of the N.W. coast of Egypt at a depth ranging from 5 to 50 m. An area of 137,460 ha in this region is suitable for fruit trees.

The amount of water which the crop needs depends on the rate of water transpired by the plant and the evaporation rate from the soil surface. In July, the maximum monthly irrigation requirements for 10 ha of orchards, olives and citrus trees on the N.W. coast of Egypt were 16,648, 18,093 and 23,784 $m^3$/(10 ha. month) respectively.

The average monthly quantity of water pumped by MoWEC on the N.W. coast of Egypt is 21,111 $m^3$ when the total dynamic head is 23.67 m. When MoWEC is used only to pump the

water required to irrigate 10 ha of orchards, olives or citrus trees on the N.W. coast of Egypt, the cost per m³ of water at a total dynamic head of 23.67 m would be 2.77, 3.92 or 3.5 € cents per m³ of water for orchards, olives or citrus respectively based on the economics of the MoWEC-prototype.

## Further research work

Energy and fresh water resources can be regarded as limited throughout the world due to the geographical situation. This is particularly true in the arid homeland Egypt. The experimental and theoretical results of this project are to be revised for application in Egyptian agriculture as follows:

**1.** In principle, the concept of MoWEC is well-suited for employment in Egypt because of its simple construction. In this connection, Egyptian operational parameters will be compiled and be provided in the context of a German - Egyptian co-operation, so that corresponding MoWEC versions can be put into operation.

**2.** Wind energy is an unstable form of energy. Therefore the question of energy storage will be placed in the center of future investigations. It is to be determined under which local wind conditions a bi-valent or mono-valent MoWEC version should be made the priority. This affects the decision to choose electrical energy storage in accumulators, or to store energy as potential energy in water containers. Questions emerge here about the amount of water hauled per unit of time due to the necessary pressure level for the selected irrigation system.

**3.** The developed irrigation technique LHBIS (Low head bubbler irrigation system) was so far examined only under laboratory conditions. Thus it is necessary to examine the laboratory results in a field test in order to evaluate the practical conversion. Also, further attempts are to be undertaken to examine the necessary filter level of the used water.

**4.** The necessity for storage basins while using wind energy for irrigation purposes should be a subject of discussion. A calculation method has to be developed to determine the optimal volume of a storage reservoir. The costs of different designs and materials for the building of a storage reservoir are to be calculated locally.

**5.** In summation, an evaluation framework has to be created to compare the newly developed “Wind Irrigation Systems” with the conventional irrigation systems. Then estimations of the extent to which this system can be put into operation at other locations in Egypt will be made. Great expectations are set on the future of water hauling with wind at Lake Nasser for the development of new areas. This project could provide a solid basis for future work in this area.

# 6 SUMMARY

## "Further development of a mobile wind energy plant for a low-pressure irrigation system"

Renewable energy is beginning to grow out of its initial status and has experienced exponential growth in usage over recent years. Wind energy is one of the most flexible of all renewable energy resources. The combination of a wind-electric system with suitable irrigation equipment for the watering of fruit trees could also supply electricity for common applications in regions without a public electrical grid.

MoWEC is the prototype of a special kind of wind energy plant. It was designed with two three-blade rotors running in opposite directions and with a yaw drive which has its travel path on a locally fixed portable frame. In the MoWEC prototype, the wing tip heights amount to 10 meters. The total rotors swept area is 80 m², because each of the two rotors has a diameter of 7.10 meters.

MoWEC has had no yaw drive system in stand alone use for low wind velocities. Such a system can be used for very high wind velocities to reduce the rotor surface facing the wind. In addition, the performance of MoWEC has not yet been measured in a field experiment. As example of the application of wind energy use, a gravity low head micro irrigation system was examined and designed for the watering of fruit trees based on the MoWEC power curve on the northwest coast of Egypt.

**The objectives of this study were:**

1. Further development of the mobile wind energy converter (MoWEC) with the goal of realizing a yaw drive control system without external energy storage in particular for stand-alone use.
2. Measurement of the MoWEC power curve in stand alone use (prototype).
3. Selection, simulation and laboratory test of a water- and energy saving irrigation technique for small orchard farms which are suitable for wind energy use.
4. Layout of an orchard farm in Egypt with this irrigation system and water provision by of MoWEC.

**MoWEC stand-alone use**

Wind energy plants in stand alone use cannot use the public grid as an energy source for the movement of the yaw drive frame. Small wind power plants – in maximum until nearly one kW – are often constructed with wind vanes. But because the MoWEC-prototype is designed for greater performance, we decided to install the simple technology of a lee-wind wheel, which is well known from historic windmills with fantails, for example.

Theoretical studies resulted in a lee-wind wheel with eight blades and an outer diameter ≥ 1.50 m. The main results of the lee-wind wheel wind tunnel experiments indicated that the blade angle φ should be 22.5 degrees and that the reduction ratio should be rw2 = 82.64:1. The installation of the lee-wind wheel system with rw2 on the MoWEC yaw drive frame results in a total reduction ratio of 1371:1. The field test proved that a modern wind energy converter works well in stand alone use with a lee-wheel yaw drive system and that this technique can also be recommended for the reduction of the effective rotor area at very high wind velocities . If the MoWEC rotors face the wind, the lee-wind wheel does not rotate. In this case, the theoretical angle θ is zero. In this position, no power is needed for the yaw drive system. In a gale, the basic position is altered by a wind vane.

**MoWC power curve and energy production**

The first power curve of the MoWEC was measured in a field test with a 10-pole permanent-magnet synchronous generator, measuring facilities for current and voltage, heating elements as a load and a digital three-cup anemometer for the wind velocity. The wind speed and the electric current in one phase were measured over a long period during the test. MoWEC´s total average power coefficient $C_{Pt}$ was calculated to be 0.32 based on the power curve, It includes the normal wind power coefficient $C_P$, generator efficiency, chain efficiency and gear box/bearing efficiency. This value $C_{Pt} = 0.32$ shall be increased through the further development of some factors of this first MoWEC prototype, e.g. the chain will be replaced by a drive shaft and the generator could be installed in a better position. A new hub will also allow the bales to be fastened in a better wind position.

A wind energy converter system (MoWEC) also enables wind energy to be used for different purposes such as irrigation, electricity generation, crop drying, grain grinding and many others. . In Egypt, like in most other developing countries, there is an increasing demand for energy. Wind energy can be very useful for lifting water and generating electricity on the N.W. coast of Egypt. The mean monthly wind speed and duration are 5.6 m/s (wind speed) and 461 h/month (duration). The actual mean annual energy production by MoWEC on the

northwest coast of Egypt was calculated to be 27,005 kWh based on the MoWEC total power coefficient of 0.32. The total initial cost of the MoWEC-prototype was 30,000 €. The cost of energy was calculated to be 15.44 € cents per kWh.

**Irrigation technique for a MoWEC application**

We chose a water and energy saving irrigation technique suitable for a MoWEC application on small orchard farms. According to a comparison of the irrigation techniques, the low-head bubbler irrigation system enabled water to be used economically, and its low operating pressure makes it particularly well-suited for combination with wind energy water pumping systems. Since design of this irrigation system is very important, the computer program LHBIS was written to make low-head bubbler irrigation design simpler and faster. Laboratory experiments were conducted to validate this computer program. The computer program was used to investigate certain factors influencing the elevation of distributor hoses along the laterals and the pressure head required at each manifold inlet of the irrigation system. In addition, the program was used to design the low-head bubbler irrigation system for 10 ha on the northwest coast of Egypt.

In July, the maximum mean monthly irrigation requirements for 10 ha orchards, olives and citrus trees on the N.W. coast of Egypt were 19,508 m³. The average mean monthly quantity of water pumped by MoWEC was calculated to be 21,111 m³. This value was enough to irrigate 10 ha of orchards, olives or citrus trees on the N.W. coast of Egypt. If only MoWEC is used to pump the water for the irrigation of 10 ha of orchards, olives or citrus trees, the average cost per m3 of water would be € cents 3.4 per $m^3$.

In the future, the wind-electrical system MoWEC can be used in a versatile manner. The described combination with a water and energy-saving irrigation system (low-head bubbler irrigation system) for fruit trees and orchards is only one targeted application. Generally, electricity generated by stand alone plants can be made available at all locations where wind velocities are sufficient, and no utility supplied electricity is available or where fossil energy is particularly expensive. Worldwide, MoWEC and the new irrigation system LHBIS thus allow a small contribution to be made towards the reduction of the water and energy shortage.

# 7 *SCHLUSSFOLGERUNGEN IN DEUTSCH*

## „Weiterentwicklung einer mobilen Windkraftanlage für ein Niederdruck-Bewässerungssystem“

Der Weltenergiebedarf nimmt kontinuierlich zu. Gründe hierfür sind die Zunahme der Weltbevölkerung, das Wirtschaftswachstum und der Energieverbrauch. Mit der heutigen Energienutzung, die hauptsächlich auf fossilen Energieträgern beruht, kann der weltweite Bedarf an Energie in den nächsten Jahrhunderten nicht mehr gedeckt werden. Der Energieverbrauch nahm stärker zu als die Weltbevölkerung. Von 1970 bis 1995 stieg der Energieverbrauch um 2,5 % pro Jahr (Verdoppelung in 30 Jahren) und die Weltbevölkerung um 1,7 % pro Jahr (Verdoppelung ca. in 40 Jahren). Von 1995 bis 2015 wird eine Zunahme des Energieverbrauchs um 2,2 % pro Jahr (Verdoppelung in 32 Jahren) und eine Zunahme der Weltbevölkerung um 1,5 % pro Jahr (Verdoppelung in 47 Jahren) erwartet [DOE (1995), IEA (1995) and PRB (1996)]. Der Zeitraum für die zukünftige weltweite Versorgung mit Öl und Erdgas wird mit ca. 50 Jahren angegeben, während Kohle noch über 100 Jahre verfügbar sein wird [BP (1994), IVANHOE (1995), BARTLETT (1995), CAMPBELL (1997), DUNCAN (1997), and YOUNGQUIST (1997)]. Diese Annahmen basieren auf der heutigen Förderung und auf der heutigen Erdbevölkerung. Wegen dieser relativ kurzen Zeiträume sollten schon heute Lösungen für morgen gefunden werden. Um ausreichend Energie auch in zukünftigen Jahrhunderten verfügbar zu haben, ist es erforderlich, die Nutzung erneuerbarer Energien weiter zu entwickeln.

Erneuerbare Energiequellen können als Energien definiert werden, die sich durch natürliche Prozesse immer wieder erneuern. Ihre Nutzung hat den Anfangsstatus verlassen und in den letzten Jahrzehnten eine exponentielle Zunahme der Anwendung erlebt. Windenergie ist eine am vielseitigsten zu nutzende erneuerbare Energie. Sie kann genutzt werden für Anwendungen wie Bewässerung, elektrische Energieerzeugung, Mahlen von Getreide und für weitere Nutzungen nach der Transformation in mechanische Energie durch einen Windenergiekonverter.

In Ägypten nimmt der Verbrauch an Elektrizität kontinuierlich zu. Deshalb hat das Ministerium für Elektrizität und Energie im Jahr 1980 ein nationales Konzept für die Nutzung und Anwendung der erneuerbaren Energien und für Maßnahmen zur Energieeinsparung vorgelegt. Darin wird eine 10%-tige Einsparung des Primärenergieverbrauchs bis zum Jahr 2005 angenommen bei einer Steigerung des erneuerbaren Energieverbrauchs auf 5 %, hauptsächlich durch Solar-, Biomasse- und Windtechnologien.

MoWEC ist der Prototyp einer mobilen Windkraftanlage mit zwei Rotoren, die bei Bedarf an verschiedenen Orten eingesetzt werden kann. Die Rotationsenergie kann wahlweise an zwei verschiedenen Positionen über eine Zapfwelle genutzt werden, z.B. für eine mechanische Wasserpumpe, einen Permanentmagnet-Generator im Insel- oder Netzbetrieb, einen Luftkompressor oder für andere passende Geräte. Verschiedene Konstruktionen in Höhe, Breite und Nennleistung sind möglich. Die Flügelspitzenhöhe des im Versuch benutzten MoWEC-Prototyps betrug 10 m und die gesamte überstrichene Rotorenfläche 80 m². Jeder der beiden Dreiblatt-Rotoren hatte einen Durchmesser von 7,10 m. Die theoretische Nennleistung ergab sich zu 20 kW bei einer Windgeschwindigkeit von 11 m/s. Das Konzept MoWEC wird seit 2002 in der Bundesforschungsanstalt für Landwirtschaft (FAL) in Braunschweig, Bundesrepublik Deutschland, entwickelt und gab Anlass zur Mitarbeit im Rahmen dieser Dissertationsschrift.

Der vorhandene MoWEC-Prototyp hatte kein automatisches Windnachführungssystem im Inselbetrieb für niedrige Windgeschwindigkeiten, das auch für sehr hohe Windgeschwindigkeiten zur Verkleinerung der dem Wind zugewandten Rotorfläche genutzt werden kann. Auch war noch keine Leistungsmessung an MoWEC im Feldversuch vorgenommen worden. Sowohl die automatische Windnachführung im Inselbetrieb als auch die Leistungsmessung stehen im Mittelpunkt dieser Dissertation. Als Beispiel für die Anwendung der Windenergienutzung wurde ein Schwerkraft-Niederdruck-Mikrobewässerungssystem mit Wasserspeicher untersucht und mit der MoWEC-Leistungskurve eine Obstbaumplantage im Nordwesten von Ägypten dimensioniert.

**Die Ziele der Arbeit waren:**

1. Weiterentwicklung der mobilen Windkraftanlage (MoWEC) mit dem Ziel, für den Inselbetrieb eine Windnachführung ohne externen Energiespeicher zu ermöglichen.
2. Messung der MoWEC-Leistungskurve im Inselbetrieb (Prototyp).
3. Auswahl, Simulation und Labortest einer für die Windenergie geeigneten wasser- und energiesparenden Bewässerungstechnik für kleine Obstbaumplantagen.
4. Layout dieses Bewässerungssystems für eine Obstbaumplantage in Ägypten mit der Wasserversorgung durch MoWEC.

Um diese Ziele erreichen zu können, wurden die Untersuchungen in vier Abschnitten vorgenommen:

**1. Ergänzung des MoWEC Windnachführungsrahmens mit einem lee-Windrad**

Der MoWEC-Prototyp benötigte ein automatisches Windnachführungssystem für den Inselbetrieb ohne externen Energiespeicher, um die Rotoren bei niedrigen

Windgeschwindigkeiten in den Wind und bei sehr hohen Windgeschwindigkeiten aus dem Wind drehen zu können. Um dies zu realisieren, wurde ein Windnachführungssystem mit einem Lee-Windrad gewählt, dimensioniert, im Windkanal getestet und an MoWEC angebaut.

Basierend auf theoretischen Untersuchungen ergaben sich für das Lee-Windrad acht Blätter und ein Außendurchmesser von $D_{wo} \geq 1{,}50$ m. Das Lee-Windrad wurde konstruiert und mit verschiedenen Blattwinkeln φ (15°, 22,5°, 35° und 45°) und zwei Getriebeuntersetzungen rw (56,82:1 oder 82,64:1) in unterschiedlichen Winkelpositionen θ zwischen dem Lee-Windrad und der Windrichtung im Windkanal getestet. Die Winkelpositionen θ zwischen dem Lee-Windrad und der Luftströmung im Windkanal stehen für die reale Luftströmung im Feldeinsatz bei Installation am MoWEC-Windnachführungsrahmen.

Die wichtigsten Ergebnisse des Lee-Windrad-Versuches im Windkanal haben gezeigt, dass der Blattwinkel φ = 22,5° betragen sollte bei einem Untersetzungsverhältnis von rw = 82,64:1. Mit diesen Werten kann das Lee-Windrad auch gut in Winkelpositionen unterhalb von θ = 20° als Windnachführung arbeiten, z.B. um ein Gewicht von 588,6 N (60 kg x 9,81 m/sec²) auch in Positionen von θ = 10° zu heben. Dieses Gewicht steht für die benötigte Kraft, um den MoWEC-Windnachführungsrahmen mit zwei Rotoren sicher bewegen zu können. In dieser Position ist der gemessene Leistungsbeiwert $C_{pm}$ = 0,1 %. Bei allen anderen Blattwinkelpositionen 15°, 35° oder 45° war der Leistungsbeiwert Null.

Die Installation des Lee-Windrad-Systems mit rw = 82,64:1 am MoWEC-Windnachführungsrahmen ergab ein gesamtes Untersetzungsverhältnis von 1371:1. Mit dem Feldtest konnte gezeigt werden, dass moderne Windenergiekonverter im Inselbetrieb gut mit einer Leerad-Windnachführung arbeiten können und auch eine Verkleinerung der wirksamen Rotorfläche bei sehr hohen Windgeschwindigkeiten mit dieser Technik empfohlen werden kann. Wenn die MoWEC-Rotoren in Windrichtung stehen, dreht sich das Leerad nicht. In dieser Position hat der Winkel θ den theoretischen Wert Null. Die Auslenkung bei Sturm erfolgt über eine Windfahne.

Der Zusammenhang zwischen der MoWEC-Rotorfläche und dem Winkel der Windrichtung zeigt, dass zur Verkleinerung der wirksamen Rotorfläche bei Sturm der Windnachführungsrahmen um einen größeren Winkel bewegt werden muss, zum Beispiel um den Winkel θ = 60°, damit die wirksame Rotorfläche halbiert wird. Wenn die Nennleistung von MoWEC überschritten wird, muss durch Querstellen des Leerades der Windnachführungsrahmen aus dem Wind fahren. Im Feldversuch wurde bestätigt, dass das Lee-Windrad genügend Energie für den Windnachführungsrahmen zur Verfügung stellen kann, um die wirksame MoWEC-Rotorfläche bei Sturm reduzieren zu können. Der Feldtest hat auch gezeigt, dass die Kräfte der

Rotorflächen auf das Antriebsrad des Windnachführungsrahmens sozusagen im handshake-Verfahren mit den Kräften des Leerades wirken und somit kein Stirnradgetriebe im Lee-Windrad-System installiert werden darf.

## 2. Messung der MoWEC-Leistungskurve

Nach Abschluss der Lee-Windraduntersuchungen wurde die erste Leistungskurve des MoWEC-Prototypen im Feldversuch durch Messung ermittelt. Benutzt wurden ein 10-poliger Permanentmagnet-Synchrongenerator mit 9 kW Nennleistung (max. 14 kW), Messeinrichtungen für Spannung und Strom, Wärmeelemente als Last und ein Dreischalen-Anemometer für die Windgeschwindigkeit. Die Windgeschwindigkeit und der Generatorstrom an einer Phase wurden über einen längeren Zeitraum in zwei Fällen bestimmt: Zuerst an der MoWEC-Konstruktion mit zwei Rotoren und dem Lee-Windrad am Windnachführungsrahmen, danach mit einem MoWEC-Rotor, der in Windrichtung fest positioniert war (Lee-Windrad außer Funktion). Mit den Messwerten konnten die Leistung von MoWEC und der Leistungsbeiwert bestimmt werden. Der benutzte Generator wurde für zukünftige MoWEC-Entwicklungen im FAL-Institut ausgelegt.

Von den Messwerten in diesen beiden Betriebszuständen ergab sich ein Gesamtleistungsbeiwert $C_{Pt}$ von 0,32. Dieser Leistungsbeiwert enthält den normalen Windenergieleistungsbeiwert $C_P$, den Generator-Wirkungsgrad, den Ketten-Wirkungsgrad und den Getriebe/Lager-Wirkungsgrad. Dieser Wert $C_{Pt} = 0{,}32$ kann durch Weiterentwicklung des MoWEC-Prototyps in Zukunft erhöht werden, z.B. sollte die Kette durch eine Gelenkwelle ersetzt werden, und der Generator könnte an einer besseren Position angebracht werden. Auch mit einer neuen Nabe könnten die Rotorblätter in einer günstigeren Windposition befestigt werden. Nach diesen Untersuchungen kann für den MoWEC-Prototyp ein elektrischer Generator mit mindestens 20 kW Nennleistung empfohlen werden. Eine Nennensleistung von 25 kW hätte den Vorteil, dass der Generator bei Windgeschwindigkeiten über 11 m/s eine genügende Gegenkraft für die Sturmsicherung aufbringen würde.

Windenergie kann genutzt werden für Anwendungen wie Bewässerung, elektrische Energieerzeugung, Mahlen von Getreide und für weitere Nutzungen nach der Transformation in mechanische Energie durch einen Windenergiekonverter. In Ägypten, wie in den meisten anderen Entwicklungsländern, gibt es einen zunehmenden Energiebedarf. Windenergie kann für das Fördern von Wasser und zum Erzeugen von Elektrizität an der N.W. Küste von Ägypten sehr nützlich sein. Das landwirtschaftlich genutzte Gebiet an der N.W. Küste von Ägypten erstreckt sich ungefähr 550 km von Alexandria nach Al-Salloum und 10-20 km südlich des Mittelmeeres. Der monatliche Durchschnitt der Windgeschwindigkeit beträgt 5,17 bis 6,03 m/s bei einer Dauer von 308 h/Monat bis 614 h/Monat. Der tatsächliche Jahresdurchschnitt der

MoWEC-Energieerzeugung von 27.233,-- kWh/Jahr an der N.W. Küste von Ägypten errechnete sich aus den durchschnittlichen Windgeschwindigkeiten und dem Gesamtleistungsbeiwert von 0,32. Die Investitionskosten des MoWEC-Prototyps, berechnet auf der Basis einer Kleinserie, beträgt 26.000,-- € plus 4.000,-- € für Generator und Wasserpumpeneinrichtungen. Damit wurden die Kosten der MoWEC-Energieproduktion mit 15,44 € cent/kWh berechnet bei einer Amortisationsdauer von 10 Jahren, 8% Jahreszins und 2% der Investitionskosten für Betrieb und Wartung.

## 3. Windenergie-Schwerkraft-Niederdruck-Bubbler-Bewässerungssystem für Obstbaumplantagen

Bewässerung ist eine der größten Energieverbraucher in der Landwirtschaft. Die Kombination eines windelektrischen Systems mit einer geeigneten Bewässerungsanlage zur Wasserversorgung von Obstbäumen kann in Regionen ohne öffentliches Stromnetz auch die Versorgung mit Elektrizität für allgemeine Anwendungen ermöglichen. In dieser Arbeit wurde ein Schwerkraft-Niederdruck-Bubbler-Bewässerungssystem gewählt, weil mit dem erforderlichen Wasserspeicher die transformierte potentielle Energie gespeichert werden kann.

Die Niederdruck-Bubbler-Bewässerung unterscheidet sich von anderen Mikro-Bewässerungssystemen. Sie basiert auf Schwerkraft mit Wasserhöhen von ungefähr 1 m und erfordert keine sorgfältige Filterung des Wassers. Ihr Auslassdurchmesser beträgt mindestens 4 mm. Damit ist dieses Bewässerungssystem für den ökonomischen Einsatz von Wasser in der Landwirtschaft geeignet, und die niedrige Wasserhöhe im Wassertank macht es besonders geeignet für die Kombination mit der MoWEC-Windenergieanlage.

Das Computerprogramm LHBIS wurde geschrieben, um Niederdruck-Bubbler-Bewässerungssysteme einfacher und schneller als auf traditionelle Weise berechnen zu können. Es erlaubt dem Benutzer, die Verteilerschlauchauslasshöhe in Bezug zum jeweiligen Verteilerrohranschluss oder die Länge für jeden Anschluss am Verteilerrohr in Abhängigkeit vom Druck und Feldbedingungen zu bestimmen.

Es wurden Laborversuche durchgeführt, um die Charakteristik der Rohrreibung zu bestimmen (Verteilerrohre und Verteilerschläuche). Der Hazen-Williams-Koeffizient des Verteilerrohres war 140 und 115 für den Verteilerschlauch. Die Laborversuche wurden auch zur Überprüfung des LHBIS-Computerprogramms verwendet. Dabei wurden u.a. die drei Neigungswinkel des Verteilerrohres (eben, ansteigend und absteigend) hinsichtlich der Durchflüsse der Verteilerschläuche und der Druckhöhe an den Verteilerschlauchanschlüssen des Verteilerrohres gemessen.

Die Durchfluss-Gleichförmigkeitswerte und der Durchfluss-Variationskoeffizient der Verteilerschläuche wurden aus den Daten des Laborexperiments errechnet. Die Durchfluss-Gleichförmigkeitswerte lagen bei 97% und die Durchfluss-Variationskoeffizienten lagen zwischen 5% bis 7%.

Die Berechnungen mittels des Computerprogramms und die Ergebnisse der Laborexperimente haben gezeigt, dass die Nutzung des Niederdruck-Bubbler-Bewässerungssystems mit unterschiedlichen Verteilerschlauch-Auslasshöhen praxisgerechter gegenüber unterschiedlichen Verteilerschlauchlängen ist, um die Obstbäume auf einem unebenen Feld gleichmäßig bewässern zu können. Dies trifft besonders dann zu, wenn die Landfläche nicht waagerecht ist (Oberflächengefälle zwischen ± 1,5%). Wenn die Bodenoberfläche dagegen eben ist, kann das Bewässerungssystem mit unterschiedlicher Verteilerschlauchlänge benutzt werden, weil die Unterschiede zwischen maximaler und minimaler Druckhöhe am Verteilerschlaucheingang den Reibungsverlusten innerhalb der Bewässerungsleitungen entsprechen (Verteilerrohr und Feldzuleitung).

Das Computerprogramm wurde benutzt, um die Faktoren zu ermitteln, welche die Verteilerschlauch-Auslasshöhe entlang des Verteilerrohres und die notwendige Druckhöhe am Beginn jeder Feldzuleitung beeinflussen. Die Ergebnisse der Analyse zeigen, dass die minimale Verteilerschlauch-Auslasshöhe bei einem Gefälle des Verteilerrohrs von minus 0,5 % erreicht wird. Die Verteilerschlauch-Auslasshöhe kann reduziert werden, wemm man den Durchfluss im Verteilerschlauch auf 40 - 60 l/h begrenzt, kurze Verteilerrohre mit einer kleinen Anzahl (≤ 13 Verteilerschlauche pro Verteilerrohrseite) verwendet sowie große Verteilerrohrdurchmesser (≥ 32 mm) und große Feldzuleitungsdurchmesser (≥ 75 mm) bei einer geringen Zahl von Verteilerrohren an der Feldzuleitung (≤ 9 pro Seite) wählt.

Der Verteilerschlauchdurchmesser hat keinen Einfluss auf die Verteilerschlauch-Auslasshöhe, aber er hat einen großen Effekt auf die erforderliche Druckhöhe des Bewässerungssystems. Die Druckhöhe erreicht eine schnelle Zunahme, wenn der Verteilerschlauchdurchmesser kleiner als 4 mm wird. Verteilerschlauchdurchmesser größer als 8 mm haben nur einen geringen Einfluss auf die erforderliche Druckhöhe am Eingang der Feldzuleitung. Luftblasen können in den Rohrleitungen des Bewässerungssystems auftreten, wenn auf ebenen Feldern die vorgesehenen Druckhöhen weniger als einen Meter betragen. Die Lufteinschlüsse im Bewässerungssystem können den Fluss des Wassers teilweise oder völlig blockieren und verringern dadurch erheblich die Gleichförmigkeit der Wasserverteilung über die Verteilerschläuche. So werden Verteilerschlauchdurchmesser von weniger als 6 mm und größer als 10 mm nicht für die Niederdruck-Bubbler-Bewässerung empfohlen, weil sich wegen der übermäßigen Reibungsverluste eine schlechte Gleichförmigkeit der Wasserverteilung zeigt.

Das untersuchte Niederdruck-Bubbler-Bewässerungssystem kann mit einem im Volumen und Wasserdruck variablen Wasserspeicher kombiniert werden. Somit ist dieses Bewässerungssystem für den Einsatz des mobilen Windenergiekonverters MoWEC geeignet.

## 4. MoWEC-Anwendung mit Wasserspeicherung: Niederdruck-Bubbler-Bewässerungssystem für Obstbaumplantagen an der Nordwestküste von Ägypten

Das Niederdruck-Bubbler-Bewässerungssystem kann gut zur Bewässerung von Obstbaumplantagen eingesetzt werden. Das Bewässerungssystem ermöglicht einen ökonomischen Einsatz des Wassers bedingt durch den niedrigen Betriebsdruck. Daher ist auch eine gute Kombination mit erneuerbaren Energien - wie der Windenergie - gegeben. Die gesamte landwirtschaftflache Fläche von Ägypten beträgt ungefähr 3,25 Millionen Hektar. Die gesamte Obstbaumfläche in Ägypten beträgt davon 13,07 %. Grundwasser steht an der Nordwestküste von Ägypten in 5 bis 50 m Tiefe ausreichend zur Verfügung. Es wird geschätzt, dass das Wasser für eine Obstbaumfläche von 137.460 ha in dieser Region ausreicht.

Die Menge des Wassers, das die Pflanzen benötigen, ist von der Evapotranspiration und der Bodenwasserversickerung abhängig. Der maximale Monatswasserbedarf für je 10 ha Obstbäume, Oliven- oder Zitrusbäume beträgt an der Nordwestküste von Ägypten im Juli 16.648, 18.093 bzw. 23.784 m³.

Das durchschnittliche monatliche von MoWEC gepumpte Wasser an der N.W.-Küste von Ägypten beträgt 21.111 m³. Bei einer Druckhöhe von 23,67 m wurde ein Wasserpreis von 2,77 € cent/m³ für Obst, 3,92 € cent/m³ für Oliven und 3,5 € cent/m³ für Zitrus aus den ökonomischen MoWEC-Daten berechnet.

## Weitere Forschungsarbeiten

In Abhängigkeit von der geografischen Lage sind die Ressourcen Nutzenergie und Süßwasser weltweit als begrenzt verfügbar anzusehen. Dies besonders im ariden Heimatland Ägypten. Die experimentellen und theoretischen Ergebnisse der Arbeit sind für die Anwendung in der ägyptischen Landwirtschaft wie folgt aufzuarbeiten:

**1.** Das Konzept MoWEC eignet sich grundsätzlich wegen der einfachen Konstruktion für den Einsatz in Ägypten. Diesbezüglich sollen für die weitere konstruktive Entwicklung Einsatzparameter aus Ägypten erarbeitet und im Rahmen einer deutsch-ägyptischen Zusammenarbeit zur Verfügung gestellt werden damit dann entsprechende MoWEC-Varianten in Betrieb genommen werden können.

**2.** Windenergie ist eine unstetige Energieform. Deshalb wird die Frage der Energiespeicherung im Mittelpunkt zukünftiger Untersuchungen stehen. Es ist zu bestimmen, unter welchen lokalen Windverhältnissen eine bivalente oder monovalente MoWEC-Version den Vorrang bekommen sollte. Dies berührt die Entscheidung über eine zu wählende elektrische Energiespeicherung in Akkumulatoren oder die Energiespeicherung als potentielle Energie im Wasser-Vorratsbehälter. Damit verbunden sind Fragen nach der zu fördernden Wassermenge pro Zeiteinheit bei Vorgabe der erforderlichen Druckhöhe für das gewählte Bewässerungssystem.

**3.** Die entwickelte Bewässerungsanlage LHBIS (Low-head bubbler irrigation system) wurde bisher nur im Labor untersucht. Somit ist es notwendig, die praktische Umsetzung zur Überprüfung der Laborergebnisse in einem Feldversuch vorzunehmen. Darüber hinaus sind weitere Versuche zur erforderlichen Filterschärfe des benutzten Wassers durchzuführen.

**4.** Die Diskussion für die Notwendigkeit eines Speicherbeckens bei der Nutzung der Windenergie für Bewässerungszwecke sollte erfolgen. Dabei ist eine Kalkulationsmethode zu entwickeln, mit der das optimale Volumen eines Speicherbeckens bestimmt werden kann. Vor Ort sind die Kosten verschiedener Bauarten und Materialen für den Bau eines Speicherbeckens zu kalkulieren.

**5.** Insgesamt ist ein Bewertungsrahmen zu erstellen, aus dem abzulesen ist, wie das neu entwickelte „Wind-Bewässerungssystem“ im Vergleich zu den herkömmlichen Bewässerungssystemen zu beurteilen ist. Danach kann eine Einschätzung abgeben werden, inwieweit sich dieses System an anderen Standorten in Ägypten einsetzen lässt. Große Erwartungen werden auf die zukünftige Wasserförderung mit Wind am Lake Nasser zur Neulanderschließung gesetzt. Diese weiterführende Arbeit könnte dafür eine gute Grundlage sein.

# 8 *ZUSAMMENFASSUNG IN DEUTSCH*

## „Weiterentwicklung einer mobilen Windkraftanlage für ein Niederdruck-Bewässerungssystem“

Die Nutzung erneuerbarer Energiequellen hat den Anfangsstatus der Anwendung verlassen und in den letzten Jahrzehnten eine exponentielle Zunahme erlebt. Windenergie ist eine am vielseitigsten zu nutzende erneuerbare Energie. Die Kombination eines windelektrischen Systems mit einer ihr angepassten Bewässerungsanlage für Obstbäume kann in Regionen ohne öffentliches Stromnetz sowohl für die Bewässerung als auch für die allgemeine Stromversorgung eingesetzt werden.

MoWEC ist der Prototyp einer mobilen Windkraftanlage mit zwei gegenläufigen Dreiblatt-Rotoren. Der Windnachführungsrahmen befindet sich auf einem ortsfest abgestellten Fahrrahmen. Die Flügelspitzenhöhe des im Versuch benutzten MoWEC-Prototyps betrug 10 m und die überstrichene Rotorfläche beider Rotoren betrug 80 m². Damit hatte jeder Rotor einen Durchmesser von 7,10 m.

Der zur Verfügung stehende MoWEC-Prototyp hatte für den Inselbetrieb keinen eigenen Antrieb des Windnachführungsrahmens. Ein Antrieb war aber für niedrige Windgeschwindigkeiten (Rotor im Wind) und für Windgeschwindigkeiten oberhalb der Nennwindgeschwindigkeit (Rotor dreht aus dem Wind) erforderlich. Auch war noch keine Leistungsmessung an MoWEC im Feldversuch vorgenommen worden. Als Beispiel für die Anwendung der Windenergienutzung wurde ein Schwerkraft-Niederdruck-Mikrobewässerungs-system mit Wasserspeicher untersucht, und es wurde mit der MoWEC-Leistungskurve eine Obstbaumplantage im Nordwesten von Ägypten dimensioniert.

**Die Ziele der Arbeit waren:**

1. Weiterentwicklung der mobilen Windkraftanlage (MoWEC) mit dem Ziel, für den Inselbetrieb eine Windnachführung ohne externen Energiespeicher zu ermöglichen.
2. Messung der MoWEC-Leistungskurve im Inselbetrieb (Prototyp).
3. Auswahl, Simulation und Labortest einer für die Windenergie geeigneten wasser- und energiesparenden Bewässerungstechnik für kleine Obstbaumplantagen.
4. Layout dieses Bewässerungssystems für eine Obstbaumplantage in Ägypten mit der Wasserversorgung durch den Einsatz von MoWEC.

## MoWEC im Inselbetrieb

Windenergieanlagen im Inselbetrieb können nicht das öffentliche Stromnetz als Energiequelle für die Windnachführung nutzen. Kleine Windenergieanlagen bis ca. ein Kilowatt Nennleistung werden häufig mit Windfahnen ausgestattet. Bei höheren Leistungen reicht eine Windfahne wegen des Gewichts nicht aus. Deshalb wurde entschieden, den MoWEC-Prototyp mit der einfachen Technik eines Lee-Windrades auszustatten. Derartige Konstruktionen sind von historischen Windmühlen bekannt. Für MoWEC musste ein neues Lee-Windrad dimensioniert, im Windkanal getestet und in der Praxis erprobt werden.

Basierend auf theoretischen Untersuchungen ergaben sich für das Lee-Windrad acht Blätter und ein Außendurchmesser von ≥ 1,50 m. Die wichtigsten Ergebnisse des Lee-Windrad-Versuches im Windkanal haben gezeigt, dass der Blattwinkel $\varphi = 22{,}5°$ betragen sollte bei einem Untersetzungsverhältnis von rw2 = 82,64:1. Die Installation des Lee-Windrad-Systems mit rw2 am Windnachführungsrahmen ergab ein gesamtes Untersetzungsverhältnis von 1371:1. Mit dem Feldtest konnte gezeigt werden, dass moderne Windenergiekonverter im Inselbetrieb gut mit einer Leerad-Windnachführung arbeiten können und auch eine Verkleinerung der wirksamen Rotorfläche bei sehr hohen Windgeschwindigkeiten mit dieser Technik empfohlen werden kann. Wenn die MoWEC-Rotoren in Windrichtung stehen, dreht sich das Leerad nicht. In dieser Position hat der Winkel $\theta$ den theoretischen Wert Null. Die Auslenkung bei Sturm erfolgt über eine Windfahne.

## MoWEC-Leistungskurve und Energieerzeugung

Die erste Leistungskurve des MoWEC-Prototyps wurde im Feldversuch gemessen. Benutzt wurden ein 10-poliger Permanentmagnet-Synchrongenerator, Messeinrichtungen für Spannung und Strom, Heizelemente als Last und ein Dreischalen-Anemometer für die Windgeschwindigkeit. Die aktuelle Windgeschwindigkeit und der Generatorstrom an einer Phase wurden über einen längeren Zeitraum gemessen. Die Messwerte ergaben einen Gesamtleistungsbeiwert $C_{Pt}$ von 0,32. Dieser Leistungsbeiwert enthält den normalen Windenergieleistungsbeiwert $C_P$, den Generator-Wirkungsgrad, den Ketten-Wirkungsgrad und den Getriebe/Lager-Wirkungsgrad. Der Wert $C_{Pt} = 0{,}32$ kann durch Weiterentwicklung des Systems in Zukunft optimiert werden, z.B. sollte die Kette durch eine Gelenkwelle ersetzt werden, und der Generator könnte an einer günstigeren Position angebracht werden. Auch mit einer neuen Nabe könnten die Rotorblätter in einer besseren Windposition befestigt werden.

Windenergie kann z.B. genutzt werden für Anwendungen in der Bewässerung, zur elektrischen Energieerzeugung und zum Mahlen von Getreide. In Ägypten, wie in den meisten anderen Entwicklungsländern, gibt es einen zunehmenden Bedarf an Energie. Beispielhaft wurde das Fördern von Wasser an der Nordwestküste von Ägypten untersucht. Der monatliche

Durchschnitt der Windgeschwindigkeit beträgt dort 5,6 m/s bei einer Dauer von 461 h/Monat. Der tatsächliche Jahresdurchschnitt der MoWEC-Energiebereitstellung wurde mit 27.005,-- kWh im Jahr berechnet auf der Basis des Gesamtleistungsbeiwertes von 0,32. Die Investitionskosten des MoWEC-Prototyps, berechnet auf der Grundlage einer Kleinserie, beträgt 30.000,-- €. Damit wurden die Kosten der MoWEC-Energieerzeugung mit 15,44 € cent/kWh berechnet.

**Bewässerungstechnik für die MoWEC-Anwendung**

Als Anwendung wurde eine geeignete wasser- und energiesparende Bewässerungstechnik für kleine Obstbaumplantagen gesucht. Durch Vergleich bekannter Bewässerungstechniken wurde das Niederdruck-Bubbler-Bewässerungssystem gewählt. Das Bewässerungssystem ermöglicht wegen des niedrigen Betriebsdruckes einen ökonomischen Einsatz des Wassers und ist deshalb gut mit einem Windpumpensystem zu betreiben. Für die Auslegung dieses Bewässerungssystems wurde das Computerprogramm LHBIS geschrieben, um die Dimensionierung eines Niederdruck-Bubbler-Bewässerungssystems einfacher und schneller vornehmen zu berechnen. Laborversuche wurden zur Überprüfung des LHBIS-Computerprogramms durchgeführt. Das Programm wurde benutzt, um Faktoren zu ermitteln, wie die Verteilerschlauch-Auslasshöhe entlang des Verteilerrohres, die notwendige Druckhöhe am Beginn jeder Feldzuleitung oder der Neigungswinkel des Verteilerrohres gewählt werden müssen. Mit Hilfe des Programms wurde zusätzlich ein Niederdruck-Bubbler-Bewässerungssystem für 10 ha an der Nordwestküste von Ägypten entworfen.

Der maximale durchschnittliche Monatswasserbedarf für je 10 ha Obstbäume, Oliven- oder Zitrusbäume beträgt an der N.W. Küste von Ägypten im Juli 19.508 m³. Das durchschnittlich im Monat durch MoWEC gepumpte Wasser an der N.W.-Küste von Ägypten beträgt 21.111 m³. Die Menge des geförderten Wassers ist somit ausreichend für die Bewässerung. Bei einer Druckhöhe von 23,67 m wurde ein Wasserpreis von durchschnittlich 3,4 € cent/m³ aus den ökonomischen MoWEC-Daten berechnet.

In Zukunft kann das windelektrische System MoWEC vielseitig eingesetzt werden. Die beschriebene Kombination mit dem wasser- und energiesparenden Bewässerungssystem LHBIS (Niedrigdruck-Bubbler-Bewässerungssystem) für Obstbaumplantagen ist nur eine Möglichkeit des Einsatzes. Allgemein kann bei ausreichenden Windgeschwindigkeiten elektrische Energie im Inselbetrieb überall dort bereitgestellt werden, wo kein öffentliches Stromnetz vorhanden oder wo fossile Energie besonders teuer ist. Somit kann mit MoWEC und dem neuen Bewässerungssystem LHBIS weltweit ein kleiner Beitrag zur Minderung der Wasser- und Energieknappheit geleistet werden.

# 9 REFERENCES

Abdel-Monem, M. H., H. E. Khalifa and Solh, M. B. (1998): Building and sustaining the high production capacity of Egypt's irrigated lands: A long-term research program. Journal of Sustainable Agriculture Vol. 11, No. 2/3:7-17.

Abu-Zaid, M. A. and Rady M. A. (1992): Water resources management and policies in Egypt. Moigne, G. L., S. Barghout, G. Geder, L. Garbus and Xie, M. (ed.): Country Experiences with Water Resources Management. Economic Institutional, Technological and Environmental Issuse. World Bank Technical Paper Number 175, World Bank, Washington, D.c, pp. 93-101.

Abu-Zaid, M. A. (1994): Egypt's efforts towards management of agricultural water demand. Proceedings of VIII IWRA World Congress on Water Resources, Cairo, Egypt, 21-25 November.

AGEB (2002): AG Energiebilanz. Die Arbeitsgemeinschaft Energiebilanzen, Köln.

ASCE Committee on Pipeline Planning (1992): Pressure pipeline design for water and wastewater. ASCE, Reston, Virginia.

Balba, A. M. (1981): Agricultural development activities in the western desert of Egypt. Advances in soil and water research. Alex. Univ. Egypt, No. 11: 35-75.

Bartlett, A. A. and Ristinen, R. A. (1995): Natural gas and transportation. Physics and Society, 24 (4): 9-10.

Baz, A. and Mobarak, A. (1981): Optimal selection of wind energy conversion systems for Egypt. Program of the German Egyptian workshop on solar collectors 31 st. January to 2 nd Februry, Cairo, Egypt, pp.1-9.

Bennett, J. and Elton, R. (1898): History of corn milling, pp. 240-241.

Betz, A. (1926): Wind-Energie und ihre Ausnutzung durch Windmühlen. Göttingen: Vandenhoeck & Ruprecht. Nachdruck: Grebenstein: OEKO-Buchverlag 1982.

BMWi (2002): Sustainable Energy Policy to Meet the Needs of the Future; Energy Report, No: 508. Bundesministerium für Wirtschaft und Technologie.

Boswell, M. J. (1984): Micro-irrigation design manual. James Hardie Irrigation Co., El Cajon, California, USA.

BP (1994): British Petroleum Statistical Review of World Energy. London: British Petroleum

Brush, C. F. (1987): Feasibility of irrigation with wind-powered centrifugal pumps. American Solar Energy Society, pp. 445-449.

Buckland, S. (1987): Lee’s patent windmill, 1744-1747. Wind and watermill section, Society for Protection of Ancient Buildings, London, UK, 19 p.

Cahoon, J. and Westesen, G.L. (1987): Wind power for irrigation systems. American Society of Agricultural Engineers, paper No. 87-2012, 10 p.

Campbell, C. J. (1997): The Coming Oil Crisis. New York: Multi-Science Publishing Company & Petroconsultants S.A.

Carr, M. and Kay, M. G. (1980): Bubbler Irrigation. Horic. Ind., pp. 11-12.

Christiansen, J. E. (1942): Hydraulics of sprinkling systems for irrigation. Trans ASCE, 107: 221- 250.

CIA (2003): Central Intelligence Agency. The World Factbook, Egypt.
http://www.odci.gov/cia/publications/factbook/geos/eg.html

Clark, H. O. (1928-29): Notes on French windmills. Transactions of the New-comen Society (T.N.S.), Vol. 9: p. 52.

Clark, R. N. and Mulh, K. E. (1992): Water pumping for livestock. Proc. Wind power, 92, AWEA, USA, October 1992, pp. 284-290.

Clark, R. N. and Pinkerton, W. E. (1988): Wind powered electric water pumping. American Society of Agricultural Engineers, paper No. 8b-4540, 10 p.

Danish (1999): Egypt - Strategy for Danish Regional Assistance 1999.
http://www.um.dk/publikationer/fremmedsprog/English/Strategy/Egypt/egypt.6.2.2.asp

David, K. (1975): Trickle irrigation design. California, USA, pp. 27-28.

Delittle, R. J. (1972): The windmill yesterday and today. London, UK, 58 p.

Derbala, A. (2003): Development and evaluation of mobile drip irrigation with center pivot irrigation machines. Dr. agr. Thesis, Justus-Liebig-Universität Giessen, Germany.

Dobesch, H. and Tran, H. V. (1999): The diagnostic wind field model ZAWIMOD2. Austrian Contribution to Meteorology and Geophysics, Vol. 22, Publ. No. 389.

DOE (1995): Annual energy outlook with projections to 2010. Washington, DC: USDOE, EIA.

Duncan, R. C. (1997): The world petroleum life-cycle: encircling the production peak. Space Studies Institute May 9: 1-8.

Duncan, R. C. and Youngquist, W. (1998): Encircling the Peak of World Oil Production. Issue # 2 Paper of the World Forecasting Program. 22 p.

El-Kady, M. M. (1999): Document of the National Water Research Center, proceedings of the first Arabic conference on water and desertification, Cairo, 17 to 19 April, 1999.

El-Mallah, A. and Soltan, A. M. (1991): Water yield from wind pumps for deserts development in Egypt. Harwood Academic Publishers; 1991. Advances in desert and arid land technology and development, Vol. 5: 211-223.

Enquete-Kommission (1995): Vorsorge zum Schutz der Erdatmosphäre des 11. Deutschen Bundestages (Hrsg.): Mehr Zukunft für die Erde. Economica Verlag. Bonn, Germany.

ENERDATA (2003): The World Energy Consumption in 2002. Statistical Yearbook
http://www.enerdata.fr/enerdata_UK/Produits/exemples/pressannu_A.pdf

FAO (1977): Doorenbos, J. and Pruitt, W.O. Crop water requirements. FAO Irrigation and Drainage Paper. Nr. 24, pp. 1-54.

Farahat, D. T. (1999): Improving the utilization of wind energy for water lifting at the N.W coast of Egypt. M. Sc. Thesis, Fac. of Agric., Alexandria University, Egypt.

Farouk, A. H. (1998): Microirrigation management and maintenance. California, USA, pp.8-14.

Fraenkel, P., R. Barlow, F. Crick and Bokalders, V. (1993): Wind pumps: A guide for development workers. IT Publications, pp. 30-33.

Franquesa, M. (1989): Kleine Windräder, Berechnung und Konstruktion. Undo Pfriemer Buchverlag in der Bauverlag GmbH. Wiesbaden und Berlin, S. 41-61.

Gad, A. (2003): Assessment of water resources and irrigation practices; Sufficiency and impact impact evaluation in Egypt. http://www.eurisy.asso.fr/events/desertification/Rabatpresentations/Gad.PDF

Gaddas, N. (2000): Promoting sustainable utilization of marginal lands in the Near East Region. Regional Workshop on Degradation and Rehabilitation of Marginal Land in the Arab Region, CEDARE. Cairo.

Gasch, R. (1996): Windkraftanlagen, Grundlagen und Entwurf. B. G. Teubner Stuttgart.

George, H. H. and Samani, Z. A. (1986): World water for agriculture precipitation management. Washington, D.C., pp. 69-74.

Godfrey, B. (1996): Renewable energy power for a sustainable future. Oxford University, UK. Pp. 27-29 and 265-312.

Gomma, A. A. (1996): Current and future global situation of grains. The Egyptian case, paper presented at the international seminar on Grains, Water, and the Political.

Gourieres, D. (1982): Wind power plants- theory and design. Pergamon Press GmbH, p. 285.

Greaves, W. F. and Carpenter, J. H. (1969): A short history of mechanical engineering. Harlow: Longmans, pp. 54-56.

Hassan, E. (2003): Biogas production from forage and sugar beets, process control and optimization – ecology and economy. Dr.- Ing. Thesis, University of Kassel, Germany.

Hau, E. (1996): Windkraftanlage - Grundlagen, Technik, Einsatz, Wirtschaftlichkeit (2., überarb. und aktualisierte Aufl.), Berlin (Springer).

Heier, S. (2000): Nutzung der Windenergie. TÜV-Verlag, S. 24-31.

Heinloth, K. (1997): Die Energiefrage : Bedarf und Potentiale, Nutzen, Risiken und Kosten.

Heywang, F., E. Nücke, J. Timm und Timm, W. (1999): Physik für Techniker. Verlag Handwerk und Technik G.m.b.H., S. 150-151.

Hull, P. J. (1981): A low-pressure irrigation system for orchard tree and plantation crops. The Agriculture Engineer, 36(2): 55-58.

ICID (2002): International Commission on Irrigation and Drainage: Sprinkler and micro-irrigated area in some member countries of ICID. ICID working group on farm irrigation systems, working paper.

IEA (1995): International Energy Annual. DOE/EIA-0219 [95]. U.S. Department of Energy, Washington, DC.

Irps, H. (2002a): The construction of the mobile wind energy plant MoWEC. ASAE Annual International Meeting/ CIGR World Congress. July 28-31. Chicago, USA: Paper 2002/4023.

Irps, H. (2002b): Mobile wind energy converter (MoWEC). World renewable energy congress VII. Cologne, Germany. World's best energy option; extended abstracts. Pergamon. 208 p.

Irps, H. (2002c): Mobile Windkraftanlage: MoWEC. Landtechnik 57 (6): 346-347.

Irps, H. and Omara, A. I. (2003): Further development of the wind energy converter MoWEC for stand alone use. RIO 3 - World Climate & Energy Event, International Conference on Renewables for a Sustainable Energy Supply. Rio de Janeiro, Brazil, 1-5 December 2003, pp. 355-360.

Irps, H. und Omara, A.I. (2004): Windkrafterntemaschine MoWEC. Landtechnik, 59 (5): 272-273.

Ivanhoe, L. F. (1995): Future world oil supplies: there is a finite limit. World Oil. October: 77-88.

Jens, P. M. (1978): Windenergie in Theorie und Praxis, Grundlagen und Einsatz. Verlag C. F. Müller Karlsruhe, 45 p.

Johansson, T. B., H. Kelly, A. K. N. Reddy and Williams, R. H. (1993): Renewable energy sources for fuels and electricity. Island Press, Washington, D.C., pp. 157-160.

John, F. W. and Jenkins, N. (1997): Wind energy technology. John Wiley & Sons, pp. 19-26.

Kay, L. and Hatcho, N. (1992): Small-scale pumped irrigation: Energy and Cost. FAO, 27 p.

Keller, J. (1990a): Modern irrigation in developing countries. Proc. 14th Int. Cong. ICID, 1-E: 113-138.

Keller, J. and Bliesner, R. D. (1990b): Splinkle and trickle irrigation. Van Nostrand Reinhold, New York, USA.

Keller, J. and Karmeli, D. (1974): Trickle irrigation design parameters. Transactions of ASAE, 17(4): 678-784.

Kruse, E. G., A. S. Humpherys and Pope, E. J. (1980): Farm water distribution system. Chapter 11 in Jensen. M. E. (ED). Design and operation of farm irrigation system. ASAE, Joseph. MI, 829 pp.

Lamont, P. A. (1981): Common pipe flow formulas compared with the theory of roughness. Journal of the American Water Works Association, 73(5), 274.

Ling, S., V. Nelson, R. N. Clark, and Vick, B. (2000): Field testing of a smart controller for wind-electric water pumping systems. A collection of the 2000 ASME wind energy symposium technical papers at the 38th AIAA aerospace sciences meeting and exhibit. Reno, NV, 10-13 January 2000, AIAA-2000-0055.

Mayr, O. (1970): The origins of feedback control. The M.I.T. Press, pp. 91-99.

Mayer, B. (2001): Assessment of and selecting criteria for irrigation methods using PVPS. GTZ Seminar, Eschborn, Germany.

McNown, J. S. (1954): Mechanics of manifold flow. Trans. ASCE, 119: 1103 -1118. American Society of Civil Engineers, New York.

Mobarak, A., H. Safwat and Abdel Hamid, A. (1991): Availability of wind energy in a typical desert location in Egypt. Harwood Academic Publishers; 1991. Advances in desert and arid land technology and development V.5: pp. 167-190.

Molly, J. P. (1990): Windenergie. (2. Aufl.)

Morcos, M. A., A. F. El-Sahrigi, M. Hanafy and Hassan, S. S. (1994): A mathematical approach to predict the pressure head inside the perforated tubes. Egypt, Misr J. Ag. Eng., 11 (4): 1041-1065.

Mortensen, N .G., L. Landsberg, I. Troen and Petersen, E. L. (1993): Wind Atlas Analysis and Application Program (WAsP). RisØ National Labs., Roskilde, Denmark.

NWSTOC (2002): National Weather Service Telecommunication Operations Center. http://www.wunderground.com/global/EG.html

NREA (2001): New & Renewable Energy Authority Egypt. Implementation of renewable energy technologies–opportunities and barriers. Risϕ National laboratory, Denmark. http://www.uccee.org/RETs/EgyptCountryStudy.pdf.

Omara, A. I. (1997): Implementation and evaluation of gated pipe for furrow irrigation system. M. Sc. Thesis, Fac. of Agric., Alexandria University, Egypt.

Omara, A. I. and Irps, H. (2003): Further development of the mobile wind energy plant MoWEC: Lee-wind wheel for yaw drive. Agritechnica, Hannover 9-16 November 2003. <http://www.fal.de/messe/agritechnica2003/themen/oma03150.pdf> (Poster).

Omara, A. I., H. Sourell, H. Irps und Sommer, C. (2004a): Low-pressure irrigation system powered by wind energy. Journal of Applied Irrigation Science, 39 (1): 83-91.

Omara, A. I., H. Irps, H. Sourell, F. Tack and Sommer, C. (2004c): First experiences with the wind energy plant MoWEC1 and its possible application on the North-west coast of Egypt to irrigate orchards with a low-head bubbler irrigation system. Landbauforschung Völkenrode, 54 (3): 153-162.

Omara, A. I., H. Irps, H. Sourell, F. Tack and Sommer, C. (2004b): Mobile wind energy plant for a low-pressure irrigation system on the Northwest coast of Egypt. Journal of Applied Irrigation Science, 39 (2): 271-281.

Omara A. I. and Irps H. (2004d): Winding the mobile wind energy converter MoWEC by using the lee-wind wheel system. International Mechanical Engineering Conference and Expostion (IMEC2004), Marriott Courtyard Hotel, Kuwait, 5-8 December 2004, (accepted paper, in press.

Patel, M. R. (1999): Wind and solar power systems. CRC Press, pp 35-41.

Peter, F. (1986): Water-pumping device. FAO, pp.17 and 99-100.

Peter, W. (2000): Irrigated agriculture in Egypt-notes of an external observer. Witzenhausen, Germany. http://www.wiz.uni-kassel.de/gear/symp2000/proceed99/irri2.pdf.

Pfeifer, T. (1972): Brockhaus, Physik. Brockhaus Verlag, Leipzig. 895 p.

Pimentel, D., M. Pimentel, and Karpenstein, M. (1999): Energy use in agriculture: An Overview. CIGR - International Commission of Agricultural Engineering. Vol. I, January 1999.

Pimentel, D., X. Huang, A. Cardova, and Pimentel, M. (1998a): Impact of a growing population on natural resources: the challenge for environmental management. Environmental Management in Practice: Analysis, Implementation, and Policy. Brussels, Belgium.

PRB (1996): World population data sheet. Washington, DC: Population Reference Bureau.

Quaschning, V. (1999): Regenerative Energiesysteme. Carl Hanser Verlag München Wien, pp. 2-30.

Ramler, J. R. and Donovan, R. M. (1979): Wind turbines for electric utilities: Development status and economics. NASA Report NASA TM-79170.

Rawlins, S. L. (1977): Uniform irrigation with a low head bubbler system. Agriculture Water Management, 1: 166-178.

Reynolds, C. A. (1993): Design and evaluation of bubbler irrigation system. M. Sc. Thesis, University of Arizona, USA.

Reynolds, C. A., M. Yitayew and Petersen, M. S. (1995a): Low-head bubbler irrigation systems. Part I: Design. Agriculture Water Management 29:1-24.

Reynolds, C. A. and Yitayew, M. (1995b): Low-head bubbler irrigation system. Part II: Air lock problem. Design procedure. Agriculture Water Management 29: 25-35.

Richard, L. H. (1996): Power from the wind, a history of windmill technology. Cambridge University Press, pp. 92-95.

Roger, M. and Ventre, J. (2000): Photovoltaic System Engineering. CRC Press, pp.1-18

Roth, R. L. (1992): Personal communication (Cited from Reynolds, C. A. 1995b).

Schnelle, W. (1999): Mühlenbau: Wasserräder und Windmühlen bewahren und erhalten. Verlag Bauwesen, Berlin, pp. 89-93.

Schofield, R. E. (1963): The lunar society of Birmingham, a social history of provincial science and industry in eighteenth century England. 74 p.

Shell I (1996): The evolution of the world's energy systems. London, Shell International, Ltd.

Smith, R. J. and Watts, P. J. (1986): Analysis and design of gated pipelines. Journal of Agricultural Water Management, Vol. 12: pp. 99- 115.

Sourell, H. (1998): Betriebstechnische Weiterentwicklung für eine umweltschonende, wasser- und energiesparende Beregnung. Landbauforschung Völkenrode H.1/1998: Seite 12-25.

Sourell, H. (1999): Landtechnik: Landwirtschaftliches Lehrbuch. Herg. H. Eichhorn, Planung von Beregnungsanlagen, Seite 209-226.

Spofford, T. (1997): National water and climate center: National Engineering Handbook; Part 652. Irrigation Guide: Chapter 6: Irrigation System Design, Part 2: pp. 59-64.

Springer, G. (1993): Elektrotechnik Energieelektronik Fachbildung. Verlag Europa-Lehrmittel, Seiten 8 und 45.

Suzanne, B. (1975): Windmills. Chariles Scribner's Sons, pp. 38-44.

Thornton, J. R. and Behoteguy, D. (1980): Operation and installation of bubbler system. ASAE, Technical Paper No. 80-2059.

Thomas, M. W., D. V. Chase and Savic, D. A. (2001): Water distribution modelling. Haestad Press Waterbury, CT USA, chapter 2.

Tostmann, H. (2002): Personal communication. Directory of the windmill in the town Peine, Germany.

UNDP/FAO (1970): Pre-Investment Survey of the North Western Coastal Region. Project ESE: SF/UAR 49 Technical Report No. 1. (Cited from Balba, M.A. 1981).

UNEP (2001): United Nation Environmental Program. Implementation of Renewable Energy Technologies-Opportunities and Barriers. Egypt Country study. ISBN: 87-550-3011-4

Wailes, R. (1945-47): Windmill winding gear. T.N.S., Vol. 25: p. 31.

Walski, T. M., T. E. Barnard and Durrans, S. R (2002): Computer applications in hydraulic engineering. Haestad Press, chapter 1.

Walski, T. M., D. V. Chase and Savic, D. A. (2003): Advanced water distribution modelling and managment. Haestad Press Waterbury, CT USA, chapter 2.

WEC/FAO (1999): The challenge of rural energy poverty in the developing countries. World Energy Council/Food and Agriculture Organization of the United Nations.

WHO (1996): Micronutrient malnutrition - half of the world's population affected. World Health Organization, 13 November 1996. No 78, pp. 1-4.

WMO (1981): Meteorological aspects of the utilization of wind as an energy source; Techn. Note No.175, WMO-No.575, Geneva, Switzerland.

Wu, I. P. and Fangmeier, D. D. (1974): Hydraulic design of twin chamber irrigation laterals. Technical Bulletin No. 216. The Agricultural Experiment Station. University of Arizona, USA.

Wu, I. P. and Gitlin, H. M. (1983): Drip irrigation application efficiency and schedules. Transactions of the ASAE, 28 (1): 92-99.

Yehia, A. (2003): Decentralisation and participatory irrigation management in Egypt. Water Demand Management Forum, Cairo, February 2003.

Yitayew M., C. A. Reynolds and Sheta, A. E. (1995): Bubbler irrigation system design and management. American Society of Agricultural Engineers, pp. 402-413.

Youngquist, W. (1997): The Inevitable Control of Earth Resources over Nations and Individuals. Portland, OR: National Book Company.

# APPENDICES / *ANHANG*

## Appendix A A-3



## Appendix B A-7

## Appendix C A-13

# Appendix A

Table A-1: Mean daily wind speed and duration in Alexandria on the N.W. coast of Egypt, with the wind speed ranging between 3.5 and 20 m/s; data from the years 1984 to 2002..

*Mittlere tägliche Windgeschwindigkeit und Dauer in Alexandria an der N.W. Küste von Ägypten im Windgeschwindigkeitsbereich von 3,5 bis 20 m/s; Daten der Jahre 1984 bis 2002.*

| Day | January | | February | | March | | April | | May | | June | |
|---|---|---|---|---|---|---|---|---|---|---|---|---|
| | $v_1$ [m/s] | MD [h/day] | $v_1$ [m/s] | MD [h/day] | $v_1$ [m/s] | MD [h/day] | $v_1$ [m/s] | MD [h/day] | $v_1$ [m/s] | MD [h/day] | $v_1$ [m/s ] | MD [h/day] |
| 1 | 4.76 | 7 | 5.05 | 11 | 5.21 | 16 | 5.77 | 20 | 4.75 | 13 | 6.46 | 16 |
| 2 | 8.08 | 14 | 6.00 | 15 | 4.89 | 12 | 7.04 | 19 | 6.13 | 22 | 5.45 | 22 |
| 3 | 7.08 | 18 | 5.23 | 24 | 5.07 | 13 | 6.10 | 21 | 5.30 | 20 | 4.87 | 13 |
| 4 | 6.63 | 9 | 4.67 | 14 | 4.73 | 15 | 6.82 | 8 | 4.44 | 8 | 5.02 | 12 |
| 5 | 7.68 | 16 | 5.37 | 16 | 4.72 | 18 | 6.47 | 10 | 4.52 | 9 | 5.54 | 13 |
| 6 | 7.34 | 20 | 4.73 | 16 | 5.11 | 16 | 7.32 | 17 | 5.08 | 15 | 5.30 | 10 |
| 7 | 7.97 | 16 | 6.26 | 11 | 4.15 | 17 | 4.82 | 24 | 4.58 | 11 | 6.06 | 19 |
| 8 | 6.46 | 24 | 4.50 | 4 | 3.74 | 4 | 5.15 | 23 | 5.31 | 20 | 4.98 | 21 |
| 9 | 8.47 | 21 | 4.63 | 7 | 4.21 | 6 | 4.79 | 16 | 4.82 | 11 | 4.42 | 12 |
| 10 | 8.50 | 24 | 4.52 | 9 | 4.68 | 12 | 4.59 | 13 | 6.62 | 23 | 6.11 | 8 |
| 11 | 5.70 | 17 | 8.23 | 20 | 6.36 | 11 | 4.63 | 8 | 5.17 | 21 | 6.56 | 21 |
| 12 | 4.11 | 1 | 8.60 | 21 | 5.43 | 11 | 4.29 | 3 | 5.66 | 9 | 5.77 | 22 |
| 13 | 3.61 | 2 | 6.40 | 21 | 6.27 | 16 | 4.70 | 8 | 7.52 | 13 | 6.40 | 24 |
| 14 | 4.30 | 3 | 3.86 | 2 | 4.72 | 13 | 4.26 | 11 | 7.54 | 23 | 5.68 | 24 |
| 15 | 4.12 | 6 | 3.61 | 3 | 4.24 | 9 | 5.57 | 17 | 7.01 | 24 | 4.93 | 22 |
| 16 | 3.86 | 2 | 4.97 | 12 | 5.61 | 18 | 6.78 | 16 | 4.87 | 22 | 5.18 | 14 |
| 17 | 3.82 | 2 | 5.60 | 17 | 5.40 | 14 | 5.81 | 23 | 5.47 | 16 | 6.17 | 12 |
| 18 | 4.88 | 4 | 5.99 | 20 | 7.37 | 9 | 6.13 | 23 | 5.71 | 19 | 6.96 | 17 |
| 19 | 4.89 | 12 | 4.23 | 9 | 7.33 | 24 | 6.27 | 24 | 5.54 | 16 | 8.21 | 23 |
| 20 | 6.78 | 16 | 4.85 | 7 | 6.57 | 24 | 6.66 | 24 | 4.70 | 18 | 6.01 | 24 |
| 21 | 5.19 | 23 | 4.26 | 11 | 6.49 | 24 | 5.61 | 20 | 5.51 | 10 | 4.86 | 20 |
| 22 | 6.66 | 23 | 5.52 | 18 | 4.60 | 19 | 4.72 | 12 | 5.95 | 24 | 4.66 | 17 |
| 23 | 3.78 | 6 | 7.27 | 15 | 7.83 | 13 | 6.30 | 20 | 6.13 | 12 | 5.14 | 10 |
| 24 | 3.50 | 0 | 8.61 | 20 | 6.49 | 16 | 6.43 | 18 | 5.82 | 22 | 5.14 | 15 |
| 25 | 3.61 | 1 | 7.47 | 17 | 6.17 | 20 | 4.99 | 16 | 4.46 | 15 | 5.39 | 15 |
| 26 | 4.32 | 5 | 5.20 | 20 | 8.16 | 19 | 4.93 | 12 | 6.01 | 13 | 5.88 | 24 |
| 27 | 3.86 | 2 | 4.67 | 14 | 7.09 | 18 | 4.67 | 11 | 5.24 | 16 | 7.29 | 24 |
| 28 | 4.43 | 5 | 5.47 | 14 | 6.52 | 21 | 5.78 | 12 | 4.89 | 16 | 7.27 | 24 |
| 29 | 5.67 | 2 | - | - | 5.75 | 23 | 5.98 | 16 | 5.15 | 9 | 5.95 | 24 |
| 30 | 5.50 | 5 | - | - | 5.39 | 15 | 5.43 | 18 | 5.79 | 12 | 5.33 | 20 |
| 31 | 5.15 | 8 | - | - | 7.54 | 24 | - | - | 5.31 | 24 | - | - |
| **MWD** | **-** | **314** | **-** | **388** | **-** | **490** | - | **483** | - | **506** | - | **542** |
| **MWS** | **5.50** | - | **5.56** | - | **5.73** | - | **5.63** | - | **5.52** | - | **5.77** | - |

Table A-1 : ***(Continued)***

| Day | July | | August | | September | | October | | November | | December | |
|---|---|---|---|---|---|---|---|---|---|---|---|---|
| | $v_1$ [m/s] | MD [h/day] | $v_1$ [m/s] | MD [h/day] | $v_1$ [m/s] | MD [h/day] | $v_1$ [m/s] | MD [h/day] | $v_1$ [m/s] | MD [h/day] | $v_1$ [m/s ] | MD [h/day] |
| 1 | 4.97 | 18 | 5.68 | 22 | 4.60 | 15 | 6.64 | 20 | 4.55 | 12 | 7.41 | 22 |
| 2 | 5.15 | 22 | 5.19 | 22 | 5.01 | 16 | 5.75 | 23 | 5.02 | 8 | 8.65 | 19 |
| 3 | 5.99 | 24 | 5.63 | 20 | 5.50 | 19 | 5.92 | 20 | 5.60 | 9 | 8.76 | 20 |
| 4 | 5.81 | 23 | 5.50 | 23 | 6.00 | 19 | 5.72 | 24 | 6.31 | 7 | 7.97 | 23 |
| 5 | 4.99 | 17 | 5.14 | 19 | 5.36 | 18 | 5.50 | 19 | 5.66 | 8 | 6.69 | 10 |
| 6 | 4.66 | 21 | 5.89 | 20 | 6.48 | 24 | 5.09 | 9 | 5.97 | 22 | 8.05 | 17 |
| 7 | 5.15 | 21 | 4.91 | 22 | 5.59 | 18 | 4.46 | 9 | 3.92 | 5 | 6.13 | 11 |
| 8 | 5.63 | 21 | 5.60 | 18 | 4.36 | 15 | 5.72 | 9 | 5.91 | 10 | 8.17 | 20 |
| 9 | 5.10 | 12 | 5.24 | 20 | 4.86 | 16 | 6.15 | 18 | 4.64 | 6 | 3.10 | 3 |
| 10 | 5.48 | 20 | 5.21 | 23 | 5.50 | 17 | 5.48 | 11 | 6.29 | 18 | 4.00 | 1 |
| 11 | 5.64 | 23 | 5.24 | 21 | 5.80 | 10 | 5.02 | 12 | 7.05 | 14 | 4.37 | 4 |
| 12 | 4.66 | 15 | 4.97 | 12 | 4.01 | 3 | 4.97 | 12 | 6.29 | 23 | 6.24 | 16 |
| 13 | 5.10 | 13 | 5.96 | 16 | 4.63 | 4 | 5.51 | 10 | 4.89 | 24 | 5.75 | 12 |
| 14 | 5.82 | 16 | 6.32 | 24 | 4.16 | 12 | 5.04 | 14 | 4.80 | 16 | 5.22 | 7 |
| 15 | 5.94 | 24 | 6.18 | 24 | 4.40 | 9 | 5.47 | 14 | 4.96 | 11 | 4.12 | 8 |
| 16 | 5.08 | 18 | 5.56 | 22 | 4.56 | 7 | 5.21 | 16 | 5.79 | 16 | 4.00 | 2 |
| 17 | 4.67 | 15 | 5.72 | 23 | 6.36 | 15 | 5.42 | 21 | 6.03 | 22 | 4.00 | 1 |
| 18 | 6.20 | 15 | 5.63 | 20 | 5.59 | 21 | 4.96 | 19 | 5.19 | 12 | 6.37 | 13 |
| 19 | 4.93 | 19 | 5.00 | 14 | 6.67 | 24 | 5.27 | 17 | 4.53 | 10 | 6.36 | 22 |
| 20 | 4.57 | 15 | 4.73 | 11 | 5.38 | 24 | 5.15 | 15 | 4.31 | 11 | 5.43 | 11 |
| 21 | 4.80 | 18 | 5.01 | 12 | 4.76 | 12 | 6.08 | 16 | 4.71 | 7 | 4.02 | 1 |
| 22 | 5.98 | 24 | 5.02 | 24 | 4.59 | 13 | 4.64 | 10 | 4.63 | 9 | 4.10 | 3 |
| 23 | 7.78 | 24 | 5.62 | 24 | 5.25 | 6 | 5.47 | 8 | 5.69 | 14 | 4.00 | 5 |
| 24 | 6.93 | 24 | 5.45 | 24 | 5.56 | 6 | 4.94 | 15 | 6.28 | 24 | 4.00 | 1 |
| 25 | 5.68 | 21 | 5.54 | 24 | 4.92 | 7 | 5.57 | 12 | 5.39 | 19 | 4.63 | 5 |
| 26 | 4.32 | 5 | 4.68 | 23 | 5.15 | 2 | 4.81 | 12 | 4.12 | 4 | 4.11 | 1 |
| 27 | 4.27 | 10 | 4.87 | 20 | 4.94 | 10 | 4.33 | 10 | 4.11 | 1 | 5.08 | 8 |
| 28 | 4.59 | 12 | 5.46 | 23 | 5.22 | 15 | 3.86 | 6 | 4.49 | 11 | 5.30 | 13 |
| 29 | 3.81 | 5 | 5.42 | 22 | 6.12 | 24 | 5.62 | 14 | 4.82 | 11 | 5.50 | 19 |
| 30 | 5.14 | 7 | 4.78 | 14 | 4.75 | 17 | 5.73 | 16 | 6.10 | 18 | 4.00 | 3 |
| 31 | 5.19 | 12 | 4.31 | 8 | - | - | 5.15 | 10 | - | - | 4.06 | 7 |
| **MWD** | **-** | **534** | **-** | **614** | **-** | **418** | **-** | **441** | **-** | **382** | | **308** |
| **MWS** | **5.29** | **-** | **5.34** | **-** | **5.21** | **-** | **5.31** | **-** | **5.27** | **-** | **5.47** | **-** |

where:

**$v_1$** = Mean daily wind speed [m/s]

**MD** = Mean daily wind speed duration [h/day]

**MWD** = Mean monthly wind speed duration [h/month]

**MWS** = Mean monthly wind speed [m/s]

Table A-2: Mean daily wind speed and duration in Mersa Matruh on the N.W. coast of Egypt, with the wind speed ranging between 3.5 and 20 m/s; data from the years 1984 to 2002.

*Mittlere tägliche Windgeschwindigkeit und Dauer in Mersa Matruh an der N.W. Küste von Ägypten im Windgeschwindigkeitsbereich von 3,5 bis 20 m/s; Daten der Jahre 1984 bis 2002.*

| Day | January | | February | | March | | April | | May | | June | |
|---|---|---|---|---|---|---|---|---|---|---|---|---|
| | $v_1$ [m/s] | MD [h/day] | $v_1$ [m/s] | MD [h/day] | $v_1$ [m/s] | MD [h/day] | $v_1$ [m/s] | MD [h/day] | $v_1$ [m/s] | MD [h/day] | $v_1$ [m/s ] | MD [h/day] |
| 1 | 5.87 | 20 | 4.17 | 9 | 3.90 | 7 | 7.02 | 20 | 5.72 | 16 | 5.31 | 15 |
| 2 | 7.98 | 19 | 4.72 | 17 | 4.11 | 4 | 8.22 | 20 | 4.91 | 11 | 5.09 | 11 |
| 3 | 6.77 | 24 | 4.91 | 18 | 3.81 | 5 | 4.89 | 18 | 4.38 | 6 | 4.50 | 8 |
| 4 | 5.93 | 17 | 4.11 | 2 | 3.92 | 8 | 7.74 | 18 | 4.43 | 10 | 4.59 | 13 |
| 5 | 8.38 | 16 | 4.68 | 10 | 3.87 | 6 | 5.30 | 17 | 5.11 | 14 | 4.68 | 9 |
| 6 | 8.48 | 23 | 4.87 | 17 | 4.18 | 8 | 6.80 | 17 | 4.49 | 11 | 4.78 | 7 |
| 7 | 8.23 | 24 | 4.79 | 12 | 4.54 | 11 | 4.57 | 17 | 4.19 | 7 | 5.48 | 12 |
| 8 | 6.13 | 23 | 4.51 | 10 | 4.63 | 7 | 3.91 | 5 | 5.99 | 14 | 4.92 | 7 |
| 9 | 7.88 | 17 | 4.72 | 6 | 5.41 | 14 | 4.70 | 9 | 6.14 | 17 | 4.32 | 5 |
| 10 | 7.11 | 19 | 7.51 | 11 | 6.03 | 21 | 4.77 | 10 | 6.58 | 24 | 4.55 | 6 |
| 11 | 6.07 | 20 | 9.24 | 24 | 8.98 | 17 | 4.76 | 15 | 4.27 | 7 | 7.69 | 24 |
| 12 | 5.20 | 17 | 9.12 | 24 | 5.56 | 15 | 4.93 | 15 | 5.70 | 13 | 6.32 | 24 |
| 13 | 4.81 | 11 | 5.43 | 22 | 6.34 | 15 | 5.96 | 20 | 5.63 | 19 | 4.72 | 17 |
| 14 | 4.12 | 3 | 4.22 | 10 | 4.78 | 14 | 5.41 | 14 | 8.30 | 19 | 5.49 | 12 |
| 15 | 4.40 | 13 | 4.11 | 1 | 4.19 | 7 | 8.27 | 12 | 7.67 | 22 | 4.74 | 10 |
| 16 | 5.24 | 16 | 4.29 | 3 | 4.36 | 15 | 5.95 | 12 | 5.02 | 13 | 5.28 | 11 |
| 17 | 3.94 | 3 | 5.96 | 17 | 4.68 | 10 | 6.08 | 16 | 4.33 | 17 | 5.40 | 8 |
| 18 | 4.48 | 10 | 4.44 | 16 | 7.76 | 12 | 6.05 | 17 | 4.63 | 8 | 5.22 | 20 |
| 19 | 4.96 | 11 | 3.72 | 9 | 7.84 | 24 | 6.62 | 22 | 4.92 | 14 | 6.21 | 24 |
| 20 | 6.61 | 22 | 4.19 | 14 | 6.96 | 19 | 7.01 | 16 | 3.97 | 7 | 5.86 | 20 |
| 21 | 6.01 | 22 | 5.98 | 13 | 6.52 | 21 | 5.52 | 11 | 7.65 | 22 | 5.61 | 24 |
| 22 | 7.62 | 21 | 5.69 | 15 | 4.45 | 17 | 4.76 | 12 | 4.61 | 23 | 4.99 | 16 |
| 23 | 5.26 | 17 | 5.86 | 13 | 8.09 | 18 | 6.01 | 16 | 4.63 | 10 | 3.61 | 4 |
| 24 | 5.51 | 7 | 7.95 | 20 | 8.53 | 20 | 5.97 | 15 | 3.67 | 8 | 5.33 | 11 |
| 25 | 4.70 | 15 | 8.20 | 19 | 8.74 | 21 | 4.08 | 12 | 4.99 | 13 | 5.79 | 16 |
| 26 | 4.65 | 15 | 4.89 | 14 | 7.38 | 23 | 3.97 | 10 | 5.75 | 17 | 6.06 | 18 |
| 27 | 3.61 | 4 | 3.94 | 3 | 7.41 | 20 | 4.40 | 9 | 5.66 | 9 | 5.49 | 18 |
| 28 | 4.69 | 9 | 4.11 | 3 | 6.96 | 22 | 5.24 | 10 | 4.19 | 7 | 6.00 | 18 |
| 29 | 4.31 | 7 | - | - | 4.83 | 13 | 5.09 | 9 | 4.93 | 14 | 4.72 | 12 |
| 30 | 4.41 | 8 | - | - | 6.97 | 16 | 3.74 | 4 | 6.31 | 15 | 4.37 | 8 |
| 31 | 4.11 | 1 | - | - | 7.36 | 20 | - | - | 5.59 | 24 | - | - |
| **MWD** | **-** | **454** | **-** | **388** | **-** | **450** | **-** | **418** | **-** | **431** | **-** | **408** |
| **MWS** | **5.73** | - | **5.56** | - | **5.91** | - | **5.59** | - | **5.30** | - | **5.24** | - |

Table A-2 : ***(Continued)***

| Day | July | | August | | September | | October | | November | | December | |
|---|---|---|---|---|---|---|---|---|---|---|---|---|
| | $v_1$ [m/s] | MD [h/day] | $v_1$ [m/s] | MD [h/day] | $v_1$ [m/s] | MD [h/day] | $v_1$ [m/s] | MD [h/day] | $v_1$ [m/s] | MD [h/day] | $v_1$ [m/s ] | MD [h/day] |
| 1 | 4.79 | 16 | 4.54 | 23 | 4.66 | 14 | 5.94 | 20 | 3.99 | 4 | 8.90 | 24 |
| 2 | 4.63 | 14 | 5.09 | 19 | 5.05 | 15 | 4.82 | 21 | 4.12 | 5 | 11.00 | 24 |
| 3 | 5.99 | 20 | 4.63 | 22 | 5.51 | 17 | 5.01 | 12 | 4.11 | 2 | 7.66 | 18 |
| 4 | 5.63 | 15 | 5.51 | 17 | 6.05 | 19 | 4.90 | 13 | 3.86 | 2 | 4.44 | 14 |
| 5 | 5.90 | 13 | 4.96 | 11 | 5.36 | 18 | 4.46 | 6 | 6.46 | 9 | 6.55 | 19 |
| 6 | 4.91 | 20 | 5.24 | 10 | 5.59 | 18 | 4.40 | 11 | 5.84 | 17 | 4.40 | 13 |
| 7 | 5.45 | 15 | 4.91 | 9 | 6.48 | 24 | 7.87 | 13 | 5.58 | 19 | 5.24 | 21 |
| 8 | 5.49 | 15 | 5.93 | 22 | 4.77 | 18 | 4.75 | 8 | 5.43 | 18 | 6.58 | 20 |
| 9 | 5.24 | 10 | 5.28 | 19 | 4.24 | 15 | 4.98 | 20 | 7.00 | 21 | 8.42 | 24 |
| 10 | 4.95 | 16 | 4.82 | 15 | 5.63 | 16 | 6.00 | 12 | 7.56 | 17 | 4.50 | 4 |
| 11 | 5.50 | 16 | 4.56 | 7 | 5.66 | 7 | 4.51 | 4 | 7.46 | 23 | 4.12 | 3 |
| 12 | 4.12 | 7 | 3.99 | 4 | 3.54 | 2 | 5.24 | 20 | 4.69 | 9 | 5.74 | 19 |
| 13 | 4.17 | 10 | 4.72 | 19 | 3.86 | 4 | 3.80 | 8 | 4.33 | 17 | 3.50 | 1 |
| 14 | 4.50 | 8 | 4.70 | 15 | 4.63 | 12 | 3.83 | 8 | 4.29 | 9 | 5.49 | 18 |
| 15 | 5.73 | 15 | 4.77 | 14 | 5.75 | 22 | 4.94 | 17 | 4.42 | 10 | 4.63 | 12 |
| 16 | 5.66 | 12 | 5.55 | 14 | 7.22 | 20 | 4.93 | 19 | 5.48 | 17 | 4.13 | 4 |
| 17 | 4.80 | 18 | 5.33 | 11 | 4.55 | 13 | 4.93 | 19 | 5.47 | 20 | 6.97 | 22 |
| 18 | 5.59 | 23 | 7.49 | 20 | 5.10 | 13 | 5.27 | 12 | 4.80 | 18 | 7.29 | 22 |
| 19 | 4.63 | 9 | 4.29 | 9 | 4.55 | 7 | 4.45 | 3 | 3.80 | 8 | 8.28 | 21 |
| 20 | 5.60 | 10 | 4.43 | 5 | 4.82 | 11 | 4.23 | 5 | 3.86 | 6 | 8.45 | 21 |
| 21 | 5.17 | 20 | 4.95 | 8 | 4.02 | 17 | 3.81 | 5 | 3.99 | 4 | 7.97 | 22 |
| 22 | 6.30 | 17 | 4.92 | 9 | 4.22 | 10 | 5.58 | 20 | 4.44 | 8 | 4.48 | 14 |
| 23 | 6.84 | 24 | 5.58 | 13 | 4.05 | 8 | 4.12 | 7 | 5.60 | 18 | 5.63 | 19 |
| 24 | 6.47 | 21 | 5.76 | 11 | 4.21 | 17 | 3.99 | 4 | 5.07 | 21 | 6.85 | 21 |
| 25 | 6.47 | 21 | 4.95 | 17 | 4.63 | 9 | 4.17 | 19 | 4.04 | 7 | 5.63 | 17 |
| 26 | 4.95 | 8 | 5.13 | 23 | 5.97 | 15 | 4.86 | 20 | 4.38 | 4 | 5.39 | 19 |
| 27 | 4.23 | 9 | 6.39 | 23 | 5.12 | 20 | 3.69 | 6 | 4.46 | 9 | 5.25 | 19 |
| 28 | 7.04 | 21 | 5.15 | 20 | 7.03 | 18 | 4.94 | 15 | 7.00 | 21 | 5.15 | 14 |
| 29 | 6.47 | 22 | 5.10 | 23 | 7.56 | 24 | 5.82 | 24 | 6.94 | 22 | 5.11 | 11 |
| 30 | 4.12 | 14 | 7.10 | 24 | 5.15 | 16 | 5.56 | 24 | 9.00 | 19 | 4.92 | 16 |
| 31 | 4.38 | 14 | 8.60 | 19 | - | - | 5.44 | 22 | - | - | 4.48 | 17 |
| **MWD** | **-** | **473** | **-** | **475** | **-** | **439** | **-** | **417** | **-** | **384** | **-** | **513** |
| **MWS** | **5.35** | - | **5.30** | - | **5.17** | - | **4.88** | - | **5.25** | - | **6.03** | - |

where:

**$v_1$** = Mean daily wind speed [m/s]

**MD** = Mean daily wind speed duration [h/day]

**MWD** = Mean monthly wind speed duration [h/month]

**MWS** = Mean monthly wind speed [m/s]

# Appendix B

Table B-1: Measured distributor hose outflow at different distributor hose elevation along one lateral. **[S = 2, SS = 2 and $q_{oh}$ = 40 l/h]**
*Gemessener Verteilerschlauchdurchfluss entlang eines Verteilerrohres mit unterschiedlich hohen Auslässen am Verteilerschlauch.*

| Nr. of DH | MDHO [l/h] at DHE | | | MDHO [l/h] at DHEZ | | |
|---|---|---|---|---|---|---|
| | $So_L$ = + 0.5% | $So_L$ = - 0.5% | $So_L$ = 0.0% | $So_L$ = + 0.5% | $So_L$ = - 0.5% | $So_L$ = 0.0% |
| 1 | 39.95 | 39.50 | 41.22 | 60.72 | 60.90 | 61.47 |
| 2 | 41.30 | 40.55 | 41.10 | 60.54 | 61.68 | 60.87 |
| 3 | 40.95 | 41.20 | 41.54 | 59.34 | 61.08 | 58.91 |
| 4 | 40.60 | 41.40 | 42.00 | 56.64 | 60.78 | 58.58 |
| 5 | 40.40 | 41.85 | 40,94 | 55.62 | 60.42 | 58.31 |
| 6 | 41.15 | 39.95 | 41.26 | 55.80 | 61.56 | 58.26 |
| 7 | 40.90 | 39.63 | 41.49 | 54.30 | 61.50 | 56.56 |
| 8 | 40.65 | 39.85 | 41.26 | 51.60 | 61.98 | 55.80 |
| 9 | 39.85 | 40.45 | 40.32 | 48.24 | 62.22 | 53.62 |
| 10 | 40.80 | 41.05 | 40.15 | 45.00 | 63.72 | 52.53 |
| 11 | 40.40 | 40.10 | 40.15 | 43.80 | 64.20 | 53.56 |
| 12 | 40.45 | 39.85 | 39.65 | 41.70 | 64.80 | 54.22 |
| 13 | 40.35 | 40.45 | 40.39 | 39.84 | 66.84 | 54.60 |
| **EU %** | **98.65** | **98.05** | **97.79** | **80.69** | **97.22** | **93.87** |
| **$q_{oh\ var}$ %** | **3.51** | **5.62** | **4.43** | **34.39** | **9.61** | **14.54** |

where **DH** is the distributor hose, **$So_L$** is the lateral slope, **MDHO** is the measured distributor hoses outflow, **DDHE** is different distributor hose outlet elevation (calculated by computer program), **DHEZ** is the outlet elevation of the distributor hoses are zero from lateral level, **S = 2** is the hose position on two lateral sides, **SS = 2** is the laterals on two manifold sides, **$q_{oh}$** is the theoretical discharge of the distributor hose, **EU** is the emission uniformity of distributor hoses and **$q_{oh\ var}$** is distributor hoses flow variation, in %.

Table B-2: Measured and calculated pressure head just before each distributor hose inlet and calculated hose outlet elevation along one lateral. **[S = 2, SS = 2 and $q_{oh}$ = 40 l/h]**
*Gemessene und berechnete Druckhöhen am Übergang vom Verteilerrohr zum Verteilerschlauch und berechnete Auslasshöhen der Verteilerschläuche.*

| Nr. of DH | $So_L$ = +0.5%, Hf = 59.9 cm | | | $So_L$ = - 0.5%, Hf = 59.9 cm | | | $So_L$ = 0.0%, Hf = 59.9 cm | | |
|---|---|---|---|---|---|---|---|---|---|
| | MPH [cm] | TPH [cm] | DHE [cm] | MPH [cm] | TPH [cm] | DHE [cm] | MPH [cm] | TPH [cm] | DHE [cm] |
| 1 | 58.60 | 57.66 | 33.64 | 59.60 | 59.66 | 35.64 | 58.90 | 58.66 | 34.64 |
| 2 | 53.40 | 53.60 | 29.57 | 59.50 | 59.60 | 35.57 | 56.20 | 56.60 | 32.57 |
| 3 | 49.50 | 49.84 | 25.82 | 59.70 | 59.84 | 35.82 | 54.20 | 54.84 | 30.82 |
| 4 | 45.80 | 46.38 | 22.35 | 60.00 | 60.37 | 36.35 | 52.70 | 53.37 | 29.35 |
| 5 | 42.40 | 43.17 | 19.15 | 60.60 | 61.17 | 37.15 | 51.40 | 52.17 | 28.15 |
| 6 | 38.90 | 40.20 | 16.18 | 61.50 | 62.21 | 38.18 | 49.70 | 51.21 | 27.18 |
| 7 | 36.20 | 37.46 | 13.44 | 62.40 | 63.46 | 39.44 | 49.00 | 50.46 | 26.44 |
| 8 | 33.30 | 34.90 | 10.88 | 63.70 | 46.90 | 40.88 | 48.10 | 49.90 | 25.88 |
| 9 | 31.10 | 32.51 | 8.48 | 65.30 | 66.50 | 42.48 | 47.90 | 49.51 | 25.48 |
| 10 | 28.90 | 30.25 | 6.23 | 67.10 | 68.25 | 44.23 | 47.50 | 49.25 | 25.23 |
| 11 | 26.90 | 28.10 | 4.08 | 68.90 | 70.10 | 46.08 | 46.70 | 49.10 | 25.08 |
| 12 | 24.80 | 26.04 | 2.01 | 70.70 | 72.04 | 48.01 | 46.70 | 49.04 | 25.01 |
| 13 | 23.40 | 24.03 | 0.00 | 73.30 | 74.03 | 50.00 | 46.90 | 49.03 | 25.00 |

where **Hf** is the pressure head at lateral inlet, **MPH** is the measure pressure head just before each distributor hose inlet, **TPH** is the theoretical pressure head calculated by the computer program and **DHE** is the distributor hose outlet elevation.

Table B-3: Measured distributor hose outflow at different distributor hose elevation along one lateral. **[S = 2, SS = 2 and $q_{oh}$ = 20 l/h]**
*Gemessener Verteilerschlauchdurchfluss entlang eines Verteilerrohres mit unterschiedlich hohen Auslässen am Verteilerschlauch.*

| Nr. of DH | MDHO [l/h] at DDHE | | | MDHO [l/h] at DHEZ | | |
|---|---|---|---|---|---|---|
| | $So_L$ = + 0.5% | $So_L$ = - 0.5% | $So_L$ = 0.0% | $So_L$ = + 0.5% | $So_L$ = - 0.5% | $So_L$ = 0.0% |
| 1 | 18.03 | 18.06 | 18.09 | 54.30 | 49.50 | 49.05 |
| 2 | 17.97 | 18.24 | 17.94 | 54.05 | 49.80 | 47.15 |
| 3 | 17.79 | 18.06 | 17.85 | 50.80 | 49.32 | 45.50 |
| 4 | 18.27 | 18.12 | 18.15 | 47.85 | 49.56 | 44.30 |
| 5 | 18.18 | 17.91 | 18.09 | 44.30 | 49.86 | 42.05 |
| 6 | 18.24 | 18.27 | 18.15 | 40.95 | 50.34 | 40.65 |
| 7 | 17.94 | 18.30 | 18.12 | 37.37 | 51.06 | 39.85 |
| 8 | 18.24 | 18.23 | 18.15 | 33.30 | 52.08 | 40.02 |
| 9 | 18.39 | 18.09 | 18.12 | 31.30 | 52.56 | 39.95 |
| 10 | 18.18 | 18.21 | 17.85 | 28.75 | 53.46 | 39.30 |
| 11 | 18.33 | 17.85 | 17.91 | 27.80 | 55.08 | 39.45 |
| 12 | 18.57 | 18.27 | 18.00 | 23.15 | 56.58 | 38.05 |
| 13 | 18.81 | 18.48 | 18.03 | 19.85 | 57.06 | 39.15 |
| **EU %** | **98.07** | **97.57** | **99.19** | **62.13** | **95.08** | **92.17** |
| **$q_{oh\ var}$ %** | **5.15** | **7.14** | **5.22** | **63.44** | **13.56** | **22.43** |

where **DH** is the distributor hose, **$So_L$** is the lateral slope, **MDHO** is the measured distributor hoses outflow, **DDHE** is different distributor hose outlet elevation (calculated by computer program), **DHEZ** is the outlet elevation of the distributor hoses (zero from lateral level), **S = 2** is the hose position on two lateral sides, **SS = 2** is the laterals on two manifold sides, **$q_{oh}$** is the theoretical discharge of the distributor hose, **EU** is the emission uniformity of distributor hoses and **$q_{oh\ var}$** is distributor hoses flow variation, in %.

Table B-4: Measured and calculated pressure head just before each distributor hose inlet and calculated hose outlet elevation along one lateral. **[S = 2, SS = 2 and $q_{oh}$ = 20 l/h]**
*Gemessene und berechnete Druckhöhen am Übergang vom Verteilerrohr zum Verteilerschlauch und berechnete Auslasshöhen der Verteilerschläuche.*

| Nr. of DH | $So_L$ = + 0.5% , Hf = 34.5 cm | | | $So_L$ = - 0.5% , Hf = 34.5 cm | | | $So_L$ = 0.0% , Hf = 34.5 cm | | |
|---|---|---|---|---|---|---|---|---|---|
| | MPH [cm] | TPH [cm] | DHE [cm] | MPH [cm] | TPH [cm] | DHE [cm] | MPH [cm] | TPH [cm] | DHE [cm] |
| 1 | 33.4 | 33.18 | 26.68 | 35.7 | 35.18 | 28.68 | 34.1 | 34.17 | 27.68 |
| 2 | 30.2 | 30.60 | 24.11 | 37.4 | 36.60 | 30.11 | 33.6 | 33.60 | 27.11 |
| 3 | 27.6 | 28.11 | 21.62 | 39.0 | 38.11 | 31.62 | 33.2 | 33.11 | 26.62 |
| 4 | 25.3 | 25.71 | 19.21 | 40.4 | 39.71 | 33.21 | 32.9 | 32.71 | 26.21 |
| 5 | 22.9 | 23.37 | 16.88 | 42.2 | 41.37 | 34.88 | 32.6 | 32.37 | 25.88 |
| 6 | 20.7 | 21.10 | 14.61 | 44.0 | 43.10 | 36.61 | 32.4 | 32.10 | 25.61 |
| 7 | 18.9 | 18.89 | 12.40 | 45.8 | 44.89 | 38.40 | 32.3 | 31.89 | 25.40 |
| 8 | 15.8 | 16.74 | 10.25 | 47.2 | 46.74 | 40.25 | 32.2 | 31.74 | 25.25 |
| 9 | 13.7 | 14.63 | 8.14 | 49.2 | 48.63 | 42.14 | 32.1 | 31.63 | 25.14 |
| 10 | 11.6 | 12.56 | 6.06 | 51.1 | 50.56 | 44.06 | 32.0 | 31.56 | 25.06 |
| 11 | 10.1 | 10.52 | 4.02 | 52.8 | 52.52 | 46.02 | 31.8 | 31.52 | 25.02 |
| 12 | 8.0 | 8.50 | 2.00 | 55.0 | 54.50 | 48.00 | 31.8 | 31.50 | 25.00 |
| 13 | 6.0 | 6.49 | 0.0 | 57.6 | 56.50 | 50.00 | 32.0 | 31.50 | 25.00 |

where **Hf** is the pressure head at lateral inlet, **MPH** is the measure pressure head just before each distributor hose inlet, **TPH** is the theoretical pressure head calculated by the computer program and **DHE** is the distributor hose outlet elevation.

Table B-5: Measured distributor hose outflow at different distributor hose elevation along one lateral. **[S = 2, SS = 1 and $q_{oh}$ = 40 l/h]**
*Gemessener Verteilerschlauchdurchfluss entlang eines Verteilerrohres mit unterschiedlich hohen Auslässen am Verteilerschlauch.*

| Nr. of DH | MDHO [l/h] at DDHE | | | MDHO [l/h] at DHEZ | | |
|---|---|---|---|---|---|---|
| | $So_L$ = + 0.5% | $So_L$ = - 0.5% | $So_L$ = 0.0% | $So_L$ = + 0.5% | $So_L$ = - 0.5% | $So_L$ = 0.0% |
| 1 | 40.75 | 39.95 | 40.16 | 50.05 | 60.72 | 55.50 |
| 2 | 40.01 | 41.30 | 41.20 | 48.76 | 60.54 | 55.60 |
| 3 | 40.89 | 40.95 | 40.92 | 47.10 | 59.34 | 54.88 |
| 4 | 41.95 | 40.60 | 40.20 | 45.45 | 56.64 | 55.45 |
| 5 | 40.47 | 40.40 | 40.92 | 45.10 | 55.62 | 55.78 |
| 6 | 41.26 | 41.15 | 40.96 | 43.65 | 55.80 | 56.65 |
| 7 | 41.49 | 40.90 | 40.32 | 42.50 | 54.30 | 57.18 |
| 8 | 41.26 | 40.65 | 40.92 | 41.85 | 51.60 | 58.60 |
| 9 | 40.32 | 39.85 | 39.88 | 41.45 | 48.24 | 58.28 |
| 10 | 40.15 | 40.80 | 40.76 | 40.68 | 45.00 | 58.95 |
| 11 | 40.94 | 40.40 | 40.96 | 40.55 | 43.80 | 60.83 |
| 12 | 41.45 | 40.45 | 41.16 | 40.95 | 41.70 | 63.40 |
| 13 | 40.85 | 40.35 | 41.16 | 41.50 | 39.84 | 63.65 |
| **EU %** | **98.65** | **98.40** | **98.13** | **80.69** | **95.22** | **93.53** |
| **$q_{oh\ var}$ %** | **3.51** | **3.20** | **4.62** | **34.39** | **13.78** | **18.98** |

where **DH** is the distributor hose, **$So_L$** is the lateral slope, **MDHO** is the measured distributor hoses outflow, **DDHE** is different distributor hose outlet elevation (calculated by computer program), **DHEZ** is the outlet elevation of the distributor hoses (zero from lateral level), **S = 2** is the hose position on two lateral sides, **SS = 1** is the laterals on two manifold sides, **$q_{oh}$** is the theoretical discharge of the distributor hose, **EU** is the emission uniformity of distributor hoses and **$q_{oh\ var}$** is distributor hoses flow variation, in %.

Table B-6: Measured and calculated pressure head just before each distributor hose inlet and calculated hose outlet elevation along one lateral. **[S = 2, SS = 1 and $q_{oh}$ = 40 l/h]**
*Gemessene und berechnete Druckhöhen am Übergang vom Verteilerrohr zum Verteilerschlauch und berechnete Auslasshöhen der Verteilerschläuche.*

| Nr. of DH | $So_L$ = + 0.5%, Hf = 59.9 cm | | | $So_L$ = - 0.5%, Hf = 43.5 cm | | | $So_L$ = 0.0%, Hf = 34.9 cm | | |
|---|---|---|---|---|---|---|---|---|---|
| | MPH [cm] | TPH [cm] | DHE [cm] | MPH [cm] | TPH [cm] | DHE [cm] | MPH [cm] | TPH [cm] | DHE [cm] |
| 1 | 58.6 | 57.66 | 33.64 | 42.8 | 43.2 | 19.23 | 33.9 | 33.66 | 9.64 |
| 2 | 53.4 | 53.6 | 29.57 | 41.9 | 43.18 | 19.16 | 31,2 | 31.6 | 7.57 |
| 3 | 49.5 | 49.84 | 25.82 | 41.0 | 43.43 | 19.41 | 29.2 | 29.84 | 5.82 |
| 4 | 45.8 | 46.37 | 22.35 | 42.3 | 43.97 | 19.94 | 27.7 | 28.37 | 4.35 |
| 5 | 42.4 | 43.17 | 19.15 | 43.2 | 44.76 | 20.74 | 26.4 | 27.17 | 3.15 |
| 6 | 38.9 | 40.21 | 16.18 | 44.1 | 45.8 | 21.77 | 24.7 | 26.21 | 2.18 |
| 7 | 36.2 | 37.46 | 13.44 | 45.3 | 47.05 | 23.02 | 24.0 | 25.46 | 1.45 |
| 8 | 33.3 | 34.9 | 10.88 | 46.3 | 48.49 | 24.47 | 23.1 | 24.9 | 0.88 |
| 9 | 31.1 | 32.51 | 8.48 | 48.0 | 50.1 | 26.07 | 22.9 | 24.51 | 0.48 |
| 10 | 28.9 | 30.25 | 6.23 | 49.7 | 51.84 | 27.82 | 22.5 | 24.25 | 0.23 |
| 11 | 26.9 | 28.1 | 4.08 | 51.2 | 53.7 | 29.67 | 21.7 | 24.1 | 0.08 |
| 12 | 24.8 | 26.04 | 2.01 | 53.2 | 55.63 | 31.61 | 21.8 | 24.04 | 0.02 |
| 13 | 23.4 | 24.03 | 0.0 | 55.9 | 57.61 | 33.59 | 22.1 | 24.03 | 0.0 |

where **Hf** is the pressure head at lateral inlet, **MPH** is the measure pressure head just before each distributor hose inlet, **TPH** is the theoretical pressure head calculated by the computer program and **DHE** is the distributor hose outlet elevation.

Table B-7: Measured distributor hose outflow at different distributor hose elevation along one lateral. **[S = 2, SS = 1 and $q_{oh}$ = 20 l/h]**
*Gemessener Verteilerschlauchdurchfluss entlang eines Verteilerrohres mit unterschiedlich hohen Auslässen am Verteilerschlauch.*

| Nr. of DH | MDHO [l/h] at DDHE | | | MDHO [l/h] at DHEZ | | |
|---|---|---|---|---|---|---|
| | $So_L$ = + 0.5% | $So_L$ = - 0.5% | $So_L$ = 0.0% | $So_L$ = + 0.5% | $So_L$ = - 0.5% | $So_L$ = 0.0% |
| 1 | 18.03 | 18.54 | 18.96 | 26.60 | 54.30 | 38.46 |
| 2 | 17.97 | 18.69 | 18.57 | 25.52 | 54.05 | 43.58 |
| 3 | 17.79 | 18.51 | 18.30 | 24.28 | 50.80 | 44.12 |
| 4 | 18.27 | 18.57 | 18.54 | 23.10 | 47.85 | 45.04 |
| 5 | 18.18 | 18.30 | 18.36 | 23.00 | 44.30 | 47.26 |
| 6 | 18.24 | 18.27 | 18.81 | 23.52 | 40.95 | 51.40 |
| 7 | 17.94 | 18.30 | 18.51 | 22.40 | 37.37 | 54.66 |
| 8 | 18.24 | 18.51 | 18.54 | 21.48 | 33.30 | 58.32 |
| 9 | 18.39 | 18.59 | 18.63 | 21.80 | 31.30 | 58.74 |
| 10 | 18.18 | 18.66 | 18.51 | 22.04 | 28.75 | 65.32 |
| 11 | 18.33 | 18.39 | 18.50 | 21.52 | 27.80 | 70.12 |
| 12 | 18.57 | 18.99 | 19.17 | 21.08 | 23.15 | 77.06 |
| 13 | 18.81 | 19.14 | 19.17 | 22.12 | 19.85 | 80.12 |
| **EU %** | **98.21** | **98.47** | **98.56** | **62.13** | **74.46** | **93.04** |
| **$q_{oh\ var}$ %** | **5.42** | **4.55** | **4.54** | **63.44** | **52.00** | **20.75** |

where **DH** is the distributor hose, **$So_L$** is the lateral slope, **MDHO** is the measured distributor hoses outflow, **DDHE** is different distributor hose outlet elevation (calculated by computer program), **DHEZ** is the outlet elevation of the distributor hoses (zero from lateral level), **S = 2** is the hose position on two lateral sides, **SS = 1** is the laterals on two manifold sides, **$q_{oh}$** is the theoretical discharge of the distributor hose, **EU** is the emission uniformity of distributor hoses and **$q_{oh\ var}$** is distributor hoses flow variation, in %.

Table B-8: Measured and calculated pressure head just before each distributor hose inlet and calculated hose outlet elevation along one lateral. **[S = 2, SS = 1 and $q_{oh}$ = 20 l/h]**
*Gemessene und berechnete Druckhöhen am Übergang vom Verteilerrohr zum Verteilerschlauch und berechnete Auslasshöhen der Verteilerschläuche.*

| Nr. of DH | $So_L$ = + 0.5%, Hf = 34.5 cm | | | $So_L$ = - 0.5%, Hf = 34.5 cm | | | $So_L$ = 0.0%, Hf = 34.5 cm | | |
|---|---|---|---|---|---|---|---|---|---|
| | MPH [cm] | TPH [cm] | DHE [cm] | MPH [cm] | TPH [cm] | DHE [cm] | MPH [cm] | TPH [cm] | DHE [cm] |
| 1 | 9.40 | 9.17 | 2.68 | 33.40 | 33.18 | 26.68 | 27.30 | 27.10 | 20.50 |
| 2 | 8.90 | 8.60 | 2.11 | 30.20 | 30.60 | 24.11 | 29.00 | 28.44 | 22.00 |
| 3 | 8.50 | 8.11 | 1.62 | 27.60 | 28.11 | 21.62 | 30.80 | 29.95 | 23.50 |
| 4 | 8.20 | 7.71 | 1.21 | 25.30 | 25.71 | 19.21 | 32.10 | 31.55 | 25.10 |
| 5 | 7.90 | 7.37 | 0.88 | 22.90 | 23.37 | 16.88 | 33.90 | 33.21 | 26.70 |
| 6 | 7.70 | 7.10 | 0.61 | 20.70 | 21.10 | 14.61 | 35.70 | 34.94 | 28.50 |
| 7 | 7.60 | 6.89 | 0.40 | 18.90 | 18.89 | 12.40 | 37.20 | 36.74 | 30.20 |
| 8 | 7.50 | 6.74 | 0.25 | 15.80 | 16.74 | 10.25 | 39.10 | 38.56 | 32.10 |
| 9 | 7.40 | 6.63 | 0.14 | 13.70 | 14.63 | 8.14 | 41.30 | 40.47 | 34.00 |
| 10 | 7.30 | 6.56 | 0.06 | 11.60 | 12.56 | 6.06 | 43.20 | 42.40 | 35.90 |
| 11 | 7.10 | 6.52 | 0.03 | 10.10 | 10.51 | 4.02 | 44.80 | 44.36 | 37.90 |
| 12 | 7.10 | 6.50 | 0.01 | 8.00 | 8.50 | 2.00 | 46.80 | 46.34 | 39.80 |
| 13 | 7.40 | 6.49 | 0.00 | 6.00 | 6.49 | 0.00 | 49.20 | 48.33 | 41.80 |

where **Hf** is the pressure head at lateral inlet, **MPH** is the measure pressure head just before each distributor hose inlet, **TPH** is the theoretical pressure head calculated by the computer program and **DHE** is the distributor hose outlet elevation.

Table B-9: Measured and theoretical distributor hose outflow along one lateral at different distributor hose length. **[S = 1, SS = 2 and $q_{oh}$ = 80 l/h]**
*Gemessener und theoretischer Durchfluss entlang eines Verteilerrohres mit unterschiedlicher Länge des Verteilerschlauches.*

| Nr. of DH from tank | MDHO [l/h] at DDHL | | | $q_{oh}$ [l/h] |
|---|---|---|---|---|
| | $So_L$ = + 0.5 % | $So_L$ = - 0.5 % | $So_L$ = 0.0 % | |
| 1 | 80.88 | 80.40 | 81.60 | 80 |
| 2 | 80.40 | 80.64 | 80.76 | 80 |
| 3 | 81.36 | 81.24 | 81.48 | 80 |
| 4 | 82.44 | 82.08 | 82.32 | 80 |
| 5 | 82.32 | 81.96 | 81.84 | 80 |
| 6 | 81.60 | 81.00 | 81.84 | 80 |
| 7 | 81.36 | 81.96 | 82.32 | 80 |
| 8 | 82.68 | 82.68 | 82.80 | 80 |
| 9 | 80.76 | 81.36 | 81.48 | 80 |
| 10 | 82.32 | 82.20 | 82.92 | 80 |
| 11 | 81.72 | 83.16 | 82.20 | 80 |
| 12 | 81.96 | 81.48 | 82.56 | 80 |
| 13 | 82.44 | 81.84 | 82.32 | 80 |
| **EU %** | **98.74** | **98.76** | **99.03** | |
| **$q_{oh\ var}$ %** | **2.76** | **3.32** | **2.60** | |

where **DH** is the distributor hose, **$So_L$** is the lateral slope, **MDHO** is the measured distributor hoses outflow, **DDHL** is different distributor hose length (calculated by computer program), **S = 1** is the hose position on one lateral side only, **SS = 2** is the laterals on both manifold sides, **$q_{oh}$** is the distributor hose theoretical discharge, **EU** is the emission uniformity of distributor hoses and **$q_{oh\ var}$** is distributor hose flow variation.

Table B-10: Measured and calculated pressure head just before each hose inlet and calculated hose length along one lateral. **[S = 1, SS = 2 and $q_{oh}$ = 80 l/h]**
*Gemessene und berechnete Druckhöhen am Übergang vom Verteilerrohr zum Verteilerschlauch und berechnete unterschiedliche Länge des Verteilerschlauches entlang eines Verteilerrohres.*

| Nr. of DH | $So_L$ = +0.5%, Hf = 72.8 cm | | | $So_L$ = - 0.5%, Hf = 72.8 cm | | | $So_L$ = 0.0%, Hf = 72.8 cm | | |
|---|---|---|---|---|---|---|---|---|---|
| | MPH [cm] | MPH [cm] | DHL [cm] | MPH [cm] | TPH [cm] | DHL [cm] | MPH [cm] | TPH [cm] | DHL [cm] |
| 1 | 69.4 | 70.56 | 179.1 | 72.0 | 72.56 | 186.7 | 71.3 | 71.56 | 182.9 |
| 2 | 65.2 | 66.49 | 163.5 | 71.9 | 72.49 | 186.5 | 68.5 | 69.49 | 175.0 |
| 3 | 60.5 | 62.74 | 149.1 | 71.5 | 72.74 | 187.4 | 66.6 | 67.74 | 168.2 |
| 4 | 57.4 | 59.27 | 135.7 | 71.5 | 73.27 | 189.5 | 65.0 | 66.27 | 162.6 |
| 5 | 53.5 | 56.07 | 123.5 | 72.0 | 74.07 | 192.5 | 63.2 | 65.07 | 158.0 |
| 6 | 49.8 | 53.11 | 112.1 | 72.9 | 75.11 | 196.5 | 61.8 | 64.11 | 154.3 |
| 7 | 48.0 | 50.36 | 101.5 | 74.0 | 76.36 | 201.3 | 61.5 | 63.36 | 151.4 |
| 8 | 46.5 | 47.80 | 91.7 | 75.1 | 77.80 | 206.8 | 60.9 | 62.80 | 149.3 |
| 9 | 42.5 | 45.40 | 82.5 | 76.9 | 79.40 | 213.0 | 60.2 | 62.40 | 147.8 |
| 10 | 39.2 | 43.15 | 73.9 | 78.3 | 81.15 | 219.7 | 59.4 | 62.15 | 146.8 |
| 11 | 37.8 | 41.00 | 65.7 | 80.1 | 83.00 | 226.8 | 59.2 | 62.00 | 146.2 |
| 12 | 36.7 | 38.94 | 57.7 | 82.2 | 84.94 | 234.2 | 59.2 | 61.94 | 146.0 |
| 13 | 35.0 | 36.92 | 50.0 | 84.4 | 86.92 | 241.8 | 59.5 | 61.92 | 145.9 |

where **Hf** is the pressure head at the lateral inlet, **MPH** is the measured pressure head just before each distributor hose inlet, **TPH** is the theoretical pressure head calculated by the computer program and **DHL** is the distributor hose length.

Table B-11: Measured and theoretical distributor hose outflow along one lateral at different distributor hose length. **[S = 1, SS = 1 and $q_{oh}$ = 80 l/h]**
*Gemessener und theoretischer Durchfluss entlang eines Verteilerrohres mit unterschiedlicher Länge des Verteilerschlauches.*

| Nr. of DH from the tank | MDHO [l/h] at DDHL | | | $q_{oh}$ [l/h] |
|---|---|---|---|---|
| | $So_L$ = + 0.5 % | $So_L$ = - 0.5 % | $So_L$ = 0.0 % | |
| 1 | 80.88 | 79.56 | 80.16 | 80 |
| 2 | 80.40 | 80.16 | 80.40 | 80 |
| 3 | 81.36 | 80.64 | 80.64 | 80 |
| 4 | 82.44 | 82.80 | 82.20 | 80 |
| 5 | 82.32 | 82.56 | 81.48 | 80 |
| 6 | 81.60 | 80.88 | 80.52 | 80 |
| 7 | 81.36 | 80.28 | 81.60 | 80 |
| 8 | 82.68 | 81.96 | 82.80 | 80 |
| 9 | 80.76 | 81.48 | 80.16 | 80 |
| 10 | 82.32 | 83.40 | 82.56 | 80 |
| 11 | 81.72 | 82.80 | 82.80 | 80 |
| 12 | 81.96 | 82.32 | 81.96 | 80 |
| 13 | 82.44 | 82.92 | 82.20 | 80 |
| **EU %** | **99.18** | **98.10** | **98.50** | |
| **$q_{oh\ var}$ %** | **2.88** | **4.60** | **2.91** | |

where **DH** is the distributor hose, **$So_L$** is the lateral slope, **MDHO** is the measured distributor hoses outflow, **DDHL** is different distributor hose length (calculated by computer program), **S = 1** is the hose position on one lateral side only, **SS = 1** is the laterals on both manifold sides, **$q_{oh}$** is the distributor hose theoretical discharge, **EU** is the emission uniformity of distributor hoses and **$q_{oh\ var}$** is distributor hose flow variation.

Table B-12: Measured and calculated pressure head just before each hose inlet and calculated hose length along one lateral. **[S = 1, SS = 1 and $q_{oh}$ = 80 l/h]**
*Gemessene, und berechnete Druckhöhen am Übergang vom Verteilerrohr zum Verteilerschlauch und berechnete unterschiedliche Länge des Verteilerschlauches entlang eines Verteilerrohres.*

| Nr. of DH | $So_L$ = + 0.5%, Hf = 72.8 cm | | | $So_L$ = - 0.5%, Hf = 26.1 cm | | | $So_L$ = 0.0 %, Hf = 47.8 cm | | |
|---|---|---|---|---|---|---|---|---|---|
| | MPH [cm] | TPH [cm] | DHL [cm] | MPH [cm] | TPH [cm] | DHL [cm] | MPH [cm] | TPH [cm] | DHL [cm] |
| 1 | 69.40 | 70.56 | 179.10 | 25.70 | 25.84 | 7.50 | 45.70 | 46.56 | 87.00 |
| 2 | 65.20 | 66.49 | 163.50 | 25.40 | 25.77 | 7.20 | 43.70 | 44.49 | 79.00 |
| 3 | 60.50 | 62.74 | 149.10 | 25.50 | 26.01 | 8.20 | 41.30 | 42.74 | 72.30 |
| 4 | 57.40 | 59.27 | 135.70 | 25.80 | 26.55 | 10.20 | 39.40 | 41.27 | 66.70 |
| 5 | 53.50 | 56.07 | 123.50 | 26.50 | 27.34 | 13.30 | 38.20 | 40.07 | 62.10 |
| 6 | 49.80 | 53.11 | 112.10 | 26.80 | 28.38 | 17.20 | 36.90 | 39.11 | 58.40 |
| 7 | 48.00 | 50.36 | 101.50 | 28.20 | 29.63 | 22.00 | 35.90 | 38.36 | 55.50 |
| 8 | 46.50 | 47.80 | 91.70 | 29.60 | 31.07 | 27.60 | 35.40 | 37.80 | 53.40 |
| 9 | 42.50 | 45.40 | 82.50 | 31.00 | 32.68 | 33.70 | 35.20 | 37.40 | 51.90 |
| 10 | 39.20 | 43.15 | 73.90 | 32.90 | 34.42 | 40.40 | 34.80 | 37.15 | 50.90 |
| 11 | 37.80 | 41.00 | 65.70 | 34.90 | 36.28 | 47.50 | 34.60 | 37.00 | 50.30 |
| 12 | 36.70 | 38.94 | 57.70 | 37.00 | 38.21 | 55.00 | 34.00 | 36.94 | 50.10 |
| 13 | 35.00 | 36.92 | 50.00 | 39.20 | 40.20 | 62.60 | 34.20 | 36.92 | 50.00 |

where **Hf** is the pressure head at the lateral inlet, **MPH** is the measured pressure head just before each distributor hose inlet, **TPH** is the theoretical pressure head calculated by the computer program and **DHL** is the distributor hose length.

# Appendix C

Figure A: Flow chart of the low-head bubbler irrigation system computer program.

*Flussdiagramm für das Niedrigdruck-Bubbler-Bewässerungssystem Computerprogramm.*

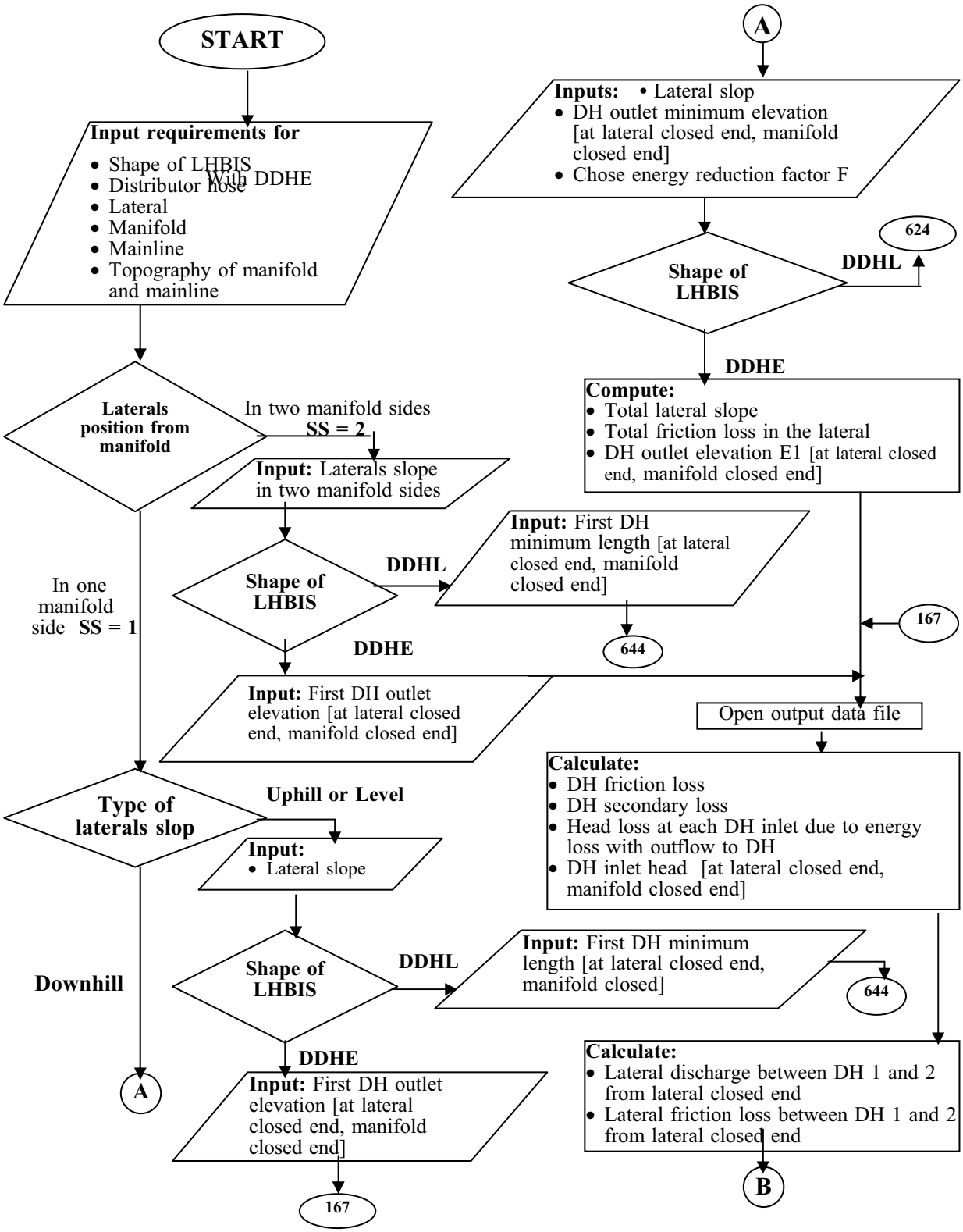

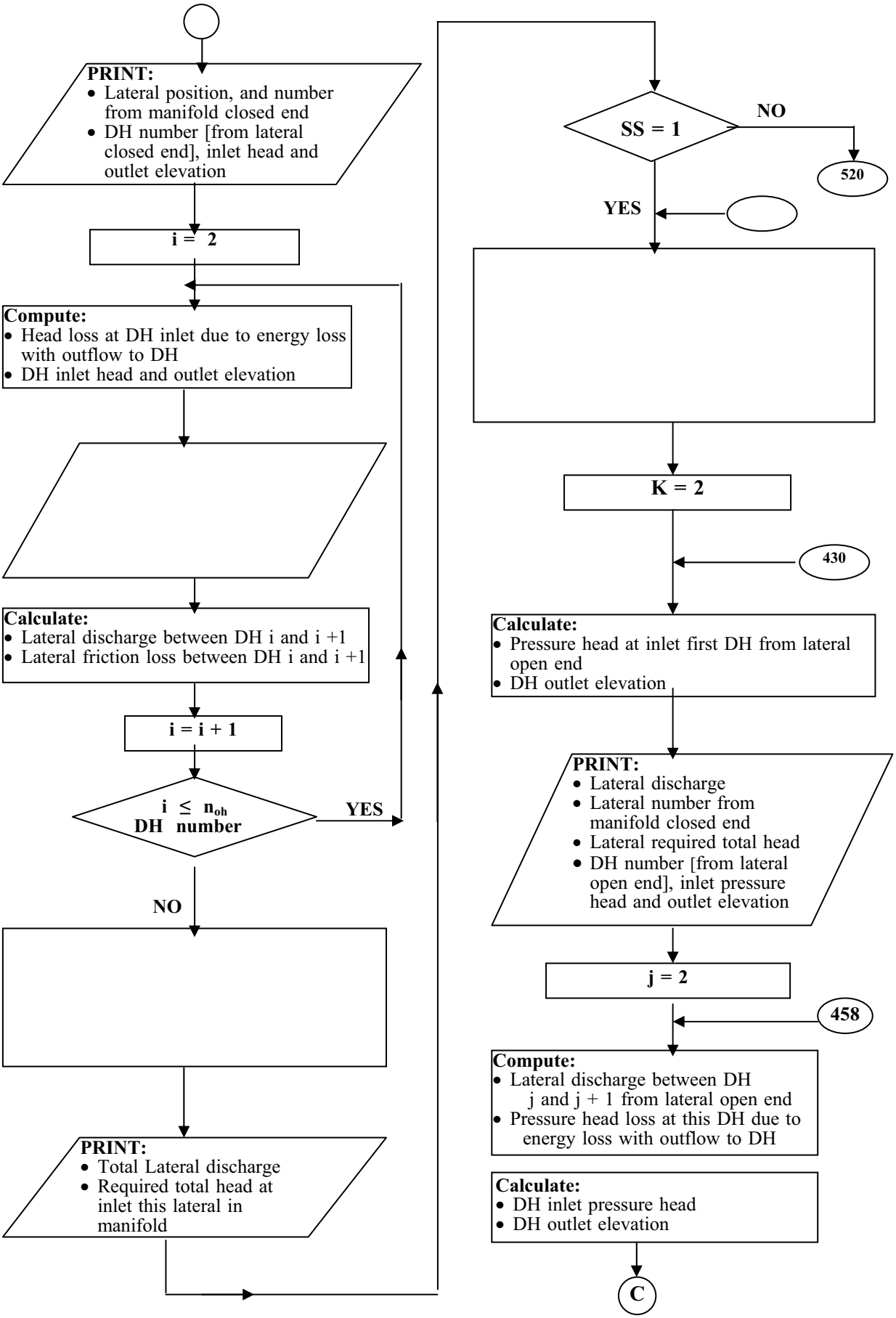
PRINT:
• Lateral position, and number from manifold closed end
• DH number [from lateral closed end], inlet head and outlet elevation
i = 2
Compute:
• Head loss at DH inlet due to energy loss with outflow to DH
• DH inlet head and outlet elevation
Calculate:
• Lateral discharge between DH i and i +1
• Lateral friction loss between DH i and i +1
i = i + 1
i ≤ n_oh
DH number
YES
NO
PRINT:
• Total Lateral discharge
• Required total head at inlet this lateral in manifold
SS = 1
NO
520
YES
K = 2
430
Calculate:
• Pressure head at inlet first DH from lateral open end
• DH outlet elevation
PRINT:
• Lateral discharge
• Lateral number from manifold closed end
• Lateral required total head
• DH number [from lateral open end], inlet pressure head and outlet elevation
j = 2
458
Compute:
• Lateral discharge between DH j and j + 1 from lateral open end
• Pressure head loss at this DH due to energy loss with outflow to DH
Calculate:
• DH inlet pressure head
• DH outlet elevation
C

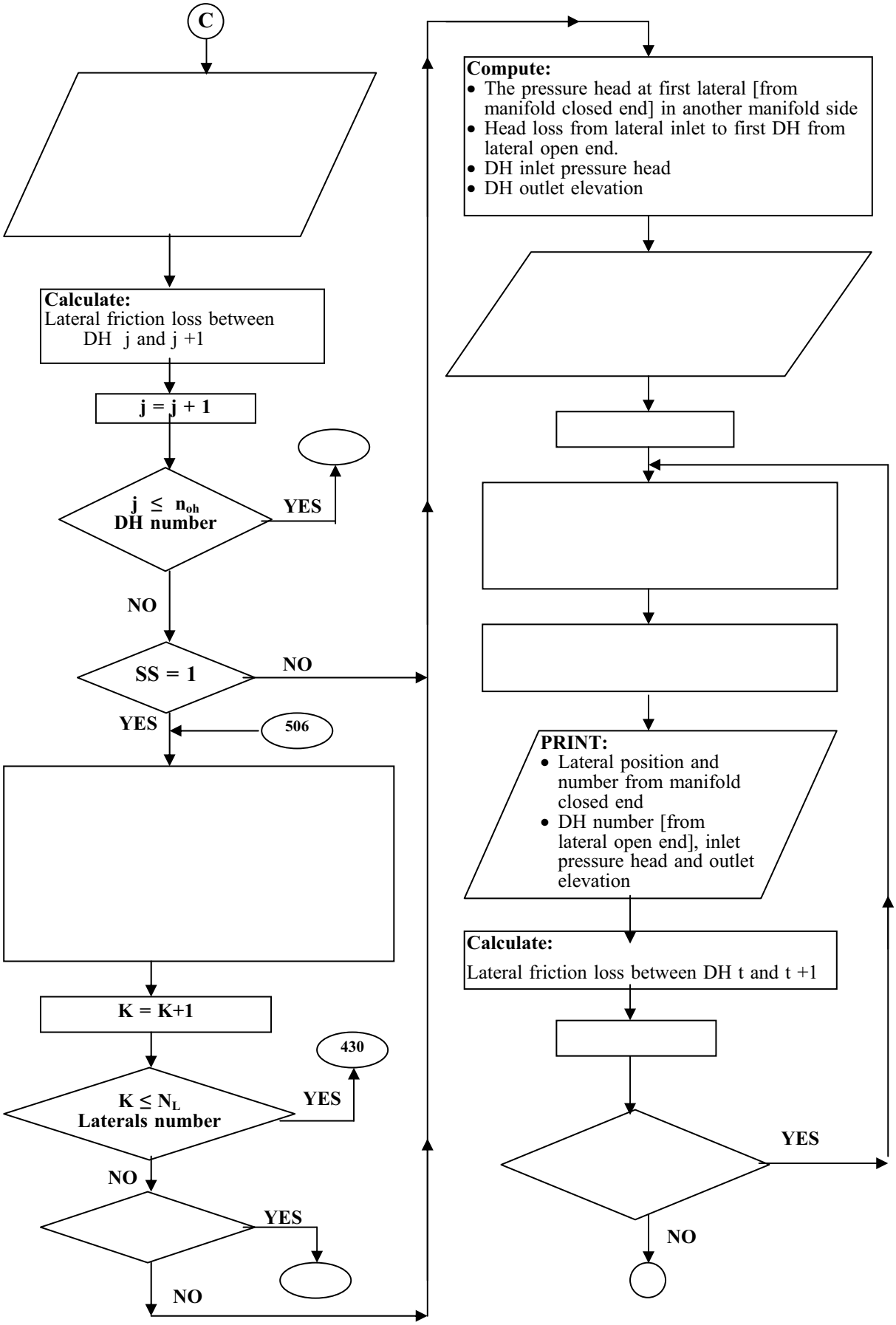
C
Calculate:
Lateral friction loss between
DH j and j +1
j = j + 1
j ≤ noh
DH number
YES
NO
SS = 1
NO
YES
506
K = K+1
430
K ≤ NL
Laterals number
YES
NO
YES
NO
Compute:
• The pressure head at first lateral [from manifold closed end] in another manifold side
• Head loss from lateral inlet to first DH from lateral open end.
• DH inlet pressure head
• DH outlet elevation
PRINT:
• Lateral position and number from manifold closed end
• DH number [from lateral open end], inlet pressure head and outlet elevation
Calculate:
Lateral friction loss between DH t and t +1
YES
NO

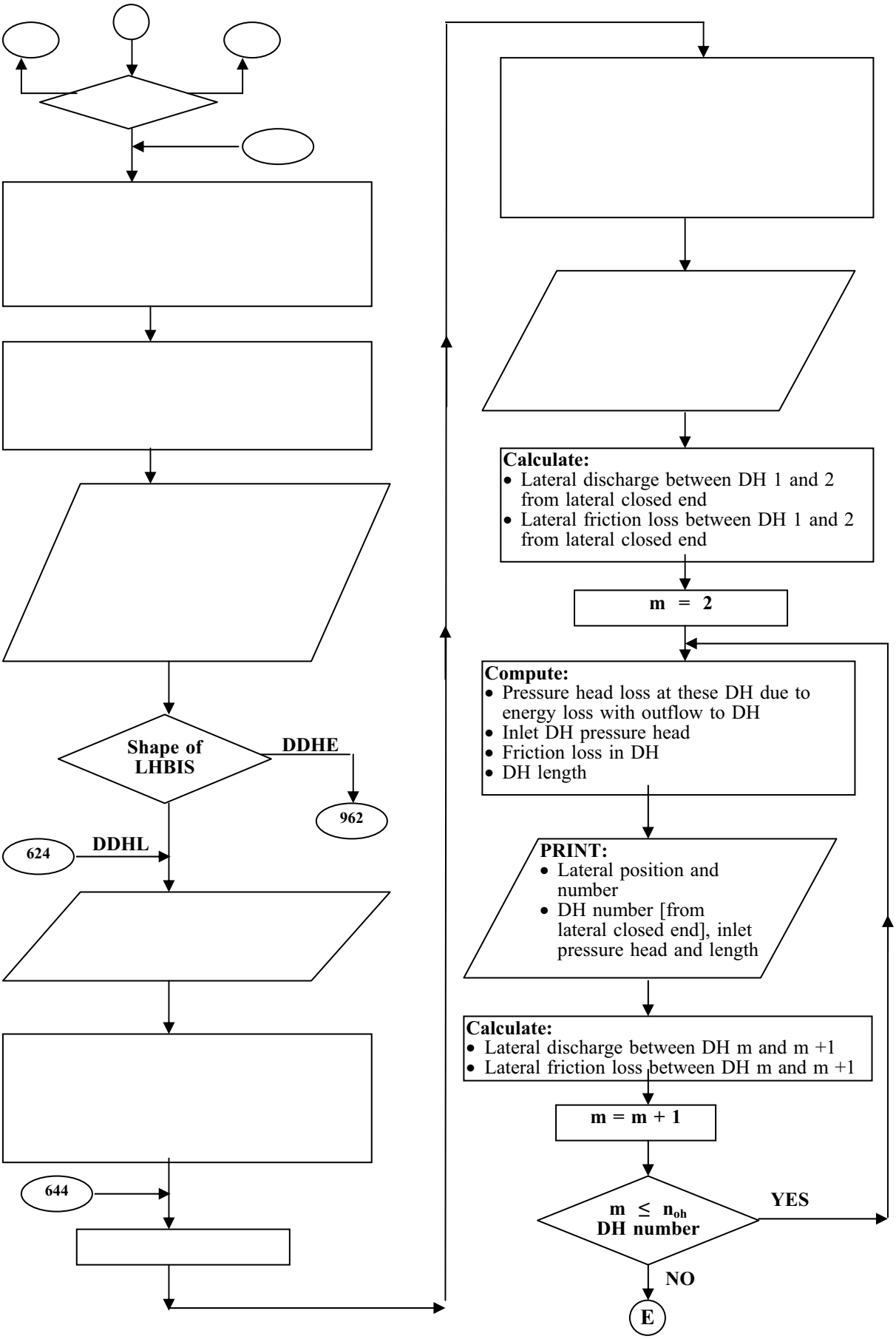
Shape of LHBIS
DDHE
962
624
DDHL
644
Calculate:
• Lateral discharge between DH 1 and 2 from lateral closed end
• Lateral friction loss between DH 1 and 2 from lateral closed end
m = 2
Compute:
• Pressure head loss at these DH due to energy loss with outflow to DH
• Inlet DH pressure head
• Friction loss in DH
• DH length
PRINT:
• Lateral position and number
• DH number [from lateral closed end], inlet pressure head and length
Calculate:
• Lateral discharge between DH m and m +1
• Lateral friction loss between DH m and m +1
m = m + 1
m ≤ n_oh
DH number
YES
NO
E

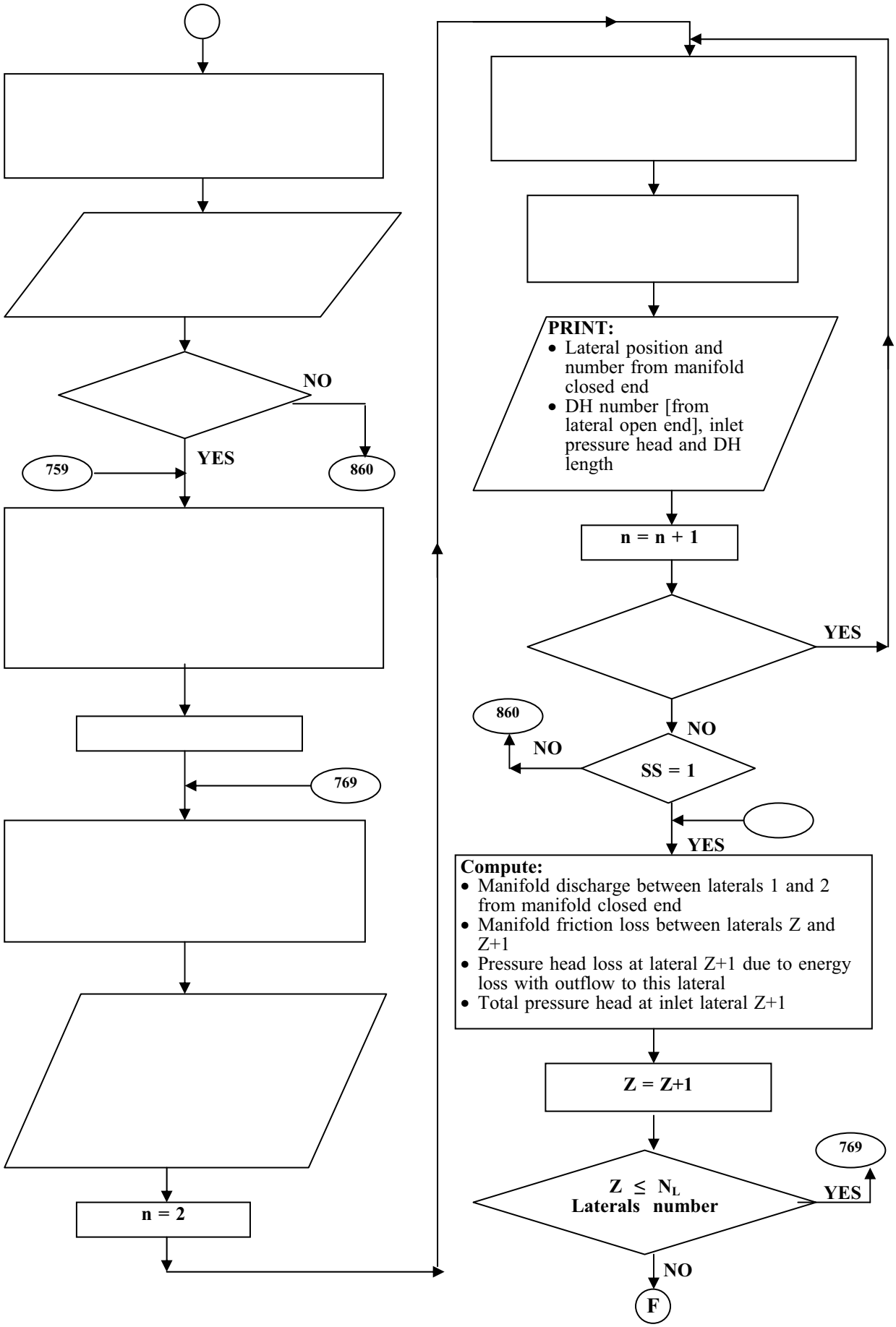
NO
YES
759
860
769
n = 2
PRINT:
• Lateral position and number from manifold closed end
• DH number [from lateral open end], inlet pressure head and DH length
n = n + 1
YES
860
NO
NO
SS = 1
YES
Compute:
• Manifold discharge between laterals 1 and 2 from manifold closed end
• Manifold friction loss between laterals Z and Z+1
• Pressure head loss at lateral Z+1 due to energy loss with outflow to this lateral
• Total pressure head at inlet lateral Z+1
Z = Z+1
769
Z ≤ N_L
Laterals number
YES
NO
F

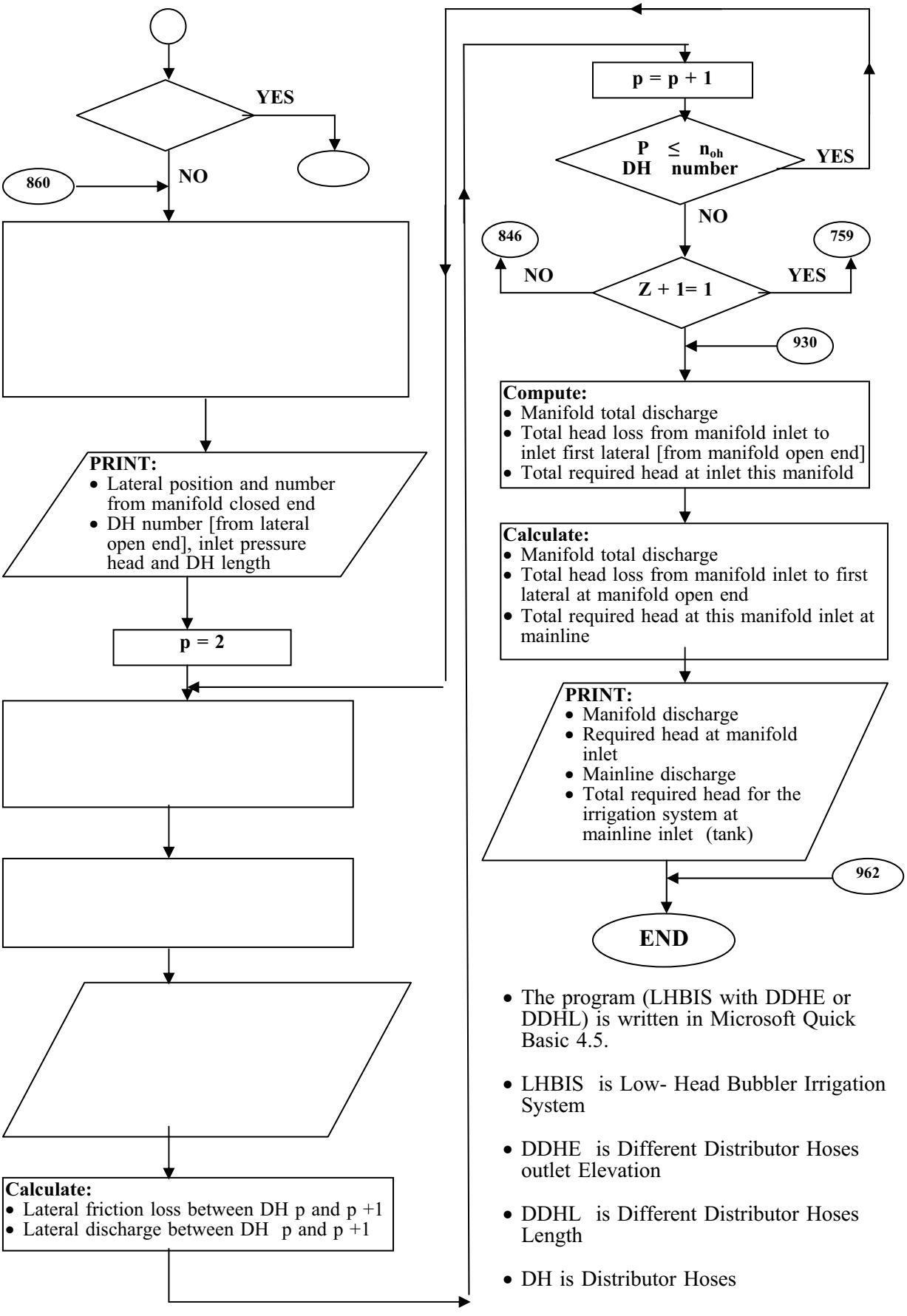


- The program (LHBIS with DDHE or DDHL) is written in Microsoft Quick Basic 4.5.
- LHBIS is Low- Head Bubbler Irrigation System
- DDHE is Different Distributor Hoses outlet Elevation
- DDHL is Different Distributor Hoses Length
- DH is Distributor Hoses

| | | |
|---|---|---|
| 239 | Axel Munack und Jürgen Krahl (Hrsg.) *(2002)*<br>**Biodiesel — Potenziale, Umweltwirkungen, Praxiserfahrungen —** | 7,00€ |
| 241 | Ulf Prüße and Klaus-Dieter Vorlop (eds.) *(2002)*<br>**Practical Aspects of Encapsulation Technologies** | 9,00€ |
| 242 | Folkhard Isermeyer (Hrsg.) *(2002)*<br>**Milchproduktion 2025** | 9,00€ |
| 243 | Franz-Josef Bockisch und Siegfried Kleisinger (Hrsg.) *(2003)*<br>**13. Arbeitswissenschaftliches Seminar** | 8,00€ |
| 244 | Anja Gassner *(2003)*<br>**Factors controlling the spatial specification of phosphorous in agricultural soils** | 9,00€ |
| 245 | Martin Kücke (Hrsg.) *(2003)*<br>**Anbauverfahren mit N-Injektion (CULTAN) — Ergebnisse, Perspektiven, Erfahrungen** | 7,00€ |
| 246 | Jeannette van de Steeg *(2003)*<br>**Land evaluation for agrarian reform. A case study for Brazil** | 7,00€ |
| 248 | Esmat W. A. Al-Karadsheh *(2003)*<br>**Potentials and development of precision irrigation technology** | 8,00€ |
| 249 | Andreas Siegfried Pacholsky *(2003)*<br>**Calibration of a Simple Method for Determinig Ammonia Votatilisation in the Field — Experiments in Henan, China, and Modelling Results** | 9,00€ |
| 250 | Asaad Abdelkader Abdalla Derbala *(2003)*<br>**Development and evaluation of mobile drip irrigation with center pivot irrigation machines** | 9,00€ |
| 251 | Susanne Freifrau von Münchhausen *(2003)*<br>**Modellgestützte Analyse der Wirtschaftlichkeit extensiver Grünlandnutzung mit Mutterkühen** | 8,00€ |
| 252 | Axel Munack . Olaf Schröder . Hendrik Stein . Jürgen Krahl und Jürgen Bünger *(2003)*<br>**Systematische Untersuchungen der Emissionen aus der motorischen Verbrennung vom RME, MK1 und DK** | 5,00€ |
| 253 | Andrea Hesse *(2003)*<br>**Entwicklung einer automatisierten Konditionsfütterung für Sauen unter besonderer Berücksichtigung der Tierleistung** | 8,00€ |
| 254 | Holger Lilienthal *(2003)*<br>**Entwicklung eines bodengestützten Fernerkundungssystems für die Landwirtschaft** | 8,00€ |
| 255 | Herwart Böhm . Thomas Engelke . Jana Finze . Andreas Häusler . Bernhard Pallutt . Arnd Verschwele und Peter Zwerger (Hrsg.) *(2003)*<br>**Strategien zur Regulierung von Wurzelunkräutern im ökologischen Landbau** | 10,00€ |
| 256 | Rudolf Artmann und Franz-Josef Bockisch (Hrsg.) *(2003)*<br>**Nachhaltige Bodennutzung — aus technischer, pflanzenbaulicher, ökologischer und ökonomischer Sicht** | 9,00€ |
| 257 | Axel Munack und Jürgen Krahl (Hrsg.) *(2003)*<br>**Erkennung des RME-Betriebes mittels eines Biodiesel-Kraftstoffsensors** | 5,00€ |
| 258 | Martina Brockmeier . Gerhard Flachowsky und Ulrich von Poschinger-Camphausen (Hrsg.) *(2003)*<br>**Statusseminar Welternährung**<br>**Beiträge zur globalen Ernährungssicherung** | 9,00€ |
| 259 | Gerold Rahmann und Hiltrud Nieberg (Hrsg.) *(2003)*<br>**Ressortforschung für den ökologischen Landbau 2002** | 8,00€ |

| | | |
|---|---|---|
| 260 | Ulrich Dämmgen (Hrsg.) *(2003)*<br>**Nationaler Inventarbericht 2004 — Berichterstattung unter der Klimarahmenkonvention der Vereinten Nationen — Teilbericht der Quellgruppe Landwirtschaft** | 7,00€ |
| 261 | Katja Hemme-Seifert *(2003)*<br>**Regional differenzierte Modellanalyse der Erzeugung von Biomasse zur energetischen Nutzung in Deutschland** | 7,00€ |
| 262 | Folkhard Isermeyer (Hrsg.) *(2003)*<br>**Fleisch 2025** | 9,00€ |
| 263 | Ernst-Jürgen Lode und Franz Ellendorff (Hrsg.) *(2003)*<br>**Perspektiven in der Tierproduktion** | 7,00€ |
| 264 | Johannes Holzner *(2004)*<br>**Eine Analyse der internationalen Wettbewerbsfähigkeit der Milcherzeugung an ausgewählten Standorten in Ostdeutschland, der Tschechischen Republik und Estland** | 10,00€ |
| 265 | Tarek Abd Elaziz Wahba Shalaby *(2004)*<br>**Genetical and nutritional influences on the spear quality of white asparagus (*Asparagus officinalis* L.)** | 7,00€ |
| 266 | Erik Zillmann *(2004)*<br>**Einsatz multi-dimensionaler Radardaten zur Erfassung der räumlichen Variabilität von Bestandesmerkmalen** | 9,00€ |
| 267 | Sergiy Parkhomenko *(2004)*<br>**International competitiveness of soybean, rapeseed and palm oil production in major producing regions** | 11,00€ |
| 268 | Martina Brockmeier und Petra Salamon *(2004)*<br>**WTO-Agrarverhandlungen — Schlüsselbereich für den Erfolg der Doha Runde<br>Optionen für Exportsubventionen, Interne Stützung, Marktzugang** | 9,00€ |
| 269 | Angela Bergschmidt *(2004)*<br>**Indikatoren für die internationale und nationale Umweltberichterstattung im Agrarbereich** | 8,00€ |
| 270 | Klaus Walter *(2004)*<br>**Analyse der Beziehung zwischen den Kosten für Tierarzt und Medikamente in der Milchviehhaltung und der Produktionstechnik, dem Futterbau, der Arbeitswirtschaft sowie der Faktorausstattung ausgewählter norddeutscher Betriebe** | 9,00€ |
| 271 | Uwe Petersen und Gerhard Flachowsky (Hrsg.) *(2004)*<br>***Workshop***<br>**Positivliste für Futtermittel als Beitrag zur Futtermittelsicherheit — Erwartungen, Konzepte, Lösungen<br>A Positive List of feedstuffs as a contribution to feed safety — Expectations, concepts and solutions** | 7,00€ |
| 272 | Gerold Rahmann und Thomas van Elsen (Hrsg.) *(2004)*<br>**Naturschutz als Aufgabe des Ökologischen Landbaus** | 7,00€ |
| 273 | Gerold Rahmann und Stefan Kühne (Hrsg.) *(2004)*<br>**Ressortforschung für den ökologischen Landbau 2004** | 7,00€ |
| 274 | Folkhard Isermeyer (Hrsg.) *(2004)*<br>**Ackerbau 2025** | 9,00€ |
| 275 | Abdelaziz Ibrahim Abdelaziz Aly Omara *(2004)*<br>**Further development of a mobile wind energy plant for a low-pressure irrigation system** | 9,00€ |
| 276 | Gerold Rahmann, Hiltrud Nieberg, Susanne Drengemann, Alois Fenneker, Solveig March, Christina Zurek (*2004)*<br>**Bundesweite Erhebung und Analyse der verbreiteten Produktionsverfahren, der realisierten Vermarktungswege und der wirtschaftlichen sowie sozialen Lage ökologisch wirtschaftender Betriebe und Aufbau eines bundesweiten Praxis-Forschungs-Netzes** | 13,00€ |

Viele frühere Sonderhefte sind weiterhin lieferbar.
Bei Interesse setzen Sie sich bitte mit Frau Röhm unter 0531-596·1403 oder *landbauforschung@fal.de* in Verbindung.